THE EFFECT OF RICE HUSK ASH ON THE MECHANICAL AND DURABILITY PROPERTIES OF CONCRETE

Binyamien I. Rasoul

A thesis submitted in partial fulfillment of the requirements of the University of Brighton for the degree of Doctor of Philosophy

2018

School of Environment and Technology

University of Brighton

United Kingdom

AUTHOR DECLARATION

I declare that the research contained in this thesis, unless otherwise formally indicated within text, is the original work of the author. The thesis has not been previously submitted to this or any other University for a degree, and does not incorporate any material already submitted for a degree.

Binyamien Ibrahim Rasoul

Brighton January, 2019

Email: br86@brighton.ac.uk,

Signature Date: 15/01/ 2019

We declare that the contents and the work described in this thesis were performed at the University of Brighton, School of Environment and Technology from October 2015 to September 2018 and under our supervision.

Friederike Günzel
Senior Lecturer,
University of Brighton
School of Environment & Technology

Email: F.K.Gunzel@brighton.ac.uk,

Imran Rafiq

Deputy HoS Quality Ass. & Enhancement,

University of Brighton

School of Environment & Technology

Email: M.Rafiq@brighton.ac.uk,

DEDICATION

This dissertation is dedicated to my Mother and Father soul, whom it was their dreams. To my wife for her patience, my son for missing his father most of the time during these difficult years, and in memory of my dears Mother and Father in law Tatiana and Nuzar Khamasurydze.

ACKNOWLEDGEMENT

Thanks for God who has given the author the courage and tenacity to complete his research thesis. The author would like to express his extremely thankful and sincere gratitude to his enthusiastic lead supervisors, Dr Friederike Günzel and Dr Imran Rafiq for their encouraging attitude, patience, sound guidance and valuable advice to complete this research. Their constant supervision and guidance helped the author to complete the research, which was otherwise not possible. The author feels very proud to have worked under her guidance and consider it a special blessing of God. Due to her benign patronage and able coaching author has been able to finish the research successfully and it is a great privilege to acknowledge her guidance. The author is also thankful to the examiners Professor, Kevin Paine of Bath University and Dr. Kevin Stone of Brighton University, for spending their valuable time.

Many thanks to staff members of the School of Environment and Technology, the Doctoral College and Aldrich Library staff at the University of Brighton for their cooperation throughout the years of study, especially Miss Sarah Longstaff who helped and guided me through the administrative process, even before applying to study in the UK. Many thanks to the staff of concrete laboratory for their cooperation in successful completion of the research. This work would not have been possible without the financial support of the Ministry of Higher Education and Scientific Research in Iraq and the Iraqi Cultural Attaché in London which have supported all Iraqi students abroad, despite all the challenges our country has faced in the last few years. Similarly, profound gratitude goes to my home University, the University of Kirkuk and the staff members of Department of Civil Engineering for their continuous support. Finally, would especially like to thank my wife, Mrs Marina Khamasurydze for her unwavering love, support, faith and encouragement. To my son Stephan for his happy faces greeting me when I see him every time back at home in Georgia. To my sisters and brothers, who always pray for my success and have been a constant source of encouragement.

Binyamien Ibrahim Rasoul

ABSTRACT

The work described in this thesis has been performed in order to gain further understanding of the effect of physical properties and chemical composition of Rice Husk Ash as an admixture on the properties of mortar and concrete in related to the percentage of replacement ratio. However, the RHA properties based on the literature had a contradiction impact on the ordinary Portland cement (OPC) concrete performance. Thus, contradiction in performance of RHA properties gives a point of view offers challenge to more investigation. To reach these objects, different types of RHA (A, B, C, C1, C2, C3, C4, and C5) with various mortar and concrete were produced. The water-binder (w/b) ratios were maintained at 0.50, with variable replacement ratio range in between 0% to 80% of cement by weight. To obtain the rice husk ash properties, the silica structure, chemical composition, physical properties and microstructure form were quantitatively analyzed using a wide range of advanced techniques such as X-Ray Diffraction (XRD), X-Ray Fluorescence (XRF), Laser diffraction particle sizing and scanning electron microscopy (SEM). These investigations are crucial for gaining a more detailed understanding on how RHA properties act as a pozzolanic admixture in OPC concrete at high replacement ratio.

The Influences of RHA on the, workability, compressive strength, splitting tensile strength, dry shrinkage, microstructure and durability of RHA mortar and concrete were evaluated. Finally, various heat treatments were applied to study the RHA silica structure. All the characteristics of these mortars and concrete containing RHA were compared to those of OPC mixtures. Overall, the results showed that RHA acts as a highly water absorbing material, which is also act as an internal curing agent in OPC. The decrease in the internal relative humidity and thus self-desiccation of OPC is reduced by the presence of RHA. The incorporation of RHA-A, B and C are improving the packing of the mortar and concrete mixtures, resulting in increased compressive and tensile strength. Moreover, with increase fineness of particles up to 4.0μm, RHA presented significant improvement in strength performance of mortar. In addition to that, with re-burned RHA-C at different temperature to time (C1, C2, C3, C4 and C5), a sustainable increase in the compressive and tensile strength were observed with C2 and C5, reactively. Drying shrinkage was another parameter was investigated and the results prove it that fineness of RHA particles effect directly on the drying shrinkage performance of concrete. Where, each of RHA-A and B (coarse particle size) strongly reduces drying shrinkage compare to RHA-C and C5.

In addition to the strength and drying shrinkage, the chloride diffusion coefficient of concrete blended RHA was investigated. The results demonstrated the extent of the effect

RHA on the chloride diffusion resistance. Where chloride diffusion coefficient drastically decreases for RHA concrete due to the improved packing of the concrete matrix. The graphical presentation of diffusion coefficient clearly demonstrates the role of variable dosage of RHA on the improvement of chloride diffusion resistance up to 50% replacement ratio regardless of the test method (NT Build 492). Based on the results it can be stated that, RHA even with relatively high crystalline silica content (RHA-A, and B), can be safely used as a partial replacement of cement up to 60% replacement ratio. Therefore, the utilization of RHA in OPC production reduces the drying shrinkage, and improves compressive, splitting tensile strength and durability of OPC concrete. Finally, the effect of temperature degree to time on the RHA silica structure was studied during the last phase of the study. A wide and exhaustive temperatures degree to time was designed in which the most reactive RHA developed.

LIST OF CONTENT

LIST OF TABLES

LIST OF FIGURES

LIST OF ABBREVIATIONS

OPC	Ordinary Portland cement
CO_2	Carbon dioxide
IPCC	Intergovernmental Panel on Climate Change
FAO	Foods and Agriculture Organization
SCM	Supplementary cementing material
C-S-H	Calcium Silicate Hydrates
CH	Calcium hydroxide
RHA	Rice husk ash
*f*c	Compressive strength of mortar or concrete
C_2S	Dicalcium Silicate
C_3A	Tricalcium Aluminate
C_3S	Tricalcium Silicate
C_4AF	Tetracalcium Aluminoferrite
S	Silicon dioxide (SiO_2)
W/C	Water to cement ratio
XRD	X-Ray Diffraction
DTA	Differential Thermal Analysis
SSA	Specific surface are
µm	Micrometer
SEM	Scanning Electron Microscope
APS	Average particle size
ASTM	American Society for Testing and Materials
ACI	American Concrete Institute
MIRHA	Microwave Incinerated Rice Husk Ash
POFA	Palm Oil Fuel Ash
FA	Fly ash
CEM I 52.5N	High early strength Portland cement
PSD	Particle size distribution
XRF	X-Ray Fluorescence
λ	Characteristic Wavelength
Δσ	Rate of change in the conductivity of saturated solution of calcium hydroxide after two minutes of adding RHA.

LOI	Loss on ignition
pH	alkalinity degree
BSI	British Standards Institution
SP	Superplasticizer
B	Binder content of concrete or mortar
C	Cement
CA	Coarse aggregate
S/A	Sand-aggregate ratio
W	Water content
W/B	Water-to-Binder Ratio
F	Maximum load at failure, in N
A_c	Cross-sectional area of the specimen on which the compressive force acts
A	Area of the cross- section broken dog-bone
M	Molarity
NT Build 942	Non-Steady State Chloride Migration (Diffusion Coefficient)
RCPT	Rapid chloride penetration test
RCM	Rapid chloride migration test
D*nssm*	Non-steady-state migration coefficient
PSD	Particle size distribution
RH	Relative humidity
f_t	Tensile strength of mortar
f_{spt}	Splitting tensile strength of concrete
BET	Nitrogen adsorption method (Brunauer-Emmett-Teller)
BCA	British Cement Association
CEN	European Committee for Standardization
AFt	Monosulphate to formation of ettringite
Wt	Weight
AAHSTO	American Association of State Highway and Transportation Officials
ϕ	Diameter of the pore
DOE	British mix design met
2θ	°2 Theta
cts	Counts

CHAPTER 1: INTRODUCTION

1.1 Background

Concrete as one of the most widely used construction material has unlimited opportunities for innovative applications, design and construction techniques. Concrete as a material consists of cement, fine aggregate, coarse aggregate, and water. According to Neville and Brooks (2008) fine and coarse aggregates constitute about 60% to 70% of concrete volume, where they influence the properties of fresh and hardened concrete. Cement is an essential element in the production of concrete where production of this material reached up to 2000 million tons in 2004 and this number doubled in 12years up to 4,200 million tons in 2016 around the world (British Geological Survey and the Statistics Portal). This high amount of cement production creates a widespread interest in the raw materials and affects not only the depletion of the natural raw materials, but also releases a significant amount of carbon dioxide gas (CO_2) as a by-product. Production of one ton of Portland cement releases about one ton of carbon dioxide (Malhotra, 1995). Carbon dioxide (CO_2) emissions from cement production are involved in the environmental issues and climate change as a result. Therefore, finding a solution to substitute part of the cement in concrete is an essential factor to increase the sustainability of concrete and reduce CO_2 gas emission (Ramezanianpour et al., 2008). On the other hand, improving concrete performance by utilisation of industrial and agricultural waste as supplementary cementitious materials gained a strong concerned in research and materials application in recent years (Imbabi et al., 2012).

Several strategies to reduce CO_2 emissions from cement production have been proposed. According to the Intergovernmental Panel on Climate Change (IPCC), replacement with waste materials, (Pozzolanic materials such as fly ash, silica fume, and ground granulated blast furnace slag), consisting of high amounts of silica could be used to reduce global CO_2 emissions (Heath and Paine, 2014). In addition to these materials, rice husk ash is one of the most pozzolanic materials produced in the worldwide yearly. RHA is the residue of completely incinerated rice husk under proper conditions. Rice husk, the outer covering of a rice kernel, is an agricultural waste from the milling process of paddy. Rice husk is abundant in many rice cultivating countries, e.g. Vietnam, India and China. Each ton of paddy rice can produce approximately 200 kg of rice husk, which on combustion produces about 40 kg of ash (Mehta, 1994). According to Food and Agriculture Organization (FAO), report the global produced an annual production rice paddy in 2017 was about 758.8 million tons, which produces approximately 145 million tons of rice husks. Normally, rice husk

from paddy rice mills is disposed directly into the environment or sometimes is dumped or burnt in open piles on the fields. This results in serious environmental pollution, especially when it is disintegrated in wet conditions.

Rice husk is generally estimated about 20% of the paddy plant (Habeeb and Fayyadh, 2009). Currently, this massive amount of waste materials creates an environmental problem of land filling; the open field combustion yields another CO_2 emission source. Rice husk ash is the end product of the rice husk burning process, where the term "RHA" exclusively refers to reactive rice husk ash in this thesis. RHA is produced in large quantities globally each year by incinerating rice husks in power stations to generate electricity, or by burning the husk of the agricultural fields. This vast amount is accompanied with difficulty in it is disposal which is in turn, becoming an environmental hazard in rice-producing countries leading to pollution of air and water. Rice husk when incinerated produces about 20% of the total weight of ash (Mehta, 1994). RHA generally consists of a high amount of silica with a variation of other elements and carbon from incomplete incineration.

Due to a high content of amorphous silica, rice husk ash (RHA) can be successfully utilized to partly replace by ordinary Portland cement (OPC) [Ganesan et al., (2008); Abu Bakar et al., (2011); etc]

According to Mehta and Pitt (1976) and Cook (1986), RHA is a natural pozzolanic material that, when used in conjunction with lime, has cementitious properties. In 1973, Mehta carried out the first attempt on the improvement of concrete blended with rice husk ash. Followed by numerous studies, showing that rice husk ash (RHA) can be used as a partial replacement for cement in concrete (Boateng and Skeete 1990; Rodriguez de Sensale 2006 and Zerbino et al. 2011).

1.2 Problem statement

1.2.1 Background to the research

As the improved performance and development of construction materials are important trends in research to improve of properties, the enhancement of service life and environmental sustainability. Development performance of the concrete properties is an object for many researchers; also, the sustainability and cost reduction of concrete production is a concern, too. In addition to the negative impact of cement production on the environment, an even concrete conventional output from ordinary Portland cement (OPC) has many defects in mechanical and durability properties such as strength (compression, splitting tensile), permeability, corrosion resistance and shrinkage (Ramezanianpour et al.,

2008). Improving concrete properties by increasing the strength and durability is the most noteworthy point concerning the use of supplementary cementitious materials. The use of these materials to achieve the high performance must determine to improve the concrete properties and find out the optimum of replacement ratio that can be affected positively on the concrete parameters (Setina et al., 2013). Rice husk ash is the second most abundant by-product material as showed in Table 1.1. It is not suitable for use as animal fodder because of it is high content of silica. However, this high rate of silica makes rice husk ash an excellent supplementary cementitious material after it is burning at appropriate temperatures. The implementation of RHA as a partial replacement of cement is viewed as a solution of reduces the CO_2 emission, cost of concrete as well as rice husk waste pollution.

Table 1. 1: The statistics of worldwide production and consumption of various wastes.

Waste	Waste source	Quantity (million ton)	Reference
Rice husk ash	Rice mills	144.9	FAO (2013)
Fly ash	Coal operated power plants	900	Malhotra (2006)
GGBFS*	Iron industry	100	Nehdi (2001)
Silica fume	Silicon industry	2	Malhotra (2006

GGBFS*: Ground granulated blast-furnace slag.

1.2.2 Hydration of cement blended with RHA

The state of art on mechanism for hydration of cement blended with RHA, is still not fully understood. It can be stated that the hydration of the binder is very complex and depends on the chemical composition, the fineness, and the number of reactive phases of RHA and the composition of the interacting solution. Generally, the inclusion of supplementary cementitious materials (SCM) with Portland cement results in a more complicated system because the hydraulic reactions of Portland cement and SCM take place simultaneously and might, interact with each other (Lee, 2005). It is proposed that the addition of SCM to Portland cement contributes extra space for the hydration products of clinker phases due to the higher water to cement ratio at the same water-binder (cement + SCM) ratio and extra nucleation sites for the precipitation of hydrated phases due to the higher fineness of SCM (RHA) in terms of finer SCM compared to cement. Moreover, the pozzolanic reaction of SCM, (amorphous silica), occurs parallel with hydraulic reaction of cement. Additionally, in comparison with other SCMs, i.e. Silica Foam, RHA particles have a highly porous structure. Consequently, the mechanism for the hydration of Portland cement blended with RHA and more complicated, and the products from RHA pozzolanic reaction may be formed. To date, this aspect has not yet been clearly understood.

1.2.3 Impacts of the RHA properties on the concrete performance

RHA is considered a pozzolanic material. When the amorphous silica (SiO_2) in the RHA reacts with calcium hydroxide resulting from the cement hydration more calcium silicate hydrate (C-S-H) gel is formed. This improves the durability and the mechanical properties of concrete. Calcium hydroxide (CH) is the most soluble of hydration products; it is considered a 'weak link' in concrete and subsequently negatively affects the durability of concrete (Malhotra et al., 1996). The chemical properties of RHA vary from one type to another, depending on the source of the husk, the process of burning and grinding process. In general, silica is the main element in the RHA with the range from 60% to 98% of the total weight of the ash, where the content of silica in RHA is different from different authors as presented in Table 1.2. The other oxide contents that also have an impact on the performance of RHA are variable and need more research on the mechanical effect on the performance of RHA. The residual carbon content is another chemical component of a direct impact on the RHA performance; it is limited up to 12% as the total weight of ash according to ASTM C618 requirement.

The physical properties of RHA also play a vital role in the performance of RHA-blended cement. The specific surface area, fineness of grain and silica form (amorphous) is the keys properties of RHA to improve concrete performance (Dakroury et al., 2008). The increased C-S-H gel in concrete blended with RHA is assigned to the high specific surface area of RHA (Feng et al., 2004). As the surface area plays a significant role in the activity of RHA, the amorphous silica content is thought most important to determine the impact of RHA on the concrete properties (Payá et al., 2001). Therefore, the physical properties of RHA are as crucial for the cement quality as the chemical composition of the RHA.

Table 1. 2: Chemical composition of RHA according to different authors.

RHA chemical composition										References
SiO_2	Al_2O_3	Fe_2O_3	CaO	MgO	SO_3	Na_2O	K_2O	P_2O_5	LOI	
82.13	4.27	0.38	0.16	1.65	-	0.14	1.23	1.44	8.60	Ikpong & Okpala(1992)
79.8	0.27	3.11	0.63	0.81	0.13	0.19	1.26	12.1	12.16	Hasparyk et al. (2004)
87.2	0.15	0.16	0.55	0.35	0.24	1.12	3.68	0.5	8.55	Zhang et al. (2005)
96.26	0.41	0.22	0.76	0.50	0.04	0.03	1.44	-	4.49	Gastaldini et al. (2007)
91.0	0.35	0.41	-	0.81	1.21	0.08	3.21	0.98	8.50	Hwang et al. (2011)
87.20	0.15	0.16	0.55	0.35	0.24	-	-	5.91	5.40	Naveen et al. (2015)

1.2.4 Discrepancies of RHA effect on the concrete properties

Up to now, to the author's knowledge, no comprehensive research has been implemented to investigate the structure of RHA in detail and the effect of the physical properties and

chemical composition of RHA on properties of fresh and hardened mortar and concrete, and it is durability at high replacement ratio. Depending on some authors, the use of RHA in concrete has led to a noticeable increase in compressive strength, a significant reduction of rapid chloride penetrability and autogenous shrinkage of ordinary and high-performance concrete (Saraswathy and Song, 2007). On the other hand, some other researchers, e.g. Ikpong and Okpala (1992) and Antiohos et al. (2013), reported that incorporation of RHA in mixtures would reduce the strength of concrete, compared to ordinary Portland cement (OPC) concrete. Another point was disputed among the researchers are the percentage of replacement. According to of Isaia et al. (2003) and Hwang et al. (2011) that, 25% replacement ratio considered as highest replacement ratio without compromising of concert properties.

Nevertheless, Habeeb and Mahmud (2010) concluded that 20% replacement ratio is found to be the highest ratio of replacement. Whereas, Leong (2015) reported that up to 5% of cement replacement by RHA increase the strength is comparable to OPC concrete. While each of Madandoust et al. (2011) and Marthong (2012) results show a reduction in strength for concrete blended RHA even with 5% replacement ratio compares to OPC control. Owing to the high specific surface area, high porosity, and irregular particle shape, RHA has a higher water demand than cement. Hence, admixtures are needed (superplasticizer) to increase the workability of fresh concrete, which is another disadvantage of using RHA as supplementary cementitious material. In addition to that, the effect of RHA on the improvement of concrete against chloride ion penetration and dry shrinkage thought as another argument points between the researchers.

1.3 Aim and objectives

1.3.1 Aim

The overall aim of the present investigation was to assess the effect of using different types of RHA at a relatively high partial replacement of cement on the workability, strength (compressive, tensile), drying shrinkage and chloride penetration of mortar and concrete. The idea of the research is to provide a further understanding of the effect of physical properties, chemical composition and microstructural characteristics of the RHA related to the concrete strength and chloride ingress. The particular aim of this thesis is tantamount to investigate the possibility of increasing the RHA content in cement above the currently known optimum. The objective is to eliminate the contradictions in contemporary literature on the effect of RHA addition to Portland cement on the quality of concrete.

1.3.2 Objectives of this Thesis

The objective of this research is to analyse the characteristics of RHA and investigate the behaviour of RHA in mortar and concrete, compared to the literature. The following aspects are investigated in this research:

i. To investigate the physical properties and chemical composition of RHA effect on the mortar and concrete performance, and relate that to the contradiction published results.
ii. To investigate the optimum replacement percentages of RHA without compromising on the concrete parameters and comparing that with literature researches.
iii. Increase the amount of replacement cement by RHA to more than 30% by weight of cement was considered, if necessary, by using the third additive.
iv. To investigate the mechanism of concrete blended RHA reducing the chloride ion penetration and drying shrinkage.
v. The effect of RHA with or without superplasticizer, on the strength (compressive and tensile) of mortar is investigated.
vi. An attempt is made to propose an incineration degree to time to produce RHA with entirely consist of amorphous silica.

1.3.3 Outline of this thesis

The content of this thesis consists of the study of key characteristics of RHA and their effect on the hydration and microstructure development, workability, compressive strength, tensile strength, drying shrinkage and durability of mortar and concrete.

CHAPTER 2: LITERATURE REVIEW

2.1 General

This chapter provides a brief and up-to-date literature review which can contribute to further understanding of the rice husk ash fundamental properties as a supplementary cementitious material in general and it is phases specifically on the mechanical and durability of concrete at different replacement ratio. The first section will begin with a general overview of the concrete microstructure complexity following by explaining the microstructure and the hydration of the cement matrix and the associated change in the presence of the fillers and mineral admixtures. The second section will describe the nature of rice husk ash, application, preparation, microstructure, fineness, and reactivity of RHA, then finally the hydration of cement blended RHA. The third part will cover the effect RHA on the strength, dry shrinkage and controlling the chloride transport property of the concrete.

2.2 Concrete

2.2.1 Preamble

Concrete is a composite material that consists mainly of the binding medium within which are embedded particles or fragments of aggregate. The paste is made up of Portland cement and water and with the addition of fine and coarse aggregates produce wet part of the paste through the hydration interaction the paste hardens and gain strength generate what is known as concrete. Nowadays concrete one of the cheapest materials in construction, because of the availability of raw materials and low rate of cost producing. However, the defect with concrete is many, such as low tensile strength, low resistance to chloride ion penetration and dry shrinkage leading to cracks in concrete. These parameters were improved by utilization of pozzolanic materials, such as fly ash and silica fume.

2.2.2 Concrete industry

With the beginning of 20 century, the concrete started to replace other construction materials, whereas there was no specific way to design concrete mix and there were no different types of cement or concrete. The Abrams (1919) relationship between the compressive strength and water-cement ratio revolutionizes the concrete production. Abram's water-cement ratio rules expression as follows.

$$fc = k_1/k_2^{w/c} \quad (1)$$

Where *fc* is the compressive strength of concrete at a designed age, while w/c is the water to cement ratio in the concrete mix, and k_1 and k_2 are the empirical constants. For different design typical curve illustrating this relationship was later developed (Fig 2.1).

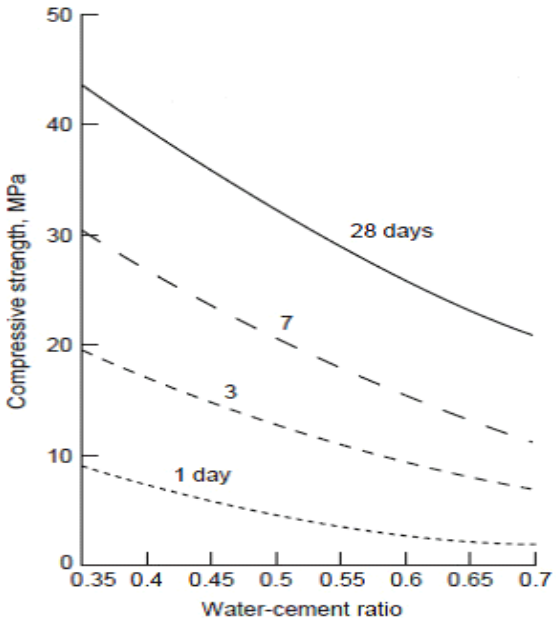

Figure 2.1: The Influence of the w/c ratio and moist curing age on concrete strength (Mehta and Monterio, 2006).

The abundance of some raw materials sand, gravel and water made concrete the main material in the construction (Mehta and Monteiro, 1993). The industry of concrete in the USA alone about 500 million tons of concrete used in 1992, which is increased to approximately 800 million tons in 2009, while in the world was about 25 billion tons (The Cement Sustainability Initiative, 2009). Concrete as a construction material has many defects as mentioned before, but in spite of that used in the construction, because of the resistance to water, unlike wood and steel. The resist capability to water action without damage makes it a perfect material for building and the high diversity options to form concrete of different size and shapes since the plastic consistency which gives a particular feature to flow into the prefabricated formwork. Whereas Portland cement, aggregate (fine, coarse), and water is commonly available almost everywhere around the world and are not expensive, there are more advantages of using the concrete as a favourite material in construction, such as maintenance, fire resistance, and resistance to cyclic loading (Mehta and Monteiro 1993).

2.2.3 Composition of the Concrete

Concrete is a composite material comprising of coarse aggregate particles dispersed in a cement matrix, which acts as a binder for the sand and gravel aggregate. It is the properties and behaviour of the cement paste that is responsible for many of the good and bad qualities of concrete. For a given aggregate, the physical and chemical characteristics of the cement paste dete1rnine the most important property of fresh concrete-workability and also the most significance engineering characteristics of hardened concrete-strength and dimensional stability (Neville 1995). To understand the formulation process of cement in concrete, cement.

2.2.3.1 Portland cement

Portland cements are hydraulic cements, meaning they react and harden chemically with the addition of water. Cement contains limestone, clay, cement rock and iron ore blended and heated up to 1500 C°. The resulting product "clinker" is then ground to the consistency of powder. Gypsum is added to control setting time. Portland cement as a multi-component, multi-phase inorganic materials major component consists of tricalcium silicate (C_3S), di-calcium silicate (C_2S), tri-calcium aluminate (C_3A), and tetra-calcium aluminoferrite (C_4AF). During the hydration of Ordinary Portland cement (OPC), the compounds C_3S, C_2S, C_3A and C_4AF react with water to form calcium silicate hydrates (C-S-H) gel which is approximately about 70% of the total cement paste, while calcium hydroxide [$Ca(OH)_2$] about 20%, sulfoaluminate 7% and 3% is secondary phases (Neville and Brooks, 2010).

2.2.3.2 Aggregate

Coarse aggregate is the term indicates to the particles size larger than 4.75mm (sieve no 4) on the other hand particle smaller than 4.75mm, but larger than 75µm (sieve number 200) indicate to fine aggregate. Whereas British Standard BS 882:1983 define coarse aggregate as an aggregate mainly retained on sieve 5.0mm and no more containing finer materials. Generally, about 60% to 75% of the concrete volume (70% to 85% by mass) is fine and coarse aggregates hence attribute significantly in the development of concrete's properties (Steven et al., 1988).

2.2.3.3 Cement chemical nomenclature and notation

Chemical formula in cement chemistry are often expressed as a sum of oxides, such as tricalcium silicate, Ca_3SiO_5, can be written as $3Ca.SiO_2$. This does not imply that the constituent oxides have any separate existence within the structure. It is usual to abbreviate the formulae of the commoner oxides to single letters, such as C for CaO, S for SiO_2 and

Ca_3SiO_5 thus becoming C_3S. This system is often combined with orthodox chemical notation within a chemical equation, e.g.

$$3CaO+SiO_2 \rightarrow C_3S \quad (2\text{-}1)$$

Or even within a single formula, as in $C_{11}A_7.CaF_2$ for $Ca_{12}Al_{14}O_{32}F_2$. The abbreviations must widely use are as follows:

C=CaO, S=SiO_2, A= Al_2O_3, F=Fe_2O_3, M=MgO, K=K_2O, S=SO_3, N=Na_2O, T=TiO_2, P=P_2O_5 and H=H_2O

The chemist notation (CCN) was developed to simplify the formulas cement chemists. It is a shorthand way of writing the chemical formula of oxides of calcium, silicon, and various cement hydration reaction formulas.

2.2.4 Hydration and microstructure of concrete

2.2.4.1 Hydration of Portland cement

The process of hydration in cement starts after mixed with sand, gravel and water produces the synthetic rock. Different chemical and physical, reactions take place during this transformation period. Chemical reactions in the admixture show the phase changes of hydration products; meanwhile, the physical reactions take place and detect the locative re-distribution of the hydration products. The final product of cement hydration is a hard-porous material. According to Tazawa et al. (1995), because of the complicity of the Portland cement, chemical hydration reaction process in concrete is complicated to be explained by one chemical equation. The cement hydration process of concrete can be characterized using following equations.

Tricalciumisilicate (C_3S)

$$2(3CaO.2SiO_2) + 6H_2O \rightarrow 3CaO.2SiO_2.3H_2O + 3Ca(OH)_2 \quad (2\text{-}2)$$

Dicalciumsilicate (C_2S)

$$2(2CaO.SiO_2) + 4H_2O \rightarrow 3CaO.2SiO_2.3H_2O + Ca(OH)_2 \quad (2\text{-}3)$$

Tricalciumaluminate (C_3A)

$$3CaO\cdot Al_2O_3 + 3(CaSO_4\cdot 2H_2O) + 26H_2O \rightarrow 3CaO\cdot Al_2O_3\cdot 3CaSO_4\cdot 32H_2O \quad (2\text{-}4)$$

$3CaO{\cdot}Al_2O_3{\cdot}3CaSO_4{\cdot}32H_2O+2(3CaO{\cdot}Al_2O_3+4H_2O \rightarrow 3(3CaO{\cdot}Al_2O_3{\cdot}CaSO_4{\cdot}12H_2O)$ (2-5)

$3CaO.Al_2O_3 + 12H_2O + Ca(OH)_2 \rightarrow 3CaO.Al_2O_3.Ca(OH)_2.12H_2O$ (2-6)

Calcium aluminoferrite (C_4AF)

$4CaO{\cdot}Al_2O_3{\cdot}Fe_2O_3 + 3(CaSO_4.2H_2O) + 27H_2O \rightarrow C_3(A.F)3CaSO_4.32H_2O + Ca(OH)_2$

(2-7)

$2CaO{\cdot}Al_2O_3{\cdot}Fe_2O_3+C_3(Al_2O_3{\cdot}Fe_2O_3)_3CaSO_4.32H_2O+6H_2O \rightarrow 3C_3(Al_2O_3{\cdot}Fe_2O_3)CaSO_4.12H_2O + 2Ca(OH)_2$ (2-8)

$4CaO{\cdot}Al_2O_3{\cdot}Fe_2O_3+10H_2O+2Ca(OH)_2 \rightarrow 3CaO.Al_2O_3.6H_2O\text{-}3CaO.Fe_2O_3.6H_2O$ (Solid solution) (2-9)

The chemical reactions show that initially by equation (3) the reaction of C_3A will form ettringite, and then transforming into mono sulfoaluminate as showed in equation (4). The interaction is followed by reaction of C_3A remaining from the shortage of gypsum as it has appeared in the equation (5). According to the curve, in Figure 2.2 introduced by Taylor (1997) that shows the paste hydration of Portland cement passed through several stages differentiated with an appearance of numbered peaks.

i. Pre-induction period: This is the first stage when water contact with cement grains immediately starts to react. In this initial stage, C_3A is the most active phase.
ii. Dormant stage: the second stage where the rapid initial reactions in the first minute followed by a period of low activity.
iii. Acceleration stage: the third stage where the reaction occurs actively and accelerates with time, reaching a maximum rate at the end of stage III.
iv. Post-acceleration stage: the fourth stage where in this period the rate of heat release slows down gradually. The C-S-H phase continues being formed, and the relative contribution of C_2S to this process increases with time.

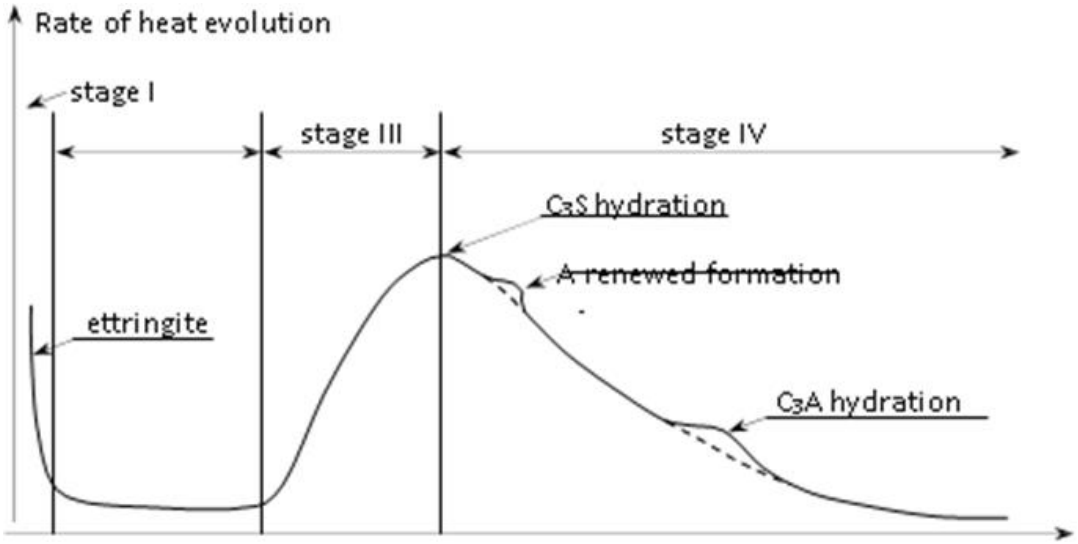

Figure 2.2: Heat rate growths during the hydration of Portland cement by Taylor (1997).

2.2.4.2 Microstructure of Portland cement

The three main hydration products, calcium silicate hydrates (C-S-H), calcium hydroxide (CH) and calcium trisulfoaluminate hydrate, called ettringite, together with other minor products formed during the hydration process can be explained by Figure 2.3.

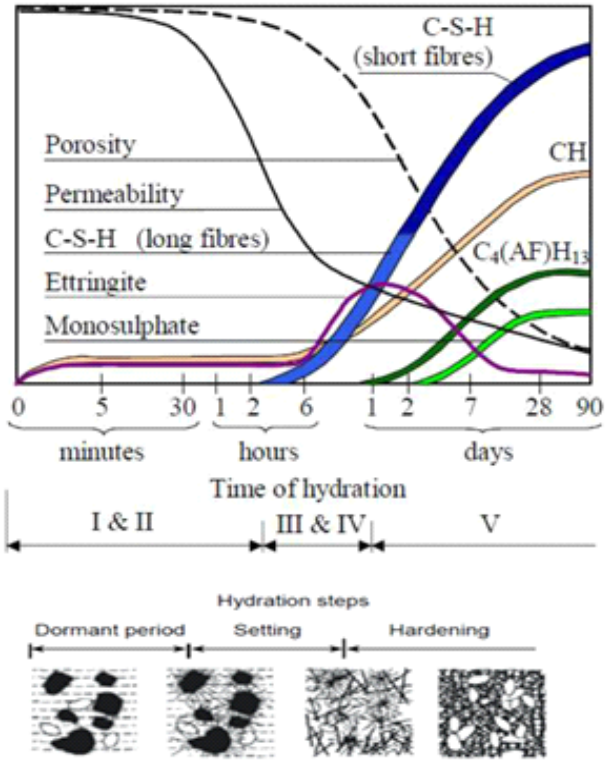

Figure 2.3: Formation of hydration Portland cement paste in relation of time and amount at an ambient temperature (Locher et al., 1976).

2.2.5 OPC Concrete industry and environmental damage

The concern of Portland cement production impact on the environment has led to a comprehensive search for substitutional clinker replacement materials (Grist et al., 2016). Moreover, the development of concrete sustainability and reduce emissions of CO_2 from cement production was the main concern for researchers in the field of construction materials to reduce the environmental damage, because of the raw materials are the manufacturing construction materials and accompanied by energy consumption producing at the same time some wastes. Concrete is composed mainly of aggregates (gravel and sand), hydraulic cement and water. Concrete consists of about 12 percent of cement, 8 percent of mixing water and the remained 80 percent in aggregate by mass (Celik et al., 2014).

Based on the British geological survey and the Statistics Portal report in 2017 about 4,180 million tons of cement produced. About 22 billion tons of concrete produced with consumption of 18 billion tons of aggregate and 2 billion cubic meters of water assuming that the mixing ratio of concrete was 1:1.5:3 and the water-cement ratio (w/c) was 0.50. Today the primary target in construction materials related to the sustainability of concrete and reduction of environmentally harmful by reduction of CO_2 emission from cement industry and decreasing of cement used by implementing waste materials or by-product materials such as fly ash and rice husk ash. The objective of use pozzolanic materials not only to reduce the use of raw materials (limestone, shale, clay) and the energy to produce cement but also to use the waste materials in concrete, which is reduce the environmental issue of waste dumping (Naik, 2008).

2.2.6 Supplementary cementitious materials

Supplementary cementitious materials or waste materials in the literature are finely divided materials, which contribute to the properties of the hardened concrete through hydraulic or pozzolanic activity, or both (CAN/CSA A3001, 2003). They are significantly beneficial for concrete properties and durability due to their sufficient physical and chemical effects on material packing and microstructure (Hassan et al. 2000; Mehta 1994). These SCMs are used to replace a part of cement, an expensive material in ready mixed concrete in mortar and concrete. Where these SCM's is agricultural or industrial by-products that are available, require little or no pyro-processing, and have inherent or latent cementitious properties. Since cement production became the worldwide concern about the deterioration of the environment, therefore SCM materials become “greener” not only through the process of replacing Portland cement but also improve the durability and the lifespan of

structures (Papatzani et al., 2014). Besides, SCM can be found as natural by-product materials, such as Limestone powder, volcanic tuff, pumicite, calcined clay, opaline cherts, and shale. Moreover, SCM can be obtained from agricultural wastes such as sugarcane bagasse and rice husk ash. Among the technically acceptable and economically available supplementary cementitious materials produced every year, RHA offers the potential for reducing a considerable amount of cement due to availability and free of cost as a by-product material.

2.3 Rice husk ash

2.3.1 Preamble

Rice husk is the outer covering part of the rice grain, a by-product resulting from rice production. World rice consumption in 2017 was nearly about 758.8 million tons (www.fao.org, 2017). The production of waste accompanies this enormous number in large quantity, and the problem of disposal has become another problem facing the environment. That most of the rice production comes from China and the Third World countries (India, Pakistan, Thailand and Vietnam, and other) where the waste is disposed by burning in open fields creating environmental problems because of the carbon dioxide (CO_2) emission and the high amount of silica content. Rice husk used in the production of fuel in brick kilns and in a low-pressure steam generation to produce electrical energy in some countries, such as India and Brazil. The amount of rice production increased from the year 1999 to 2013 by about 22% as shown in Table 2.1 (FAO, 2017).

Table 2.1: World rate of rice paddy production (FAO organization, 2017).

Country	Year (Quantity in million ton)			
	1999	2007	2013	2017
China	200.5	192.5	205.7	207.7
India	131.2	142.5	150.0	163.7
Indonesia	49.50	60.60	69.00	72.3
Vietnam	31.40	37.90	43.70	19.1
Bangladesh	29.90	46.10	50.70	52.1
Thailand	23.30	31.90	37.80	33.7
Rest of the world	130.7	164.4	173.3	210.2
Total	596.5	675.9	730.2	758.8

The percentage of husk in rice depends on many factors, such as location, season, cultivation method, the variation in the amount of bran and broken rice, etc. Houston (1972) reported that the rice husk estimated from 16.3 to 26% percentages by weight of the rice grain. In

general, 20% to 23% considered the acceptable of rice husk as an average value. Incineration of rice husk yields as a result rice husk ash (RHA) which is approximately 20% of rice husk weight (Govindarao, 1980). The high amount of silica (SiO_2) content makes rice husk ash (RHA) very active pozzolanic material. The silica (SiO_2) content of the rice husk ash (RHA) may reach about 95% percent according to Singh et al. (2008), while it can be as high as 90–98% of total ash weight according to Patil et al. (2014). Rice husk incineration generally produces an amorphous form of silica at burning temperature ranged in between 350°C to 750°C, while crystalline silica formed at a temperature over 800°C (Boating and Skeet, 1990). Utilization of RHA, as a pozzolanic material in concrete brought the attention of researchers as alternative materials for cement, because of the high amount of silica content, availability, siliceous nature and the low cost.

2.3.2 Nature of Rice Husk

Rice husk is composed of two parts: organic and inorganic mineral materials. The natural materials consisting of cellulose, lignin, pentosanes and a small amount of protein and vitamins. The inorganic mineral major component in rice husk is silica. However, rice husk is distinguished by composition, because of different factors, such as rice variety, broken rice during the milling process, geographical location, the method of analysis and relative humidity (Govindarao, 1980 cited in Olawale et al., 2012). Naturally, the silicon is taken up from the soil by roots of rice plant as monosilicic acid, by a transition of the soluble silica to the outer surface of the plant, where cellulose-silica membrane formed (Yoshida et al., 1957 cited in Bui, 2001). The bulk density of rice husk ranges between 85 to125kg/m^3 after milling, where the specific gravity about 0.75kg/m^3. Rice husk burning does not give flame as other fuel, because of the volatile matter consist are very low, and the high range of silica that led to low efficiency, while resulting in high content of unburned carbon (Kapur et al., 1984).

2.3.3 Application of Rice Husk

The composition of rice husk determines the suitability to use for different application depending on the chemical properties. Generally, rice husk can be used as;

i. Power Plant Fuel: As fuel in boilers, with incineration rice husk produces heat energy. Rice husk benefit is in two ways: first, by producing electric power from a local source, and second, by reducing the pollution of rice husk waste. To produce 1MWh of electricity, approximately one ton of rice husk is required. In addition, rice

husk can be used as alternative fuel for household energy and, as fuel, in brick kilns in furnaces (Kumar et al., 2012 cited from Thipwimon et al., 2009).

ii. Source of Silica: As about 20% of rice husk are silica, which is a promising source of silica. The presence of silicon compounds in rice husk is silicon carbide, silicon nitride, silicon tetrachloride, zeolite, silica, and pure silicon. The applications of such materials derived from rice husks are quite comprehensive. (Matori and Haslinawati, 2009 cited in Kumar et al., 2012).

iii. Other uses: Rice husk is a raw material to produce xylitol, furfural, ethanol, acetic acid and lingo sulphuric acids although used as cleaning or polishing agent in metal and machine industry, in the manufacturing of building material (Mehta, 1978). Rice husk also used as an industrial raw material, such as an insulating board material, fillers in plastic, filling material, building materials, for making panel board and activated carbon (Farooquea et al., 2009).

2.3.4 Rice Husk Ash (RHA)

Rice husk as a cellular structure by incineration the cellulose-lignin composition leaves behind porous ash where the main component is silica, with a minor amount of alkali and other elements. The amount of silica, particle size and specific surface area is different and varies up to the source, incineration methods and temperature (Zhang et al., 1996). The high amount of non-silica materials in rice husk ash is Alkali, where the majority is potassium. Generally, ranged in between 0.18% to 3.68% of ash weight [(Mehta, 1992); Dakroury and Gasser (2008)]. While sodium contents are not exceeded of 1.12% (Giaccio et al., 2007). According to the ASTM C-618 the sum of all of the silicon oxide (SiO_2), iron oxide (Fe_2O_3) and aluminum oxide (Al_2O_3) should not be less than 70% of total weight of the pozzolanic material. The main impurities in RHA are residual carbon and alkali oxides. Chemical properties of RHA vary according to the source, because of that it is difficult to obtain RHA with the same or nearly same composition. This variation in composition presented in Table 2.2. RHA particles are un-regular, ranging in diameter from less than 1 micron to 150 microns, the majority being less than 45 microns. Generally, the RHA from open heap incineration is coarser than from controlled combustion. Moreover, RHA from the combustion of open heap contains more residual carbon content and less reactive of ash.

Table 2.2: Chemical composition of RHA from various countries.

RHA origin source	RHA components (% wt. of RHA)									Reference
	SiO_2	Al_2O_3	Fe_2O_3	CaO	MgO	K_2O	Na_2O	SO_3	LOI	
Malaysia	93.1	0.21	0.21	0.41	1.59	2.31	-	-	2.36	
Brazil	92.9	0.10	0.43	1.03	0.35	0.72	0.02	0.01	-	Bui (2001)
Vietnam	86.9	0.84	0.73	1.40	0.57	2.46	0.11	-	5.14	
Iraq	86.8	0.40	0.19	1.40	0.37	3.84	1.15	1.54	3.30	
USA	95.5	-	-	0.25	0.23	1.10	0.78	1.13	-	
Tanzania	90.8	-	0.24	0.78	0.53	1.13	-	0.25	2.49	Cizer et al. (2007)
Nigeria	68.1	1.06	0.78	1.01	1.31	21.2	-	0.13	18.2	Dabai et al. (2009)
Egypt	94.6	0.30	0.30	0.40	0.3	1.3	0.20	1.00	1.8	Nehdi et al. (2003)
China	91.7	0.36	0.90	0.86	031	1.67	0.12	-	3.13	Xu et al. (2012)

2.3.5 RHA Preparation

There are two parameters of impacts are the rice husk ash production (temperature and grinding process). Numerous researchers have investigated the effect of incineration on the RHA composition especially the content of amorphous silica. Mehta (1978) reported that under controlled temperature and time, can produce ashes with the amorphous form of highly reactive by maintaining the incineration temperature lower than 500°C under the oxidizing condition, or by exposure of the rice husk to 680°C for one minute. Yeoh et al. (1979) indicated that RHA silica could remain in the amorphous form even when burned temperature up to 900°C if the combustion time less than 1hrs. Beyond this range of temperature and duration of time, the silica converted to crystalline. Chakravarty et al. (1988) burned rice husk at 700°C for 1.5h, 3h, 4h and over 30h. The author used X-Ray diffraction (XRD) analysis to confirm that RHA does not convert to crystalline silica even with per longed time of incineration. Della et al. (2002), de Sensale (2006) and Onojah et al. (2013) they reported that at burning temperature below than 700°C, the RHA silica appearances in high reactive amorphous form. Moreover, Shinohara and Kohyama (2004) concluded that the transformation of amorphous form silica to crystalline start at a temperature from 867°C to 1000°C. While Cizer et al. (2006) find out about temperatures between 800°C to 1000°C the silica in RHA turned into crystallization form.

Ibrahim et al. (1980) investigated the influence of incineration condition of boiled rice husk on the silica properties during thermal treatment. The author stated, no sign of crystalline silica was detected up to 900°C. Nevertheless, the crystalline form of silica begun at 1000°C, while Tridymite stage began to appear at 1200 °C. Sooriyakumaran and Ismail

(1979) used differential thermal analysis (DTA) to analyze RHA mineral composition, where they spotted an endothermal peak when rice husk incinerated at 760°C`, because of the transformation of amorphous silica to crystalline form. While, by using same theory of analyzing RHA mineral composition (DTA), Shah et al. (1979) reported that RHA silica converted to crystalline at 600°C. This discrepancy in DTA results let James and Rao (1986) argue that the Differential Thermal Analysis (DTA) technique, as it is not suitable methods to determine the transformation point of silica from the amorphous form to crystalline.

Hwang and Wu (1989) concluded that by incineration of RHA at 400°C, 600°C and 900°C, there was no transition of silica to crystalline. Cook (1984) proved that the crystallizations phase of silica began at a temperature lower than 600°C, while Dass (1987) concluded that the crystallization process starts at 500°C. Kapur (1981) reported that with 15h exposers the crystallization takes place even at 300°C. These differences of temperature in which the thermal process begin crystallization phase in rice husk ash led to variation in the opinions of researchers. Two different theories explained the transformation process of amorphous silica to crystalline. Kapur (1981); Boating and Skeete (1990) admitted that transformation of amorphous silica process begins with converted silica to quartz and later to cristobalite at 1000°C with the prolonged process than tridymite as following.

$$\text{Amorphous} \rightarrow \text{quartz} \rightarrow \text{cristobalite} \rightarrow \text{tridymite} \qquad (2\text{-}10)$$

However, Ibrahim et al., (1980) thought that amorphous silica converted to cristobalite at the first stage and then with increasing heat converted to tridymite. Onojah et al., (2013) have another point of view, with burning RHA at 600°C, amorphous silica structure produces. While, increasing combustion degree over 600°C, silica convert to Quartz at the first stage and with increasing temperature over 800°C turns to tridymite and at 1470°C silica fully transformed into cristobalitete. James and Rao (1986) concluded that the transformation phenomenon of silica from amorphous to crystalline is related to the existence of the minor element in the RHA, such as Na, K, Mg, and Ca lead to decreasing transformation silica temperature. Generally, according to the previous researchers, there is no exact temperature where the amorphous silica converting to crystalline and this subject need more investigate.

2.3.6 RHA reactivity

Rice husk ash defines as a very fine pozzolanic material when completely burning leaving behind a porous ash silica structure (Mehta, 1992 cited in Zhang et al., 1996). Where, a pozzolan is defined "as a siliceous or siliceous and aluminous material which in it itself

possesses little or no cementitious value but which will, in finely divided form and in the presence of moisture, chemically react with calcium hydroxide at ordinary temperature to form compounds possessing cementitious properties (Mehta, 1978). RHA is a very fine material composed mostly of silica in amorphous form (≥70%) and it has a highly micro-porous structure which is suitable to replace cement through it is pozzolanic reaction (Lun, 2015). Reactivity of RHA defines as a degree of reactive silica content, which is basically depend on the form of silica (amorphous) and the degree of fineness of RHA particles (Zhang et al., 1996). Bui (2001) reported that the RHA actual specific surface area ranges from 20 to 270 m^2/g. In addition to the burning process effect on the specific surface area and particle size distribution, also the appropriate duration of grinding time is essential.

Habeeb and Fayyadh (2009) concluded that the enhancement of RHA pozzolanic reactivity linked to the high surface area. Where the extension of grinding time the specific surface area will be increased; as a result, pozzolana activity increased. Mehta (1979), find out that RHA particles with a high degree of fineness will reduce the pozzolana activity. On the other hand, each of James et al. (1986); Kraiwood et al. (2001) and Paya et al. (1995) stated that with increasing fineness of particle size the reactivity of RHA would be increased. Generally, the relationship between the reactivity of RHA to the fineness of particle has a disagreement between researchers. While, each of Zain et al. (2011); Shukla et al. (2011), Raman et al. (2011), and Khan et al. (2015), stated that RHA reactivity of ash it dependent on the amount of amorphous silica, fineness of particles and specific surface area. However, Mehta (1994) confirmed that the reactivity of amorphous silica is directly proportional to the specific surface area of ash.

2.3.7 Physical characteristics of RHA

RHA is a very fine material with a mean particle size ranging from 5 to 10μm (Siddique, 2008). The physical characteristics of RHA like fineness, particle shape and size, and colour mainly depend on the combustion temperature of the rice husk. Generally, the physical properties of RHA have a greater influence on the performance of fresh concrete such as workability, bleeding, segregation etc. Fineness of the RHA has an influence on pozzolanic activity and workability of concrete. It also affects the water content and admixture demand in concrete. Most of RHA particle size is in range in between 4 to 75μm (Mehta, 2002). In addition to the particle size distribution, RHA consist of a very high specific surface area (SSA) which is significantly governed by the porous structure of RHA particles. Zhang and Malhotra (1996) related the high of the specific surface area of RHA to the porous of honeycomb microstructure of RHA particles. Physical properties depend on burning

conditions. Notably, the period and temperature of burning affect the microstructure and characteristics of RHA (Nagataki 1994). Therefore, with the comparison of physical properties published by the previous researcher, there is remarkable variation, as is shown in Table 2.3.

Table 2. 3: The physical properties of RHA, as reported by several authors.

Author		Surface area (m^2/g)	Determination theory	Mean particle size (μm)
Yu et al. (1999)		55.10	*BET fineness	15.4
Isaia et al. (2003)		20.20	BET fineness	11
Tashima et al. (2004)		1.619	**Blaine fineness	12.34
Gastaldini et al. (2007)		40.00	BET fineness	-
Ganesan et al. (2008)		36.47	BET fineness	3.80
Chindaprasirt et al. (2008)		1.120	Blaine fineness	10
Rukzon et al. (2008)	RHA1	0.320	Blaine fineness	28
	RHA2	0.780	Blaine fineness	17
	RHA3	1.250	Blaine fineness	10
Kartini et al. (2010)		20.50	BET fineness)	25.83
Swaminathen and Ravi (2016)		27.40	BET fineness	7
Antiohos et al. (2013)	RHA-8	0.382	Blaine fineness	
	RHA-12	0.393	Blaine fineness	

*BET fineness: Brunauer -Emmett –Teller theory (Nitrogen gas absorption).
**Blaine fineness: Air Permeability Method.

The importance of the RHA particle size comes from the direct impact on the properties of concrete. The RHA particle size influence on the pore structure by refinement and chain the development of un-favorable crystals produced in the hydration process (Givi et al., 2010). Where, hardening of mortar or concrete linked to the higher fineness of RHA when applied in the cementitious system, because of filling or densification of microstructure [Khan et al., (2014); Shukla et al. (2011) and El-Dakroury and Gasser, (2008)]. However, there is an optimum grinding time/fineness of RHA to achieve a maximum compressive strength were beyond that decreased (Nugan et al., 2013). According to the author, with increasing grinding particles, the particle size of RHA decreases (Fig. 2.4), involving the collapse of the porous structure of RHA particles and in result leading to agglomeration. Which is confirmed by Mehta (1992) point of view were great fineness of RHA particles should be avoided since the pozzolanicity of RHA derives from the internal surface area.

While, Givi et al. (2010) reported that by using ultra-fine RHA (average particle size about 5μm), concrete reaches greater strength than RHA with an average particle size of 95 μm. Despite the fact that a lot of researchers have carried out on the effect of RHA finesses on the concrete properties, the information is scarce in the literature (Bui et al., 2005; Habeeb and Fayyadh. 2009). Therefore, it is necessary to find out the appropriate fineness of RHA,

to enhance the RHA performance. Finally, the particle shape and size mainly depend upon the mineralogical phase and grinding time. The color of RHA may range from light grey or grey to almost black depending on the rice husk combustion process. The moisture content in RHA is basically a problem related to only handling, storage (large hoppers) and distribution.

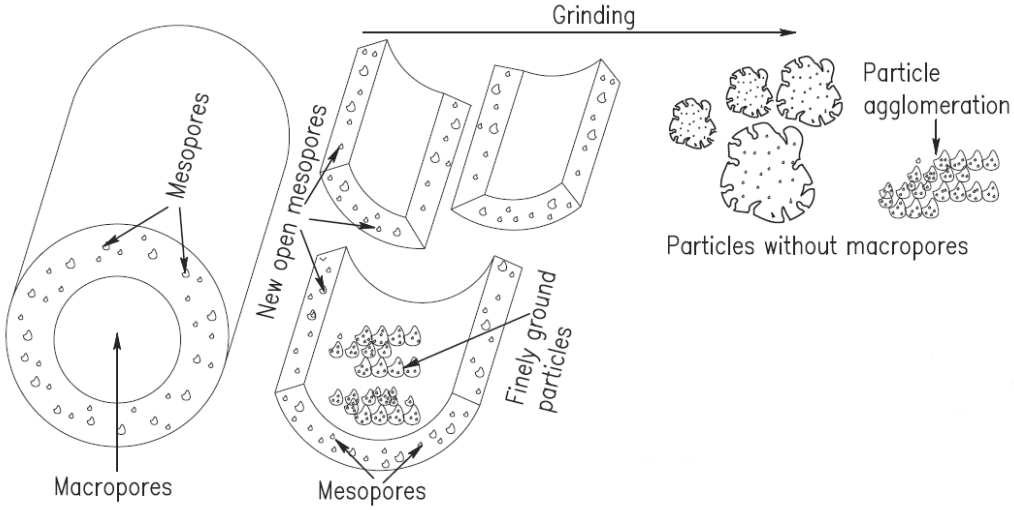

Figure 2.4: Different stages of RHA particles and it is effect on the pore volume during grinding process.

2.3.7.1 Specific surface area determination method

Based on the literature in Table 2.3, two different methods were used to determine the specific surface area (SSA) of RHA (BET and Blaine). Each method has a different principle to present the result. The Brunauer-Emmett-Teller method (BET) analysis provides precise specific surface area evaluation of materials by nitrogen multilayer adsorption measured as a function of relative pressure using a fully automated analyser (Gelb and Gubbins, 1998). The technique encompasses external area and pore area evaluations to determine the total specific surface area in m^2/g yielding important information in studying the effects of surface porosity and particle size in many applications. While the principle of Blaine theory operation is that the permeability of a bed of fine particles is proportional to the fineness of the particles (Harrigan, 2013). Therefore, the test is a measurement of the flow rate of air through a bed of cement particles with vacuum on one side and atmospheric pressure on the other. The relationship between the air permeability of a powder and its surface area comes directly from the Kozeny–Carman approximate theory (equation 2-11), which assumes a packing of mono-sized spherical particles.

$$S = \frac{Ss\sqrt{T}}{\sqrt{Ts}} \quad (2\text{-}11)$$

Where
S_s is the surface area of the reference material.
Ts is the time of flow using the reference material.
T is the time of flow of the material under test.
S is the surface area of the material under test.

2.3.8 RHA chemical composition

RHA is a fine particulate material with the main chemical constituents being SiO_2. These chemicals are responsible for it is pozzolanic activity. It also consists of Al_2O_3, Fe_2O_3, CaO, MgO, TiO, P_2O_5, SO_3, Na_2O and un-burnt carbon. There is a possibility for variation of composition from plant to plant and even in one plant from time to time. The general variation in two principal constituents will be as follows: SiO_2 +$A1_2O_3$+ $Fe_2O_3 \geq 70\%$, residual carbon content (loss on ignition) ≤12%. The structure of RHA is mostly non-crystalline silica (amorphous). With incineration rice husk in the moderately oxidizing environment under the controlled temperature between 500°C to 800°C for appropriate time length generally ranging from 15 minutes to 1h produce RHA, which consists mainly of silica (SiO_2) with a high amount of amorphous form (Nagataki, 1994). Generally, based on variation in chemical composition, RHA cannot be classified as fly ash; however, consider as a very pozzolanic materials. These variations are presented in Table 2.4.

Della et al. (2002) prepared different types of RHA at four different temperatures (400°C, 500°C, 600°C and 700°C) at three different periods of time (1, 3 and 6 hrs.) for each sample. The chemical analysis has shown that RHA sample incinerated at 700°C for 6h consist of the highest percentage of silica. Generally, the main content of RHA is silica (more than 70% wt. of SiO_2). However, there are varying proportions of elements which cannot be ignored such as aluminate (Al_2O_3) and potassium oxide (K_2O). Furthermore, the residual carbon content (LOI) percentage, considered as very important as it has come to the second stage regarding total weigh of ash.

Table 2.4: Major oxide contents of RHA used by various researchers.

Oxide Composition (% wt. of RHA)									Authors
Al_2O_3	Fe_2O_3	CaO	MgO	Na_2O	K_2O	P_2O_5	C	LOI*	
4.27	0.38	0.16	1.65	0.14	1.23	1.44	-	8.60	Ikpong and Okpala (1992)
0.47	0.19	1.43	-	1.22	4.10	-	-	3.49	AlKhalaf and Yousif (1984)
0.15	0.16	0.55	0.35	1.12	3.68	0.50	5.91	8.55	Zhang et al. (1995)
0.25	0.41	0.38	0.21	0.05	2.78	0.36	0.41	2.93	Yu et al. (1999)
0.30	0.10	0.50	0.30	0.10	1.60	-	-	9.10	Isaia et al. (2003)
0.41	0.22	0.76	-	0.03	1.44	-	-	4.49	Gastaldini et al. (2007)
6.19	3.65	2.88	1.45	-	1.82	1.10	-	5.43	Memon et al. (2011)

LOI*: Loss on ignition.

2.3.8.1 Effect of SiO_3, AL_2O_3 and Fe_2O_3

The characteristics of RHA chemically it depends on their $SiO_2 + Al_2O_3$ and Fe_2O_3 contents. ASTM C 350-1954, specified a minimum limit of SiO_2 content as 40% in fly ash. In 1960, the sum of SiO_3, Al_2O_3 and Fe_2O_3 by weight was made to be a minimum of 70%. The intention to specify this limit is to ensure that sufficient silica is available to produce more C-S-H gel, as a result of reaction with CH of cement hydration. As RHA not classified; therefore, treat as same as fly ash.

2.3.8.2 Effect of Alkalis (K_2O+ Na_2O_3)

The presence of alkalis ($K_2O + Na_2O_3$) causes the efflorescence and alkali-silica reaction, leading to serious expansion and cracking in concrete, resulting in major structural problems and sometimes necessitating demolition (Farny and Kerkhoff, 1997). K_2O consider as the second highest of the elemental oxides in concentration in RHA, ranged in between 0.72–3.84% (Muthadhi et al., 2007). However, this variable in concentration may increase or decrease depending on the nature of the soil and the geographical area of the crop. While Na2O3 availability is too small and not exceed 1.5% of total ash weight as presented in Table 2.4.

2.3.9 Microstructure of RHA

Scanning electron micrographs of RHA microstructure according to different researchers are shown in Figs. 2.5 (a, b), and 2.6. Figure 2.5 (a), clearly indicates the hull like shape of the ash particle. However, these particles are quite fragile, and some particles tend to break down during handling, thereby losing the hull like shape. A higher magnification micrograph of the ash particle (Fig. 2.5, b) shows the internal skeleton structure of silica. While, the necklace-shaped cross-section of the rice husk ash particles can be observed in Fig. 2.6, (a).

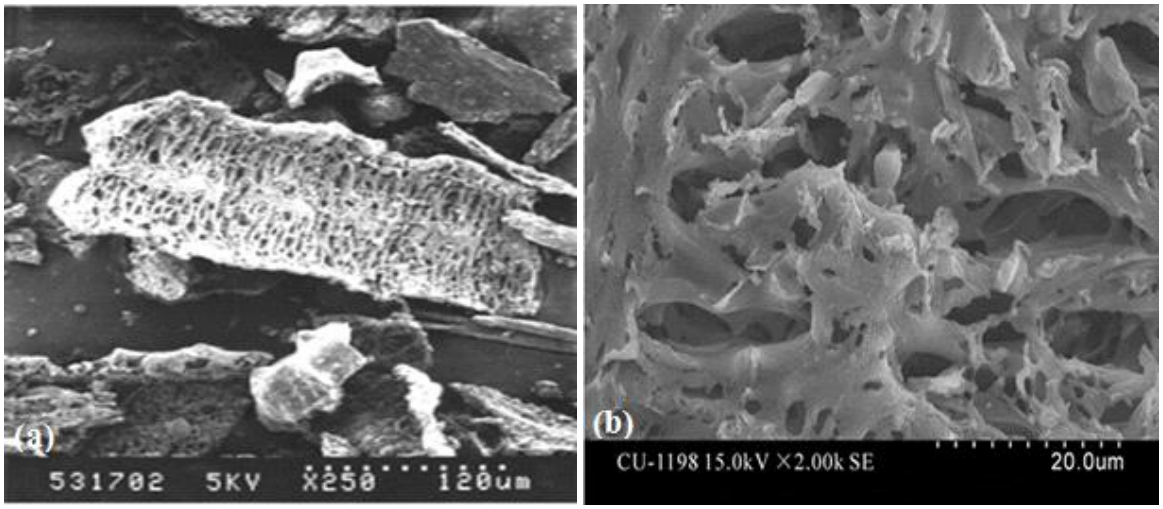

Figure 2.5: Scanning electron micrographs of RHA microstructure; a), internal structure through view of cross section of rice husk ash (Li et al., 2009); b) porous surface structure of RHA particle (Sarkar and Bandyopadhyay, 2010).

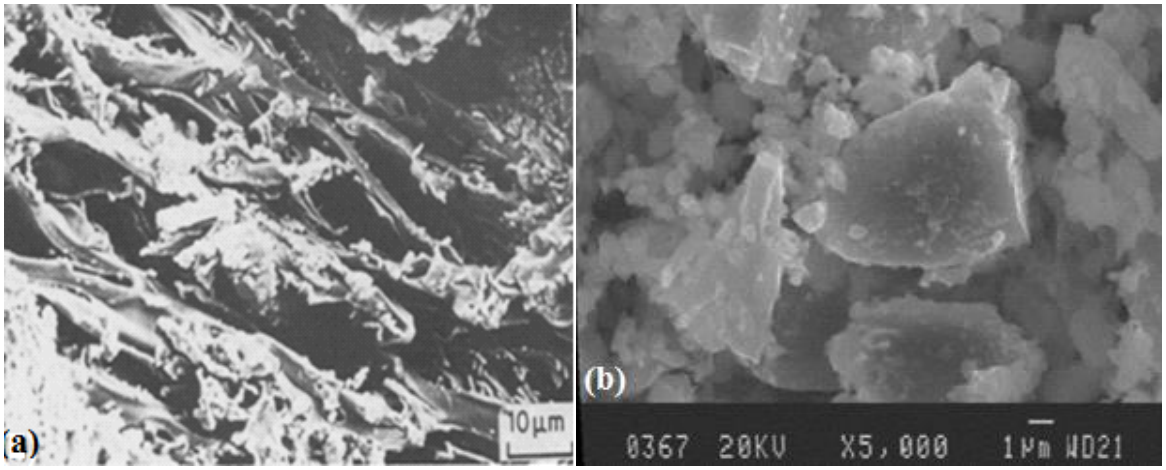

Figure 2.6:Micrograph of RHA particles under SEM image of RHA particle size; a) The necklace-shaped cross-section of the internal skeleton structure of silica (Das et al., 1986); b) the micro structure of particles size distribution of RHA (Zhang and Malhotra, 1996).

The most effective factor effect on the microstructure of RHA is the grinding time (Chindaprasirt, 2008). A comparison between RHA particle before and after ground (Fig. 2.7) shown that the extent of the effect of grinding on the particles of as-received RHA. Therefore, finer RHA particles lead to large pore segmentation, and the number of nucleation sites is increased to precipitate the hydration products of cement paste (Mehta, 1987). In result, this accelerates the reaction and forms smaller crystals of calcium hydroxide.

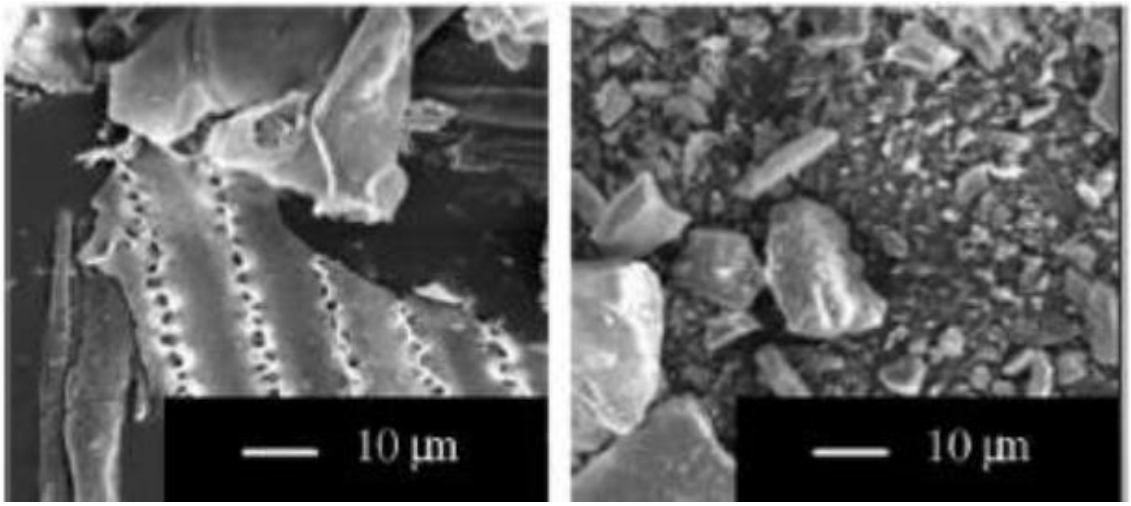

Figure 2.7: SEM image of RHA, before and after grinded according to Chindaprasirt (2008).

2.3.10 Effect of unburnt carbon content on the RHA performance

Rice husk ash (RHA) can be obtained by burning of rice husk under controlled temperature or in open fields. The amount of residual carbon (loss on ignition) in the ash depends directly on the burning process. Bui (2001) found that the uncompleted combustion of RHA leaves a high amount of unburnt carbon with an extensive surface area, causing increased demand for water, which effects on the workability of concrete. Zain et al. (2011) recommended that carbon content in RHA should be a small percentage. Cordeiro et al. (2009) supposed that RHA with a high rate of residual carbon (loss on ignition) considered as low-quality pozzolanic material. Moreover, the presence of large amounts of residual carbon in ash influencing negatively on the strength of mortar or concrete. Cordeiro et al. (2009) stated that the homogeneity and pozzolanic activity of RHA could be increased with residual carbon content about to12% when grinding procedures adopted.

Venkatanarayanan et al. (2013) compared between two types of RHA (Low residual carbon, and high residual carbon content). The author concluded that RHA particles with low and high carbon content have a porous and cellular microstructure with approximately similar particle size distribution. Moreover, the SEM analysis of the microstructure of single high and low carbon RHA particles of both RHA (Fig.2.8) appears to be comparable. Nair et al. (2008) and Karim et al. (2012) reported that the pozzolanic activity of RHA influenced by many factors such as silica content, silica crystallization phase, particles size distribution, the specific surface area of the ash and percentage of residual carbon content. Where the existence of un-burnt carbon can adversely affect the activity of rice husk ash. Wansom et al. (2010) stated that the main factor for good pozzolanic activity of RHA is low unburnt carbon content.

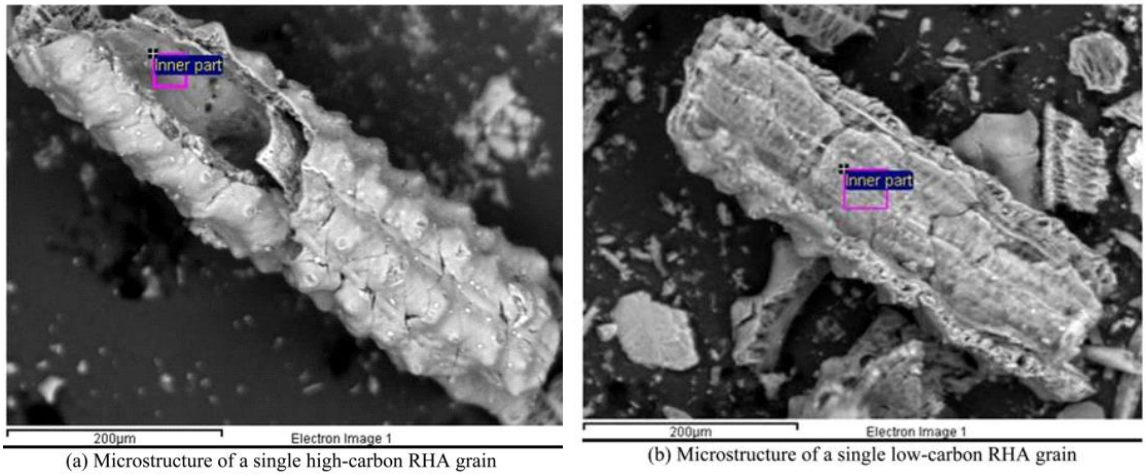

(a) Microstructure of a single high-carbon RHA grain (b) Microstructure of a single low-carbon RHA grain

Figure 2.8: SEM analysis of single high- and low-carbon RHA particle.

2.4 Hydration of cement blended RHA

Adding RHA to the mortar or concrete mix, the pozzolanic reaction will start when $Ca(OH)_2$ is released from cement hydration. In silica-lime reaction, OH^- and Ca^{2+} react with the SiO_2 or Al_2O_3-SiO_2 structure to form calcium silicate hydrate (C-S-H), calcium aluminate hydrate (C-A-H), and calcium aluminate ferrite hydrate (C-A-F-H) as following (Givi et al., 2010; Ngun et al., 2010);

Calcium silicate hydrate:

$$2SiO_2 + 3Ca(OH)_2 \rightarrow 3CaO.2SiO_2.3H_2O \quad (2\text{-}12)$$

Calcium aluminate hydrate:

$$Al_2O_3 + Ca(OH)_2 + H_2O \rightarrow CaO.Al_2O_3.Ca(OH)_2.H_2O \quad (2\text{-}13)$$

Calcium aluminate ferrite hydrate:

$$Fe_2O_3 + Ca\ (OH)_2 + A1_2O_3 + H_2O \rightarrow Ca(OH)_2.A1_2O_3.Fe_2O_3.H_2O \quad (2\text{-}14)$$

With time progress the crystallized compound of C-S-H and C-A-H, (cement gel) as a result of silica and alumina reaction in RHA with $Ca(OH)_2$ of cement hydration. The reaction leads to hardened and forms a continuous binding matrix with a large surface area that is attributed in development of concrete strength in the cement paste (Kassim et al., 2004 cited in Givi et al., 2010). Hwang et al. (2011) explained the interaction process of the hydration process reaction in cement paste with RHA by dividing the process of interaction to four consecutive stages of time as shown in Fig. 2.9. According to the author, after 40 hours, the pozzolan reaction additionally binds Si to RHA with CH to form a C-S-H gel. Where water previously

adsorbed and available in RHA particles amplifies the pozzolanic reaction in the inner cell spaces.

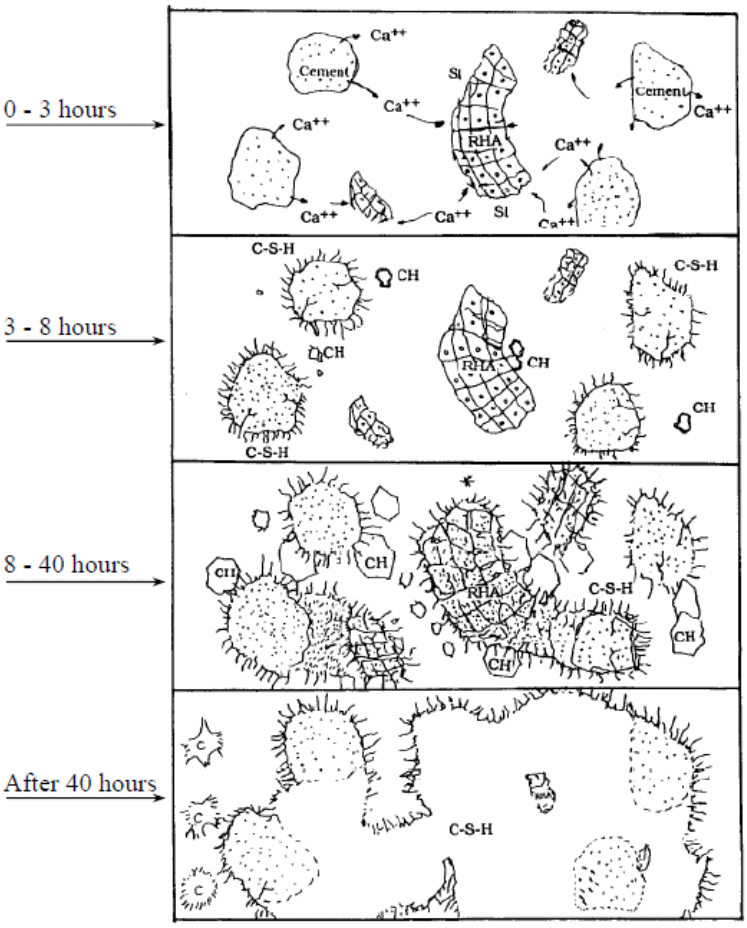

Figure 2.9: Hydration development of cement paste with RHA [(Hwang et al., (2011) cited from Hwang and Chandra, (1997)].

2.4.1 Microstructure of cement blended RHA

Hwang and Wu (1989) observed by using of scanning electron microscope (SEM) that the CH crystal in the cement paste containing RHA appears between anhydrous cores, where the C-S-H gel appears after 5 hours. The size of this crystal in matrix increased up to 4, 8 and 26 times after 6.5, 7.5 and 12.5 hours respectively. This phenomenon does not occur without the availability of RHA. Sivakumar and Ravibaskar (2009) reported that after one hour of mixing RHA cement that the surface of RHA particles covered by hydration products. After 24 hours, most of the CH compounds had reacted with RHA producing some hexagonal plates (about 0.1μm) grow on the surface of RHA particles similar to that of mono sulfoaluminate (AFm), the ettringite (AFt) needles disappear, and the CH crystals decreased due to the silica reaction. After 72 hours, the dense fibers bond with the matrix

within the larger pore, and in one week, these pores filled with the RHA. Further magnifying the cement hydrate area as depicted in Fig.2.10 (b), two distinct phases can be seen: The C-S-H gel and the needle-like crystals. According to Xu et al. (2016), the flake-shaped of calcium hydroxide crystalline period does not appear on the glassy phase surface of RHA concrete (Fig 2.10, b), indicating that to the reactive silica in RHA can enhance and accelerate secondary hydration reaction of $Ca(OH)_2$ in cement matrix.

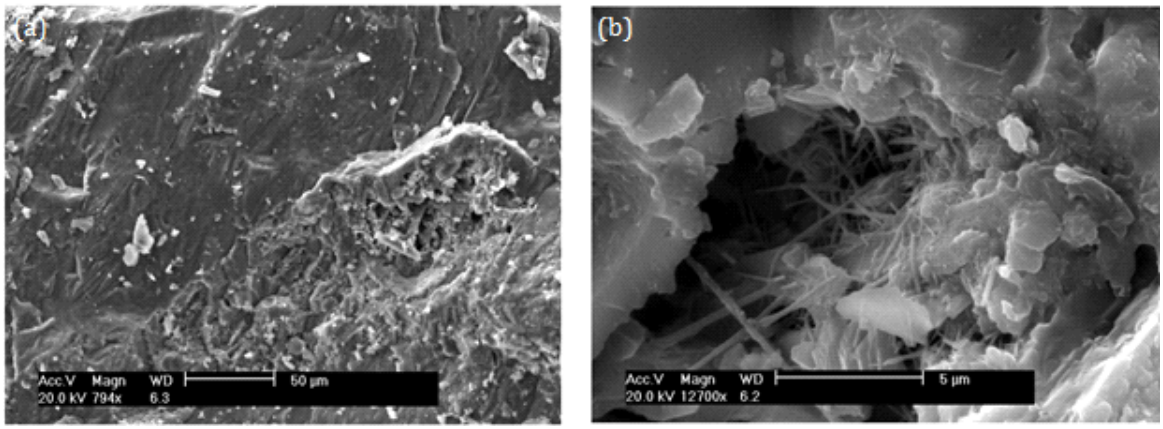

Figure 2.10: SEM of RHA concrete (28days): (a) with magnification of 794x; (b) with magnification of 12700x (Xu et al., 2016).

Nugan et al. (2013) stated that the pozzolanic reactivity of RHA lies on mesoporous structure, where the mesoporous structure of RHA particles absorbs the water and as a result it renders possible that calcium ions diffuse into internal parts of RHA particles. This facilitates the hydration products of the pozzolanic reaction to intergrowth intensely with the cement matrix (Fig.2.11).

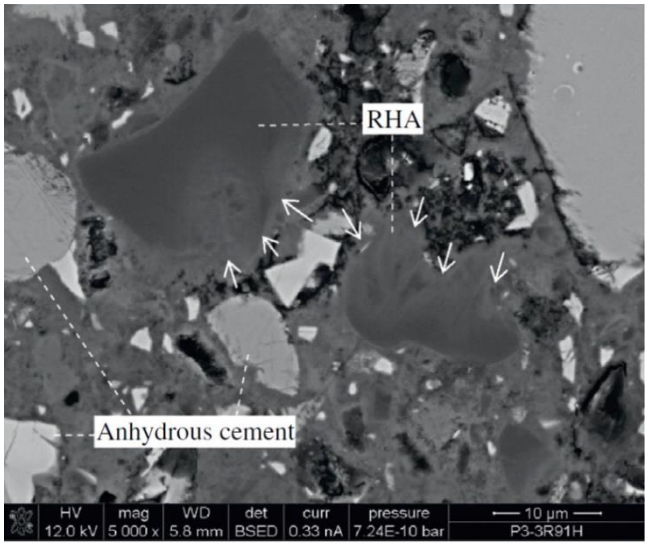

Figure 2.11: SEM image of RHA particle in cement paste at after 91days hydration (Nugan et al., 2013).

2.5 The effect of RHA on the properties of mortar

2.5.1 Flowability of RHA mortar

Flowability is a property of freshly mixed mortar which determines the ease and homogeneity with which it can be mixed, placed, consolidated and finished (Christopher et al., 2017). Generally, flowability of mortar blended RHA has been investigated by a few researchers. The results of investigators Chanu and Devi (2013), Apriantis (2015), and Rashid (2016) on the effect of RHA on the flowability of mortar converge at the conclusion that mortar progressively becomes unworkable as the percent of replacement ratio of cement with RHA increases unless water-reducing admixtures are used. Even more so the dosage of admixtures (superplasticizer) needs to be increases with the increase in replacement level of RHA (Chanu and Devi, 2013). This happening because of the quantum of RHA with higher fineness and porosity could attribute to increased surface area of matrix to absorb more water. According to each of Le et al. (2012) and Van et al. (2013), RHA is a porous material with macro and meso-pores inside and on surface of the particles resulting in a very large specific surface area. Therefore, more water is required to make the mortar more workable with increase in RHA content. However, small addition (2–3% by weight of cement) of RHA may be helpful for improving the stability and workability of mortar or concrete by reducing the tendency towards bleeding and segregation (Mehta, 1983, 1992). In conclusion, to attain the required flowability, mixes containing RHA will required higher water content than the conventional mortar, and this demand increases with increase of RHA replacement ratio in the mix (Le et al., 2014).

2.5.2 Compressive strength

RHA as a potential substitute for cement in mortar has less attention than that of concrete by researchers. Akasaki et al. (2005) made comparative studies between the RHA amorphous and crystalline. For the comparative two ashes were used in the study: the crystalline ash (A0) and the amorphous ash (A1). These two ashes were submitted to a milling process with five different milling times (20, 30, 40, 50, and 60 minutes). Two replacement ratios of cement by RHA (5% and 10%) were tested in order to analyze the effect of the RHA fineness on the development of compressive strength. The test results indicated that the improvements in the RHA mortars compressive strength reached the optimum (67.8MPa at 5%RHA1) with mean particle size of 13μm. However, beyond that compressive strength start to decrease gradually to reach 52.7MPa at 10% RHA1, compare

to 53.9MPa of control mix. Moreover, 5% replacement ratio yielded an increase of 10% in compressive strength of mortars with the crystalline ash (sample 0), and an increase of 26% with amorphous ash (sample 1) with fineness of 13.0μm.

Xu et al. (2012) have studied the microstructure and reactivity of rich husk ash. The author used four different combustion degrees (500°C, 600°C, 700°C, and 800°C) to prepare RHA. To determine the variation in combustion degree on the compressive strength of mortar, 10% RHA was used as replacement ratio. According to the data presented by the author, the compressive strength of RHA blended mortar depends on the calcination temperature. Where, the compressive strength of mortar with RHA prepared at 500°C was almost similar to that of control mix. While, RHA mortar with calcination temperature of 600°C achieved the highest compressive strength in comparison to control mix, the percentage increase at the age of 28 days came out to be 20%. The author attributed that to the high silica content and high specific surface area. Beyond of 600°C, the compressive strength dropped gradually as the calcination degree increased to 700 and 800°C. The author related that to amount of crystalline silica content.

Potty et al. (2014) in his paper "Properties of rice husk ash (RHA) and Microwave Incinerated Rice Husk Ash (MIRHA) mortars" investigated the effects of design water binder ratio on the replacement. The replacements varied from 5 to 30% by weight of ash. The results of compressive strength of RHA mortars showed an increase in the strength at 5% replacement and decrease thereafter. According to the author this is due to the coarser grain size of RHA than the cement which produced porous surface and more voids inside the mixtures. Moreover, the incorporation of RHA in varied w/b did not give significant contribution to the properties of the mortars. Rashid (2016) studied the effect of rice husk ash on strength of cement mortar. Mortar samples were made with a diversity of replacement levels of the cement by RHA (0, 10, 15, 20 and 30%, respectively). The test results of the compressive strength indicated that strength decreased with increase replacement ratio of RHA at the early age (7 days) and even at 28 days age; however, on ward 90 days became higher than control mix. In addition to that, RHA mortar compressive strength reach maximum value at 20% replacement ratio. According to that the author concluded that the optimum replacement level of ordinary Portland cement by RHA might be 15 or 20% by considering other parameters.

2.5.3 Direct tensile strength

Among all supplementary cementitious materials, the effect of RHA on the tensile strength of mortar it doesn't have enough attention by the researchers; therefore, few researches addressed this side of mortar are available. Saraswathy et al. (2014) in his paper "Improved durability performances in cement mortar with rice husk ash" studied enhancing durability of concrete by using RHA with variable replacement ratio (0%, 10%, 15%, 20%, 25% and 30%). According to the data present by the author, tensile strength of mortar decreased with increase replacement ratio to reach 2.31MPa compare to 2.94MPa of control mortar at age of 28 days. However, the results confirmed that the tolerable limit of replacement of RHA is found to be 10%. Beyond 10% RHA there is a reduction in strength observed due to the delayed formation of C-S-H gel.

Ganesan (2014) in his thesis assessed the performance of RHA and bagasse ash blended concretes for durability properties. To evaluation that, direct tensile strength values of blended cement mortars after 28 days of curing was carried out. The author used variable replacement ratio of RHA ranged in between 5% and 35%. The data presented by the author showed a gradual increase in direct tensile strength when OPC was replaced from 5 to 20% of RHA, and then decreased up to 35%. At 30%, the direct tensile strength (3.05 MPa) of RHA admixed mortar was equivalent to OPC mortar (3.13MPa). In conclusion the author stated that these data again confirmed that optimal level of replacement of RHA as 30%. Rasoul et al. (2017) evaluated the effect of rice husk ash properties on the early age and long-term strength of mortar. The author used four different types of RHA (A, B, C and D) with variable replacement ratio ranged in between 5% to 60% of cement weight. The author found that the improvement in tensile strength reached maximum value with 20% replacement ratio, and up 50% replacement ratio (RHA-C and D) without any adverse effect on the strength of mortar. The author attributed that to the high reactivity of the amorphous silica and fine grain size.

2.6 The effect of RHA on the mechanical properties of concrete

Concrete is a heterogeneous mixture of cement, aggregate (fine, coarse) and water with some other materials (additives) for specific properties. The strength and durability of concrete is normally to be governed by such factors as water binder ratio (cementitious content), the efficiency of curing, compactness, admixture and also content of cement in the mix. The increase of concrete strength means good packing of materials, higher density and

therefore good performance. There are many investigations regarding the use of pozzolanic materials to improve the properties of concrete were carried out. To understand the influence of RHA on the concrete performance need to review the previous researchers then compared to the obtained results. This comparison will provide a clear vision of the impact of RHA properties on the concrete performance.

2.6.1 Workability

Workability is defined by ACI as; that property of freshly mixed concrete or mortar that determines the ease with which it can be mixed, placed, consolidated, and finished with a homogenous condition (Zulu, 2017). A growing body of literature has claimed that besides leading to sustainable concrete and improving the durability of hardened concrete, the use of RHA improves the workability of fresh concrete and the strength and durability of hardened concrete (Bapat, 2012; Shetty, 2005). Generally, particle size and surface area of RHA are traditionally considered to be responsible for their higher water demands (Hwang and Chandra, 1997). However, Givi et al. (2010), revealed that the use of RHA, especially with coarser average particle size, reduces the water demand of mixtures. The slump test result observation shown increase in workability from 50% to 100% for proportionate replacement of RHA from 5% to 20%. Therefore, cement particles are effectively dispersed and could trap large amounts of water, resulting in a decrease in water requirements for the system to achieve an acceptable consistency. In addition to that, reduced water demands also associated with the particle packing. According to that, the author concluded that the workability of cement partially replacement by RHA is improved. This improvement increased further with coarser RHA particle (average particle size of 95μm) and increases the replacement ratio. Similar conclusion was reported by each of Bui (2001) and Stroeven et al., (2002).

On the other hand, a study conducted by Hamid et al. (2013) found that for the same percentage of RHA replacement ratio, the increment of RHA grinding time decreases the concrete workability. The author attributed that the absorptive characteristic, which is also pointed out by Kartini et al. (2006). Each of Zhang et al., (1996), Ganesan et al., (2008) and Habeeb and Fayyadh (2009), referred to the fineness of particles results in high water demand to wet the surface area of RHA, therefore decrease the workability. Irregularity shape of RHA particles another factor has a negative impact on the workability of refreshes concrete (Srinivasreddy et al., 2013). Depending on the author, high water demand of RHA particles leads to reduce the workability of concrete in comparison to control mix. A similar

conclusion was issued by Triantafyllou et al. (2017). Therefore, this transparency in RHA physical properties effect on workability of concrete need more investigation.

2.6.2 Compressive Strength

The strength of hardened concrete is of fundamental importance to structural designers. Strength is defined as the ability of a material to resist stress without failure (Neville, 2005). In general, for a given set of cement and aggregates, and under the same mixing, curing and testing conditions, the compressive strength of concrete primarily depends on w/b ratio, mixture composition, and the ratio of cement replacement. The rate of strength development at early ages is related to the rate of hydration of cement (National Ready Mixed Concrete Association, 2006). Strength gain contributed by PC occurs very rapidly at early ages up to about seven days, after which it slows markedly. Therefore, the inclusion of RHA in concrete affects all aspects of concrete properties. As a part of the composite that forms the concrete mass, RHA acts in part as fine aggregate and in part as a cementitious component (Ganesan, 2014). It influences the rheological properties of the fresh concrete, the strength, the finish, the porosity and the durability of the hardened mass, as well as the cost and energy consumed in the manufacture of the final product (Mehta and Monteiro, 2017).

Recently, RHA as supplementary cementitious materials (SCM) has received a research attention in developing of concrete properties. Indeed, RHA is proven to contain a large amount of amorphous silica, which is essential for the SCM reaction in concrete (Saad et al., 2016). Therefore, RHA used by many researchers up to 30% of cement (Fig.2.12, a) to improve compressive strength of concrete [Saraswathy and Song, (2007), Ganesan et al., (2008), and Zareei et al., (2017)]. However, usage of conventional RHA is unfavourable in current concrete industry. One of the reasons that restrain the utilization of conventional RHA nowadays is due to it is properties inconsistency namely chemical and mineralogical properties. This phenomenon occurs due to sensitivity of the material towards burning temperature. Accordingly, some other researchers presented data with reduction in compressive strength (Fig.2.12, b) with concrete blended RHA [Ikopong and Okpala (1992), Kartini et al., (2006), and Ramakrishnan et al., (2014)]. This variation in compressive strength of concrete blended RHA lead up to discrepancy in effect of RHA as supplementary cementitious materials. To understand this contradiction in results, the published literature was divided in two parts, as following.

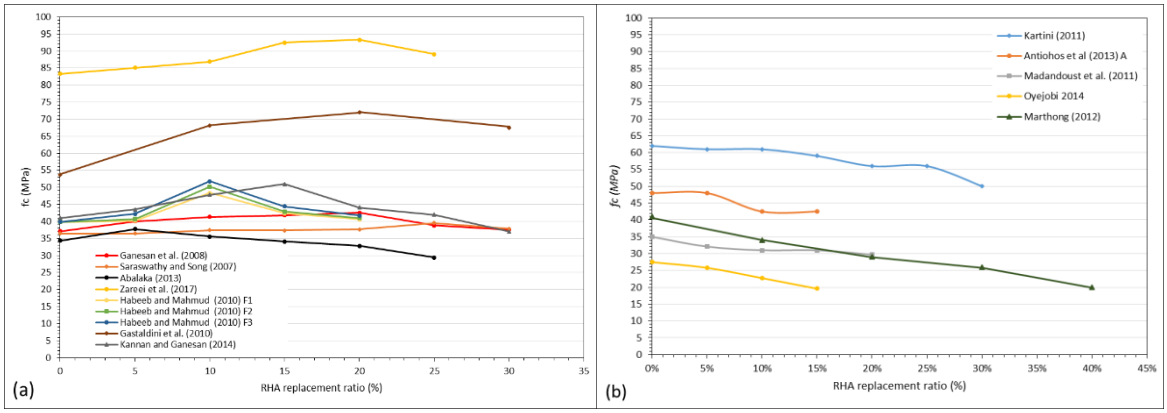

Figure 2. 12: Variation in compressive strength based on the literature at age of 28 days; a) Improved the compressive strength, b) Decrease the compressive strength.

2.6.2.1 Research presented positively effect of RHA on the compressive strength of concrete

Habeeb and Mahmud (2010) have compared the effect of three different average particle size with a variable dosage of superplasticizer on the strength development of concrete with incorporation of 5, 10, 15 and 20%RHA. Specifically, his paper discusses the effect of fineness on strength. The RHA used was rich in silica (88.32%), and the loss on ignition was relatively high (5.81%). The authors based on the experimental results, the following conclusions were drawn:

i. Increasing RHA fineness enhances the strength of blended concrete.
ii. 20% replacement could be valuably replaced by cement without adversely affecting the strength.
iii. Grinding RHA to finer average particle size (APS) has slightly increased it is specific surface area.

Ganesan et al. (2008) made an assessment of optimal level of replacement for strength and permeability properties of concrete. To reach that aim, the author used a variable replacement ratio ranged in between 5 to 35% of cement weight. The RHA used in the experimental research was consist of 87.32% silica, 2.10% loss on ignition and 4.14% $K_2O+Na_2O_3$, with very high specific surface area 36470 m^2/kg and very fine mean particle size (3.80μm). The author concludes that as high as 30% by weight of OPC can be replaced with re-burnt RHA without any adverse effect on strength properties.

Zareei et al. (2017), in their study evaluated the durability and mechanical properties of concrete by investigating RHA as a partial replacement of cement in high strength concrete containing micro silica. The chemical characteristics of the ash used in the experimental research shown that it is consisting of 86.73% silica, 0.54% LOI, and relatively high amount

of Na_2O_3 (9.76%). Five mixtures with proportions of 5, 10, 15, 20 and 25% RHA by weight of cement in addition to 10% micro- silica was used. The result indicated that the compressive strength increased in containment of RHA up to 20%, then decreased by more ratios of replacements.

Abalaka (2013), in his paper "Strength and some durability properties of concrete containing rice husk ash produced in a charcoal incinerator at low specific surface", has compared the different w/b ratio (0.35, 0.40, 0.45, 0.50, 0.55) with very low specific surface are of RHA (235 m^2/kg) on the compressive strength of concrete. To evaluated that different approaches are identified, by increase in water/binder (w/b) ratio of the concrete mixes with increase RHA replacement ratio. The authors conclude that the low specific surface of RHA could replace 15 % of OPC at w/b ratio of 0.50 without reduction in both compressive and tensile strength of concrete. However, low w/b mixes tended to lower optimum RHA replacement level.

Saraswathy and Song (2007) have studied the corrosion performance of rice husk ash blended concrete. The author made a realistic approach using different techniques such as compressive strength, bond strength, split tensile strength etc. RHA used was consist of 92.95% SiO_2, 2.14% K_2O + Na_2O_3, and 1.97% LOI with mix proportion ranged in between 5-30%. They conclude that incorporation of RHA up to 30%, reduces the chloride penetration, decreases permeability, and improves strength and corrosion resistance properties. Gastaldini et al. (2010) have discussed the influence of curing time on the chloride penetration resistance of concrete containing rice husk ash. Concrete with admixtures (fly ash, RHA, and slag) at three different w/b ratio (0.35, 0.50, and 0.65) was investigated. Compressive strength and chloride penetration at 28 days were assessed according to American Society for Testing and Materials (ASTM) C1202, with concentrations of 10%, 20% and 30% RHA. Based on the performance of the compressive strength the author has made the following recommendations:

i. The mixtures with RHA display better performance but depending on the curing time used and level of compressive strength desired.
ii. Higher w/b ratios may be necessary, which would adversely effect on the strength and durability of RHA concrete.
iii. Longer curing times reduced Coulomb charge values for all mixtures in the study, and again the reduction increased as w/b ratios were increased.
iv. 20% RHA consider being the optimum replacement ratio, where strength reaches the maximum value.

2.6.2.2 Research presented negatively effect of RHA on compressive strength of concrete

Utilization of RHA in concrete partially, modify the physical and chemical properties of mortars and concretes, and the compressive strengths can be separated into fractions of strength related to physical and chemical effects of mineral admixtures. When mineral admixtures are added, three effects can be quantified including, dilution, heterogeneous nucleation (physical) and pozzolanic reaction (chemical) depending on the amount and solubility of amorphous silica. Heterogeneous nucleation is a physical process leading to a chemical activation of hydration of cement such that mineral admixture particles act as nucleation centres for the hydrates thus enhancing cement hydration. A smaller amount of powder has an optimum efficiency and results in a significant increase in compressive strength while the use of a considerable amount of powder has a smaller effect (Rizwan, 2006).

In contrary to that, Incorporation of RHA in cement-based materials generally reduces the strength. Coutinho and Papadakis (2011), in their paper "RHA-importance of fineness for it is use as a pozzolanic and chloride-resistant material" investigated the fineness effect and pozzolanic activity of the RHA, in order to understand RHAs performance. Two different types of RHA (A, and Θ) with two replacement ratios (10 and 15%) were used. RHA-A was consisting of 89.05% silica (81.43 are reactive), 3.04% Al_2O_3+ Fe_2O_3, 3.05% CaO, and 2.15% MgO. While, RHA-Θ consist of 86.50% SiO_2 (78.64% reactive), 2.70% Al_2O_3+ Fe_2O_3, 4.40% CaO, and 1.97% MgO, respectively. The author found that as far as the RHA fineness increased the compressive strength increased.

However, the strength was lower than control mix and decreased with increase of replacement ratio. According to the author, increase the fineness of RHA-A particles led to the development of smaller grain sizes than those of cement. Where small grain sizes of ash strengthen (through the filler effect) packing among aggregates (especially in the case of fine aggregates) and cement grains. Madandoust et al. (2011) have studied the mechanical properties and durability assessment of RHA concrete. To establish the suitable proportion of RHA for the partial replacement of cement, concrete mixtures with 0-30% RHA were produced and their mechanical properties were determined. The author concludes that the growth in strength is lower for RHA concrete compared to the control specimens and decreased with increase replacement ratio. However, with progression of time the strength development is comparable to normal concrete at the age of 270 days.

Marthong (2012) in his paper "Effect of RHA as partial replacement of cement on concrete properties" made comparative between three grades of ordinary Portland cement (OPC) namely; 33, 43 and 53, respectively. Percentage replacement of OPC with RHA was 0, 10, 20, 30 and 40% respectively. Compressive strength, water absorption, shrinkage and durability of concrete were all tested. The test data of compressive strength showed that as far as RHA percentage increase, compressive strength decrease gradually. However, the author demonstrated that compressive strength of concrete increases with grade of cement, where the rate of strength gain by RHA-33 grades OPC is lower as compared to 43 and 53 grades. The author suggested that the use of RHA as partial replacement of cement up to a maximum of 10% by volume in all grades of cement.

2.6.3 Splitting tensile strength

Splitting tensile strength is of utmost significance in the construction of concrete slabs and beams as they are subjected to tensile stresses due to bending action (Atis, 2005). Available literature shows that the splitting tensile strength of RHA concrete tends to follow the trend of compressive strength. Generally, the effect of RHA on the splitting tensile strength of concrete from the different sources was evaluated. According to the literature RHA concretes shown variable effect on the development of splitting tensile strength of concretes. Concretes with the finer RHA mixture have a direct impact on the strength development due to the increased pozzolanic reaction and the packing ability of the RHA fine particles (Zhang et al., 1996). Ganesen et al. (2008) have observed that tensile strength value increases with RHA content up to 20% and then at 30% RHA, the splitting tensile strength is equivalent to that of OPC concrete. The author states that more research need on the effect of RHA on the splitting tensile strength. Kartini et al. (2006) in their paper, "rice husk ash – pozzolanic material for sustainability" evaluated the RHA influence on the splitting tensile strength of concrete. The author concludes that the RHA does not improve the tensile strength of concrete.

Shukla et al. (2011) have studied the effect of replacement ratio of RHA on the splitting tensile strength of concrete. The test data presented by the author showed that splitting tensile strength significantly decreased as the percentage of RHA increased. Tushir et al. (2016) in their paper, “Effect of Rice Husk Ash on Split Tensile Strength of Concrete” have made a comparative study in between two grades of RHA concrete (M30, M60). The author found that, there was reduction in split tensile strength in both the concrete mixes. The author linked this reduction in splitting tensile strength to the fact that concrete is brittle

material and cannot handle tensile stress. Therefore, as the percentage of rice husk ash increased strength decreased.

Habeeb and Fayyadh (2009) have studied the effect of RHA average particle size on mechanical properties and drying shrinkage of concrete. A comparative between three different sizes of RHA particles (31.3, 18.3, and 11.5μm) have been made. The author reported that, tensile properties have been significantly enhanced with increase fineness of RHA particles, while the coarser RHA particle mixture showed the least improvement in tensile strength. Madandoust et al. (2011) have studied the mechanical properties and durability assessment of rice husk ash concrete. In their study, data on selected properties of fresh and hardened concrete are presented. Constant replacement level of 20% by mass of cement was used. They concluded that concretes containing 20% RHA as cementitious material lowered the tensile strength of RHA concrete than normal concrete at ages up to below 90 days. However, it became equivalent or greater than normal concrete at the later ages.

Ramezanianpour et al. (2009) have investigated the influence of RHA on mechanical properties and durability of sustainable concretes. Three different replacements ratio of RHA varied from 7%, 10% and 15% by weight were studied. The test results indicated that the more the cement was replaced by RHA, the more tensile strength increased. Where, 15% RHA concrete increased the splitting tensile strength up to 5.62 MPa compare to 4.58, 4.90, and 5.21MPa for control concrete, 5% RHA, and 10%RHA, respectively. In conclusion it can be observe from the literature review that the substitution of cement by RHA presented a contradiction on the splitting tensile strength of concrete. In addition to that, the optimum replacement of cement by RHA is another argument point between the researchers. This is very important for the experimental studies in the next chapters relating to concrete containing RHA. Therefore, to assess the effect of RHA characteristics on the splitting tensile strength of concrete, it is very important to use a comparative methodology between different types of RHA and with wide range of replacement ratio.

2.6.4 Effect of replacement ratio

The major effect of RHA in Portland cement blends beside the pozzolanic effect; it is the amount of replacement ratio. Which is effect directly on the reaction that takes place between the silica in the RHA and $Ca(OH)_2$ formed by the hydration of Portland cement. Where, Calcium silicate hydrates are thus formed these contribute to the strength development of the concrete. Therefore, RHA content consider very important to develop the performance of concrete properties. Ganesan et al. (2010), have studied the effectiveness

of RHA with wide range of replacement ratio (0, 5, 10, 15, 20, 25, 30, and 35%). The author found that RHA could replace up to 30% of cement without any adverse effect on the strength and durability properties of concrete. Habeeb and Mahmud (2010) suggested that with respect to compressive strength, the incorporation of RHA in concretes up to 20% replacement ratio improve the performance of concrete properties. Moreover, this improvement particularly increased with increase fineness of RHA particles.

Khan et al. (2015) have studied the mix proportioning of cement with RHA as a partial replacement of cement up 30% of cement weight. The author found that as high as 25% by weight of OPC can be replaced with RHA without any adverse effect on the compressive strength of self-compacted concrete. Dakroury et al. (2008) discussed the effect of RHA replacement ratio on the strength of the cemented waste. RHA in concrete replacing Portland cement by 0%, 10%, 20%, 30%, 40% and 50%. The test data showed that the compressive strength of the concrete containing up to 30% of the RHA was higher than that of the control Portland cement. In addition to that, the strength of the concrete increased with decreasing w/b ratio. Same conclusion was reported by Saraswathy et al. (2007). However, Chindaprasirt et al. (2008) have proved that the compressive strength of 40% mortar blended RHA is greater than control mortar after 90 days of curing. Similar to that, Nehdi et al. (2003) reported that RHA enhanced the compressive strength of concrete up to 40%.

Isaia et al. (2003) investigated the effect of replacement ratio (0%, 12.5%, 25% and 50%) with the water binder ratio (w/b) on the strength development of concrete. Three differences water to binder ratio was used (0.35, 0.50 and 0.65). The author demonstrated that, even at 50% replacement ratio, the compressive strength of RHA concrete was higher than that of OPC control at the w/b ratio of 0.35. While, almost same of OPC control concrete at the w/b ratio of 0.50%. However, decreased about 13.50% compared to OPC control at 0.65 to binder ratio. To confirm variability of use high replacement ratio on improvement of concrete strength, Ettu et al. (2013) used wide variable replacement ratio (5%, 10%, 15%, 20%, 25%, 30%, 35%, 40%, 45% and 50%). The results revealed that the strength of concrete blended RHA was higher than conventional concrete up to 10% then gradually decreases.

2.7 Shrinkage of concrete

Problems associated with the three to seven days of concrete life are crucial to the long-term properties of the hardened concrete. Poor construction, conditions, casting and curing, and harsh environmental conditions can together create unwanted effects such as plastic, drying,

thermal shrinkage and, eventually, cracking on a concrete. Generally, many factors mainly an effect on the shrinkage of concrete, such as stiffness, coarse aggregate and porosity matrix (Zerbino et al., 2011). Furthermore, type of cement and mineral additions can also influence on mortar and concrete shrinkage. Where, the presence of minerals additional effect on the water movement inside the cement paste and as a result differed strain (Zerbino et al., 2011). In general, concrete shrinkage are divided into two different phases, early and late age. Both aspects should be evaluated together as a general shrinkage of the concrete. The early age of contraction refers to the first day that concrete is applied and solidification begins. Long-term age, concrete refers to 24 hours after casting or longer. Concrete shrinkage types can be divided into plastic shrinkage, chemical shrinkage (autogenous shrinkage) and drying shrinkage. Despite different types of shrinkage exhibited in concrete, there are two types of shrinkage are participating in total concrete shrinkage. First, the autogenous shrinkage, which is the bulk deformation of a closed isothermal, cementitious materials system not subjected to external forces (Jensen and Hansen, 2001). Drying shrinkage, which is defined as the reduction in volume in the cement matrix as a consequence of an overall loss of water to the environment through evaporation.

Generally, drying shrinkage to strains associated with the moisture loss within the unloaded concrete. Factors affecting drying shrinkage are ambient relative humidity, temperature, wind velocity, and time of exposure (Neville, 1995). The physical significance of shrinkage drying leads to a decrease in the volume of concrete. In dry and hot conditions, it is expected that the rate and amount of shrinkage will be higher than under moderate climatic conditions. The net effect of drying shrinkage is a reduction in the compressive strength of concrete. Drying shrinkage is a long-term process that develops for several weeks, months and even years.

2.7.1 Drying shrinkage of concrete blended RHA

Generally, the definition of drying shrinkage is a phenomenon that is mainly caused by the moisture drying from the pore system of the hardened paste and thus leads to volume shrinkage of the concrete (Yang et al., 2017). Among the different types of shrinkage, drying shrinkage usually results in the most significant volume change as a result of changes in capillary stress, disjointing pressure, and surface free energy (Deshpande et al., 2007). Commonly, the entire shrinkage strain is assumed to be from drying shrinkage, and any contribution of autogenous shrinkage to the average strength of concrete is neglected (Malhotra and Mehta, 1996). Supplementary cementitious material (SCM) can significantly

influence the shrinkage of the mixture. The available literature is shown that for such a mix the incorporation of slag cement has marginal influence on the increase in drying shrinkage. While a high content of silica fume can increase the drying shrinkage in the short-term ages. However, in the long-term, silica fume may not cause an increased shrinkage with less replacement ratio (Rao et al., 2000). Class F fly ash used in binary mixtures may reduce drying shrinkage with increasing replacement dosages compared to plain Portland cement concrete. The properties of both freshly mixed and hardened concretes are intimately and complexly associated with the characteristics and relative proportions of the material used in their manufacture. One of these properties are directly associated to materials characteristics and proportions is drying shrinkage of concrete and mortar. Studies on the effect of RHA on the drying shrinkage of concrete are still not detailed, and deformation properties of concrete containing RHA have not been sufficiently explored.

Chatveera and lertwattanaruk (2011) in their "Durability of conventional concretes containing black rice husk ash" they investigated the drying shrinkage performed of concrete. The concrete was made based on Japanese concrete institute (JCI, 1998). Two different replacement ratios of cement by RHA, 20% and 40%, with three different water binder ratios (0.6, 0.7 and 0.8) were used. The author concluded that the use of RHA replacing Portland cement has a negative effect on the drying shrinkage of concrete. However, the drying shrinkage of concrete with 40% RHA replacement ratio is comparable to the OPC concrete. In addition to that, water binder ratio affected directly on the value of drying shrinkage. Where with increase w/b ratio from 0.60 to 0.70 and 0.80. The drying shrinkage of RHA concrete increased for the same replacement ratio.

Habeeb and Fayyadh (2009) have studied the effect of RHA particle size on the drying shrinkage of concrete at 20% replacement ratio. The author used RHA with three different mean particle size of 31.3µm (20F1), 18.3µm (20F2), and 11.5µm (20F3), with specific surface area of 27400m^2/kg (20F1), 29100m^2/kg (20F2), and 30400m^2/kg (20F3), reactively. The author concludes that the drying shrinkage was significantly affected by RHA fineness; 20F3 recorded the higher shrinkage value. While 20F1 exhibited lower values than the control, this could be mainly due to the effect of the micro fine particles. Wu and Peng (2003) have comparative of two different types RHA and silica fume at five different temperatures: 65, 80, 120, 150 and 180°C were assessed with replacement ratio 15, 20, 33, and 50% by mass of cement were used. The result indicated that the total amount of the drying shrinkage is less with increase temperature than that of normal temperature curing (25°C).

Zhang and Malhotra (1996) in their study of high-performance concrete incorporating rice husk ash as a supplementary cementing material, made comparative in effect of 10% RHA to 10% SF and OPC concrete on the drying shrinkage of concrete. The authors found that, concrete with 10% RHA exhibited higher drying shrinkage compare to 10%SF and OPC concrete. However, with progression of time became lower than OPC concrete. Moghadam and Khoshbin (2013) in their paper "Mechanical properties and shrinkage and expansion assessment of rice husk ash" they compared the effect of different replacement ratio on the compressive strength, tensile strength and drying shrinkage of concrete. Variable replacement ratio of RHA ranged in between 5 to 30% was used. The authors found that, the deformation of drying shrinkage for the RHA specimens were more than that of the control concrete specimens. Moreover, the amount of deformation increased with increase replacement ratio. The author attributed that to the reactivity of ash, where the capillary pores in hydration products are increased. Therefore, concrete blended RHA has more shrinkage than OPC concrete.

Alvarez and Arboleda (2008) studied the possibility of use RHA as a partial substitute for cement, and affect that on the concrete performance. RHA by 10% and 20% replacement ratio at two different water binder (w/b) ratios, (0.40 and 0.55) were used. The test data showed that the drying shrinkage of RHA concrete was significantly lower than for normal concrete, where at 10% replacement ratio exhibited maximum reduction. In addition to that with increase water binder ratio, drying shrinkage increased. Khassaf et al. (2014) in their study; investigation the properties of concrete containing rice husk ash to reduction the seepage in canals, concrete specimens were molded with 10%, 20%, and 30% of (RHA) replacing the cement, and measured it to workability, compressive strength, splitting tensile strength, dryings shrinkage. They had observed that the drying shrinkage of concrete was decreased with increased of RHA%, the maximum decreased given by 30% RHA it was about 28% of normal concrete shrinkage after 90days age. As a result, from the previous published researches survey on the drying shrinkage of concrete, there is a clear discrepancy in effectiveness of use of RHA on the performance of concrete. In addition to that, there is another contradiction also in the extent of the effect of RHA replacement ratio, which is very important for the experimental studies in the next chapters.

2.8 Durability of OPC concrete blended RHA

2.8.1 Definition of concrete durability

The durability of concrete is considered as the second significant concrete properties in addition to the strength. Where strength is the ability to resist the stress, durability is the ability to resist deterioration (Shahroodi, 2010). The American Concrete Institute (ACI 116R) defines the concrete durability as it is the ability to withstand weathering action, chemical attack, abrasion and other conditions of service.

2.8.2 Durability problems

Water penetration (with corrosive agents) is the main problem of the concrete durability. According to Neville (1995), the kinetics of chloride ingress can be identified as the diffusion of chloride ion, because of difference in the concentration gradient and absorption due to capillary action. Exposure to various environmental conditions (i.e., high temperature or water freezing) and chemical reaction (i.e., chloride ion reaction) leads to significant cracking and therefore deterioration of concrete. There are two categories effect on the durability of concrete and causes of deterioration: first, physical causes, which include surface wear (abrasion, erosion and cavitation) and cracking (volume changes, loading damage, and extreme temperature damage). Second, chemical causes (i.e., alkali-aggregate reaction, sulphate attack, chloride penetration lead to corrosion).

2.8.3 Durability concrete in aggressive environment

2.8.3.1Theoretical Background

There are three main ways to penetration of chloride ion in concrete: diffusion, capillary absorption and hydrostatic pressure, where the diffusion is the most known method. The diffusion of chloride ion can be described as the movement of chloride ions under a concentration gradient (Stannish et al., 1997). The process of chloride ingress into the concrete occurred by three ways; first, when the concrete has continued liquid phase with chloride ion concentration gradient, second, the penetration of chloride ion driven under the hydraulic head on the concrete face which leads to penetrate into the concrete. Third, with the capillary absorption when dry face concrete in touched with the water containing chloride (Thomas et al., 1996).

2.8.3.2 Concrete properties influence on the chloride ion penetration

The pore structure of concrete plays a major role on the rate of chloride ion penetration, where age, materials and construction practices factors are affecting on the process of

penetration. Certainly, the pore structure of the cement paste matrix identifies the permeability of concrete influenced by water-cement ratio and supplementary cementitious materials utilization, which work on the division of the pore structure as well as concrete hydration degree (Mc Grath, 1997). According to the Luping and Nilsson (1992) and Bamforth (1997), the pozzolanic materials react slowly with $Ca(OH)_2$ of hydration cement give more extended time to more development in the pore structure of concrete. The capacity of chloride ion penetration in concrete by use of supplementary cementing materials is controlled. Nevertheless, the exact effects on the penetration of chloride ion in concrete are unclear [Byfors, (1986) and Thomas et al., (1995)].

2.8.4 Chloride ion penetration in concrete blended RHA

The main factor of the concrete deterioration primarily is due to the chloride ion, and it is present either freely or in bound form. Concrete containing RHA have received considerable attention as supplementary cementitious materials to improve the durability of concrete. As with the compressive strength, contradicting results are presented in the literature shown in Fig. 2.14.

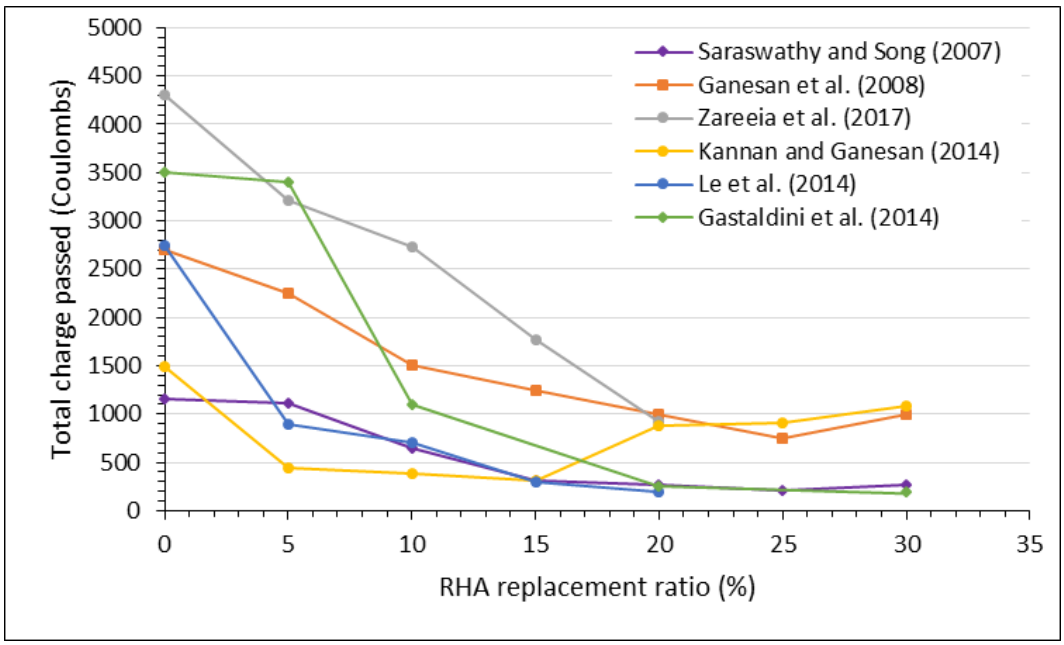

Figure 2.14: Chloride diffusion of RHA blended concretes according to the literature.

The effect of RHA on the chloride diffusion is varies between researchers, especially in high replacement ratio. Generally, the improvement is mainly caused by the reduction of permeability/diffusivity in blended concrete. Nahdi et al. (2003) compared the performance of four different types of RHA, three Egyptian RHA given name of A, B, C, and the fourth

one from USA. RHAs were consisting of 94.6%, 93.7%, 91.6% and 89.1% silica and variables mean particle size of 7.15, 7.63, 7.41 and 6.8µm, respectively. Three replacement ratios (7.5, 10 and 12.5%) with constant w/b ratio of 0.40 were used. The result indicated that the effect of RHA was dependent upon the replacement ratio and quality of the RHA used. Where, with increased replacement ratio, RHA concrete resistance to chloride ion penetration increase. Moreover, this improvement increased either with increasing silica content (RHA-A) or decrease mean particle size (US RHA).

Saraswathy and Song (2007) in their paper "Corrosion performance of rice husk ash blended concrete" evaluated RHA concrete corrosion performance using different techniques (open circuit potential measurements, rapid chloride ion permeation test and impressed voltage test). The author found that, incorporation of RHA up to 30% replacement ratio reduces the chloride penetration, decreases permeability, and improves strength and corrosion resistance properties. Nevertheless, the authors concluded that up to 25% replacement ratio of RHA is recommended. Chindaprasirt et al. (2008) made a comparative in between the performance of RHA, palm oil fuel ash (POA) and classified fly ash (fine fly ash, FA) mortars to the chloride penetration and chloride ion diffusion coefficient at two different replacement ratios (20 and 40%). In comparison with POA and FA, RHA presented a further reduction in the rapid chloride penetration and chloride ion diffusion coefficient. Moreover, this improvement in performance was increased with increase replacement ratio to 40%. Ganesan et al. (2008) have studied the assessment of optimal level of replacement for strength and permeability properties of concrete. The concrete was made following Indian code and up to 35% of cement replacement was made using RHA. The authors based on the results, the following conclusions were drawn:

1. Replacement with 30% of RHA leads to substantial improvement in the permeability properties of blended concrete when compared to that of unblended OPC concrete, namely

1.1. About 35% reductions in water permeability.

1.2. About 28% reductions in chloride diffusion.

1.3. About 75% reductions in chloride permeation.

2. A linear relationship is found to exist among the sportively, chloride penetration in term of total charge in coulombs and chloride diffusion coefficient.

3. When RHA re-burned, which is consisting of less of loss on ignition value compared to RHA before re-burned, the resistance to chloride permeation is substantially improved. This may probably due to a decrease in electrical conductivity of concrete due to lowering of

unburnt carbon content in RHA, in addition to pore structure refinement and conductivity of pore solution.

4. Chloride permeability resistance of RHA blended concretes reached optimum reduction at 30% replacement ratio. While, with chloride diffusion resistance of RHA blended concretes the optimum decrease was reported at 25% replacement ratio.

Kannan and Ganesan (2014) have presented data on the chloride and chemical resistance of self-compacting concrete containing RHA and Metakaolin. The author found that even with very fine particles (mean particle size 6.27μm), mixture with 15% RHA was the most durable and it may be considered as an optimum level of replacement for OPC as supplementary cementitious materials. While Zahedi et al. (2015) reveal that RHA concrete reached the maximum enhancement of chloride resistivity at 20% replacement ratio. The author attributed that to an increase in porosity and pore size refinement due to their filler packing. Madandoust et al. (2011) investigated the durability of concrete mixtures with 0-30% RHA consist of 90.9% silica, where 81.25% is amorphous. After eleven months of exposure, the specimens to aggressive environment, the results show that the higher the RHA content, the lower the chloride penetration has appeared are compared to control samples. According to the author, by blending concrete with RHA leads to lower porosity and finer pore structures, in result inhibiting penetration of chloride.

In a more recent study by Gastaldini et al. (2014) in their paper "Total shrinkage, chloride penetration, and compressive strength of concretes that contain clear-coloured rice husk ash", the author demonstrated that there is a connection between the rate of chloride ion penetration to the replacement ratio of cement by RHA and water binder ratio. Three different water binder ratio (0.35, 0.50 and 0.65) and 5 to 30% RHA replacement level were used. RHA consists of 93.54% silica with surface area 18890 m^2/kg. The results showed that there was an increase in the passing charge of chloride ion with increase water binder ratio (w/b). In addition to that, there was a decrease in the passing charge as the RHA contents increased.

Le et al. (2014) revealed that with four different RHA replacement ratios (5, 10, 10 and 20%) consist of 86.81% silica and 8.42μm mean particle sizes, the lowest value of the charge passed was obtained at 20%of RHA. The author stated that RHA with pore structure might be regarded as an internal curing agent lead to prolonging hydration of cement. Therefore, the permeability of concrete is lowered. Furthermore, the capability of RHA pore-refining in concrete has been presumed to enhance the chloride penetration resistance.

Antiohos et al. (2014) investigated the silica reactive and fineness of RHA on the resistance of RHA concrete to chloride penetration. The researchers used two types of RHA (RHA8, RHA12) consist of 89.47% and 93.15% silica, each type with two different fineness [(380 and 700 m^2/kg) RHA8, (390 and 655m^2/kg) RHA12] at replacement ratio of 10%, 20% and 30% respectively. Comparing the output of the experimental work (Table 2.6), of the two types of RHA concrete, reveal a definite difference in the effect of silica content and fineness of the resistance of RHA concrete to chloride penetration.

Table 2. 5: Chloride resistance results according to Antiohos et al. (2014).

Components (kg/m^3)	OPC	RHA8		RHA12	
		10%	20%	10%	20%
Charge passed (Coulombs)	3135	3896	1962	2962	996
Adjusted charge passed (Coulombs)	2719	3380	1702	2569	864
Permeability class	Moderate	Moderate	Low	Moderate	Very low

2.9 Effect of SP on the strength of concrete blended RHA

Superplasticizers, also called as high range water reducing (HRWR) admixtures, are micro-molecular organic or chemically synthesized agents. According to their chemical contents, have been divided into the following four groups: Sulphonate melamine formaldehyde, Sulphonate naphthalene formaldehyde, Modified lignosulphonates and Copolymers containing sulphonic and carboxyl groups which may contain polycarboxylates and polyacrylates (Plank and Winter, 2008). Regarding to the investigations on the usages of superplasticizer (SP) and RHA, previous studies were made mostly for the purpose of increase the flowability of concrete and mortar. The effect of SPs in OPC paste, mortar and concrete has been widely evaluated by several authors such as Chandra and Björnström (2002); Msinjili et al. (2017) and others. Recently, some studies have been conducted on the effect of the SPs on other pozzolanic material, such as fly ash, slags and SF. On the contrary, effect of the SPs on RHA strength development has been received less attention. Moreover, the effect of SP dosage with the presence of RHA influences mortar strength still remains unknown.

2.10 Summary points

The review of the literature was undertaken to report the state of the art of the current understanding of the effect of RHA physical properties and chemical composition to replacement ratio on the strength, dry shrinkage and durability of concrete. The author has dealt with the important topics of positively and negatively effect of RHA on the

compressive and tensile strength of mortar and concrete, drying shrinkage, chloride ion penetration and diffusion at different replacement ratio with different RHA properties at different ages. The examination of the literature reveals the following key observations:

i. Comparing the RHA composition of the previous studies there is a clear difference in the chemical composition and physical properties, this difference in properties led to a difference in effect (positive to negative impact) on properties of mortar and concrete. This variation in RHA properties needs more investigation to find out the contribution factors to enhance concrete properties.

ii. The relationship between reactivity and fineness of RHA to hydration and mechanical properties of blended cement containing various amounts of RHA needed to be investigated.

iii. Effect of RHA fineness of particles as a filler on the performance of mortar or concrete in related to the amount of the replacement ratio wasn't investigated.

iv. The literature survey showed a contradiction on effect of RHA fineness on the workability of mortar and concrete.

v. There is a discrepancy in between the researchers on the effect of RHA implementation as supplementary contentious materials on the strength of concrete development.

vi. The optimum replacement percentage of cement with RHA without adversely effect on mortar or concrete properties is varying from research to another and it is the second controversial point.

vii. Effect of residual carbon content (loss on ignition) of the RHA performance scarcely investigated, to clarify the impact on RHA performance more research need.

viii. Drying shrinkage is another parameter of mortar blended RHA where rarely investigated, especially with high replacement ratio.

ix. There is no clear vision of the relationship between micro fines of RHA particles to the deformation resistance of drying shrinkage of concrete.

x. Effect of RHA properties on the chloride penetration resistance was presented in many published papers. Despite that, most of the researchers agree on the positive impact of RHA increase the resistance to chloride ion penetration. However, there were many discrepancies on the optimal limitation of RHA replacement ratio and the impact of the fineness of particles on the durability of concrete.

xi. The effect of superplasticizer dosage on the RHA concrete properties needs further investigation.

CHAPTER 3: METHODOLOGY AND EXPERIMENTAL PROCESS

3.1 Introduction

This chapter presents the experimental techniques and methodology implemented satisfies the objectives of this research. These include descriptions of the research materials, testing techniques and experimental lab work.

3.2 Materials and Methods

3.2.1 Cement

Cement type CEM I 52.5N was used in the experimental study. The properties and mineral composition of cement shown in Table 3.1, was provided by the manufacturer (CEMEX UK Cement Ltd) according to BS EN 197-1: 1996.

Table 3.1: Specification of high strength cement type CEM I 52.5N according to manufacturer (CEMEX UK Cement Ltd).

Physical properties										
Specific surface area						$0.415m^2/g$				
Initial setting time						130 minutes				
Expansion						1mm				
Chemical composition										
Oxides	SiO_2	Al_2O_3	Fe_2O_3	CaO	MgO	Na_2O	SO_3	Cl^-	FI	LOI*
% wt. of Cement	19.7	4.70	3.10	63.9	1.10	0.69	3.30	0.05	3.40	2.80

LOI*: loss on ignition (residual carbon content).

3.3 Rice husk ash

Several types of RHA with varied physical properties and chemical composition were used in the experimental to accomplish the different project tasks successfully. Initially, three RHA types labelled as A, B and C, were brought from Navdanya Food PVT. LTD Odisha, India. Further, five types marked C1, C2, C3, C4 and C5 respectively were obtained from re-incinerated of RHA-C at different temperatures and times (400°C/30min, 400°C/2h, 500°C/2h, 600°C/2h and 550°C/6h) in University of Brighton Laboratories. The RHA ashes used in this study were selected to give a wide range in fineness, specific surface area,

reactivity (silica structure), silica content and loss on ignition. Emphasis on these properties is due to the fact that RHA performance is primarily affected by these factors. Careful consideration was made in preparation of the re-incinerated series (C1 to C5), of RHA, to isolate these effects. Each type of RHA had a different composition and different fineness.

3.3.1 RHA physical properties

Determination of Physical properties of RHA considered very important to assess the impact on the mechanical and durability of concrete. Particle size distribution, specific surface area, and the mean particle size of RHA samples were determined using the Mastersizer 2000 (Malvern, UK) laser diffractometer. The principle of a laser diffractometer is based on the fact that the spatial distribution of scattered light is a function of the particle size of the analyzed sample (Agrawal and Mc Cave, 1991). Laser diffraction measures particle size distributions by measuring the angular variation in intensity of light scattered as a laser beam passes through a dispersed particulate sample. Large particles scatter light at small angles relative to the laser beam and small particles scatter light at large angles, as illustrated below (Fig.3.2, i). The angular scattering intensity data is then analyzed to calculate the size of the particles responsible for creating the scattering pattern, using the Mie theory of light scattering. The particle size is reported as a volume equivalent sphere diameter.

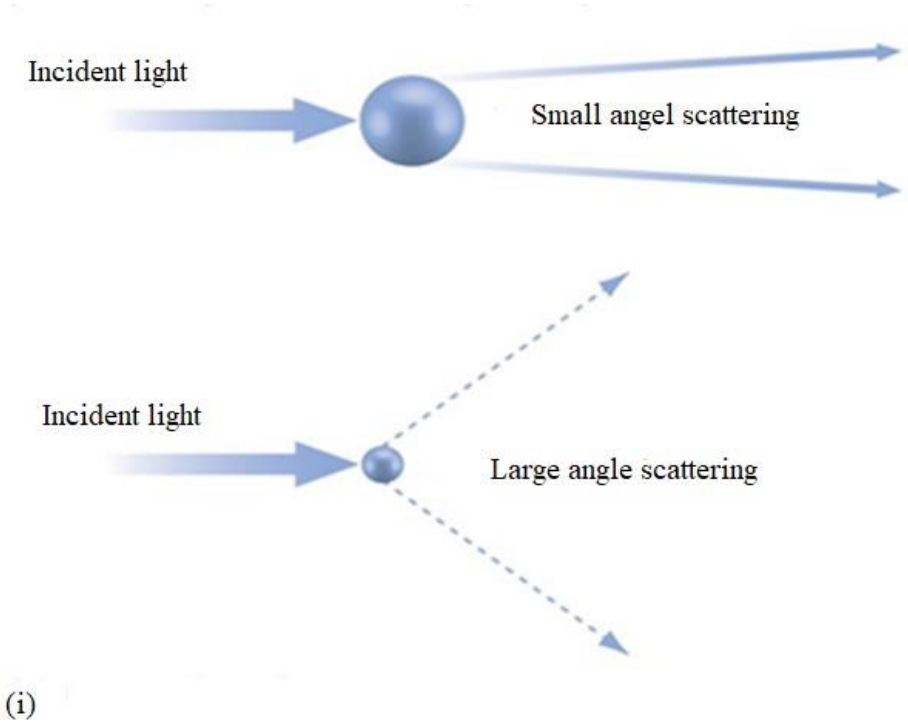

(i)

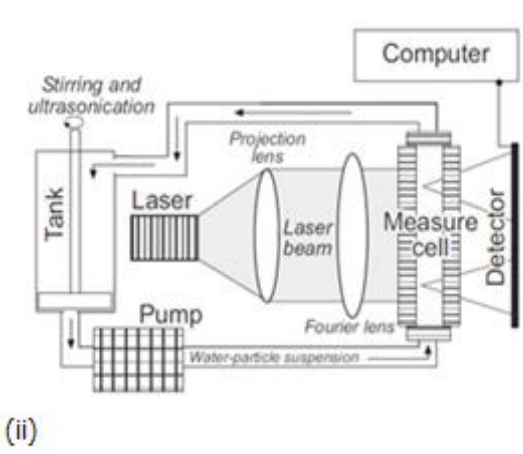

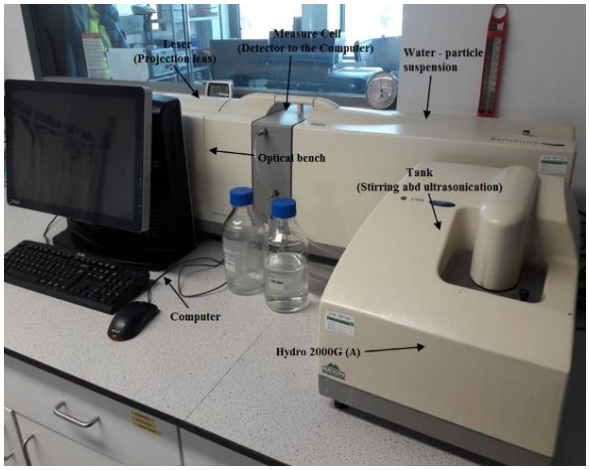

Figure 3.1: (i) Scattering of light from small and large particles; (ii) Schematic graph showing the main components of a laser diffraction particle size analyser (Mastersizer 2000, Malvern instrument).

3.3.2 Chemical composition of RHA samples

To achieve the purpose of this research and taking into account the effect of chemical composition of RHA, it is very important to determine the chemical composition of RHA. To identify and quantify the major and minor oxide elements present in the samples of obtained RHA, X-Ray Fluorescence (XRF) analysis was carried out using Bruker AXS S4 spectra plus (Figure 3.2), with soil-LE-FP method and duration of 60 seconds. Prior to the test, RHA samples were prepared as a flat disc with a diameter of 20mm. Pressed pellets were prepared by pressing loose powder filled in a flat disc using a set of dies and press machine. Ease of RHA powder palletization depends on the RHA silica characterization (amorphous to crystalline) and grain size. To improve that, a sufficient amount of pulverization (3 to 5 drops) was used with continuous stirring the powder up to 5 minutes.

Figure 3.2: X-ray fluorescence test used Bruker AXS S4 spectra plus instrument.

3.3.3 Silica structure of RHA

To evaluate the suitability of RHA silica as supplementary cementitious materials, determine the crystalline compounds of the silica is important. X-ray Diffraction (XRD) test was carried out using XRD crystallography (PANalytical X'Pert Pro MPD, powered by a Philips PW3040/60 X-Ray generator, Figure 3.3). The process of obtaining the diffraction data of RHA samples began with preparation of samples by packing about 15g of RHA tightly into the metal sample holder. The process of sample preparation is shown in Figure 3.3 (a). The principles of XRD measurement according to Kugler (2003) is the capability to differentiate between different crystalline substances their diffraction patterns. The powder samples were exposed to Cu-Kα X-ray radiation, which delivers a characteristic wavelength (λ) of 1.5418Å. X-rays are generated by a Cu anode supplied with 40kV and a current of 40mA. The data were gathered over a range start position °2θ is 5.0052 to end position of °2θ is 69.9892 with a step size of °2θ =0.0080 and nominal time per step of 10.1600s, using the scanning X'Celerator detector.

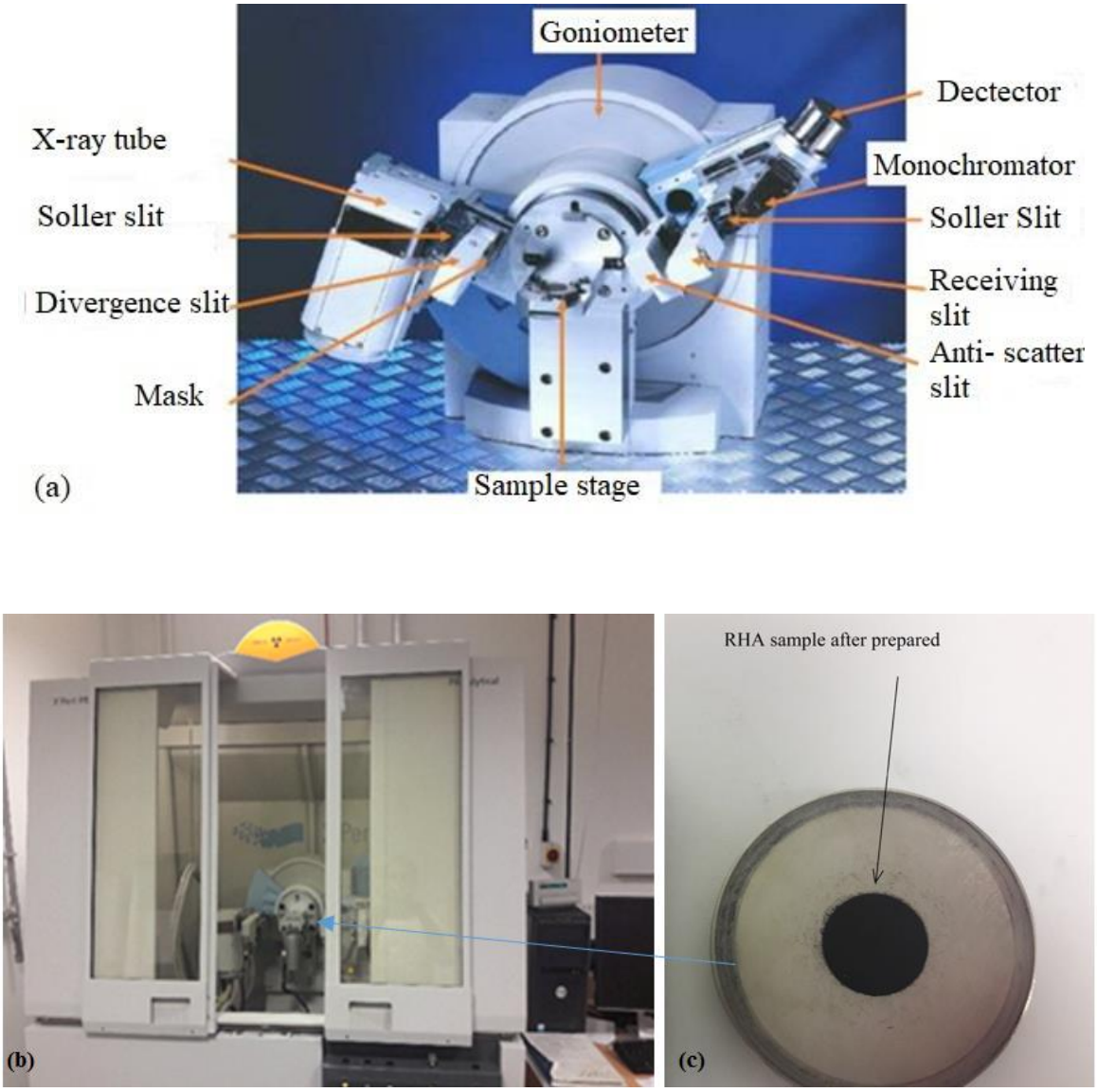

Figure 3.3: (a) XRD device detailed, (b) XRD device at University of Brighton, (c) the prepared sample of RHA used.

3.3.4 Pozzolanic activity of RHA (Electrical conductivity method)

Pozzolanic activity is the extent of the chemical reaction occurring between the active constitutes of pozzolana, calcium hydroxide, and water. Therefore, to evaluate the reactivity of RHA on the mechanical and durability of mortar and concrete, indirect method through the variation in the electrical conductivity in the first two minutes was used. The method of measuring the electrical conductivity of saturated solution of calcium hydroxide developed by Luxán, et al. (1989) was used. The method is based on the interaction of the Ca+ and OH^- ions of a saturated $Ca(OH)_2$ solution with amorphous silica (SiO_2); some of these ions react with the silica reducing the conductivity of the solution over time. The rate of change in the conductivity of the solution two minutes after adding RHA ($\Delta\sigma 2min$) was used to classify the pozzolanic quality of RHA. RHA conductivity $\Delta\sigma 2min < 0.4$ indicates 'non-

pozzolanicity', while $0.4 \leq \Delta\sigma 2\min \leq 1.2$ refers to 'variable pozzolanicity' and $\Delta\sigma 2\min > 1.2$ indicates 'good pozzolanicity' (Luxán, et al., 1989). This method used by Yu et al. (1999) and Nair et al. (2008), who confirmed it is applicability to assess the pozzolanic activity of RHA.

3.3.5 Microstructure of RHA

To investigate the microstructure of the RHA particles, Scanning Electron Microscope (SEM) model Jeol JSM-6480 LV as shown in Fig.3.4, was used. SEM has become one of the most widely utilized instruments for materials characterization. BSE mode was used to determine the microstructure of RHA at two magnifications, 4.00kx and 5.00kx for each sample, two images were captured in order to provide more confidence in the results of the image analysis.

Figure 3.4: Philips- Jeol JSM-6480 LV, used for RHA microstructural observation.

3.3.6 Loss on ignition

The residual carbon content is the more important component of loss on ignition and it affects the water requirement for mortar and concrete. The carbon content of RHA which has high porosity and a very large specific surface area causes the absorption of water and organic admixtures such as water reducing agents. ASTM C 618-89 has allowed only

maximum of 12% of total weight of RHA, therefore it is very important to quantify the total content of loss on ignition. Residual carbon content "LOI" of RHA samples was obtained according to EN 196-2:1994 s. After drying for 24h at 105°C, the pre-weighted RHA samples (1 ± 0.05g) were placed in a crucible beaker with a lid and heated in a muffle furnace at 975 ± 25°C for 5 minutes. After that, the cover was removed and the samples were heated for a further 10min. After the muffle furnace was turned off, the samples were left to cool down to room temperature in the crucible beaker. The loss on ignition was calculated by using the following equation.

$$LOI = \frac{m7-m8}{m7} \times 100 \quad (3\text{-}1)$$

Where: m7: Mass of the RHA sample before combustion.
m8: Mass of the RHA sample after combustion.

3.6.7 pH of RHA Solutions

With regard to the chemical composition of the RHA powder, one notable point in the properties of RHA is K_2O percentage. This possibly causes a different effect of the pH value (alkalinity) of the pore solution in the cement paste or concrete, when RHA is added in the system. In fact, the high content of K_2O in RHA will contribute a high alkalinity of the pore solution and may help to offset the decrease in pH value of the pore solution due to the pozzolanic reaction between the silica of RHA and the calcium hydroxide [Hwang and Wu, (1989); Bui, (2001)]. Whereas, pH effect on the durability of concrete by meaning of initiation of corrosion. Low value of pH "pH less than 9" is considering critical threshold for initiation corrosion. With regard to the chemical composition of the RHA powder, one notable point in the properties of RHA is that RHA has a comparatively content of K_2O.
This possibly causes a different effect of the pH value of the pore solution in the cement paste or concrete, when RHA is added in the system. Therefore, in this study will be quantified for the raw materials (RHA) to determination their effect on the durability of the cementation's materials. The pH of RHA blended mortar was measured. RHA samples with four different types of at replacement ratios ranged in between 0% to 60% of total weight of cement were tested according to BS 6068-2-50:1995. A Mettler Toledo AG portable pH meter was used (Fig.3.5. b). The pH measurement of the mortar blended RHA solutions included the following procedures:

1. Place 1g ± 0.05 of RHA in a 50ml test tube.
2. Add 20 ml of sterilized water.

3. The samples are set in a multi-rotator device model PTR-60 (Grant-bio) as shown in Fig.3.6 (b).
4. Samples are stirred for 3 minutes, then left for 24h.
5. pH measurements: The pH of the expressed pore solution was measured directly with a pH meter and a micro combination pH electrode, as shown in Figure 4, e. This electrode is designed to measure the pH ranged from 0–14. Before performing the pH measurements, the pH electrode system was calibrated by two standard buffer solutions. The pH measurements were conducted at an ambient temperature within a range of 20–25 ◦C. The calibrated micro-combination pH electrode remained in the solution until the pH value was constant.

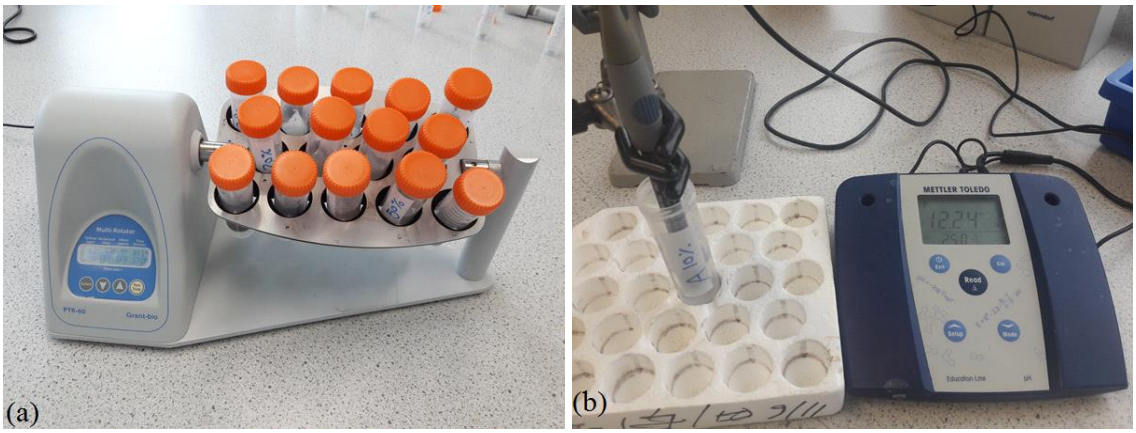

Figure 3.5: pH measurement device used to determine the pH of RHA motors; (a) multi-rotator model PTR-60 (Grant-bio), (b) Mettler Toledo AG pH meter.

3.4 Aggregates

3.4.1 Fine aggregate

3.4.1.1 Silica Sand

The silica sand used in the mortar experimental study conformed to the graded standard requirements of BS EN 12620:2002:2008. The silica sand properties are provided by the manufacturer (Sibelco UK Ltd) presented in Table 3.2.

Table 3.2: Physical properties of silica sand as provided by the manufacturer (SIBELCO).

Sieve (μm)	Typical cumulative passing (%)	Typical cumulative passing (%)	Typical cumulative retained (%)	Typical retained each sieve (%)	Sand retained (%)	Category
1000	100.0	100.0 Min	0.00	0.00	0.0	Very coarse
710	100.0	99.6 Min	0.00	0.00	0.3	Coarse
500	99.70	97.0 Min	0.30	0.30	0.3	Coarse
355	95.80	-	4.20	3.90	34.1	Medium
250	65.60	-	34.4	30.2	34.1	Medium
180	24.30	-	75.7	41.3	61.1	Fine
125	4.50	7.0 max	95.5		61.1	Fine
90	0.80	-	99.2	3.70	4.4	Very fine
63	0.10	0.3 Max	99.9		4.4	Very fine
<63	-	-	100.0	0.1	0.1	Silt/Clay

3.4.1.2 Sand (Fine aggregate)

Fine aggregate was used for concrete experimental. The size distribution of sand was determined according to BS EN 12620:2013. The sieve analyses are shown in Table 3.3.

Table 3.3: Sieve distribution of the fine aggregate.

Sieve No:	Weight (g)	Weight percentage (%)	Cumulative passing (%)
4mm	11	2.2	97.8
2.8mm	43	8.6	89.2
1.4 mm	97	19.4	69.9
600μm	140	27.9	41.9
300μm	159	31.7	10.2
150μm	45	9.0	1.2
75μm	4	0.8	0.4
63μm	1	0.2	0.2
< 63μm	-	-	-

3.4.2 Coarse aggregate

Un-crushed coarse aggregate maximum size of 10mm conforms to BS EN 12620:2013 was used in the concrete batches. The sieve analysis is presented in Table 3.4.

Table 3.4: Sieve distribution of coarse aggregates.

Sieve No:	Weight (g)	Weight percentage (%)	Accumulative passing (%)
9.5 mm	15	3.0	97
8 mm	48	9.6	87
4 mm	34.1	68.1	1

3.5 Superplasticizers

The use of RHA in a cementitious system can significantly increase the water demand. This is mainly attributed to the fact that RHA is a porous material, which also has a large specific surface, and angular structure (Cordeiro et al., 2011; Chau-Lung., 2011). Therefore, superplasticizers (SP) are used to limit the water demand whilst improving the workability. A Polycarboxylate polymer superplasticizer was used in this project. According to the manufacturer (Fosroc International Ltd.), this superplasticizer has high range water reducing capabilities and excellent scattering levels with reliable performance. The specification of the superplasticizer complies with EN 934 –2; it is presented in Table 3.5.

Table 3.5: Properties of Fosroc Auracast 200 according to the manufacture (Fosroc International Ltd).

Nature	Liquid
Color	Dark Straw
Specific gravity	1.050 – 1.070
pH	4 +/- 1
Chloride content	<0.1%
Na_2O equivalent	<0.5%
Freezing point	Sensitive to freezing
Air entrainment	typically less than 2% additional air is entrained at normal dosage

3.6 Water

According to BS EN 1008:2002 specification, the quality of the mixing water for production of concrete can influence the setting time, the strength development of concrete and the protection of the reinforcement against corrosion. Therefore, water should be free from undesirable salts and organic material compounds. In this project, the water used was obtained from the domestic water supply pipe in the concrete laboratory.

3.7 Mortar mixture

For the mortar samples a constant water/binder ratio of 0.50 and a constant binder/sand ratio of 1:2.25 was used. Therefore, the RHA-replacement percentage and superplasticizer addition were the only variable parameters. The average density of the mortar was determined according to ASTM C 270 as ρ =2200 kg/m^3.

$$\text{Cement quantity (C)} = \frac{2200}{[1+(\frac{W}{C})+(\frac{S}{C})]} \quad (3.2)$$

Where: W/C = 0.50, S/C = 2.25

Sand quantity (S) = 2200 – C – W

Where: C: cement content, W: water content

To study the effect of RHA properties on the performance of mortar, cement type CEM I 52.5N, with three different series of RHA mortars and variable replacement ratio were created. Series 1 was mortars blended with RHA- A, B, C and C5 at replacement ratio ranging from 0% to 60% (RHA-A, B and C5) and up to 80% RHA-C. Series 2 consists of mortars blended with RHA-C1, C3 and C4 at a constant replacement ratio of 5%, while RHA-C2 content up to 60%. Series 3 included three different types of RHA (RHA-A, B and C) ground for four different periods at a constant replacement ratio of 5%. To improve the flowability of mixes, superplasticizer was used. The superplasticizer dosage is given as dry weight to the amount of binder (i.e. cement and pozzolans). The superplasticizer content had to be increased for high RHA contents to keep the workability of the mortar in acceptable limitations. Details of the mix proportion are presented in Table 3.6.

Table 3.6: RHA mortar mix proportions.

RHA%	Cement (kg/m^3)	RHA (kg/m^3)	Silica Sand (kg/m^3)	Water (kg/m^3)	SP (%wt. of binder)
0%	587	-	1320	293.5	0.25%
5%	558	29	1320	293.5	0.25%
10%	528	59	1320	293.5	0.25%
15%	499	88	1320	293.5	0.25%
20%	470	117	1320	293.5	0.25%
30%	411	176	1320	293.5	0.50%
40%	352	235	1300	293.5	1.00%
50%	293.5	293.5	1320	293.5	2.00%
60%	235	352	1320	293.5	4.00%

3.8 Concrete

The mean target of concrete strength mixtures was 50 ± 3MPa for the OPC control mixture at 28days. The total binder content was 460 kg/m^3, fine aggregate 785kg/m^3 and coarse aggregate 800kg/m^3, the water to binder ratio (w/b) was kept constant at 0.50. Superplasticizer was used to keep the mixtures workability within the permitted limit (varied to maintain a slump of 50-200 mm) for all mixtures. The moisture content of coarse and fine aggregate was determined to adjust the mixing water content half an hour before batching. Three series of concrete blended RHA (A, B and C) with the water-binder ratio of 0.50 were investigated.

Table 3.7: Concrete mixture proportions.

RHA%	Cement (kg/m^3)	RHA (kg/m^3)	Water (kg/m^3)	SP (%wt. of binder)
0%	460	0	230	0.25%
5%	437	23	230	0.25%
10%	414	46	230	0.25%
15%	391	69	230	0.25%
20%	368	92	230	0.25%
30%	322	138	230	0.50%
40%	276	184	230	1.00%
50%	230	230	230	2.00%
60%	184	276	230	4.00%

SP*: Superplasticizer (%wt. of total binder)

3.9 Sample specimen

For each mortar mix, five cubes (50mm×50mm×50mm) and 'dog-bones' 44.86mm × 74.6mm × 25.4mm (see Fig. 3.6) were cast and placed with vibration. The intensity and duration of the vibration was adjusted according to the flowability of each mix. The samples were demolded after 24hrs and then stored at 100% humidity at constant temperature of 20±3°C. Drying shrinkage tests of mortar were performed using prisms size 70mm×70mm×280mm, the samples were kept at temperature of 20±3°C after demolding. For each mix of concrete, cube size 100mm×100mm×100mm was used according to BS 12390-1:2012. For splitting tensile strength and durability (chloride penetration) test, cylinders size 100mm diameter × 200mm high were used. All samples were cured in 100% humidity till the day of testing. The total numbers of specimens are presented in Table 3.8.

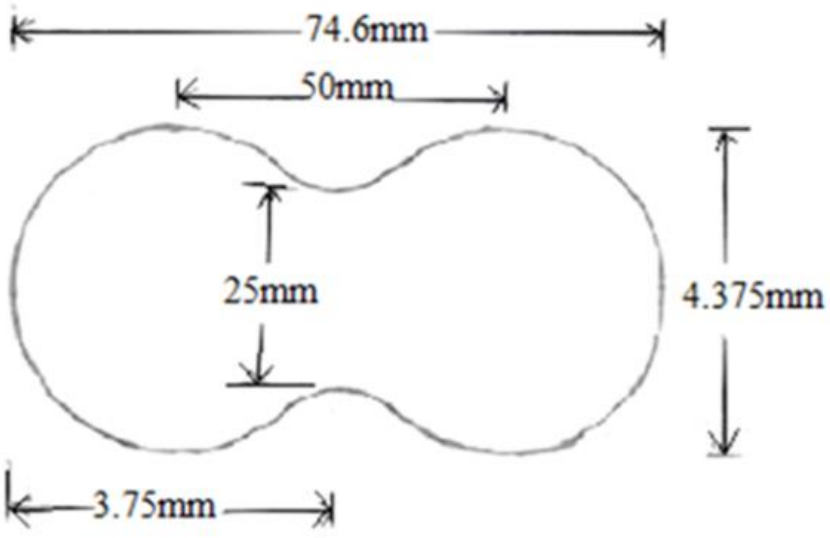

Figure 3. 6: Dog-bone specimens dimension sued to determine tensile strength of mortar.

Table 3. 8: Total numbers of specimens used in the experimental tests.

Mix type		Test type	
Mortar	compressive strength	tensile strength	drying shrinkage
OPC	15	15	2
RHA-A	40	40	16
RHA-B	40	40	16
RHA-C	50	50	20
RHA-C1	40	40	-
RHA-C2	40	40	-
RHA-C3	40	40	-
RHA-C4	40	40	-
RHA-C5	50	50	16
Concrete	Compressive strength	splitting tensile strength	chloride penetration
OPC	9	9	2
RHA-A	24	24	16
RHA-B	24	24	16
RHA-C	24	24	20

3.10 Mixture preparation

3.10.1 Mortar mixture

The mixing was carried out using a Hobart N50-60 heavy-duty countertop 5 quart, three-speed commercial mixer as shown in Figure 3.7. Mixing of binder materials start at slow mixing (145 rpm) for 30 seconds, and then water was added and mixed for another 30 second. After that, the silica sand was added and mixed for another 120 seconds at 285 rpm. Mixing the RHA blended mortars required more mixing time (maximum about 20 minutes for 60%RHA-A), depending on the replacement ratio and type of RHA (particle size distribution, loss on ignition and crystalline silica content). The blended mixes looked very viscous due to the irregular, abrasive and internally porous particles of RHA. Directly after the flowability tests, the mixture was poured into the molds in three layers. Each layer was vibrated for 20 seconds; however, vibrating time increased with increase replacement ratio (maximum 85sec for 60%RHA-A) as a consequence of low workability. The molds were kept for 48hrs, then de-molded. The specimens were preserved in curing tank till the date of testing at a room temperature 22°C±3.

Figure 3.7: Hobart N50-60 heavy-duty countertop 5-quart, 3 speed commercial mixer.

3.10.2 Concrete mixture

For the concrete mixes, the coarse aggregates and sand was mixed in the mixer for 3 minutes, then cement and RHA was added. Then the mixture of water with superplasticizer was added slowly within 30 seconds. The mixing process continued after all materials were added for a further 3-5 minutes. With high replacement ratios over 50%, the mixing process was continued further until the mixture reached acceptable homogeneity. The workability of mixtures was determined with slump tests according to BS EN 12350-2:2009. After that, the mixes are poured in the cube and cylinder molds in three layers; each layer was vibrated for about 60 ± 5 seconds. However, for high replacement ratios (50% and over) the vibration time was increased as a result of low workability of mixtures. Thereafter, the concrete surfaces were levelled; samples were demolded after 24hrs. However, at high replacement ratio (60% and over) due to the low reactivity of RHA at the early age the specimens were demolded after 48hrs. All samples were kept in the curing tank at a constant temperature of 20±3°C until the date of the test.

3.10 Workability of mortar and concrete

3.10.1 Flow table measurement of mortar

Standard mortar flow test was conducted using flow table in accordance with BS EN 1015-03:2004. This test was conducted to examine the mortar flowability with different RHA types and replacement ratio. These measurements were made using a mini-slump cone. The target flow level was 18±1cm. The increased superplasticizer dosage required to give the target flow for the RHA blended mixes was determined by trials.

3.10.2 Concrete slump test

To determine the workability of concrete mixtures the slump tests was conducted based on BS EN 12350-2 (2009).

3.11 Compressive strength

The compressive strength considers as the main characteristic of cementitious materials that describe the mechanical properties of mortar and concrete. Therefore, it is very important to determine the contribution the pozzolanic reaction to the compressive strength of mortar and concrete from physical and chemical effects of RHA. In order to achieve that, compressive strength of RHA concrete at different replacement ratio were determined through experiment followed by the BS EN 12390-3:2009 standard. Cube specimens of dimensions 50mm × 50mm × 50mm used for mortar and 100mm×100mm×100mm cube for concrete. Three different moisture curing time (7, 28 and 91day) were selected. The cubes after curing were tested for compressive strength by loading the sides of the cubes uniformly with a compressive strength testing machine until fracture appeared. The maximum load in KN at which fracture occurred was recorded and used to calculate the compressive strength as:

$$f_c = F/A_c \qquad (3.3)$$

Where;

f_c: is the compressive strength, in MPa (N/mm²);

F: is the maximum load at failure, in N;

A_c: is the cross-sectional area of the specimen on which the compressive force acts, calculated from the designated size of the specimen (see EN 12390-1) or from measurements on the specimen if tested according to Annex B, in mm^2

3.12 Tensile strength

Tensile strength is defined as the ability of a material to support axial load without rupture and is determined through the tensile test. Therefore, it is very important to study the effect of RHA properties (physical and chemical) on tensile strength performance of mortar and concrete. To achieve that direct tension (dog-bone) for mortar and splitting tension was used for concrete. In this test, a cylindrical specimen is loaded in compression diametrically between two plates. According to the theory of elasticity, this loading generates almost uniform tensile stress along the diameter, which causes the specimen to fail by splitting along a vertical plane. The split tensile test was conducted as per BS EN 12390-6-2009. The direct tensile strength of mortar is given by the formula:

$$ft = \frac{F}{A} \tag{3.4}$$

Where:
ft: is the tensile splitting strength, in mega Pascal's (MPa) or in Newton's per square millimetre (N/mm²).
F: is the maximum load, in Newton's (N).
A: is area of the cross- section broken dog-bone.

While, the splitting tensile strength for concrete is given by the formula:

$$f_{pt} = \frac{2 \times F}{\pi \times L \times d} \tag{3.5}$$

Where:
fspt: is the tensile splitting strength, in mega Pascal's (MPa) or in Newton's per square millimetre (N/mm²).
F: is the maximum load, in Newton's (N);
L: is the length of the line of contact of the specimen, in millimetres (mm);
d: is the designated cross-sectional dimension, in millimetres (mm).

3.13 Curing

The circulation of water in the tank between the cubes are necessary to leave adequate space between them and the side of the curing tank to give all cubes same curing environment to assist strength development equally.

3.14 Drying shrinkage of mortar

Drying shrinkage, defined as the time dependent deformation due to loss of water at constant temperature and relative humidity (Hansen, 1987). This shrinkage causes an increase in tensile stress, which may lead to cracking, internal warping, and external deflection, before

the concrete is subjected to any kind of loading. Therefore, development of drying shrinkage of mortar and concrete consider very important. To achieve this objective four different types of RHA (A, B, C and C5) were used at replacement ratios from 0% to 60%. The reading initial reading was taken directly after samples were de-molded according to BS ISO1920-8:2009. The sample as fixed at both ends to the device (digital length comparator BS812-120). The room temperature and humidity were recorded each time using a sensor (N090AQ). The experimental setup was used to measure the length change and temperature of three 40mm×40mm×250mm sized samples shown in Figure 3.9. After being measured and weighted, the samples are kept in the laboratory under constant temperature and humidity to avoid any possible influence on the measures of the sensor. The calculated change length of specimens at any age was as follows:

$$L = \frac{(Lx - Li)}{G} \times 100 \qquad (3.6)$$

Where:

L = Change in length at x age, %.

L_x= length of specimen at time x minus length of reference bar the same time in millimeters.

L_i= Initial length of specimen minus length of reference bar at that same time in millimeters.

G = Nominal gauge length (250).

Figure 3.8: Drying shrinkage of RHA mortar measurements; (a) Calculation of length change setup according to BS812-120, (b) Temperature and humidity at time of length change measurement.

3.15 Durability of concrete (chloride ion penetration)

Chloride ion penetration is the most common defect in reinforced concrete (RC) structure resulting corrosion either by exposure to de-icing salt or sea water (Jones, 1997). Several laboratories testing methods have been developed to quantify the penetration of chloride ion in concrete short-term and long-term. Because of the cost, the time consuming and laborious long-term methods are usually not preferred (Spiesz and Brouwers, 2009). To evaluate the effect of RHA properties on the concrete durability, a none-steady-state migration test (NT Build 492) was used. For each concrete batch, two cylinders' size 100mm (diameter) × 200mm (high) up to 60% replacement ratio were cast. For the chloride migration (diffusion coefficient) tests the NT Build 492 (Nord Test) equipment was used. The non-steady state migration test, also known as the rapid chloride migration test (RMT) was initially proposed by Tang and Nilsson (1992) and Tang (2010). This test can be used for different types of concrete (Tang and Nilsson, 1992).

The depth of chloride penetration in concrete is measured to determine the chloride migration coefficient. Penetration of chloride ion into the sample is enforced by an applied external electrical voltage. Due to the difference in potential between the electrodes (Anolyte) and chloride (Catholyte), the ions migrate from the 10%NaCl solution, through the concrete specimen, towards the 0.3M NaOH solution for a defined period. After that, the sample is split and sprayed with $AgNO_3$ as indicator for chlorides; the depth of discoloration is referred as chloride penetration. For the chloride ion penetration test three samples for each mixture of RHA concrete were used. After sawing, washing, drying the samples and the vacuum treatment (10–50 mbar/1–5 kPa for three hours) the concrete samples were saturated with $Ca(OH)_2$ for 19 hours (one hour with the maintained steady vacuum level and subsequently 18 hours after turning off the pump).

The container of catholyte and anolyte were filled with the solutions. The catholyte is a 10% NaCl solution (100g NaCl in 900g distilled or de-ionized water, about 2N), the anolyte is a 0.3N NaOH solution (approximately 12g NaOH in 1-litre water). The applied electrical potential, which is drives the chloride ion into the concrete sample is 30V DC. The duration of the test selected depending on the initial current and test voltage are presented in Table 3.9.

Table 3. 9: NT Build 492 method test voltage and duration (NT BUILD 492. 1999).

Initial current I_0 (with 30 V) [mA]	Applied Voltage U (After adjustment) [V]	Possible new Initial current I_0 [mA]	Test duration (hour)
$I_0 < 5$	60	$I_0 < 10$	96
$5 \leq I_0 < 10$	60	$10 \leq I_0 < 20$	48
$10 \leq I_0 < 15$	60	$20 \leq I_0 < 30$	24
$15 \leq I_0 < 20$	50	$25 \leq I_0 < 35$	24
$20 \leq I_0 < 30$	40	$25 \leq I_0 < 40$	24
$30 \leq I_0 < 40$	35	$35 \leq I_0 < 50$	24
$40 \leq I_0 < 60$	30	$40 \leq I_0 < 60$	24
$60 \leq I_0 < 90$	25	$50 \leq I_0 < 75$	24
$90 \leq I_0 < 120$	20	$60 \leq I_0 < 80$	24
$120 \leq I_0 < 180$	15	$60 \leq I_0 < 90$	24
$180 \leq I_0 < 360$	10	$60 \leq I_0 < 120$	24
$I_0 < 360$	10	$I_0 \geq 120$	6

The depth of the chloride ion penetration is measured by the AgCl color that is visible after 15 minutes of spraying (Fig 3.8). This process is called the colorimetric method, which is characterized by it is simplicity and quickness.

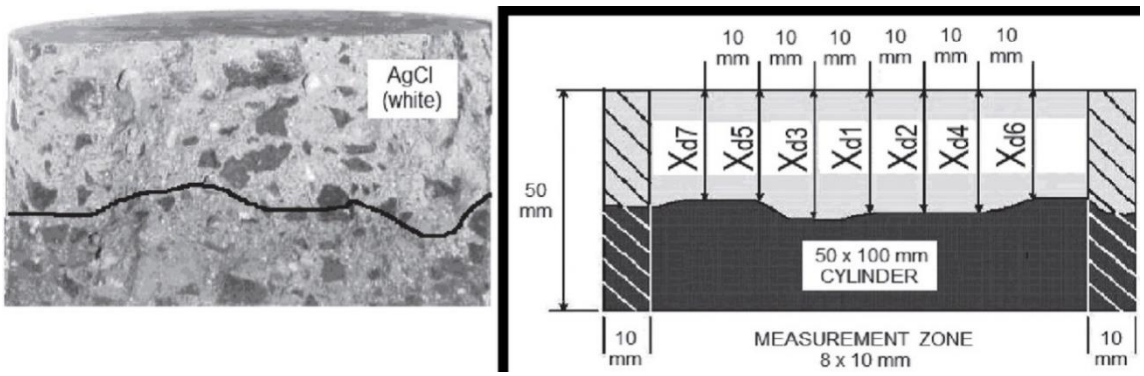

Figure 3. 9: Test of the chloride ion penetration of concrete using the NT Build 492 method. Measurement of chloride penetration depths (Stanish et al., 2004; Tang et al., 2011).

The measurement of chloride ion penetration of the concrete specimens should be to an accuracy of 0.1mm (Tang et al., 2012). The measurement is starting from the center of the sample to the edges at each 10mm (Fig.3.3) by using a suitable Caliper. Shi et al. (2012) reported that no measurement should be made in the zone within about 10mm from the edge because of a non-homogeneous saturation degree or possible leakage. For each sample, an average of six readings should be taken to determine the non-steady-state chloride migration coefficient "D_{nssm}". The non-steady-state chloride migration coefficient will be determined based on the measurement of the voltage, the temperature of anolyte at the beginning and

end of the test and the depth of penetration of chloride ions (Tang and Nilsson, 1992). The non-steady state migration coefficient is calculated from equation (3.7):

$$D_{nssm} = \frac{0.0239(273+T)L}{(U-2)t}\left(x_d - 0.0238\sqrt{\frac{(273+T)L\,x_d}{U-2}}\right) \quad (3.7)$$

Where:

D*nssm*: non-steady-state migration coefficient, $\times 10^{-12}$ m^2/s;
T: average value of the initial and final temperatures in the anolyte solution, °C;
L: thickness of the specimen, mm;
x_d: average value of the penetration depths, mm;
t: test duration, hour.
U: ultimate voltage
To evaluate the chloride penetration resistance of concrete blended RHA, the chloride migration coefficient presented by Tang (2010) in Table 3.10, are adopted.

Table 3.10: Evaluation of concrete resistance to chloride ion penetration (Tang, 2010).

Chloride migration coefficient [D*nssm*, m^2/s]	Resistance to chloride penetration
$< 2 \times 10^{-12}$	Very good
$2 – 8 \times 10^{-12}$	Good
$8 – 16 \times 10^{-12}$	Acceptable

CHAPTER 4: RHA CHARACTERISTICS RESULTS

4.1 Introduction

The experimental data and discussion of the observed trends of RHA characteristics are presented in this Chapter. First, the silica structure of the as-received RHA (A, B and C) and re-incinerated RHA-C5 are presented. The characterization techniques entail tests of silica structure, crystallinity measurement of particles, chemical composition and physical properties. Following that loss on ignition, data are presented and correlated to RHA characteristics. Next, the pozzolanic reactivity of RHA samples determined according to Luxán's et al. (1989) theory is presented. Finally, the microstructure of RHA particles is addressed. To achieve those different techniques, i.e. X-ray fluorescence, and scanning electron microscopy (SEM) were used.

4.2 Characterization of RHA silica structure

The reactivity of RHA is considered to be the main factor impact on the RHA performance. Therefore, to evaluate RHA properties, determining the silica structure (amorphous to crystalline silica) content is essential. To identify the degree of the reactivity of RHA samples, X-Ray Diffraction (XRD) is used; here, the total X-Ray scattering of both the crystalline and amorphous phases are used to determine the crystallinity. The process of assessing crystallinity is explained in Chapter 3, section 3.3.3. The X-Ray Diffraction pattern results are shown in Figure 4.1, while the peaks are listed in Table 4.1. The results of the X-Ray Diffraction show there are a variation in the intensity of broad peaks. The NIOSH manual of analytical methods (NMAM, 2003) was used as reference to analyses the XRD results. Where the RHA peaks in the X-Ray Diffraction results can be assigned to tridymite 20.93°, cristobalite at 21.93°, possibly cristobalite or tschernichite at 22.04°, quartz at 20.85°, 26.7° and 68.4° and brownleeite at 44.40°.

A general RHA X-ray spectrum will have a broad amorphous peak. However, if the RHA has crystallinity, it will show up as a sharp peak on the top of the large amorphous peak (Fig.4.1). In general, the broad peak observed for RHA-C sample indicates the amorphous nature of silica. Similar results were obtained for RHA-C5 samples with a trace of crystalline reflections. However, RHA-B showed some reasonably sharp and intense reflections, evidencing that consist of cristobalite and quartz respectively. Furthermore, these peaks become more intense with RHA-A, where they mostly refer to cristobalite.

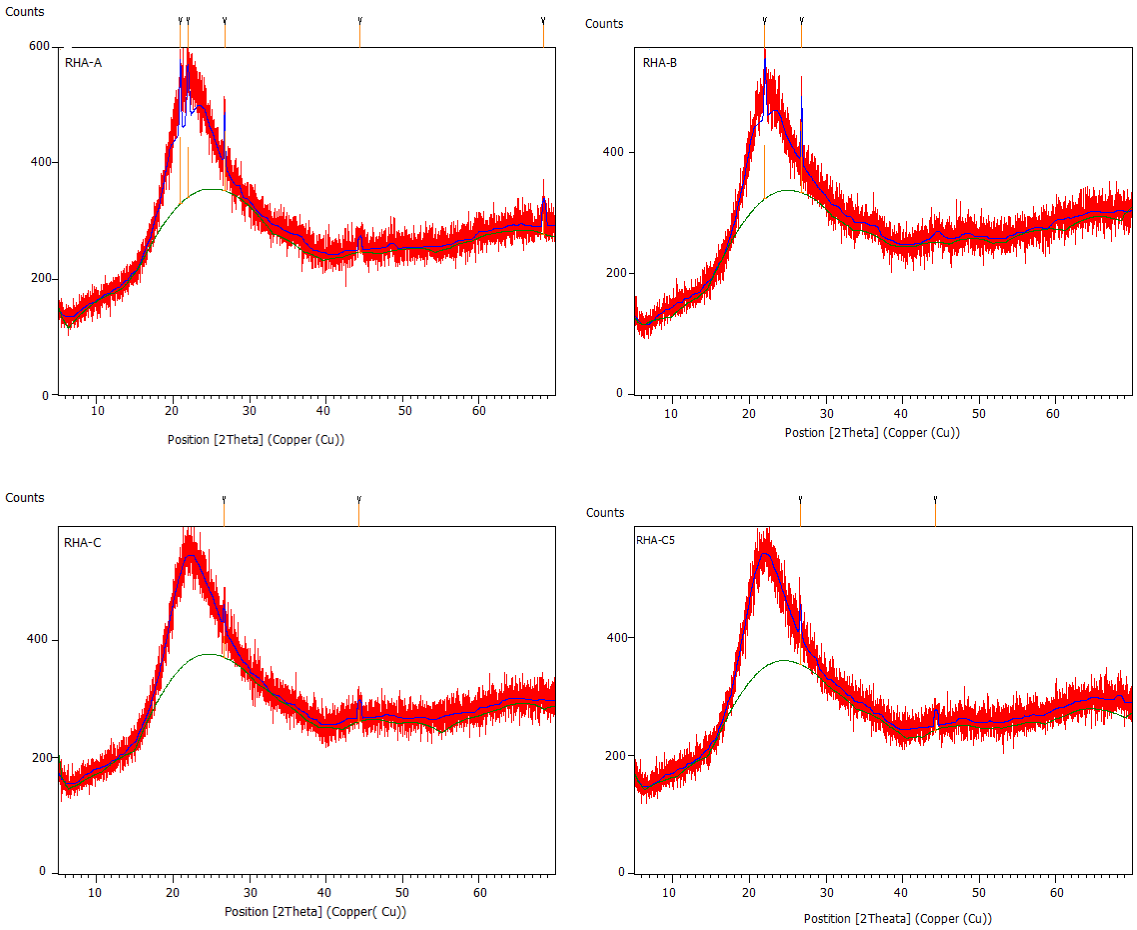

Figure 4.1: X-Ray Diffractogram of RHA-A, B, C and C5 samples.

Table 4. 1: The X-ray diffraction peaks of RHA samples.

RHA sample	Position [°2θ]	Height [Counts]
RHA-A	20.9363	116.40
	21.9453	86.60
	26.7445	104.45
RHA-B	22.0390	89.26
	26.7997	116.72
RHA-C	26.6621	37.69
RHA-C5	26.6662	52.39

4.2.1 Crystallinity measurement of RHA

The spectrum is the sum of crystalline peaks and an amorphous peak. The true area of the crystalline peaks and the amorphous peak can be determined from a computer XRD software package performing a mathematical deconvolution of the peaks. Generally, quantification of amorphous content can be divided into two categories, direct and indirect. The direct method relies on the ability to accurately assess contribution of both the crystalline and amorphous phases to the diffraction pattern. The indirect method only uses

the crystalline phases; however, it requires a specific amount of a known crystalline standard to be added. Quantification of amorphous content using the direct method can be difficult for several reasons. Broad amorphous peaks can be difficult to observe, particularly if the amount of amorphous fraction is small, which is true in RHA-C and C5. Therefore, it is often difficult to clearly low broad amorphous peaks and their associated tails from the pattern's background intensity. So, it is not practical to measure amorphous material directly as a constituent of a larger crystalline phase to the accuracy required. Therefore, in this study, an indirect technique, used to determine the amount of crystalline silica. The Rietveld simulation standard, was used to quantify amorphous content. The determination was carried out by running an XRD profile of the sample is spiked with amount of ~20% by mass of known crystalline phase "quartz ground to very fine particles, 10μm" (Wolford, 2015). The results are shown in Table 4.2.

Table 4.2: The crystalline to amorphous percentage of RHA ashes (A, B, C and C5) based on XRD test.

XRD pattern peak position	Intensity (Counts)	Semi-quantitative estimate SiO_2 (%)	Amorphous (%)	Rietveld refinement SiO_2	Amorphous (%)
26.60 20.93 21.94	104.45 116.40 86.60	6.3	93.8	23.4	76.6
26.57 22.03	116.72 89.26	2.0	98.0	15.6	85.4
26.60	38	0	100	0.0	100.0
26.66	52	0	99	1.375	98.76

4.3 Physical properties of RHA

The particle size and specific surface area of RHA was determined by laser particle size analysis. The results are shown in Tables 4.3, 4.4, and plotted in Fig. 4.2. The results are an average of three measurements for each RHA type. RHA particle sizes mostly ranged in between 7 and 31μm. The median particle diameter typically varied between 12.640 and 23.397μm. Usually, particle sizes of RHA are variable, and it depends on the grinding time. The grain sizes of most of the RHA sample in published literature vary from <1μm to 100μm. According to Mehta (2002), particle sizes of RHA between 6 and 15μm are preferred for workability and cohesiveness of concrete.

Table 4. 3: RHA physical properties.

Physical properties	RHA			
	A	B	C	C5
Specific surface area (m^2/g)	0.537	0.587	0.692	0.808
Mean particle size (µm)	23.397	20.948	15.804	12.64

Table 4. 4: Cumulative particle size distribution of RHA.

Particle size (µm)	% of total volume			
	A	B	C	C5
0.060	6.850	7.920	9.750	12.08
3.900	8.710	10.19	14.33	17.90
7.800	17.51	19.72	25.39	29.48
15.60	30.92	30.17	26.68	25.21
31.00	29.16	25.02	17.35	12.22
63.00	6.830	6.720	5.190	3.010
125.0	0.020	0.250	0.680	0.110
250.0	0.000	0.000	0.530	0.000
Mean particle size	23.39	20.94	15.80	12.64

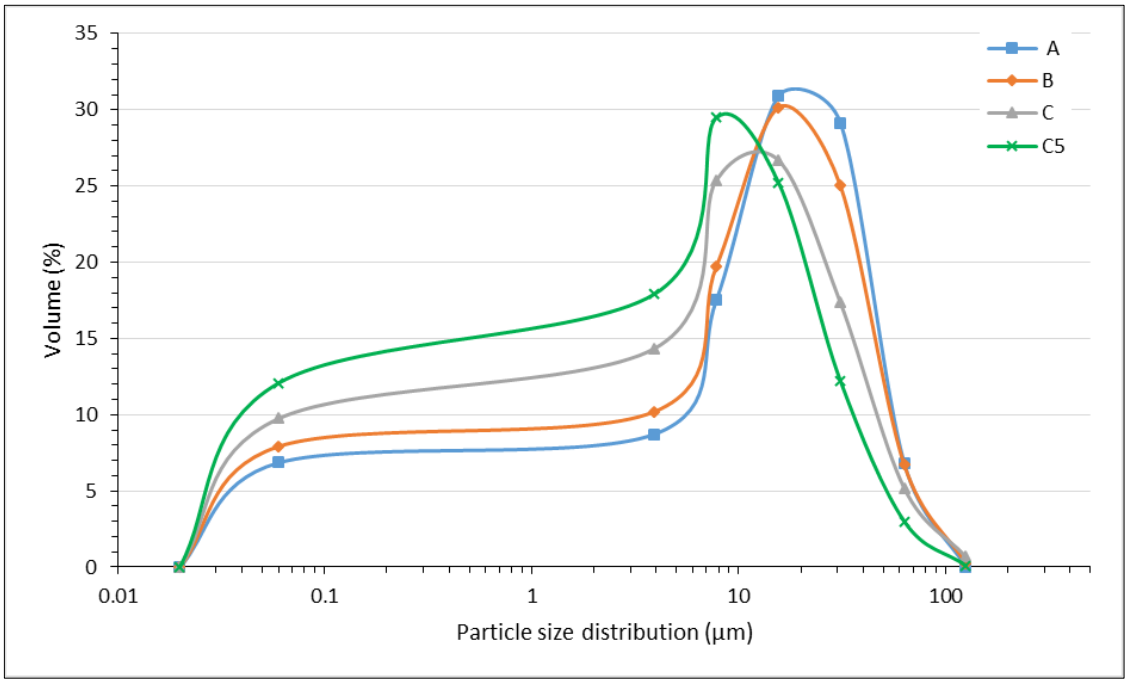

Figure 4. 2: Mean particle size distribution curve of RHA (A, B, C and C5) samples.

4.4 Chemical composition of RHA

The chemical oxide compositions in weight percent of the RHA samples, determined used X-Ray Fluorescence are presented in Table 4.5. For each RHA type, three individual pellets were produced and analyzed by XRF, the average concentrations of each component are

given in the Table 4.5. The results showed obvious variation of silica content with minor differences in contents of other oxides except for Al_2O_3 and K_2O. The results indicate that all samples of RHA had combined percentages of silica (SiO_2), Alumina (Al_2O_3) and ferric oxide (Fe_2O_3) of more than 70%, which is conform to ASTM C618. The results also demonstrate the remarkable effect that re-burning RHA-C improved the chemical quality of the ash (RHA-C5) by increasing the contents of most accompanying oxides. The increase contents of SiO_2, Al_2O_3, Fe_2O_3, CaO, K_2O and SO_3 are 9.83%, 10.12%, 13.37%, 24.92%, 4.10% and 1.19% respectively, while P_2O_5 and MnO decreased about 1.78% and 20.14% comparing to RHA-C. Furthermore, RHA-C5 has a light grey color resulting from of the reduction of residual carbon (85.46% compared to RHA-C). That means the designated burning stages (temperature to time) of RHA to produce ash with ultimate properties are necessary to control the residual content of the carbonaceous materials in the ash. The black color of RHA-C is an indication for the un-completeness of the combustion process and the high level of remaining inorganic impurities.

Table 4. 5: Chemical composition of RHA samples based on X-ray fluorescence test results.

RHA sample	Chemical composition (% wt. of ash)							
	SiO_2	Al_2O_3	Fe_2O_3	CaO	K_2O	P_2O_5	SO_3	MnO
RHA-A	92.10	1.066	0.241	0.719	1.366	0.403	0.076	0.109
RHA-B	89.31	1.389	0.391	0.987	1.813	0.747	1.104	0.166
RHA-C	84.30	1.066	0.175	0.729	1.522	0.675	0.083	0.144
RHA-C5	93.49	1.186	0.202	0.971	1.587	0.663	0.084	0.115

4.5 RHA loss on ignition

The residual carbon content (loss on ignition) of RHA samples are presented in Table 4.6. The result (based on EN 196-2:1994) show that RHA-C contains the maximum quantity of residual carbon. The black color of RHA-C is also an indicator for the high carbon content. However, it is within the limitation of ASTM C618-94a (12% wt. of the total weight of ash). The re-burning process of RHA-C converted the black ash to a light gray color (RHA-C5) resulting remarkably improvement in the silica content of ash. RHA-A and B have a low carbon content.

Table 4. 6: Loss on ignition of RHA samples.

RHA Samples	RHA-A	RHA-B	RHA-C	RHA-C5
Loss on ignition (% wt. of RHA)	3.80	5.10	11.35	1.65

4.6 Pozzolanic activity

To determine the pozzolanic activity several methodologies are developed by various researchers, such as accelerated pozzolanic strength reactivity index (Van Tuan et al., 2013). Another method is the rapid evaluation of pozzolanic activity by conductivity measurement, which is reported by Luxan et al. (1989). This method measures the conductivity level of a calcium hydroxide [$Ca(OH)_2$] saturated solution before and after adding pozzolanic material. Pozzolanic activity is the extent of the chemical reaction occurring between the active silica, calcium hydroxide, and water. Thus, the pozzolanic activity of RHA is directly related to the content of amorphous silica in the ash. This aspect (pozzolanic activity) was evaluated by the indirect method through the variation in the electrical conductivity in the first two minutes as introduced in the experimental method part 3.3.4. Table 4.7, shows the difference in the electrical conductivity of the RHA solutions using RHAs with different mean particle sizes of RHA. The results indicate that the reactivity of RHA is lower for ashes with coarse particles (RHA-A and B). However, with increasing fineness of RHA particles (RHA-C and C5) indicating of the high reactivity of ash. This may be caused by the grinding level, which influences the exposed surface area of RHA particles and also the porous structure of RHA, i.e. collapsing the structure of particles as suggested by Mehta (1994), Bui et al. (2005), and Van Tuan et al. (2010).

Table 4.7: The evolution of electrical conductivity of RHA pozzolanic activity at 40°C.

RHA Samples	RHA-A	RHA-B	RHA-C	RHA-C5
Variation in the electrical Conductivity variation (mS/cm)	0.90	1.07	1.81	1.73
Mean particle size (μm)	23.39	20.94	15.80	12.64

4.7 pH value of RHA samples

The result of the pH value of RHA dispersed in demineralized water is presented in Table 4.8. It is evident that pH of the RHA solution increased with increasing reactivity of ash. This is likely to affect the pH value of the pore solution in the mortar or concrete, when RHA is added in the system. The change of the pH value of the de-ionized water in the presence of RHA, with the maximum pH value of 9.44 with RHA-C5. Which is confirmed the relationship between the pozzolanic reactivity and pH value of ash.

Table 4. 8: pH value of RHA dispersed in the demineralized water ashes.

RHA	A	B	C	C5
pH degree	8.89	9.04	9.79	9.57

4.8 Microstructure of RHA samples

It is essential to know the shape, size and morphological characteristics of the RHA particles used to understand and explain some of the results on flow, strength, and shrinkage. The microstructure of RHA samples was investigated with a scanning electron microscopy (SEM ZEISS model Gemini SEM500). The scanning electron micrographic (SEM) observation of 5.00KX (500 times magnification) with a resolution of 10µm and 2µm for RHA (A, B, C and C5) samples are presented in Figures 4.3 and 4.4. The observation from scanning images show that the surface of the RHA-A particle structure looks like overlapping sheets with protuberances, distributed over a wide size range with variation in particle size shapes. Comparing particles of RHA-B to RHA-A, it is dispersed better with irregular and vesicular appearance with more porous microstructure. RHA-C structure shows more porous microstructure, systematic and uniform size compared to RHA-A and B.

Microscopic observation of RHA-C5 ash reveals the small particles that are formed by deformation or collapse of the structure in some parts of the inner shell of RHA-C after burning at 550°C/6h (Fig.4.3). Additional nano and macro pores in the range of 0.060 and 7.80 µm are observed after the fracturing of some parts of RHA-C5 sample. Finally, the results of the SEM investigations can now be used to interpret the particle size distribution and specific surface area of the RHA samples calculated via laser diffractometer. The intraparticle meso-and macrospores of the RHA samples generate the remarkably high specific surface area of the materials. RHA-A and B has showed smaller specific surface areas compared to RHA-C and C5. The result of the RHA-A and B interaction of various factors like (i) formation of larger particles via agglomeration of some smaller particles; (ii) increase in the macro porosity and iii) formation of crystalline silica. These phenomena do not occur in the RHA-C and C5 samples.

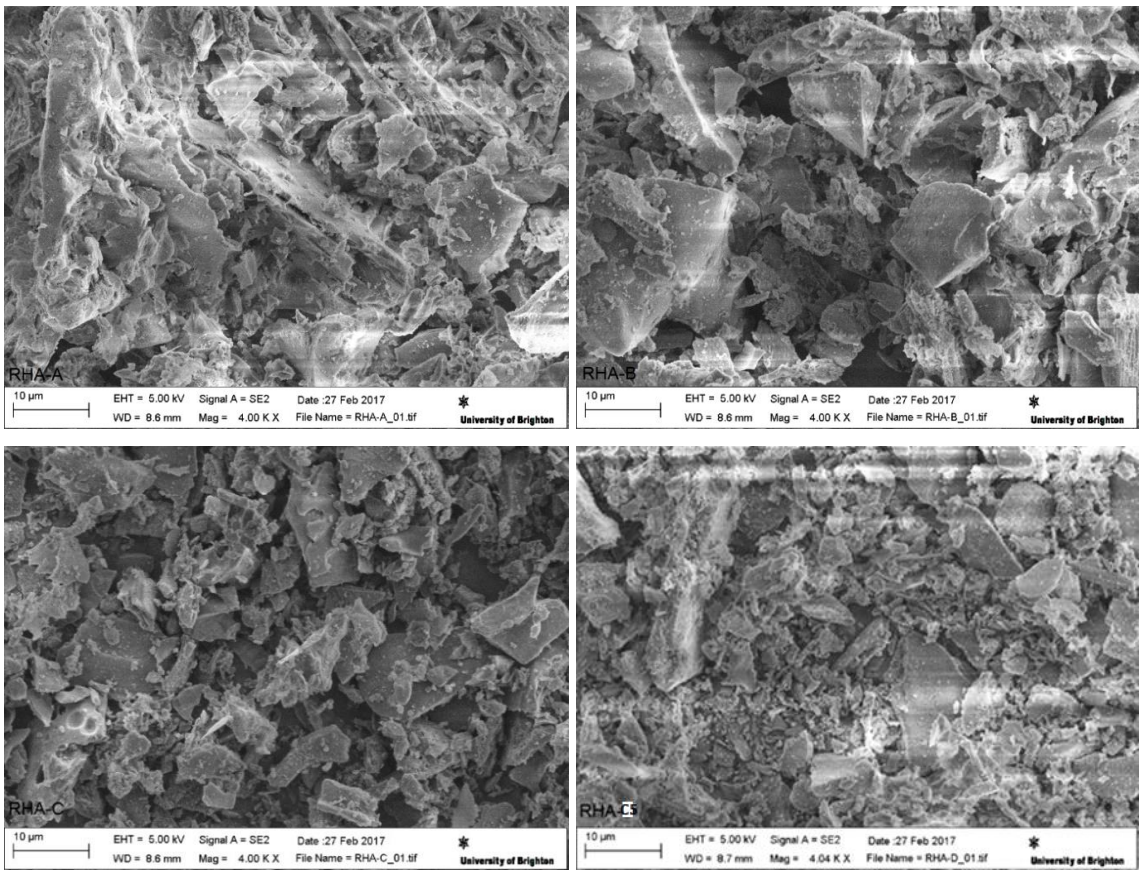

Figure 4.3: Scanning electron micrograph (SEM) of RHA particles ground for: RHA-A, RHA-B, RHA-C and RHA-C5 at 10µm.

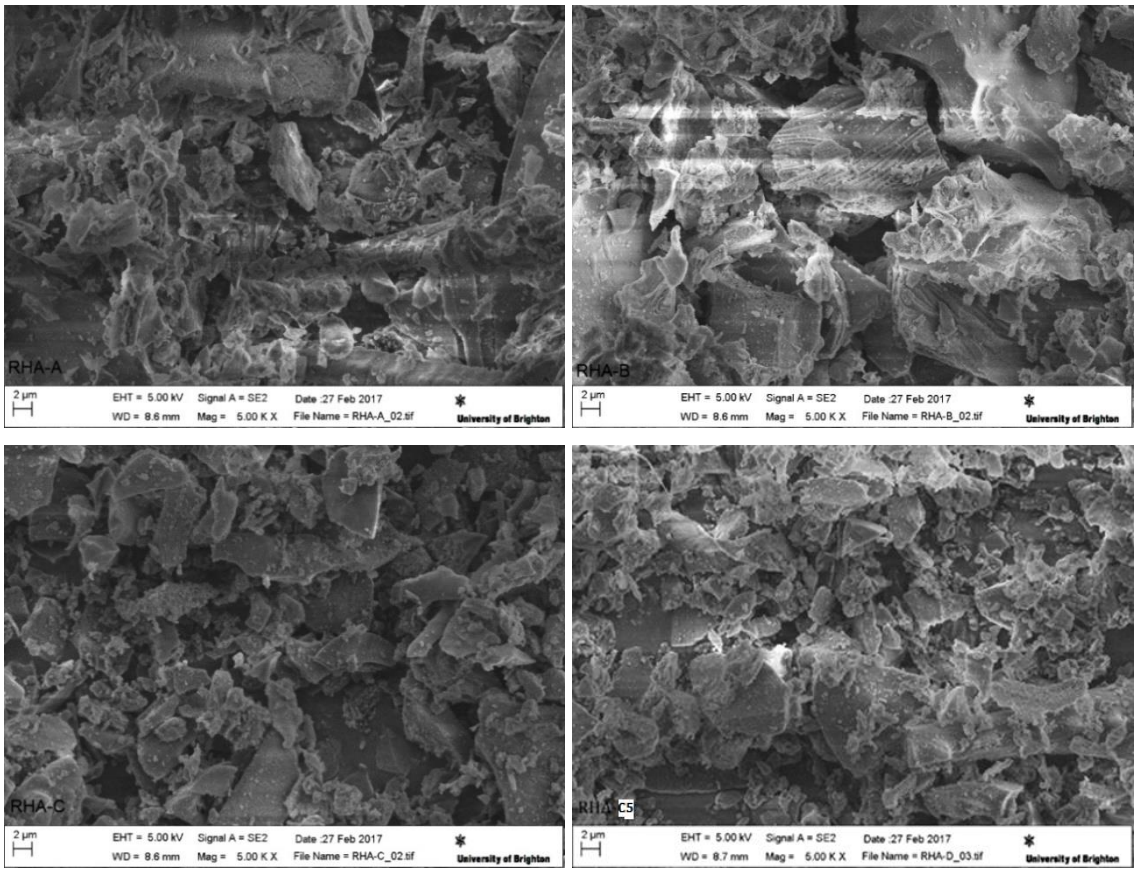

Figure 4.4: Scanning electron micrograph (SEM) of RHA particles ground for RHA-A, RHA-B, RHA-C and RHA-C5 at 2μm.

4.9 Conclusion

From the results obtained, the following conclusions can be drawn:

i. Re-burning of rice husk ash (RHA-C) at 550°C for 6hrs decreases the particle size of RHA and increase the specific surface area (RHA-C5).
ii. RHA properties were suitable for producing mortar or concrete mixtures, as they met the ASTM specified physical and chemical requirements.
iii. The chemical compositions of the RHA shown that the chemical components were also confirm to ASTM and no impurities were present above the maximum permissible limit is, such as loss on ignition.
iv. Heat treatment (550°C for 6hrs) of RHA-C sample lead to an increase of silica content and reduction of carbon content by about 85%.
v. Rice husk ashes with high contents of amorphous silica (RHA-C) are very porous and have extensive specific surface area.
vi. The particle size analyses of the RHA materials revealed that all RHA types were well-graded and lower than OPC cement particles size.

CHAPTER 5: EFFECT OF RHA PROPERTIES ON THE STRENGTH AND DRYING SHRINKAGE OF MORTAR

5.1 Introduction

It has been observed from literature review in Chapter two that there are variable effects of RHA properties on the performance of concrete. Therefore, the aim of the experimental investigation was to examine the chemical composition and physical properties of RHA on the possibility of using RHA as a blending material for cement at high replacement ratio (> 30%). The evaluation was based on the investigation of the pozzolanic activity, silica content, and fineness of particles of four types of RHA. The change of the hydration products in the cement paste containing different types and amounts of RHA was also investigated.

5.2 Materials and methods

The materials used throughout this Chapter were introduced in Chapter Three. The test programme included three basic materials, cement, RHA and silica sand. In the test programme, constant water to binder ratio of 0.50 was used. The mix design was used in the experimental studies is shown in detail in Chapter 3, section 3.6.1. The study was based on thirty-two mixtures; the measured parameters are workability, compressive and tensile strength. The superplasticizer dosage was constant (0.25%) up to 20% replacement ratio; beyond that, it was increased with increasing replacement ratio.

5.3 Experimental results

5.3.1 Flowability of RHA mortar

Consistency (flowability) of the RHA reference mortar is shown in Fig.5.1 and presented in Table 5.1. Flow ability was evaluated by table flow according to BS EN 1015-03:2004. It can be seen that the incorporation of RHA decreased flowability compared to the reference sample from 255mm (OPC) to 98mm (80% RHA-C5 + 46% SP). This decrease in flowability occurs due to the high specific surface area of the RHA. The reduction of flowability caused by RHA is partially counter-acted by the increasing dosage

superplasticizer as shown in Fig. 5.1. A similar approach was used by many authors, e.g. Bui et al. (2005), Khan et al. (2012). In general, the flowability of mortar relies on the water-binder ratio and the sand (Safiuddin et al., 2011). With increasing replacement ratio, RHA will subsequently absorb a certain amount of mixing water on it is surface and, in the pores, resulting in a decrease in free water and lower flowability (Christopher et al., 2017). The flowability values are not what may expect from the specific surface area of RHA-A, B, C and C5 (0.537, 0.587, 0.691 and 0.808 m^2/g, respectively) as the mortar with coarser RHA particles (RHA-A and B) with irregular shape and coarser particles shows lower flowability. This slightly paradox result can be explained by the porous structure of the RHA particles. The porous structure of very finely ground RHA collapses. Therefore, the coarser RHA types have a higher water demand as more water is trapped inside the pores of the RHA particles. These results agree with the conclusions of Bui et al. (2005) results; however, contradict of the results reported by Cordeiro and Filho (2008). According to these authors, the high specific surface area of RHA decreases the flowbility of fresh mixture. With increasing replacement ratio up to 70%, RHA-A and B mortars reached a point where no more flowability was exhibited even when the superplasticizer dosage was increased to 10 - 12% of total weight of the binder. This limited the replacement ratio of RHA-A and B up to 60%. In addition to the grain size, the higher content of crystalline silica of RHA-A and B may be another factor resulting in decrease in workability of the mixtures. Crystalline silica is reported to have a higher internal porosity resulting in reduced followability (Bui et al., 2012).

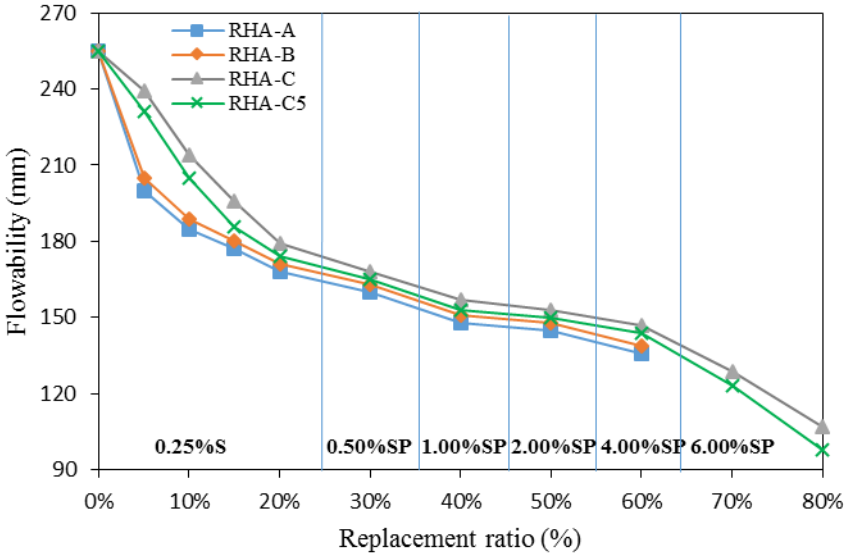

Figure 5.1: Flowability of RHA mortars mixtures at different replacement ratio.

Table 5.1: Flowability of the RHA mortar mixtures.

RHA %	Flow table (mm)				SP*(%)
	RHA-A	RHA-B	RHA-C	RHA-C5	
5%	200	205	239	231	0.25
10%	185	189	214	205	0.25
15%	177	180	196	186	0.25
20%	168	171	179	174	0.25
30%	160	163	168	165	0.50
40%	148	151	157	153	1.00
50%	145	148	153	150	2.00
60%	136	139	147	144	4.00
70%	-	-	129	123	6.00
80%	-	-	107	98	6.00
OPC	255				0.25

SP*: Superplasticizer (%wt. of binder

5.3.2 Compressive strength

5.3.2.1 Compressive strength of RHA mortar at 7 days' age

The average compressive strength of five RHA mortar specimen at various replacement ratios is shown in Table 5.2, and presented in Fig.5.2, while the ratio of strength development compare to the reference sample are presented in Table 5.3. It is obvious that at early ages, the higher content of crystalline silica, coarse particles size and RHA replacement ratio, the lower the compressive strength. Despite the expected slow reaction of RHA as pozzolanic material, the compressive strength of the RHA samples (RHA-C and C5) are higher than that of the OPC control mortar up to 10% RHA-C and 15% RHA-C5. Micro particles may act as fillers or crystallization nuclei accelerating the formation of C–S–H gel (Givi et al., 2012). Compressive strength was reduced with increasing of RHA replacement ratio. The most likely explanation for this effect is the increase of replacement ratio (Engelhard et al., 1995 and Chindaprasirt and Rukzon, 2008).

Table 5.2: Compressive strength results of control and RHA mortars at age of 7-days.

%RHA	SP%	RHA			
		A	B	C	C5
5	0.25	32.75	33.87	37.97	38.32
10	0.25	31.87	31.04	36.13	37.40
15	0.25	31.02	30.39	34.94	35.07
20	0.25	29.08	28.82	32.97	33.67
30	0.50	28.91	26.77	30.55	30.47
40	1.00	26.82	23.12	27.24	28.64
50	2.00	20.00	17.16	20.82	27.81
60	4.00	11.16	9.59	16.34	23.02
OPC mortar	0.25	35.40			

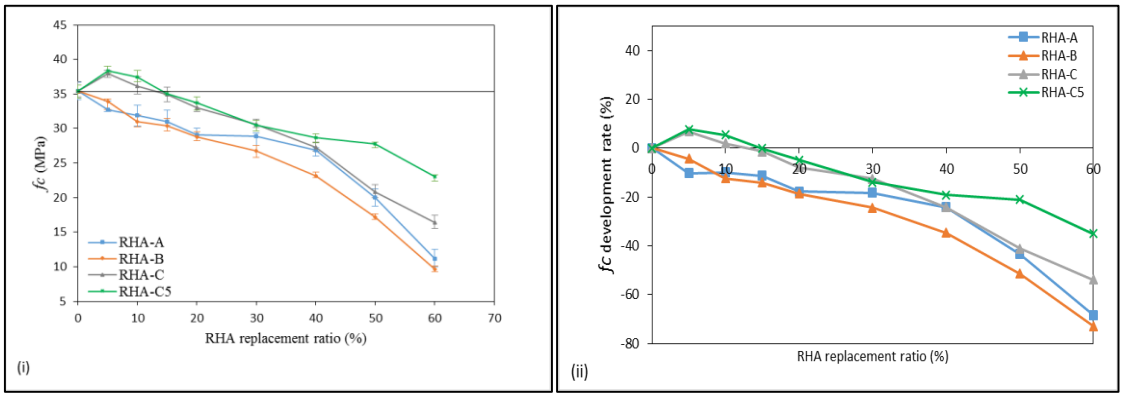

Figure 5.2: Compressive strength development of RHA mortar at age of 7-days; (i) compare compressive strength to replacement ratio, (ii) % rate of compressive strength development to replacement ratio.

Table 5.3: The rate of RHA mortar compressive strength compared to OPC mortar at 7 days.

% Replacement ratio	RHA types			
	A	B	C	C5
5%	-10.31	-4.320	6.769	7.620
10%	-9.970	-12.32	2.020	5.350
15%	-11.24	-14.15	-1.300	-0.093
20%	-17.85	-18.59	-7.790	-4.890
30%	-18.33	-24.38	-12.63	-13.92
40%	-24.24	-34.69	-24.29	-19.10
50%	-43.50	-51.53	-41.19	-21.14
60%	-68.47	-72.91	-53.84	-34.97

5.3.2.2 Compressive strength of RHA mortar at age of 28 days

The compressive strength results of the RHA samples at 28 days are presented in Table 5.4, and shown in Fig.5.3. In general, the increase in compressive strength of RHA-C and especially the RHA-C5 series mortar from 7 to 28-days of curing is a result of the smaller

grain size of these RHA types. The strength of RHA-C and RHA-C5 is higher than the control up to 30% and 40% replacement ratio, respectively. There is a maximum replacement ratio for each type of RHA. Beyond that the strength is lower than control mortar. This reduction in compressive strength may be because the quantity of RHA present in the mixture exceeds the amount of liberated lime during the hydration process (Al-Khalaf and Yousif, 1984) or the slower pozzolanic reaction. Moreover, the RHA porosity also plays an essential role. The higher the volume of the pores, the lower the strength of the concrete will be (Hwang et al., 2011). This may explain the low strength of RHA-A and RHA-B mortars, which is lower than the control mortar, except at replacement ratio of 30% and 20% respectively.

Table 5. 4: Compressive strength results of control and RHA mortars at age of 28-days.

%RHA	SP%	RHA			
		A	B	C	C5
5	0.25	40.42	43.07	48.53	49.17
10	0.25	42.76	44.42	50.24	50.56
15	0.25	43.83	45.08	49.91	53.95
20	0.25	44.90	47.42	48.10	56.43
30	0.50	46.30	42.66	47.79	55.94
40	1.00	43.38	40.61	45.43	48.96
50	2.00	35.36	31.16	39.72	42.55
60	4.00	24.08	19.12	32.82	39.59
OPC mortar	0.25	45.50			

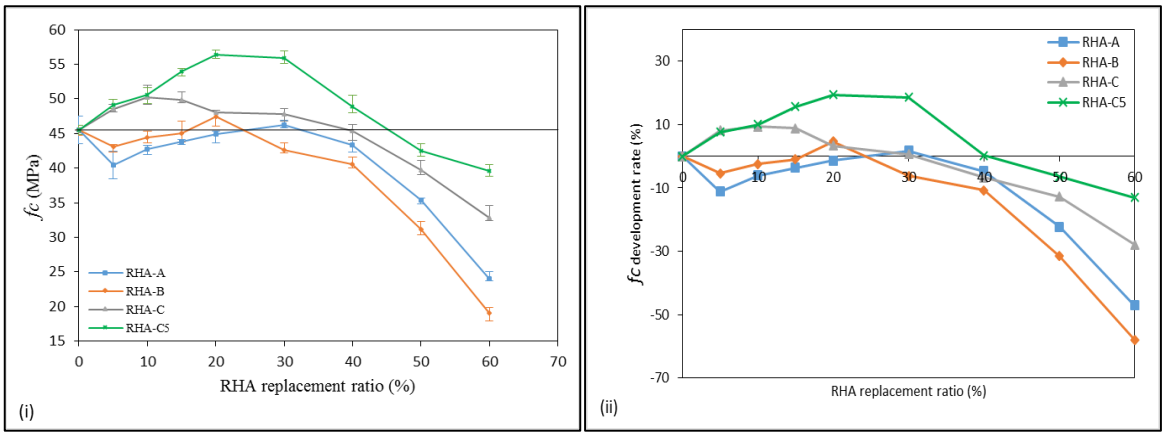

Figure 5.3: Compressive strength development of RHA mortar at age of 28-days; (i) compare compressive strength to replacement ratio, (ii) % rate of compressive strength development to replacement ratio.

5.3.2.3 Compressive strength results at the age of 91-days

The average compressive strength results of various replacement ratios are presented in Table 5.5 and shown in Fig. 5.4 (i, ii), while the rate of strength development versus time (7, 28, and 91-days) are presented in Figure 5.4 (iii, iv, v and vi). Generally, there has been

a great improvement of the strength of nearly all RHA mortar at the age of 91-days. The incorporation of the RHA increases the strength of RHA mortar at 91 days, possibly due to the internal water curing effect. Furthermore, the pozzolanic reaction of RHA indicated by the CH consumption occurs to the great extent at this age inducing a significant pore refinement. Even if all CH of cement hydration is consumed by the pozzolanic reaction, RHA grains can act as filler and reduce the porosity of the mixtures significantly (Fig.5.5). These results in an increase in the compressive strength of mortar samples containing RHA compared to that of the reference sample at late ages.

Table 5. 5: Compressive strength results of control and RHA mortars at age of 91-days.

%RHA	%SP	RHA			
		A	B	C	C5
5	0.25	45.20	49.66	55.65	57.91
10	0.25	49.25	52.10	56.15	59.41
15	0.25	51.29	53.16	56.47	61.79
20	0.25	52.38	55.00	60.21	63.01
30	0.50	54.70	52.08	57.79	64.25
40	1.00	52.57	51.86	55.71	59.24
50	2.00	50.38	48.04	54.44	55.97
60	4.00	47.04	42.20	53.34	54.16
OPC mortar	0.25	48.81			

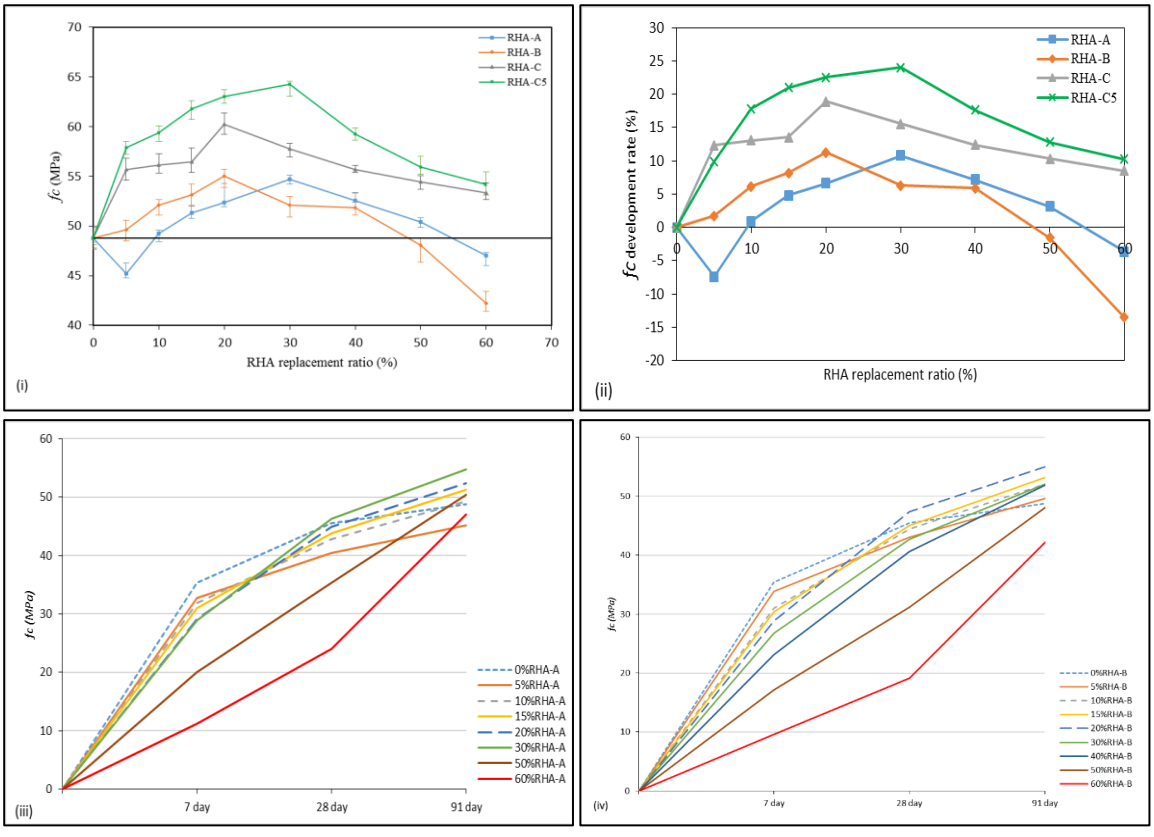

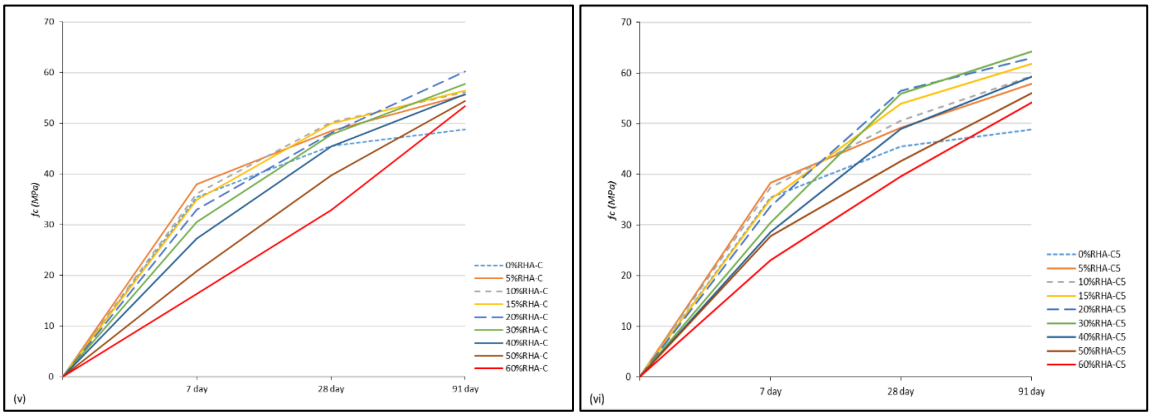

Figure 5.4: Compressive strength development of RHA mortar at age of 91-days; (i) compare compressive strength to replacement ratio, (ii) % rate of compressive strength development to replacement ratio, (iii, iv, v and vi) Compressive strength (f_{cu}) versus time (7, 28 and 91-days).

The continuous progression in compressive strength is a result of the reaction of RHA; it proves the validity of the theory by Engelhard et al. (1995). With higher contents of amorphous silica in RHA more C-S-H gel will be produced by rpozzolanic reaction (Ikpong and Okpala, 1992). The improvement in compressive strength of RHA-A blended mortar compared to the control mortar ranged in between 0.893% to 10.77%, which is showing a remarkable strength gain, despite the lower compressive strength at an early age (7days). Similarly, RHA-B has demonstrated noteworthy development in compressive strength up to 40% replacement ratio. RHA-B achieved better compressive strength than RHA-A at a replacement ratio between 5% and 20%.

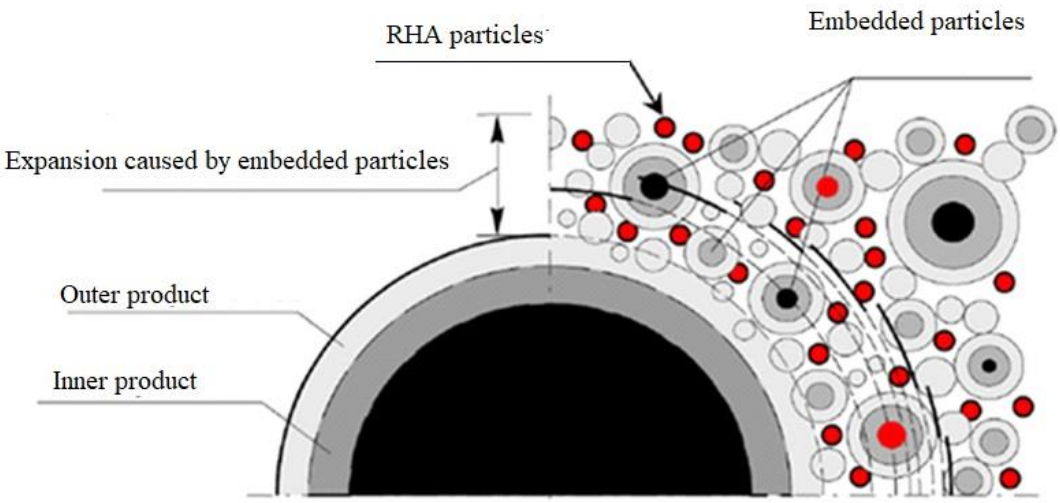

Figure 5. 5: The embedding of RHA particles concept

The better performance of RHA-B compared to RHA-A, up to 20% replacement ratio can be attributed to the higher amount of amorphous silica content. To evaluate the obtained experimental results, the results reported by other researchers are shown in Table 5.7 for comparison. Previous work showed a discrepancy in RHA effect, where the results presented by Jamil et al., (2013) and Chindaprasirt et al. (2008) shown improvement in strength up to 30 and 40% replacement ratio. On the other hand, Coutinho and Papadakis (2011) results show a remarkable reduction in RHA mortar strength at 10 and 15% replacement ratio compared to OPC control. Generally, this contradiction in strength results can be attributed to the the fineness of RHA particles which is dramatically influences it is pore structure.

Hence, the pozzolanic reaction process and the cement hydration process in the blended cement paste, thus results in a difference in the development of the compressive strength of mortar. However, the experimental results show that the positive effect of RHA on the compressive strength of mortar incorporating RHA with various mean particle size (MPS) can be explained as follows: The fine RHA improves the packing density of granular mixture because of it is filler effect. RHA particles might be the weakest point in the matrix especially at the late age because of their pore structure. The negative effect of RHA is more significant with the coarser particles. Therefore, it can be suggested that the positive effect of the finer MPS of RHA might be dominant at the late age resulting in the higher compressive strength of finer RHA containing sample compared to the coarser RHA containing sample and the reference sample. As a conclusion, partial replacing of cement up to maximum 60 weight percent by RHA (C and C5) could considerably improve the compressive strength of concrete due to the formation of more C–S–H gel.

Table 5. 6: The rate of RHA mortar compressive strength development compare to OPC mortar at age of 28 and 91days.

RHA%	RHA compressive strength (28-days)				RHA compressive strength (91-days)			
	A	B	C	C5	A	B	C	C5
5%	-11.16	-5.34	8.14	7.64	-7.401	1.711	12.29	9.89
10%	-6.022	-2.374	9.43	10.01	0.893	6.14	13.07	17.84
15%	-3.67	-0.92	8.84	15.66	4.835	8.183	13.56	21.01
20%	-1.32	4.68	3.4	19.37	6.637	11.25	18.93	22.54
30%	1.73	-6.24	0.63	18.66	10.77	6.279	15.54	24.03
40%	-4.66	-10.75	-6.75	-2.99	7.152	5.881	12.39	17.6
50%	-22.29	-31.52	-12.7	-6.48	3.116	-1.578	10.34	12.79
60%	-47.08	-57.98	-27.87	-12.99	-3.626	-13.54	8.493	10.21

Table 5. 7: Compressive strength results of RHA blended mortars according to the literature.

RHA (%)	w/b	Compressive strength (MPa)			References
		7	28	91	
0%	0.50	38.7	48.0	53.3	Coutinho and Papadakis (2011)
10%A		37.0	42.5	48.4	
15%A		37.5	42.9	49.0	
10%Θ		38.6	44.6	49.1	
15%Θ		37.0	42.6	47.7	
0%	0.50	43.5	57.0	60.0	Chindaprasirt et al. (2008)
20%		44.5	59.5	63.5	
40%		33.0	56.5	62.0	
0%	0.50	-	37.0	-	Jamil et al. (2013)
5%		-	38.9	-	
10%		-	42.8	-	
15%		-	46.7	-	
20%		-	39.8	-	
25%		-	38.3	-	
30%		-	37.0	-	
35%		-	36.0	-	

5.3.3 Tensile strength

5.3.3.1 Tensile strength performance at age of 28 days

The results of tensile strength and rate of development to OPC mortar are presented in Table 5.8, and plotted in Fig.5.6. As with the compressive strength, the results indicate that the effect of RHA on the tensile strength is different with different characteristics of RHA. Considering the tensile strength values of mortars made with all four RHA types against the control values, it can be concluded that the RHA-C and C5 ashes showed a remarkable improvement. In this way the values of tensile strengths of these mortars are a consequence of the formation of hydrated compounds, like calcium silicates, resulting from the pozzolanic reactions. On the other hand, the tensile strength of RHA- A and B tend to decline with the coarser particles. The decrease in tensile strength of RHA-A and B at high replacement ratio may be due to the RHA particles acting as porous micro-fine aggregate. Therefore, the results indicate that the pozzolanic reaction and formation of crystallization nuclei may be more prominent than the filler effect, as fillers are not expected to increase the tensile strength. These weaken the matrix and pores may act as starting points of micro-cracks, hence reduce the tensile strength of RHA mortar (Le et al., 2014).

Table 5.8: Tensile strength and ratio of strength development results of RHA mortars compare to OPC mortar at age of 28-days.

%RHA	RHA							
	A	% to OPC	B	% to OPC	C	% to OPC	C5	% to OPC
5	3.19	15.9	3.05	12.1	3.23	17.0	3.66	26.8
10	3.30	18.8	3.13	14.4	3.61	25.8	3.82	29.8
15	3.12	14.1	2.97	9.76	3.70	27.6	3.97	32.5
20	2.94	8.84	2.80	4.29	3.79	29.3	4.18	35.9
30	2.78	3.59	2.59	-3.35	3.87	30.7	4.08	34.3
40	2.63	-1.86	2.27	-15.3	3.55	24.5	3.78	29.1
50	2.48	-7.46	2.15	-19.7	3.39	20.9	3.61	25.8
60	2.31	-13.8	2.06	-23.1	3.19	11.8	3.32	19.3
OPC mortar	2.68							

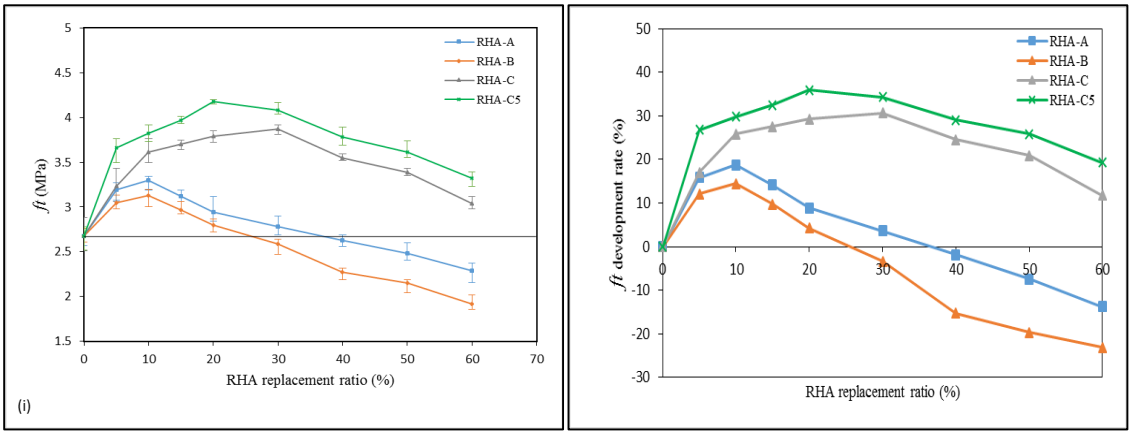

Figure 5. 6: (i) Tensile strength of RHA blended mortar at age of 28 days; (ii) Tensile strength performance in relation to the RHA replacement ratio.

5.3.3.2 Tensile strength performance at age of 91 days

The tensile strength and rate of development to OPC mortar formulated from different types of RHA are given in Table 5.9, and displayed in Fig.5.7 (i and ii), while the development of tensile strength versus time presented in Figure 5.7 (iii, iv, v and vi). It can be seen that tensile strength of mortar containing the fine RHA (RHA-C and C5) were higher than that of the sample containing coarse one (RHA-A and B) regardless of age. Therefore, it can be said that the fine RHA has a stronger effect on tensile strength than the coarse one at late ages, e.g. 91days. This result of tensile strength fit is well with the result of the pozzolanic reactivity of RHA analyzed previously. Tensile strength of the RHA-C5 with that of RHA-C was significantly higher. The result is closely related to the 91-day pozzolanic reactivity of RHA-C5 indicated by the consumption of CH. Generally, the development of tensile strength of RHA mortar is correlated to the time-dependent pozzolanic reactivity of RHA, the cement hydration process and the microstructure development (Lee, 2015).

Incorporation of the porous RHA increases the degree of cement hydration at 91 days, possibly due to the internal water curing effect. Furthermore, the pozzolanic reaction of RHA indicated by the CH consumption occurs to the great extent at this age inducing a significant pore refinement. Fineness of RHA dramatically influences it is pore structure, specific surface area (SSA) and hence the pozzolanic reaction process and the cement hydration process in the blended cement paste. The pozzolanic reaction takes place on both surface areas successively. The hydrated products, i.e. C-S-H phases, generated from the "external pozzolanic reaction" refine the pore structure of the cement matrix surrounding RHA particles meanwhile the whole or a main part of products of "internal pozzolanic reaction" consolidates the pore structure of RHA particles.

Table 5.9: Tensile strength and ratio of strength development results of RHA mortars compare to OPC mortar at age of 91-days.

%RHA	RHA							
	A	% to OPC	B	% to OPC	C	% to OPC	C5	% to OPC
5	3.25	7.38	3.12	3.52	3.98	24.4	4.48	32.8
10	3.77	20.2	3.35	10.1	4.19	28.2	4.58	34.3
15	4.14	27.3	3.89	22.6	4.47	32.7	4.82	37.6
20	4.25	29.2	4.07	26.0	4.86	38.1	5.14	41.4
30	4.46	32.5	4.33	30.5	4.56	34.0	4.81	37.4
40	4.04	25.5	3.95	23.8	4.22	28.7	4.32	30.3
50	3.56	15.4	3.46	13.0	3.97	24.2	4.13	27.1
60	3.11	3.21	3.00	-0.33	3.84	21.6	4.06	25.7
OPC mortar	3.01							

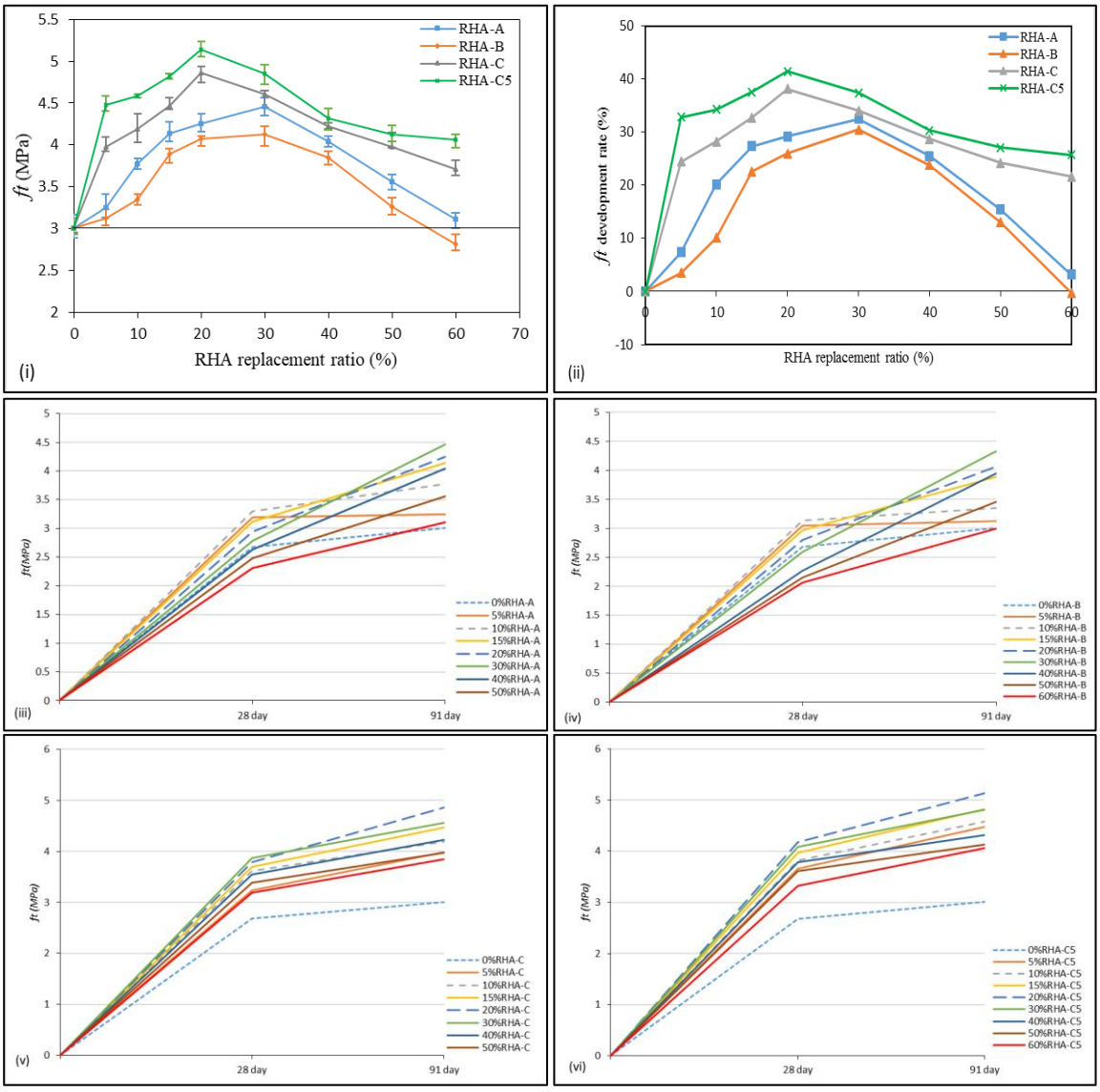

Figure 5. 7: (i and ii) Effect of RHA properties on tensile strength of mortar at age of 91days, (iii, iv, v and vi) rate of tensile strength development versus time (28 and 91days).

5.3.3.3 Comparison the results to the literature

In general, there are very rare attempt to obtain tensile strength in mortar containing RHA. Except the research has been carried out by Saraswathy and Kwon (2014), therefore it has to combine results with splitting tensile strength of concrete to understand more the RHA factors influencing the strength for normal mortar. Results of tensile strength conducted to RHA mortar at 28 days are compared to literature data of similar tests shown in Table 5.10. With increase replacement ratio the tensile strength is decreased. The works of Le et al. (2014) also witnessed an increase up to 10% replacement of cement with RHA, and then began to be decrease onward. RHA used by the author consist of 86.81% silica, 4.6% loss on ignition, 1.04% CaO, and 8.42μm mean particle size. Using the data obtained in the investigation carried by Abalaka (2013) where RHA content of 95.41% silica, which is consist of 90% amorphous silica, 0.77% loss on ignition, and 235m^2/kg specific surface area (SSA).

Sarawathy & Kown (2014) stated that tensile strength results are confirmed that the tolerable limit of replacement of RHA found to be 10%, where RHA used content of 85.49% silica, loss on ignition 3.02%, and 3.68% CaO, which is considered high for RHA. Comparison the results of pervious researchers, it is clear that the good performance of Abalaka (2013) results can be attributed to the high silica content (95.41%) and very low LOI (0.77%) compare to 86.81% silica and 4.6%LOI of RHA used by Le et al. (2014). According to the previous researches, at least up to 10% cement replacement with RHA will result in strength development comparable to the control specimens which is aligned with results of RHA-A and B. However, the optimum replacement level of RHA in this study shown that RHA increase tensile strength up to 30% (RHA-C). The experimental results also shown that tensile strength was recorded for RHA-C and C5 at 60% replacement ratio are higher than OPC mortar (see Table 5.6). Generally, this high performance of each of RHA-C and C5, were mainly due to the amorphous silica content and high specific surface.

Table 5.10: Tensile strength of RHA mortar according to the published literature (28-days).

Mix	w/b	*ft* (MPa)	rate of strength development (%)	Reference
0%		2.94	-	
10%		3.10	5.16	
15%	0.52	3.05	3.61	Sarawathy & Kown (2014)
20%		2.89	-1.70	
25%		2.54	-13.61	
30%		2.31	-21.43	
0%		5.1	-	
5%		5.6	8.93	
10%	0.32	6.5	21.54	Le (2014)
15%		6.0	15.00	
20%		5.4	5.56	
0%		2.62	-	
5%		3.48	24.71	
10%	0.50	3.40	22.94	Abalaka (2013)
15%		3.69	28.99	
20%		3.29	20.36	

5.3.3.4 Tensile to compressive strength correlation of RHA mortar

In the experimental results of tensile strength (f_t) and compressive strength (f_c') were plotted against the calculation results by means of the existing equations listed in Table 5.11, as shown in Fig.5.9. Based on the results, the empirical relation suggested by ACI Building Code (Neville, 1995) where used.

$$f_t = 0.56\ (f_c)^{0.5} \tag{5.1}$$

According to the results, the 28 age of mortar were not proportional to 0.5 power of *fc'*. Where, RHA-A results are closely to the 0.47 power of *fc'.* Similar commentaries were also given by each of Neville (1996) and Gajendran et al. (2015).

$$f_t = 0.56\ f_c^{0.47} \tag{5.2}$$

While, RHA-B results are close to 0.44 power *fc.*

$$f_t = 0.56\ f_c^{0.44} \tag{5.3}$$

Meanwhile, 0.485 power of *fc*' seems to be close more with the test results of RHA-C and C5. Whereas, the results of 91 days found to be very close to the empirical relation equation in the prediction of f_t with types of RHA-A. While, less accuracy with RHA-B, even not proportional to 0.5 power of *fc'*; however, the relationships fitted best with the following equation:

$$f_t = 0.56\ (f_c)^{0.47} \tag{5.4}$$

According to the results of 28 days, the RHA-C and C5 is 0.485 power of *fc*' as shown in equation 5.5:

$$f_t = 0.55\ (f_c)^{0.485} \quad (5.5)$$

Additionally, as shown in Fig.5.9, the predicted results of RHA-C and C5 mortar f_t from *fc'* based on the results, were found to fit to the empirical relation suggested by ACI Building Code expressed as;

$$f_t = 0.59\ (f_c)^{0.5} \quad (5.6)$$

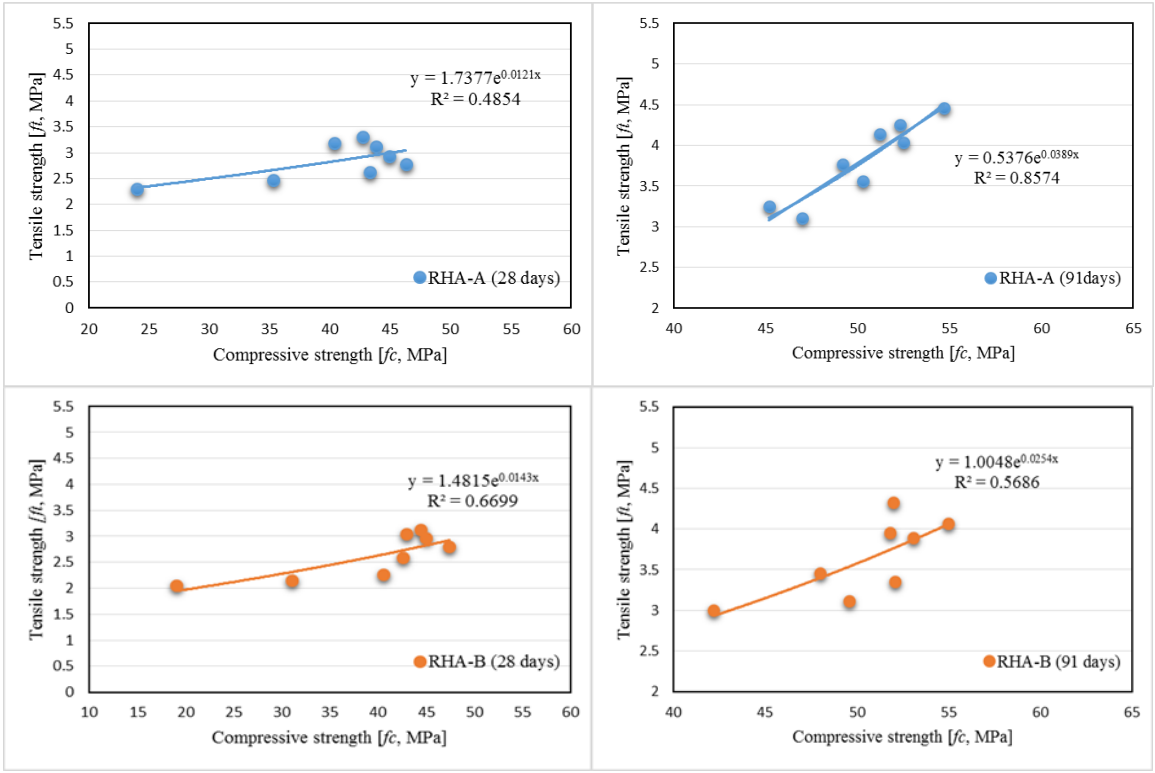

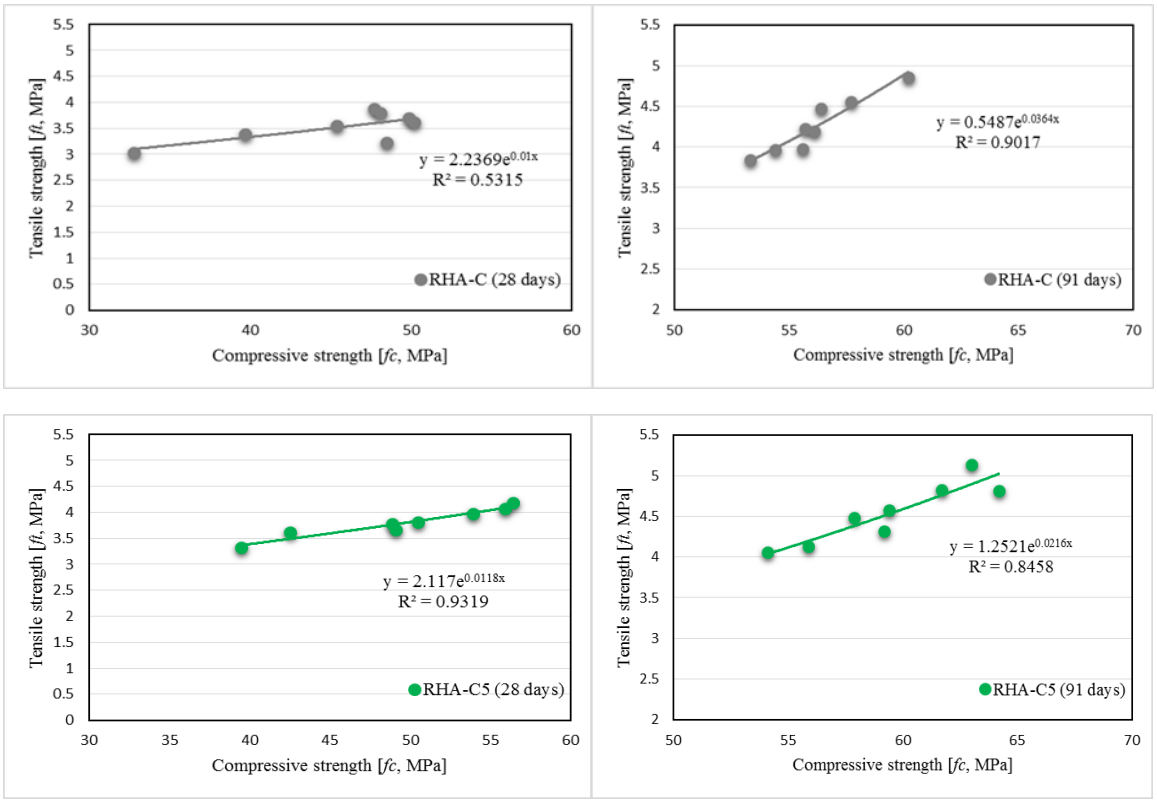

Figure 5. 5: Tensile-compressive strength relationship for RHA mortars at age of 28 and 91-days.

Table 5. 11: Tensile strength to compressive strength of RHA mortars at age of 28 and 91-days.

Mixture	Tensile to compressive strength ratio (%)											
	RHA-A						RHA-B					
	28day			91day			28day			91day		
	fc	*Ft*	*ft/fc*	*fc*	*ft*	*ft/fc*	*fc*	*ft*	*ft/fc*	*fc*	*ft*	*ft/fc*
5%RHA	40.4	3.19	7.89	45.2	3.25	7.19	43.0	3.05	7.08	49.6	3.12	6.28
10%RHA	42.7	3.30	7.72	49.2	3.77	7.65	44.4	3.13	7.05	52.1	3.35	6.43
15%RHA	43.8	3.12	7.12	51.2	4.14	8.07	45.0	2.97	6.59	53.1	3.89	7.32
20%RHA	44.9	2.94	6.54	52.3	4.25	8.11	47.4	2.8	5.90	55.0	4.07	7.40
30%RHA	46.3	2.78	6.00	54.7	4.46	8.15	42.6	2.59	6.07	52.0	4.33	8.31
40%RHA	43.3	2.63	6.06	52.5	4.04	7.68	40.6	2.27	5.59	51.8	3.95	7.62
50%RHA	35.3	2.48	7.01	50.3	3.56	7.07	31.1	2.15	6.90	48.0	3.46	7.20
60%RHA	24.0	2.31	9.63	47.0	3.11	6.61	19.1	2.06	10.7	42.2	3.00	7.11
OPC mortar	28day								91day			
	Fc			*ft*			*ft/fc*		*fc*	*ft*		*ft/fc*
	45.5			2.68			5.89		48.48	3.01		6.17

Mixture	RHA-C					RHA-C5					
			91day			28day			91day		
	ft	*ft/fc*	*fc*	*ft*	*ft/fc*	*fc*	*ft*	*ft/fc*	*fc*	*ft*	*ft/fc*
5%RHA	3.23	6.66	55.6	3.98	7.15	49.1	3.66	7.44	57.9	4.48	7.74
10%RHA	3.61	7.19	56.1	4.19	7.46	50.5	3.82	7.55	59.4	4.58	7.71
15%RHA	3.7	7.41	56.4	4.47	7.92	53.9	3.97	7.36	61.7	4.82	7.80
20%RHA	3.79	7.88	60.2	4.86	8.07	56.4	4.18	7.41	63.0	5.14	8.16
30%RHA	3.87	8.10	57.7	4.56	7.89	55.9	4.08	7.29	64.2	4.81	7.49
40%RHA	3.55	7.81	55.7	4.22	7.57	48.9	3.78	7.72	59.2	4.32	7.29
50%RHA	3.39	8.53	54.4	3.97	7.29	42.5	3.61	8.48	55.9	4.13	7.38
60%RHA	3.04	9.26	53.3	3.84	7.20	39.5	3.32	8.39	54.1	4.06	7.50

5.3.4 Hydration of mortar formulated from RHA

Generally, properties of concrete (strength and durability) are dependent on the hydration of cement. The main products of the chemical reactions of cement clinker with water, are calcium silicate hydrates (C-S-H), calcium aluminate hydrates (C-A-H) and calcium hydroxide (Papatzani et al., 2014). The hydration is responsible for the "setting and Hardening", which is a sudden loss of plasticity in cement paste due to it is conversion into a solid material that occurs before the development of compressive strength during the hardening of cement (Lea, 1998). The OPC cement hydration process is commonly divided into several periods. These periods are the time of the onset (I), the induction phase (II), the acceleration time (III) and the retardation period phase (IV). (See Chapter 2, Fig.2.2).

The hydration of OPC involves a series of reactions of anhydrous calcium silicate (C_3S and C_2S), aluminates (C_3A and C_4AF), and calcium sulphate phases with water to form hydrated phases (Newman and Cho, 2003). Upon wetting the reactions in Eqs, 1 to 5 occurs (see Chapter 2, section 2.4.1). In general, each of C_3S and C_2S reacts with water and produce a similar type of C–S–H gel which is the primary component giving strength to the cement paste. The hydration of C_3S and C_2S creates calcium hydroxide $Ca(OH)_2$, (CH), which precipitates. Using the chemical reactions and the molecular weight (see Table 5.12) of each element, it is possible to calculate the amount of $Ca(OH)_2$ produced from a certain amount of OPC.

Table 5.12: Molecular weights of cement component.

Molecular weights						
H	O	Ca	Si	Al	Fe	S
1.0079	15.9994	40.078	28.0855	26.9815	55.845	32.065

C_3S equation;

$$2(3CaO{\cdot}SiO_2) + 6H_2O \rightarrow 3CaO{\cdot}2SiO_2{\cdot}3H_2O + 3Ca(OH)_2 \quad (5.7)$$

$456.646 + 108.0924 \rightarrow 342.454 + 222.2844$
$2C_3S \quad 6H \quad 3C\text{-}S\text{-}H \quad 3CH$

1kg OPC contains 623g of C_3S, therefore 303g CH are formed
$623 + 147.6 \rightarrow 467.2 + 303.3$

C_2S equation;

$2(2CaO{\cdot}SiO_2) + 4H_2O \rightarrow 3CaO{\cdot}2SiO_2{\cdot}3H_2O + Ca(OH)_2$ (5.8)

344.5 + 72.1 → 342.5 + 74.1
$2C_2S$ 4H 3C-S-H CH

1kg OPC contains 105.4g of C_2S, therefore 28g CH are formed
105.4 + 22.2 →105.4 +22.8

C_3A equation;

$3CaO{\cdot}Al_2O_3 + Ca(OH)_2 + 12H_2O \rightarrow 3CaO{\cdot}Al_2O_3{\cdot}Ca(OH)_2{\cdot}12H_2O$ (5.9)

270.1944+ 74.092 + 216.1848 → 560.4712
$3C_3A$ CH 12H 3CAC

1 kg OPC contains 73g of C_3A, therefore 20.017g CH are consumed

73+ 20.017+ 58.407 → 151.425 g

C_4AF equation;

$4CaO{\cdot}A1_2O_3{\cdot}Fe_2O_3 + 10H_2O + 2Ca(OH)_2 \rightarrow 6CaO{\cdot}AI_2O_3{\cdot}Fe_2O_3{\cdot}12H_2O$ (5.10)

339.1405 + 180.15 + 148.184→ 667.4785
$4C_4AF$ 10H 2CH C_4AF-hydrate

1kg OPC contains 95g of C_4AF, therefore 42g of CH are consumed

95+ 50.46+41.509 → 186.974

Calcium Sulphate (Gypsum);

According to Uddin and Quayyum (2012) cited from Bensted (1983), calcium sulphate reacts with calcium aluminate hydrate ($4CaO{\cdot}Al_2O_3{\cdot}19H_2O$) to form ettringite as following;

$3(CaSO_4{\cdot}2H_2O)+4CaO{\cdot}Al_2O_3{\cdot}19H_2O+8H_2O\rightarrow 3CaO{\cdot}Al_2O_3{\cdot}3CaSO_4{\cdot}32H_2O+Ca(OH)_2$ (5.11)

1183.131+ 144.123 →1253.32 + 74.0948

$3CS_4H+CAH\rightarrow CA$

1kg OPC contains 50g of Gypsum, therefore 3g CH are produced

50+ 6.090 → 52.966 + 3.131g (CH)

5.3.5 Pozzolanic reaction of RHA silica and calcium hydroxide

With entirely hydrated cement, and no further reaction takes place to form additional C-S-H compounds. Excess calcium hydroxide can affect the strength of concrete. This is simply because it tends to have crystalline growth in one direction (Papadakis et al., 2002). Pozzolanic reaction refers to the process of a siliceous material reacting with calcium hydroxide CH (Papadakis et al., 2002). Pozzolanic reaction will occur when active silica or Al_2O_3-SiO_2 and CH is available in the concrete and form C-S-H gel (Sumadi and Lee, 2008). The reaction is slow and begins after one week and results in more permeable concrete in the early age, which becomes denser with time (Givi et al., 2010). The delay of the reaction is due to two reasons: Firstly, the pozzolan particles form precipitation sites for the early hydration of the OPC components, which delays the reaction. Secondly, glassy silica only can be broken down by the alkalinity of the pore water which requires some period to attain the high pH after the hydration process. Cement gels can reduce the pore size of concrete and by blocking the capillary pores to make the concrete more durable and stronger (Sumadi and Lee, 2008). Based on the chemical equilibrium, the possible reaction between silica and $Ca(OH)_2$ is presented below.

$$2SiO_2 + 3Ca(OH)_2 \rightarrow 3CaO{\cdot}2SiO_2{\cdot}3H_2O \quad (5.12)$$

$$120.17 + 222.76 \rightarrow 342.48$$

2S 3CH C_3-S_2-H_3

For 1kg OPC, 268g of CH are produced, which theoretically can react with 145g of silica:
$145 + 268 \rightarrow 412g$
Therefore, the maximum ratio of SiO_2 to $Ca(OH)_2$ (S/CH ratio) that allows all active silica to react is 0.53945.

5.3.5.1 The microstructure of cement blended with RHA

RHA particles are randomly distributed in the Portland cement. The C-S-H phase produced by the pozzolanic reaction of RHA will grow RHA particles, similar to the growth of cement gel with the hydration time. In addition, the CH phase taken up by the RHA pozzolanic reaction is represented as a decrease in particle diameter (Lee, 2015). Based on the experimental results in this study, the mechanism for the successive pozzolanic reactions of RHA is proposed as illustrated in Fig. 5.9 following:

i. OH^- ions from the pore solution attack Si-O-Si bonds, dissolving amorphous silica from the external surface of RHA particles into the aqueous solution, and a certain

amount of water is absorbed into the pores of RHA particles. Ca^{2+} and OH^- ions in the pore solution react with silica to create Ca/Si C-S-H hydrates which then precipitate on the surfaces of RHA particles; they can also take up some foreign ions, e.g. sodium, potassium, and aluminium.

ii. Over time, the pozzolanic reaction occurs not only on the external surfaces but also in the pores of RHA particles possibly due to the diffusion of Ca^{2-} ions from the cement matrix into the pores of RHA particles. The products formed by the internal pozzolanic reaction fill up the pores inside the RHA particles first. A main part of the internal pozzolanic reaction products consolidates the pore structures of RHA particles, and is not effective in reducing the pore structure of the RHA blended cement matrix. Therefore, the pore structure of the coarse RHA blended matrix is greater than of the fine RHA blended cement matrix [Le, (2015), Chindaprasirt, (2009)]

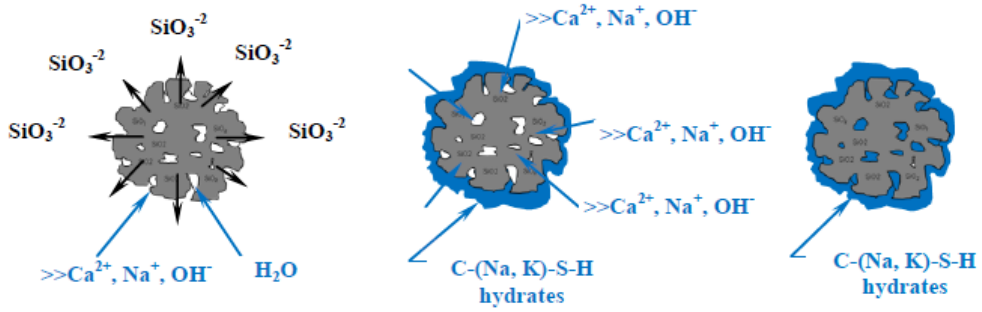

Figure 5. 6: Schematic representation of the mechanism for successive pozzolanic reactions of RHA particles (Lee, 2015).

5.3.6 Calculation of silica to calcium hydroxide ratio

The fact that addition of RHA increases the degree of cement hydration at later stages may be attributed to the release of water from the porous structure of RHA particles as discussed earlier. The CEM I 52.5N cement used in this study contains 62.3%C_3S, 10.6%C_2S, 7.5%C_3A, 9.5%C_4AF and about 5% calcium sulphate (Gypsum). The SiO_2 (S) to CH ratio is calculated for each type of RHA and replacement ratio as follows: 1kg of CEM I 52.5N cement produces 268.014g of calcium hydroxide (CH). The active silica content of each RHA was taken from Table 5.13. These values were multiplied with the replacement values. For example, 5% RHA-C (84.30% amorphous) contain 42.15g active silica and 95% of OPC produce254.6g of calcium hydroxide. Hence, the S/CH ratio for 5% RHA-C will be; S/CH ratio = 42.15/ 254.6 → 0.165

Table 5. 13: Calculation of maximum RHA contribution in reaction with CH of cement hydration

%RHA-A	%Cement	Total amount of CH delivered by 1kg of cement	RHA-A, 92.10% silica *76.6% amorphous	S/CH ratio	SiO_2 reacted with CH (g)	SiO_2 as a filler (g)	23.4%Crystalline silica as a filler (g)
0	100	268.014	-	-	-	-	-
5	95	254.613	35.270	0.1384	35.27	-	10.77
10	90	241.2	70.550	0.2924	70.55	-	21.55
15	85	227.812	105.82	0.4645	105.8	-	32.33
20	80	214.414	141.09	0.658	112.4	28.690	43.10
30	70	187.61	211.65	1.1415	98.42	113.22	64.65
40	60	160.80	282.19	1.1281	84.34	197.65	86.21
50	50	134.01	352.74	2.6322	70.28	282.45	107.7
60	40	107.19	423.29	3.9488	56.22	367.06	129.3
17.1	82.9	222.99	119.85	0.5387	116.69	-	36.64
%RHA-B	%Cement	Total amount of CH delivered by 1kg of cement	RHA-B, 89.31% silica *85.4% amorphous	S/CH ratio	SiO_2 reacted with CH (g)	SiO_2 as a filler (g)	14.6%Crystalline silica as a filler (g)
0	100	268.01	-	-	-	-	-
5	95	254.61	38.135	0.1497	38.13	-	6.52
10	90	241.20	76.270	0.3162	76.27	-	13.04
15	85	227.81	114.41	0.5022	114.4	-	19.56
20	80	214.41	152.54	0.7114	114.5	40.26	26.08
30	70	187.61	228.81	1.2196	98.42	130.4	39.12
40	60	160.80	305.08	1.8972	84.36	220.6	52.16
50	50	134.01	381.35	2.8457	70.30	311.1	65.20
60	40	107.19	457.62	4.2691	56.23	401.4	78.24
15.5	84.5	226.46	118.20	0.5219	118.8	-	24.51

%RHA-C	%Cement	Total amount of CH delivered by 1kg of cement	RHA-C, 84.30% silica *100% amorphous	S/CH ratio	SiO_2 reacted with CH (g)	SiO_2 as a filler (g)	0%Crystalline silica as a filler (g)
0	100	268.01	-	-	-	-	-
5	95	254.61	42.15	0.1655	42.15	-	-
10	90	241.20	84.300	0.3495	84.30	-	-
15	85	227.81	126.45	0.5550	119.0	6.940	-
20	80	214.41	168.60	0.7863	112.7	55.91	-
30	70	187.61	252.90	1.3480	98.43	154.5	-
40	60	160.80	337.20	2.0970	84.36	252.8	-
50	50	134.01	421.50	3.1453	70.30	351.2	-
60	40	107.19	505.80	4.7186	56.23	449.5	-
70	30	80.404	590.10	7.3391	42.18	547.9	-
80	20	53.602	674.40	12.581	28.12	646.3	-
14.66	85.34	222.01	122.24	0.5495	120.0	-	-
%RHA-C5	%Cement	Total amount of CH delivered by 1kg of cement	RHA-C5, 934.9 g silica *98.76% amorphous	S/CH ratio	SiO_2 reacted with CH (g)	SiO_2 as a filler (g)	1.34% Crystalline silica as a filler (g)
0	100	268.01	-	-	-	-	-
5	95	254.61	45.899	0.1824	45.90	-	0.56
10	90	241.20	91.798	0.3851	91.79	-	1.12
15	85	227.81	137.69	0.6115	117.9	19.76	1.74
20	80	214.41	183.59	0.8664	112.5	71.12	2.32
30	70	187.61	275.38	1.4852	98.42	176.9	3.48
40	60	160.80	367.18	2.3104	84.36	282.8	4.64
50	50	134.01	458.98	3.4671	70.30	388.7	5.80
60	40	107.19	550.78	5.1985	56.23	494.5	6.96
70	30	80.404	642.58	8.0844	42.18	599.8	8.11
80	20	53.603	734.37	13.863	28.12	706.3	9.27
13.43	86.57	232.22	123.27	0.5377	121.8	1.474	1.56

5.3.7 Experimental verification of the chemical contribution of RHA

Validation of the chemical contribution of RHA in blended cement carried out by Jamil et al. (2013) will be considered as the basis of these considerations. Essentially, in this study, it was assumed that with increasing replacement ratio, the strength of mortar and concrete would be maximized by a combination of chemical effect up to a limitation. The results range between 13.4% and 17.1% replacement. Therefore, maximum strength is expected to be close to this replacement ratio of RHA.

5.3.8 X-Ray diffraction analysis of OPC and blended mortars

X-Ray diffraction analysis of OPC and blended mortar samples enables the identification of the amount of CH still available in the cement paste. The analysis was performed with a Philips PW 3040/60 X'pert system diffractometer (see Chapter 4, section 4.2.2.3). The diffraction peaks are 29.5° for C-S-H, 18.3° and 34.3° for CH and 26.7° for SiO_2 (Sanchez, 2008). The contents of CH and C-S-H are given in Table 5.14, and plotted in Fig. 5.10. The ratio of C-S-H to CH was used to determine how much CH has reacted with silica to form C-S-H. The data clearly show that the CH declines with increasing replacement ratio. The maximum C-S-H contents for RHA mortar mixtures reached 30% for RHA-A, 20% for RHA-B and C, and 15% for RHA-C5. These results supported this hypothesis that the hydration reaction was a dominant phase while the reactivity of RHA was maximal (RHA-C). It was also noticeable that CH decreased with the increase in RHA content. This phenomenon was considered to be the result of two factors: the large quantity of RHA used to replace cement resulted in an adequate level of reaction (RHA-A), and high fineness of RHA allowed the pozzolanic reaction to react (RHA-C and C5).

5.3.9 Optimum replacement ratio

Generally, enhancement in strength of RHA mortar came from producing more C-S-H gel due to the reaction among RHA amorphous silica and calcium hydroxide in hydrating cement (Yu et al., 1999). However, the optimum replacement ratio where RHA mortar reaches the maximum strength is controversial among researchers. Based on the experimental strength results, RHA ashes reached optimum strength at 20% (RHA-B and C) which is aligned with results obtained by each of Chindaprasirt et al. (2008), Jamil. (2013), and Ganesan et al. (2008). While, with RHA-A and C5 maximum strength obtained at 30% replacement ratio, which is aligned with the results obtained by each of Mehta and Pitt (1976) and Dakroury et al. (2008). These results confirm the X-Ray diffraction results of RHA mortar.

Table 5.14: X-Ray diffraction results of OPC and RHA mortars at age of 365-days.

RHA%	RHA-A				RHA-B			
	CH		C-S-H	C-S-H/CH	CH		C-S-H	C-S-H/CH
	18.3° (counts)	34.3° (counts)	29.5° (counts)		18.3° (counts)	34.3° (counts)	29.5° (counts)	
5	273.14	448.94	322.25	1.18	360.40	405.97	386.23	1.07
10	269.54	327.73	429.48	1.59	281.33	419.25	409.24	1.45
15	226.47	301.91	487.54	2.15	229.04	326.26	453.97	1.98
20	207.35	285.17	514.02	2.48	195.42	299.29	475.77	2.43
30	173.29	208.51	548.09	3.16	157.20	247.56	459.83	2.92
40	130.25	173.35	440.23	3.38	135.75	182.63	433.14	3.19
50	-	-	347.19	-	120.83	170.71	406.18	3.36
60	-	-	263.46	-	111.96	126.26	320.01	2.86
OPC	CH				C-S-H			C-S-H/CH
	18.3° (counts)		34.3° (counts)		29.5° (counts)			1.35
	311.33		428.63		421.47			

RHA%	RHA-C				RHA-C5			
	CH		C-S-H	C-S-H/CH	CH		C-S-H	C-S-H/CH
	18.3° (counts)	34.3° (counts)	29.5° (counts)		18.3° (counts)	34.3° (counts)	29.5° (counts)	
5	319.50	421.60	408.23	1.28	316.44	468.05	424.57	1.34
10	291.30	437.69	438.31	1.50	252.64	403.07	464.24	1.84
15	204.43	277.62	504.31	2.47	141.55	254.74	519.25	3.69
20	124.55	251.95	592.54	4.76	95.14	243.16	517.60	5.44
30	81.44	144.48	570.20	7.00	44.08	111.47	390.67	8.86
40	64.06	110.56	497.55	7.77	24.96	78.21	376.15	15.23
50	42.82	80.78	475.82	11.12	15.59	75.62	389.06	24.94
60	-	50.98	463.66	-	-	58.35	315.79	-

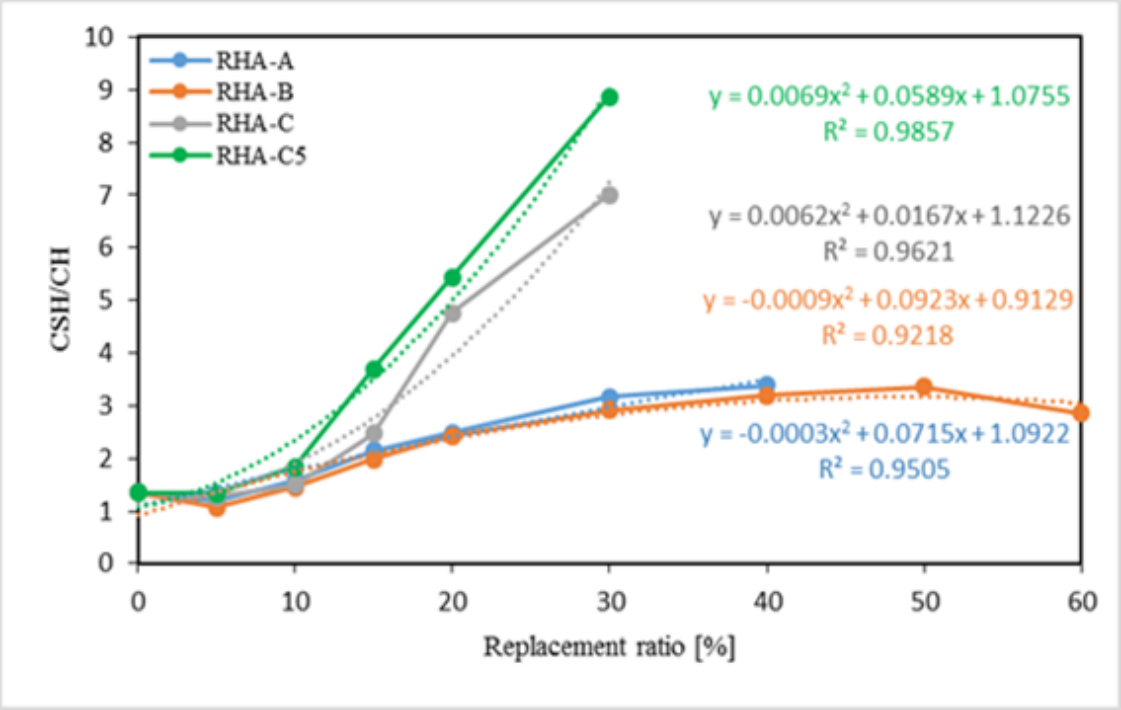

Figure 5. 10: Correlation between CH to C-S-H of OPC and RHA mortar mixture at age of 365-day.

5.3.10 Effect of RHA fineness on the strength of mortar

Based on the mean particles size distribution, it can be seen that compressive strength of mortar containing the finer grained RHA-C and C5 was higher compared to mortar containing the coarser grained RHA-A and B. The development of compressive strength of the RHA-C and C5 samples is higher or similar to that of the control sample after 7 days up to 15% replacement ratio. However, with the progression of time, the compressive strength of RHA-C and C5 became higher than control mortar up to 30% replacement ratio at the age of 28 days. In addition, the development of the compressive strength of the RHA-C5 samples is larger than that of the RHA-C. The higher compressive strength of the RHA-C5 specimens compared to that of RHA-C is possibly due to the better filler effect (the amount of nanoparticles increased (see Table 4.6), high silica amount, and lower carbon content. Re-burning decreased the mean grain size of RHA-C from 15.80µm to 12.64µm.

Furthermore, the nanoparticles size of 0.06µm increased from 9.750% to 12.08% of total volume of ash, which is meant an increase of approximately 19%. In addition to that, the content of particle size 3.90µm was increased from 14.33% to 17.90%. In another word, with re-incinerated RHA-C, the fineness of particles size under 3.9µm increased about 40% of total amount of ash. According to that, the improved performance of RHA-C5 can be attributed partially to the increase of fineness. Whereas, the range of nano- particles

(0.060µm) content of RHA-A to B were 6.85% - 7.92% and the content of micro-particles content under 3.9µm was 8.710% to 10.19%, respectively. Nonetheless, with increasing replacement ratio over 20%, it is shown that the performance of RHA-A is better than RHA-B. This better performance of RHA-A may be due to the higher amount of silica content and lower residual carbon content than RHA-B.

5.3.11 pH of OPC and RHA mortars

The pH variations of the OPC and RHA mortar solutions were measured by the Mettler Toledo AG portable pH meter (see Chapter 3, section 3.3.7); results are given in Table 5.15, and plotted in Fig.5.11. The results show that all RHA mortar exhibited a slight decrease in alkalinity up to 20% replacement ratio. However, pH reduced more with increasing replacement ratio. Where, the reactivity of RHA, the higher is the higher the drop in the pH of the solution (Vayghan et al., 2013). The higher active RHA types C and C5 reduce the pH more. Whereas both RHA-A and B showed less reduction of mortar alkalinity. However, the limitation of the minimum alkalinity to destroy the passive iron oxide layer is pH=11.0 (Neville and Brooks, 1987). Therefore, with the implementation of RHA in mortar maintenance of alkalinity remains in the acceptable limitation even at high replacement ratios (60%).

Table 5.15: pH of OPC and RHA mortars at age of 365-days.

RHA (%)	RHA-A	RHA-B	RHA-C	RHA-C5
5	12.27	12.27	12.26	12.26
10	12.24	12.26	12.23	12.24
15	12.19	12.19	12.13	12.14
20	12.17	12.16	12.06	12.03
30	11.99	12.04	11.79	11.78
40	11.95	11.96	11.68	11.59
50	11.62	11.81	11.29	11.52
60	11.35	11.69	10.84	11.25
OPC	12.27			

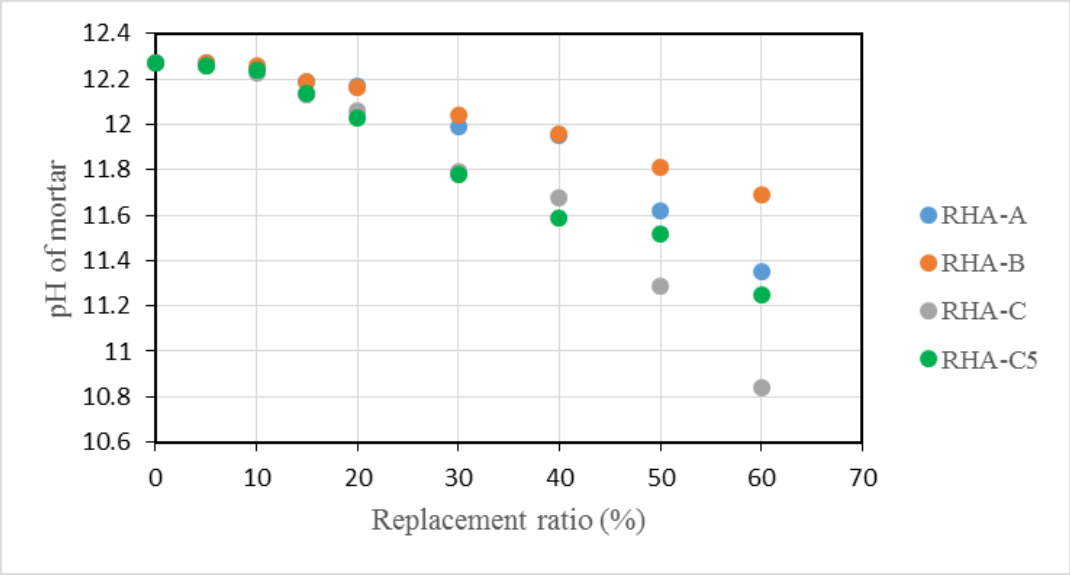

Figure 5. 7: pH rate of RHA mortar at different replacement ratio (age 365-days).

5.4 Effect of superplasticizer dosage on RHA mixture properties

It has been known that the flowability of mortar is affected by the degree of RHA particles and replacement ratio which can be optimized by increase the superplasticizer dosage. Generally, the flowability of RHA mortars at 0.25%SP over 20% replacement ratios were under the target. Therefore, the objective of this section was to identify the behavior of RHA mortar with variation of superplasticizer as a main parameter.

5.4.1 Effect of SP on the flowability and strength of RHA mortar

5.4.1.1 Flowability

As presented in Table 5.16, and plotted in Fig.5.12, the fresh-mixed mortars for RHA-C specimens were produced with an equivalent of unit cement 587kg/m^3, and sand of 1320kg/m^3 for W/B = 0.50. In this series, SP dosage is the only parameter. The dosages of 0%, 0.25%, and 0.50% were introduced in the mixes in order to examine it is effect on mortar, flowability, compressive and tensile strength. Similarly, to mortar mixture (Chapter 3, section 3.10.1), the mixing time was also 3 minutes. Figs. 5.13 show the evaluation of mortar containing RHA when increasing the dosages of superplasticizer from 0.0% to 0.50% by weight of binder materials. As expected, the mixtures showing greater flowability when mixed with 0.5% superplasticizer compare to 0.0%, and 0.25%. Additionally, as shown in Fig 5.13, flowabilty are decreased with increase replacement ratio. According to Aitcin et

al., (1994), mechanism of the superplasticizers is known as adsorption by C_3A, which breaks the agglomeration by repulsion of the same charges and releases entrapped water. Therefore, with increasing RHA replacement ratio, reduction in C_3A content resulted in lower flowability of mixtures.

Table 5.16: Flowability of RHA-C mortar at different dosage of superplasticizers.

Mix	Flow ability (mm)		
	Superplasticizers dosage [% wt. of total binder]		
	0%	0.25%	0.50%
OPC	181	255	293
5%	166	239	257
10%	161	214	238
15%	155	196	226
20%	147	179	214

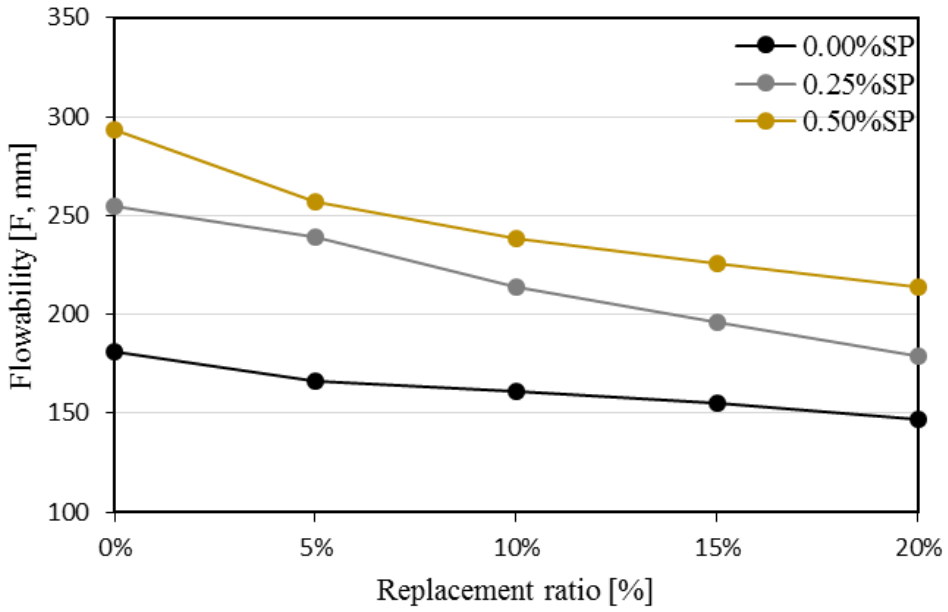

Figure 5. 8: Flow ability of RHA-C with variable dosage of superplasticizer.

5.4.1.2 Effect of superplasticizer dosage on the compressive strength of RHA-C mortar

The effect of superplasticizer (SP) dosages on compressive strength of mortar can be observed in the experimental results as given in Tables 5.17 and plotted in Fig. 5.13. It can be seen that SP dosage caused a change in mortar compressive strength development. The strength of mortar reached maximum of 55.59MPa at 15% replacement ratio when SP/C was 0.0%. However, when SP content was 0.25%, and 0.50% content, the dispersion of cement particles could be improved leading to an increment of compressive strength to reached 59.72MPa and 68.04MPa at 15% replacement ratio (age of 91days) as observed in

the experimental results. Advantageously, this finding agreed with the results of other researchers in the literature reviews. This test is conducted on 7, 28 and 91 days. From the figure, continuous strength gain for superplasticizer is observed for all replacement ratios and ages. At an early age (7 days), strength increased up 5% RHA-C. Adding 0.25 SP increased the compressive strength by about 3MPa; the same increase was observed again for 0.5% SP. The graphs for the three SP contents are more or less parallel; all have the maximum at 5% RHA.

Only at higher replacements, the strength of samples without SP drops slightly more. A very similar picture is visible for 28-day strength values. Here the maximum strength at 15% RHA; again, the three graphs are nearly parallel, only at 0.5% SP the peak at 10% RHA is more pronounced. For 91-day the maximum strength at 15% replacement; nearly all replacement ratios show a larger strength increase from 0.25% SP to 0.5% SP than for 0% SP to 0.5% SP. The addition of SP provides more free water in the cement paste by de-flocculation of cement particles. The obtained results agree with outcomes of Khan et al. (2012), Gamal et al. (2012) and Ahmed et al. (2005). On the other hand, Alasadey (2012) stated that the strength increased with increasing superplasticizer dosage up to 1.0% and beyond that reduces the strength significantly. According to the author, this phenomenon occurs since over dosage of SP will cause bleeding and segregation, which will affect the cohesiveness and uniformity of the concrete. As a result, compressive strength will be reduced, if the used dosage is beyond the optimum dosage.

Table 5.17: Compressive strength of RHA-C mortar at different superplasticizer dosages.

Mix (%RHA)	Compressive strength [*fc*, MPa]								
	0.00%SP			0.25%SP			0.50%SP		
	7day	28day	91day	7day	28day	91day	7day	28day	91day
5%	35.51	47.70	49.29	37.79	48.53	55.65	40.28	52.61	58.85
10%	34.43	49.47	52.59	36.13	50.24	56.47	39.61	58.79	65.03
15%	30.25	48.92	55.59	34.94	49.76	59.72	38.36	55.39	68.04
20%	28.93	46.03	50.27	32.58	47.16	51.93	37.05	52.34	58.85
OPC	32.40	42.24	45.66	35.4	45.50	48.81	37.49	49.42	51.91

Therefore, the maximum limit for the use of SP depends strongly on the water demand of the mix and therefore on the RHA content. SP addition de-flocculates the cement particles, giving a larger surface area for reaction and a more homogeneous structure to the cement paste. Without SP the water trapped between cement grains will leave large pores, and in result reduce the strength (James and Rao, 1986).

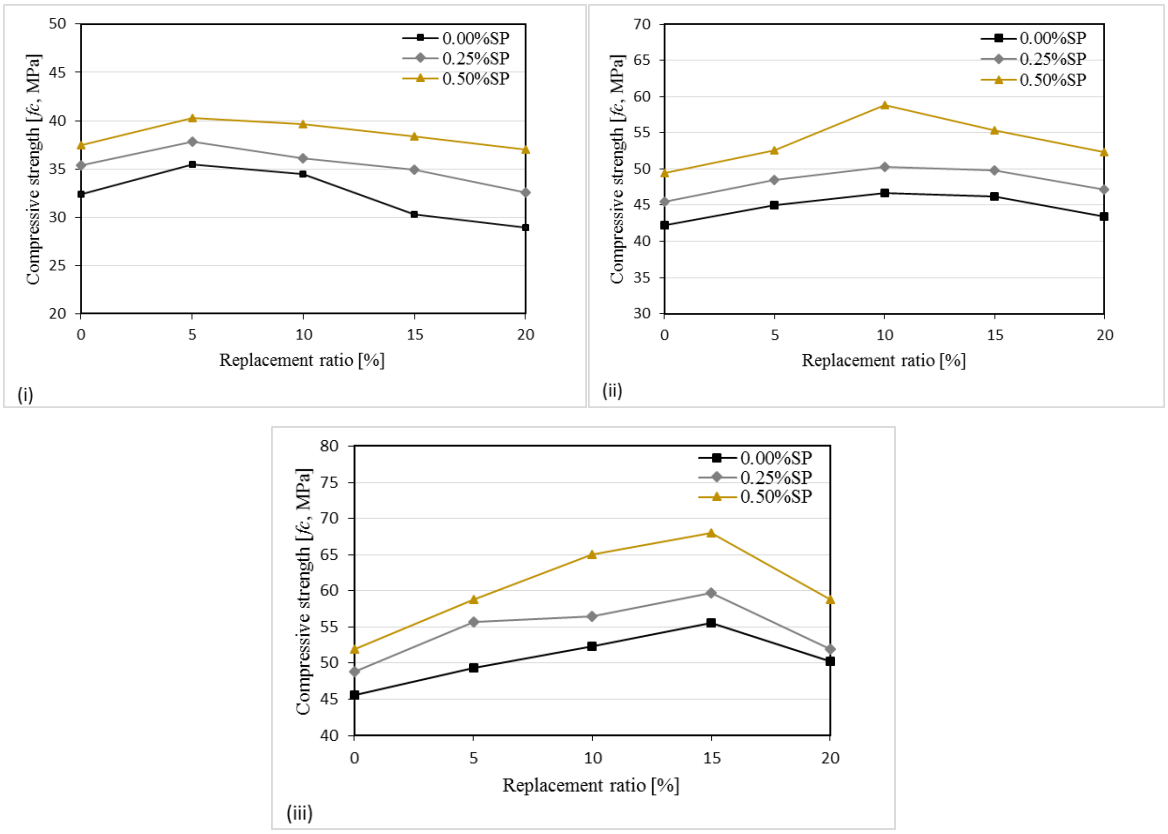

Figure 5.9: Rate of compressive strength development with different dosage of superplasticizer for OPC and RHA-C mortars at age of; (i) 7-days, (ii) 28-days and (iii) 91-days.

Table 5.18: Rate of compressive strength enhancement with two variable superplasticizer dosage, compared to RHA-C mortar mixture without SP.

Mix (% RHA)	0.25%SP			0.50%SP		
	7day	28day	91day	7day	28day	91day
5%	6.033	7.27	11.43	11.84	14.46	16.24
10%	4.700	7.11	6.87	13.08	20.62	19.13
15%	13.42	6.05	6.92	21.14	16.68	18.30
20%	11.20	7.93	3.97	21.92	17.04	14.58
OPC	8.470	7.16	6.45	37.49	14.53	12.04

SP*: Superplasticizer

5.4.1.3 Effect of superplasticizer dosage on the tensile strength of RHA-C mortar

The effect of superplasticizer rate on the development of tensile strength with age is shown in Table 5.19 and Fig. 5.14. Same as for the compressive strength, the graphs for 0%, 0.25% and 0.5% SP run parallel with a slightly higher strength gain from 0.25% to 0.5% SP than for 0% to 0.25% SP. Both 28 day and 91-day strength data show increasing strength up to 20% RHA replacement.

Table 5.19: Tensile strength results of OPC control and RHA-C mortars.

Mix (% RHA)	0.00%SP		0.25%SP		0.50%SP	
	28day	91day	28day	91day	28day	91day
5%	3.05	3.60	3.23	3.98	3.64	4.46
10%	3.31	3.87	3.61	4.19	3.93	4.79
15%	3.52	4.13	3.70	4.47	4.18	5.15
20%	3.39	4.41	3.79	4.86	4.22	5.33
OPC	2.27	2.73	2.68	3.01	3.33	3.87

SP*: Superplasticizer

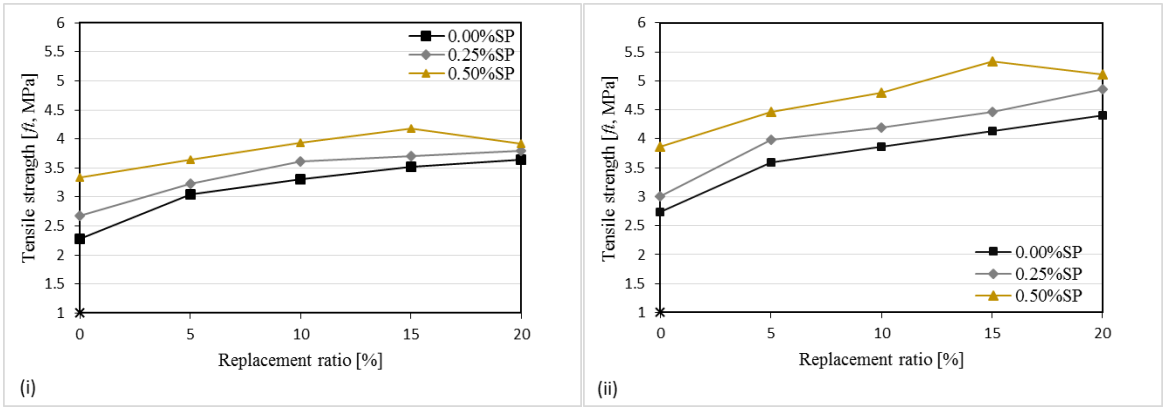

Figure 5.10: Rate of tensile strength development with different dosage of superplasticizer for OPC and RHA-C mortars at age of; (i) 28-day, (ii) 91-day.

5.4.1.4 Correlation of direct tensile to compressive strength

The relation of compressive to direct tensile strength is shown in Table 5.20 and Fig.5.15. At 28 days the three curves are very similar, with slightly higher tensile strength for the samples with SP. For 91 days the curves for 0% SP and 0.25 % SP are practically identical; the tensile strengths for 0.5% SP are significantly higher relative to the compressive strength except for 10% replacement. This relative increase of tensile strength may be attributed to the reduction of pores by de-flocculation of cement grains.

Table 5.20: Ratio (%) of direct tensile to compressive strength at different SP dosage.

Mix	0.00%SP		0.25%SP		0.50%SP	
	28day	91day	28day	91day	28day	91day
OPC	5.35	5.98	5.89	6.16	6.74	7.46
5%	6.39	7.30	6.66	7.15	6.92	7.58
10%	6.57	7.36	7.19	7.42	6.68	7.37
15%	7.20	7.43	7.44	7.48	7.55	8.73
20%	7.36	8.77	8.04	8.85	7.49	10.27

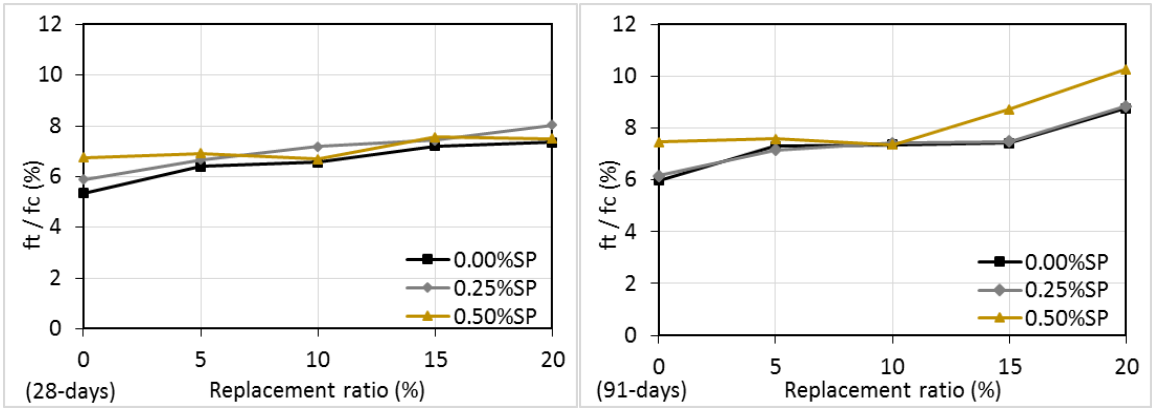

Figure 5.11: Correlation of direct tensile to compressive strength.

5.5 Drying shrinking of RHA mortar

5.5.1 Introduction

The impact of RHA properties on drying shrinkage of mortar is a potential problem, especially in the context of the increasing use of new generation solutions and the development of new materials to ensure sustainability. In this section, the results of the tests on drying shrinkage of RHA concretes are presented. The drying shrinkage specimens were transferred to the ambient environment in the laboratory and monitored over a period of 180 days. The effect of variations in different replacement ratio, RHA particles size (fineness) and silica structure on the drying shrinkage of mortar blended RHA are investigated. Comparisons are made at ages ranging from 3 days to 180-days. The experimental drying shrinkage data are evaluated with the published literature. Drying shrinkage is the volumetric contraction of hardened concrete by the removal of water held by hydrostatic tension in small capillary pore of the hydrated cement paste and loss of physically adsorbed water from C–S–H (Wongkeo et al., 2012). The size of capillary pore smaller than 50 nm has the highest effect on the drying shrinkage. The pore size reducing is the main cause to induce drying shrinkage particularly of cement containing pozzolanic or supplementary materials. The additional C–S–H gel formed by the pozzolanic reaction will thus have the effect of the pores by filling the micro pore in cement paste. The drying shrinkage of mortar was measured as the decrease in length of test specimens under controlled drying conditions according to BS ISO 1920-8:2009.

5.5.2 Preparation of mortar specimen for drying shrinkage test.

5.5.2.1Specimen preparation and test procedure

Mortar was mixed according to ASTM C 270. Prism moulds (Fig.5.16) were used to cast the specimens. Mixing and casting of the mortar samples was identical to that described in Section 3.10.1. The mould dimensions were according to BS ISO 1920-8:2009 (Fig. 5.16 a, b). Measurement were made using a vertical digital dial gage length comparator (Fig. 5.61, c) with an accuracy of 0.00254 mm and a total range of 10 mm. To facilitate the measurement of length change, gage studs that were knurled at one end and threaded at the other were embedded in both ends of the specimens. After the initial measurements were made the prisms were stored in a controlled dry room allowing the movement of the air around the prisms. The temperature inside the room was maintained at 22+3°C. The relative humidity was maintained at 50% ±5%.

BS ISO 1920--8:2009
ISO 1920-8:2009(E)

Dimensions in millimeters

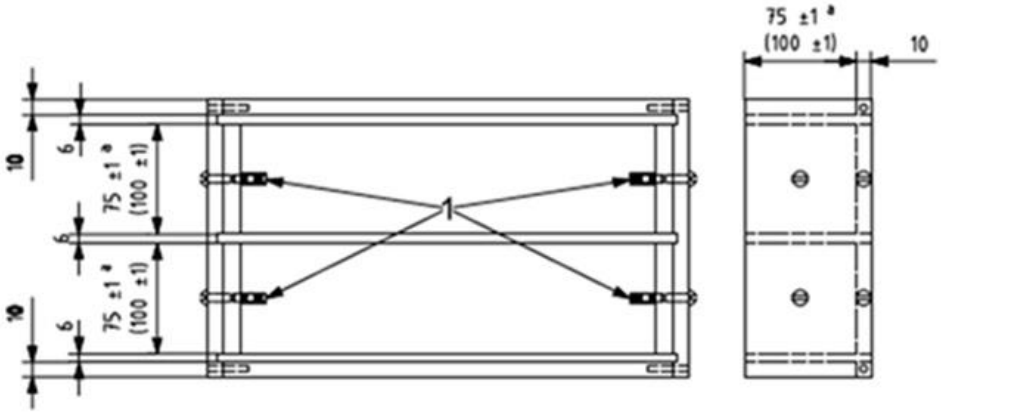

(i) Double Mould

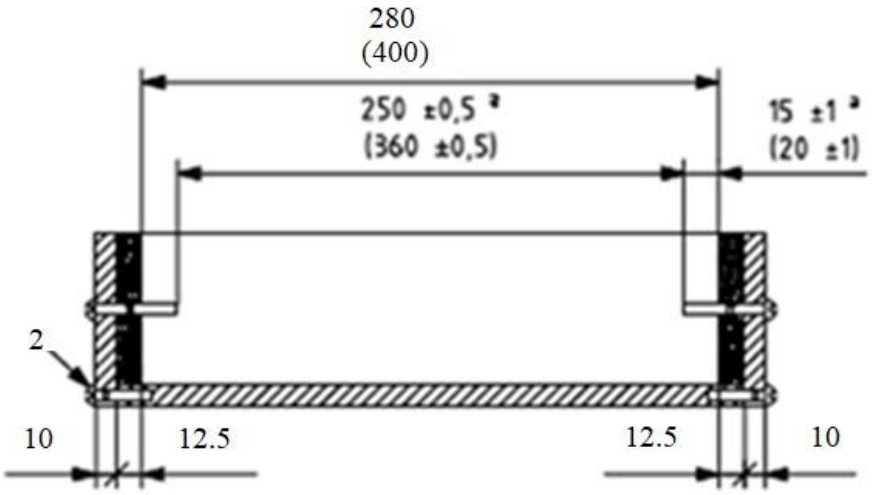

Selection of Mould

(ii)

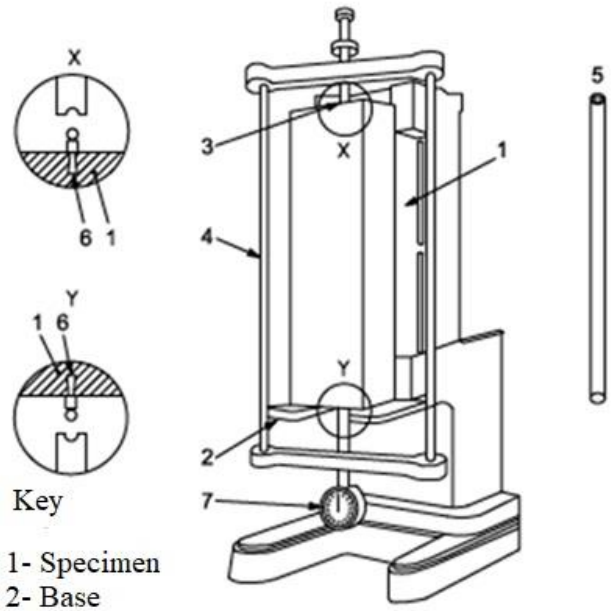

Key

1- Specimen
2- Base
3-Point
4-Frame for a measuerment
5- Reference bar
6-Guage stud
7-Dial guage

(iii) Vertical length comparator

Figure 5.12: Mould used to prepare prism for mortar drying shrinkage test; (i) Double mould prism, (ii) Selection drying shrinkage prism, (iii) Digital dial gage length comparator (BS ISO).

5.5.2.2 Materials and mix proportion

The materials used in this study are presented in Tables, 3.2, 3.4.1.1, 3.5 and 3.6 (Chapter 3). The mix proportions of the batches are given in Table 3.6 (see Chapter 3, section 3.7).

5.5.2.3 Drying

A temperature and humidity controlled drying room was used to store the specimens during drying and data collection. The specimens were stored on a work bench with a minimum clearance of 5mm. The specimens were allowed to dry from all sides. The relative humidity inside the drying room was maintained at 50 ± 5 percent. The temperature was maintained at 23 ± 2°C. The length comparator was located in the drying room, and the readings were taken in the drying room.

5.5.3 Specimens length change measurement

The lengths change measurement of the specimens was determined using a length comparator in accordance with BS ISO 1920-8:2009. The detailed of calculation change length of specimens are presented in section 3.13.1 (Chapter 3).

5.5.4 Results

The drying shrinkages of RHA cement mortars under different replacement ratio are presented in Table 5.21, and plotted in Fig.5.17. Comparisons are made over the full test period and at specific ages ranging from 3 to 180days. Drying shrinkage values are expressed as linear strain as a function of age. At early ages, the RHA mortars have not fully matured, and the high early drying shrinkage strain obtained at this stage were expected. A high proportion of the drying shrinkage strain for all RHA mortars occurred during the initial 28 days, after which the shrinkage gradually increased with increase in age and then became somewhat stabilized with time until the end of the test period. According to the data obtained in this investigation, mixtures with cement replaced partially by 5%RHA-C5 showed the highest drying shrinkage strain values at the early age (3days) and later at 180 days at 50 and 60% replacement compare to OPC control.

The reason for the higher drying shrinkage of mortar containing RHA-C5 may be due to high reactivity and fineness of particles (see Table 4. 3, Chapter 4), which fill the capillary pore of cement paste and the greater pozzolanic reactivity (Habeeb and Fayyadh, 2009). Therefore, the high amount of silica content of RHA-C5 (93.49% wt. of silica), high reactivity of ash (98.87% amorphous) and very high specific surface area (0.808 m^2/g)

strongly influence the determining factors for the development of shrinkage, which are porosity, and the degree of hydration. At the end of the test period, the drying shrinkage strain of all the RHA mixtures varied between 1016 (60%RHA-A) and 1391(60%RHA-C5) micro-strains. In contrast, the RHA-A and B mortar showed a significant reduction in drying shrinkage, with increase replacement ratio and progression of time. With increase replacement ratio to 10%, all RHA mortars mixtures exhibited reducing in drying shrinkage than OPC mortar especially mortars with RHA-A and B. With increase incorporation of RHA to 15% replacement ratio RHA-A and B significantly reduced the drying shrinkage to reach the maximum decrease in comparison to OPC. Fine RHA (C, and C5) also significantly reduced the drying shrinkage of mortar but to a lesser extent. RHA mortars reached maximum drying shrinkage reduction with incorporation of 20% RHA. Although these drying shrinkage strain levels are either comparable to/or in a manner similar to those observedby each AI-Khalaf and Yousift (1984), and Item et al. (2011).

As expected, with increase replacement ratio over 20%, RHA mortars exhibited increase in drying shrinkage strain. The higher drying shrinkage of mixes is probably due to higher binder content. In addition, at a constant water binder ratio, drying shrinkage increases with an increase in the cementitious content resulted in a large volume of hydrated cementitious paste which is liable to drying shrinkage (Hung, 1997). This tendency is observed for all RHA mixtures. The influence of coarse grain and crystalline silica amount influenced on the drying shrinkage at long-term drying shrinkage at high replacement ratio (40%, 50% and 60%). These factors reduced drying shrinkage of RHA-A and B to 18.63%, and 13.17% compared to OPC control. These results are brought into line with the conclusion reported by Mehta and Monteiro (2006) and Chandra (1997).

Table 5.21: Drying shrinkage strain (mm/mm) of RHA mortars at different replacement ratio compare to OPC mortar at different ages.

Time (day)	5%RHA				10%RHA				15%RHA			
	A	B	C	C5	A	B	C	C5	A	B	C	C5
3	0.0118	0.0040	0.0278	0.0462	0.0112	0.0034	0.0172	0.0254	0.0056	0.0018	0.0158	0.0300
7	0.0346	0.0224	0.0463	0.0644	0.0328	0.0214	0.0370	0.0408	0.027	0.0158	0.0336	0.0396
14	0.0486	0.0482	0.0533	0.0770	0.0414	0.0458	0.0502	0.0532	0.0356	0.0390	0.0438	0.0530
28	0.0594	0.0714	0.0766	0.0990	0.0546	0.0612	0.0636	0.0742	0.0502	0.0550	0.0598	0.0680
56	0.0758	0.0912	0.0936	0.1154	0.0646	0.0776	0.0832	0.0890	0.0568	0.0662	0.0694	0.0794
91	0.0776	0.0980	0.1054	0.1264	0.0664	0.0816	0.0882	0.0982	0.0646	0.0762	0.0806	0.0862
180	0.0796	0.0995	0.1068	0.1298	0.0689	0.0853	0.0891	0.1024	0.0659	0.0785	0.0819	0.0881
Time (day)	20%RHA				30%RHA				40%RHA			
	A	B	C	C5	A	B	C	C5	A	B	C	C5
3	0.0023	0.0046	0.0138	0.0178	0.0034	0.0032	0.0100	0.0152	0.0092	0.011	0.003	0.0134
7	0.0216	0.0232	0.0298	0.0358	0.0284	0.0246	0.0196	0.0400	0.0330	0.0282	0.0084	0.0406
14	0.0290	0.0362	0.0390	0.0506	0.0334	0.0334	0.0362	0.0512	0.0443	0.0464	0.0228	0.0529
28	0.0484	0.0536	0.0564	0.0660	0.0544	0.0489	0.0538	0.0648	0.0604	0.0664	0.0462	0.0730
56	0.0596	0.0646	0.0683	0.0780	0.0624	0.067	0.0714	0.0788	0.0724	0.0748	0.0826	0.0966
91	0.0646	0.0700	0.0744	0.0840	0.0664	0.0746	0.0808	0.089	0.0801	0.0828	0.0928	0.1016
180	0.0685	0.0721	0.0768	0.0852	0.0702	0.0773	0.0827	0.0910	0.0829	0.0881	0.0937	0.1043
Time (day)	50%RHA				60%RHA				OPC			
	A	B	C	C5	A	B	C	C5				
3	0.0122	0.0140	0.0076	0.0176	0.0176	0.0144	0.0116	0.0234	0.0424			
7	0.0388	0.0350	0.018	0.0406	0.055	0.0436	0.0272	0.0582	0.0500			
14	0.0558	0.0560	0.0322	0.0656	0.0644	0.0712	0.0423	0.0768	0.0590			
28	0.0770	0.0786	0.0626	0.0856	0.0832	0.0872	0.0699	0.0944	0.0794			
56	0.0874	0.0892	0.0926	0.1076	0.0934	0.0972	0.1052	0.1176	0.1004			
91	0.0926	0.0954	0.1048	0.1164	0.0994	0.1027	0.1162	0.1326	0.1120			
180	0.0939	0.1002	0.1065	0.1198	0.1046	0.1089	0.1187	0.134	0.1143			

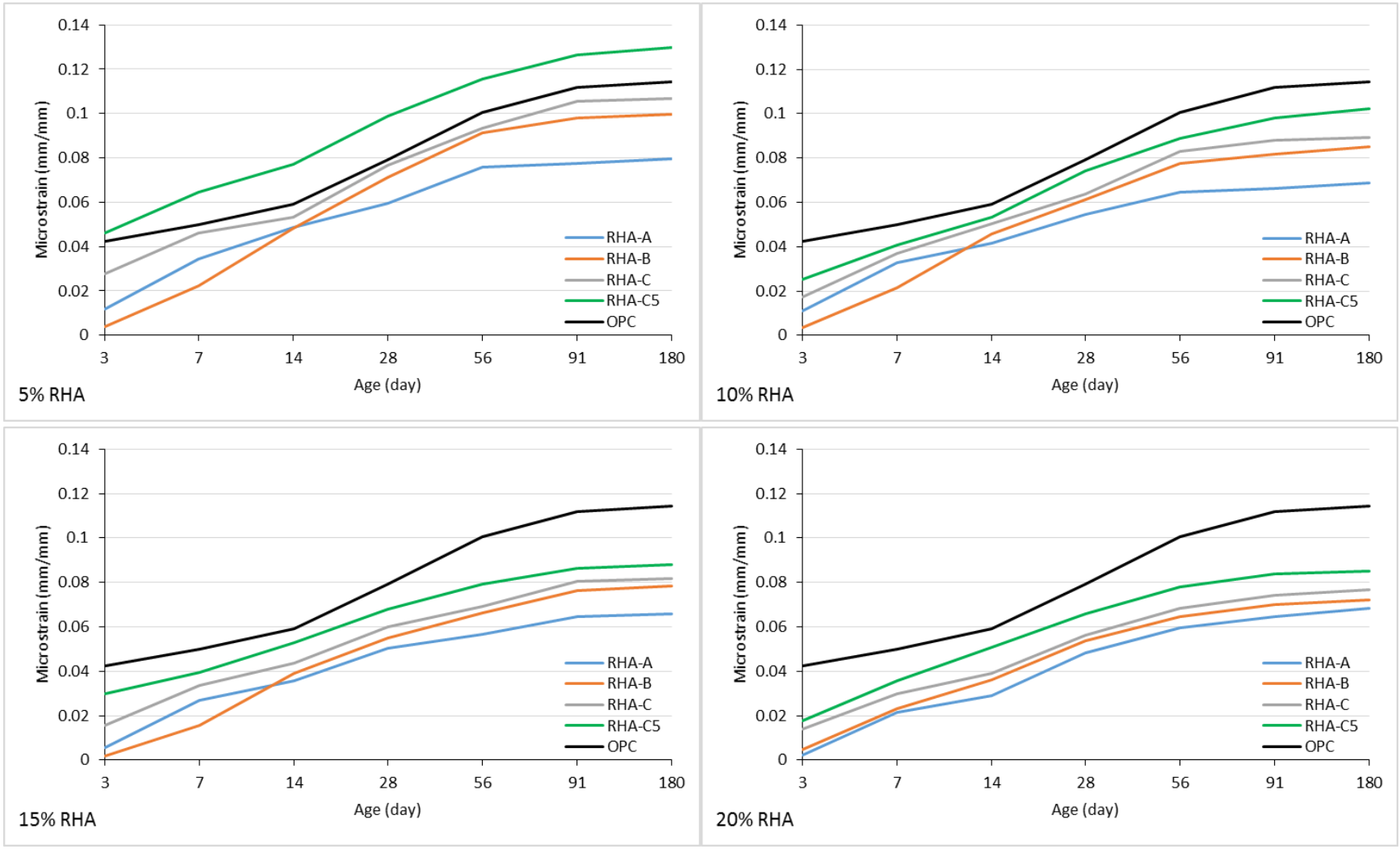
0.14
0.12
0.1
0.08
0.06
0.04
0.02
0
Microstrain (mm/mm)
3
7
14
28
56
91
180
Age (day)
RHA-A
RHA-B
RHA-C
RHA-C5
OPC
5% RHA
10% RHA
15% RHA
20% RHA

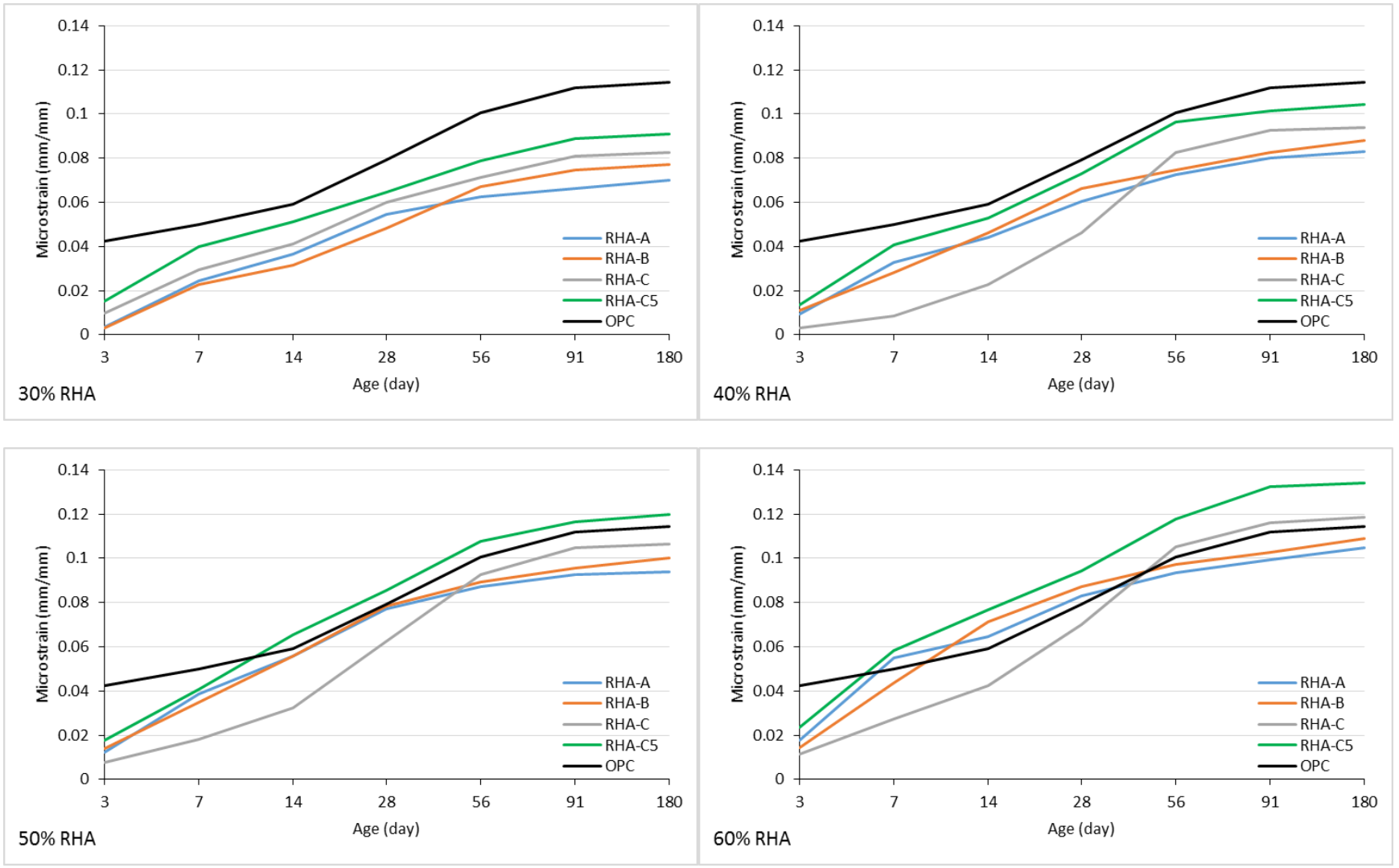

Figure 5.13: Drying shrinkage strain vs. curing time for RHA mortar at different replacement ratio compared to OPC.

5.5.5 Effect of RHA content

The effect of the RHA content on drying shrinkage was examined. In consideration of Figure 5.17, there is a general trend of drying shrinkage decreasing with increasing replacement ratio up 15% RHA-A, and 20% RHA-B, C and C5. The relative drying shrinkage versus RHA content for the set of data gathered here. The drying shrinkage was found to depend upon the RHA content and properties, varying between approximately an 8.49% decrease in drying shrinkage at 60%RHA-A, to increase about 3.71% at 60% RHA-C5 content. This is can be justified by the amorphous silica of RHA [Zhang and Malhotra, (1996); Habeeb et al., (2009); and Chatveera & Lertwattanaruk, (2011)].

According to the results, the increased drying shrinkage of RHA-C5 can be explained by the pozzolanic and the filler effects (Habeeb et al., 2009). Despite of RHA-C content totally amorphous silica, exhibited lower dry shrinkage compared to OPC mortar. This behavior of RHA-C specimens can be assigned to the high residual carbon content. On the other hand, the drying shrinkage of RHA mortar specimens was noticeably reduced by the addition of RHA-A and B. Specimens at 180 days, showed a reduction in drying shrinkage strain by 30.11% and 12.64% compared to OPC. Implementation of RHA partially crystalline silica with coarse particles size provides a positive effect on the drying shrinkage of mortar, which is ascribed to the filler effect. According to Mehta & Monteiro (2006) and Chandra (1997), concrete incorporating pore refinement additives will usually show higher shrinkage and creep values.

5.5.6 Effect the fineness of RHA particles

In consideration of Fig.5.18, there is a general trend of drying shrinkage decreasing with increase replacement ratio up to 15% RHA-A, and 20% RHA-B, C and C5, then increase with increase replacement ratio. This is due to the increased fineness of the binder derived from increased addition rate of RHA. From the data presented in Fig. 5.18, it can be noted that all of the mortar blended RHA-A and B, exhibited lower drying shrinkage than that of OPC mortar. However, RHA-C and C5, presented significant difference at high replacement ratio (60%RHA-C, and 50% and 60%RHA-C5). Consideration the particle size distribution presented in Table 4-4 (see Chapter 4, section 4.3) show that, there is a remarkable portion of RHA-A equal to 31µm (29.16%). Compare to 25.02 , 17.35 and 12.22 µm of RHA-B, C and C5, respectively. The indication of coarser particles became important when considering the drying shrinkage of the blends (South, 2009). In addition to that, there is a

linear correlation between the particle size distributions to the development of drying shrinkage of RHA mortar which is presented in Fig.5.19. This correlation was determined for 20% RHA; however, it's similar for other RHA replacement ratio.

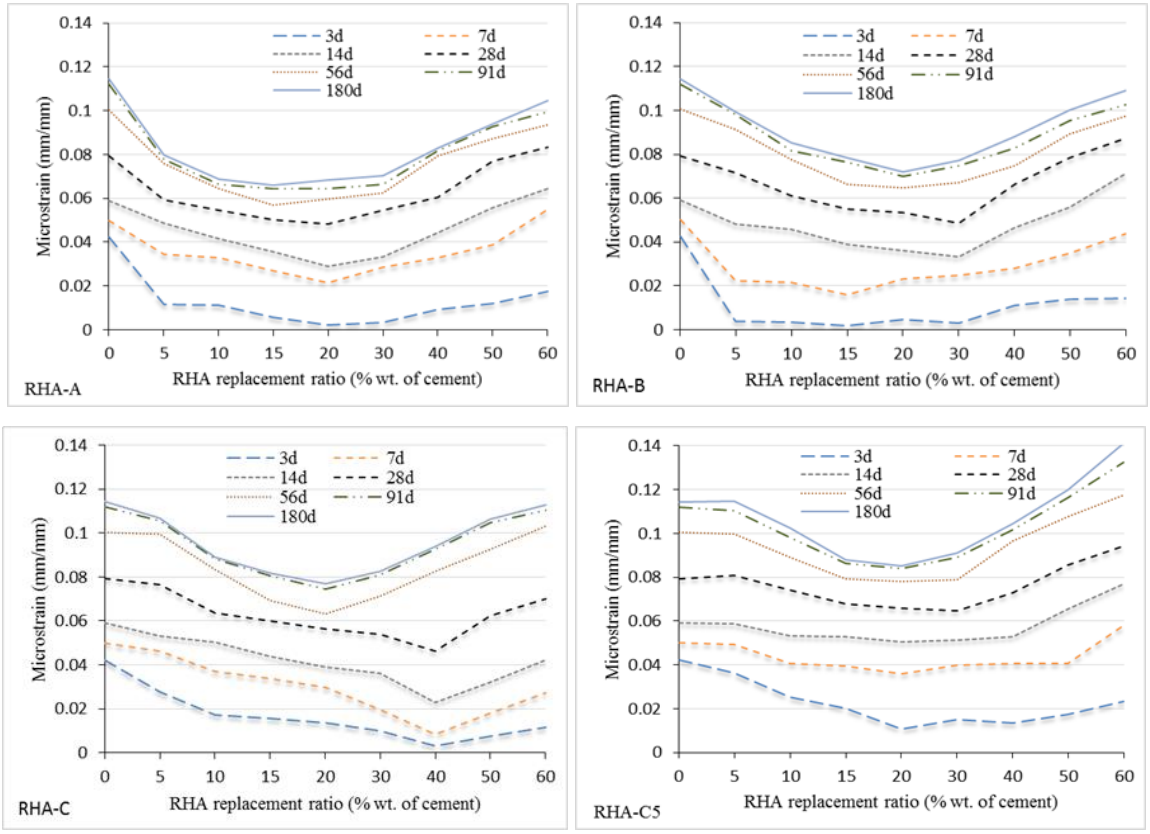

Figure 5.14: Correlation between drying shrinkage of OPC and RHA mortar to RHA replacement ratio.

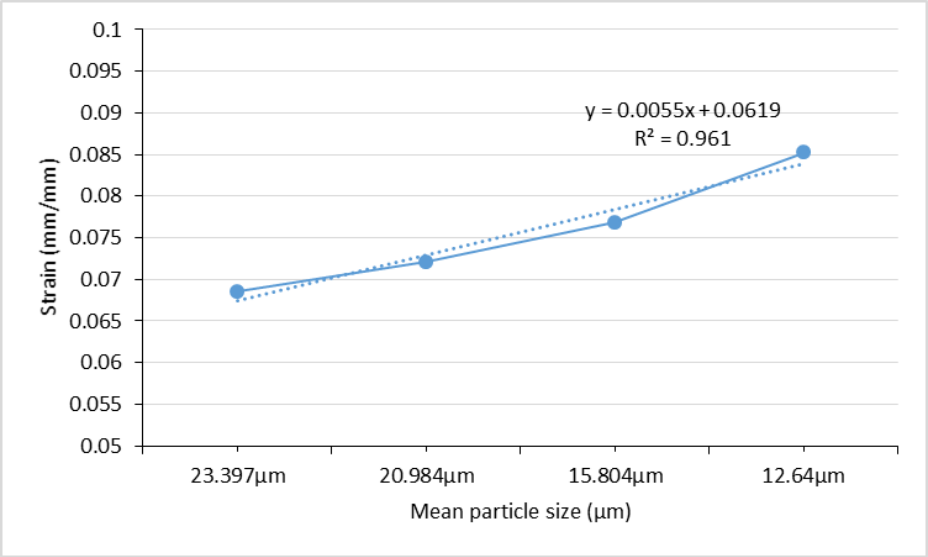

Figure 5.15: Relationship between mean particles size of RHA to strain of 20%RHA mortars.

5.5.7 Correlation between compressive strength and drying shrinkage

The relationship between the drying shrinkage and compressive strength of RHA mortar are shown Fig.5.20. According to the results, there is a good correlation between compressive strength and RHA-A-C and C5 mortar drying shrinkage at age of 91 days. However, the relationship is less strong with RHA-A, and more developed with RHA-B. Depending on the development of compressive strength and the dry shrinkage strain, the optimum compressive strength value, offset by the minimum dry shrinkage strain. This relation is clearer with the progression of time. By representing the shrinkage strain with compressive strength for each type of RHA mortar in Fig.5.19, it will be noted that this correlation not a single and depends mainly on the RHA properties and the amount of the replacement ratio.

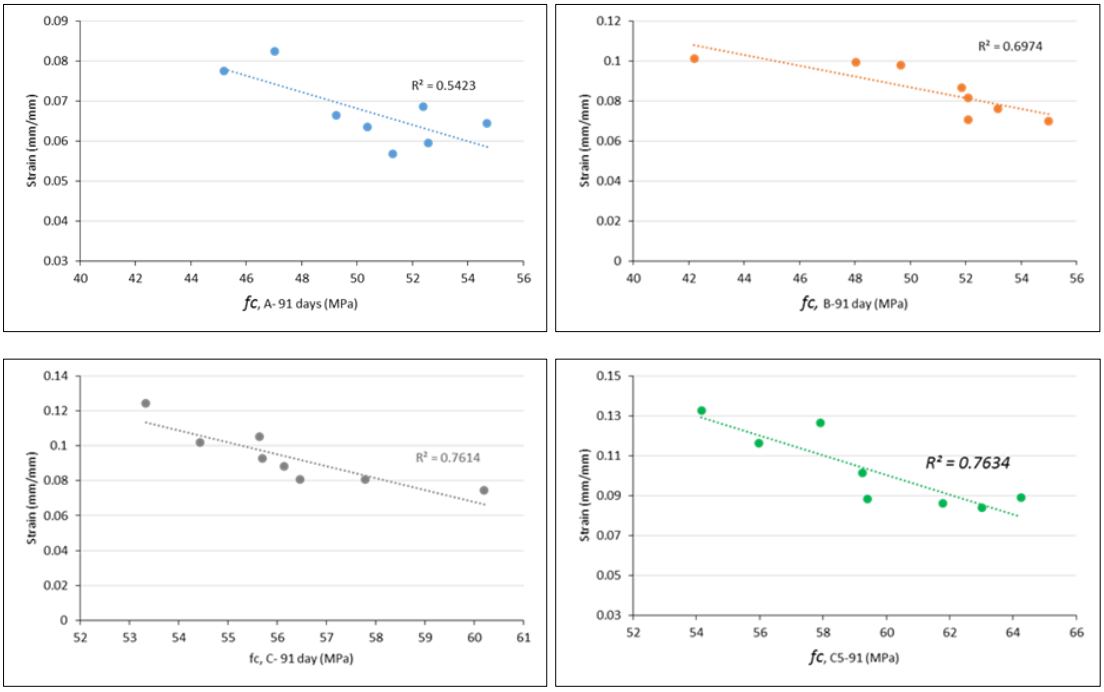

Figure 5.16: Correlation between RHA mortar compressive strength to RHA mortar drying shrinkage of RHA ratio of RHA at age of 91days.

5.5.8 Conclusion

Relatively few investigations have been carried out on drying shrinkage of mortar containing RHA. The intention of this experimental program was to understand the influence of RHA fineness and silica form on the drying shrinkage of mortar. The experimental results, however, indicated that the replacement of cement by 60% RHA (by total mass) decreasing drying shrinkage with RHA consist of coarser particles. Generally, from the experimental results, it was observed that, when compared to the control mortar mix. Replacement of cement by RHA decrease the drying shrinkage up to 20% replacement ratio, particularly RHA-A and B mortar mixture showed lowest shrinkage. Generally, RHA-A and B provides a positive effect on the drying shrinkage deformation, since early ages (3-7 days) which is attributed to the filler effect, when compared with the hydration effect of an equal dosage of RHA-C and C5. The decrease in drying shrinkage at the age of 28 days were 39.04% (20%RHA-A), 38.41%, 34.18% and 18.39% of 30% RHA-B, C and C5, compare to control mortar.

Generally, the increase in drying shrinkage of RHA-C5 might be due to pozzolanic reaction and pore size refinement (Itim et al., 2011). After 180 days, it is to be noted that the drying shrinkage of RHA-A mortar improves with the age for 20% replacement rate. Where the drying shrinkage decreased about 40.07%, compare to 32.37%, 27.65% and 20.38% of RHA-B, C and C5, respectively. The drying shrinkage decreases when the replacement rate of RHA is increase up to 20%RHA-A, and 30% RHA-B, C and C5. These results are aligned with those presented by Item et al. (2011). However, when the replacement rate reaches 40% and over, the drying shrinkage becomes remarkably high; this result is in agreement with those reported by AI-Khalaf and Yousift (1984).

5.6 Effect of RHA residual carbon content on the strength of mortar

5.6.1 Introduction

The reactivity of RHA is considered to be influenced by many factors, such as silica structure and particle size distribution. However, residual carbon content (loss on ignition), which is dependent on the burning temperature and duration of incineration is considered another crucial factor. Therefore, the present experimental study was aimed to improve understanding of the effect of residual carbon content on the performance of RHA-blended

mortar. Various ashes were prepared by re-incineration of RHA-C at different temperatures to time. The properties of the ashes were determined using scanning electron microscopy and X-ray fluorescence; blended mortar samples were created to determine effect of re-incineration on the workability, compressive and tensile strength.

5.6.2 Experimental program

5.6.2.1 Preparation of RHA

Generally, RHA-C (the blackish ash) which is consisting of high residual carbon content (11.35% wt. of ash) sorted out by burning rice husk at 400°C for 3h (Navdanya Food PVT. LTD Odisha, India). Since the black colour considered due to high residual carbon content which is effect adversely on the activity of ash (Yamamoto and Lakho, 1982). Therefore, to improve RHA-C quality by re-incineration of ash was carried out in a furnace with controlled temperature in order to investigate the effect of burning temperature and time on the amount of residual carbon content and silica reactivity. An electrical muffle furnace model 'Carbolite' was used to re-incinerate four different types of RHA under various temperatures and time. RHA-C was selected to investigate because of it is high carbon content and completely amorphous silica structure. RHA-C ash was re-incinerated in 200g portions to produce four different types of ashes (RHA-C1: 400°C/30min, RHA-C2: 400°C/2hrs, RHA-C3: 500°C/2hrs and RHA-C4: 600°C/2hrs). For each burning temperature, the sample was left for another 30min in the muffle furnace after it was turned off to reach the room temperature.

5.6.2.2 Physical properties of ashes

A laser particle size analyser was used to determine the particle size distribution and specific surface area of the re-incinerated RHAs. The particle size distribution of RH ashes is presented in Fig. 5.21 and Table 5.22. The results indicated that specific surface area (SSA) increased from 0.691 m^2/g (RHA-C) to 0.741 m^2/g (RHA-C2) then decreased to 0.639 m^2/g (RHA-C4). The mean particles size increased from 15.8μm (RHA-C) to 17.51μm (RHA-C4). This increase in the specific surface area directly proportional to heating temperature and time is caused by agglomeration effect and diminishing porosity (Della et al., 2002).

However, with prolonged combustion time to 6hrs at temperature of 550°C (RHA-C5), RHA exhibited very high specific surface area with reduction of mean particles size to 12.64 µm, coincides with slightly reduction of activity due to transforming of small part of silica to crystalline.

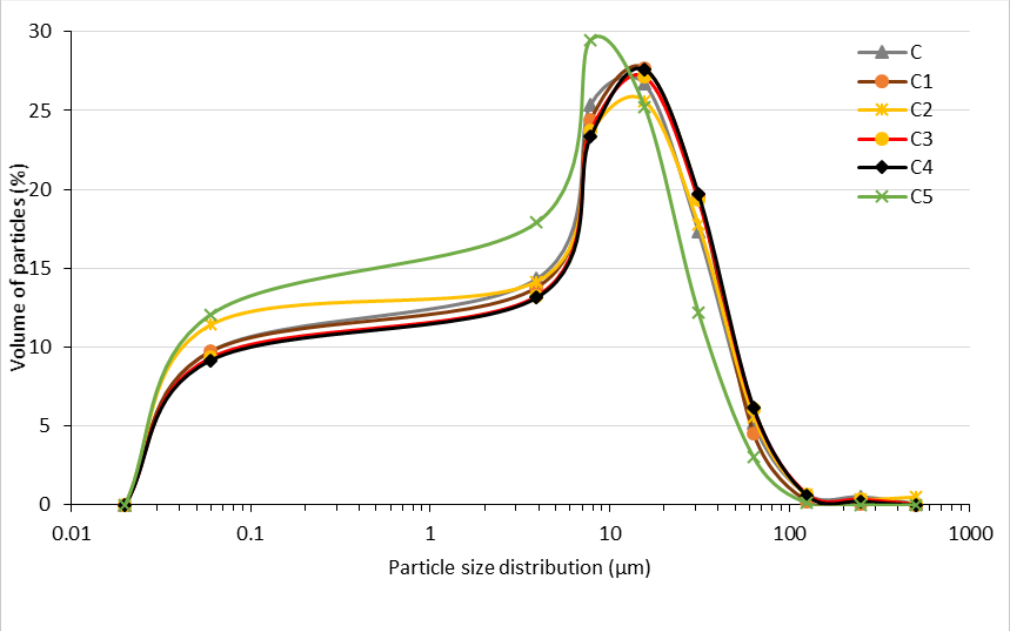

Figure 5.17: Particle size distribution of RHA samples.

Table 5.22: Particle size distribution and specific surface are of RHA ashes.

Particle size distribution (µm)	% Volume of particles					
	C	C1	C2	C3	C4	C5
0.060	9.75	9.74	11.43	9.34	9.18	12.08
3.900	14.33	13.79	14.17	13.24	13.14	17.9
7.800	25.39	24.43	23.59	23.76	23.36	29.48
15.60	26.68	27.68	25.61	27.14	27.61	25.21
31.00	17.35	19.58	17.79	19.33	19.74	12.22
63.00	5.19	4.51	5.60	6.06	6.14	3.01
125.00	0.68	0.24	0.63	0.69	0.6	0.11
250.00	0.53	0.04	0.35	0.37	0.23	0
500.00	0.1	0	0.51	0.07	0	0
Mean particle size (µm)	15.8	15.85	15.93	17.08	17.51	12.64
SSA (m^2/g)	0.691	0.695	0.741	0.663	0.639	0.808

5.6.2.3 Chemical composition of RHA

The chemical composition of RHA samples was measured using X-Ray Fluorescence (XRF, Philips, model PW 2400); the results are presented in Table 5.23. The results showed that

with increase combustion degree, oxide amount of ash is increased. This relative increase in silica content allows establishing a relationship in between pozzolanic activity of RHA and the burning temperature and duration.

Table 5.23: Chemical composition of RHA samples.

RHA	Chemical composition (wt. %)								
	SiO_2	Al_2O_3	Fe_2O_3	CaO	K_2O	P_2O_5	SO_3	MnO	LOI
RHA-C	84.30	1.066	0.175	0.729	1.522	0.675	0.083	0.144	11.35
RHA-C1	87.81	1.136	0.186	0.776	1.621	0.718	0.089	0.153	7.57
RHA-C2	90.27	1.142	0.187	0.780	1.630	0.722	0.089	0.154	5.08
RHA-C3	91.33	1.155	0.189	0.789	1.649	0.731	0.090	0.156	3.96
RHA-C4	92.34	1.168	0.191	0.798	1.667	0.739	0.091	0.157	2.90
RHA-C5	93.49	1.186	0.202	0.971	1.587	0.663	0.084	0.115	1.65

5.6.2.4 Loss on ignition

Loss on ignition was obtained according to EN 196-2:1994 (see Chapter 3, section 3.3.6). The loss on ignition test results are shown in Table 5.23, which indicates that with increasing combustion temperature and duration, the residual carbon content decreased. This change in residual carbon content can be evaluated from the gradual shift in ash colour. According to Huston (1972), RHA can be classified to a high-carbon material (black colour), low carbon (grey colour) and carbon-free pink or white ash. The colour of the ashes changed from black (RHA-C) to light grey with increasing heating temperature.

5.6.2.5 Silica structure and Pozzolanic activity of RHA

As a reference to analysis the XRD peaks results, The NIOSH manual of analytical methods (NMAM, 2003) was considered. RHA peaks in the X-Ray Diffraction results can be assigned to tridymite 20.93°, cristobalite at 21.93°, possibly cristobalite or tschernichite at 22.04°, quartz at 26.67° and brownleeite at 44.40°. The X-ray diffraction patterns shown in Fig.5.22, and presented in Table 5.24, indicated that RHA-C burned at 400°C/30min (C1) and 400°C/2h (C2) remained amorphous and there were no crystalline phases of silica. On the other hand, results for RHA-C3 and C4, re-incinerated at a temperature of 500°C/2h, and 600°C/2h, exhibited of development of silica into a quartz crystalline phase. Further, to study the relationship between the pozzolanic activity of RHA and the burning temperature, RHA samples (C1 to C4) are compared to RHA-C and RHA-C5 (RHA-C burned at 550C/6h). Obviously, the broad peak of RHA-C5 silica (550°C/6h) shown some trace of crystalline (quartz), however less than RHA-C4 (600°C/2h) but higher than RHA-

C3 (550C/2h). Which is prove that, transformation of amorphous silica to crystalline depend on the temperature degree more than applied time.

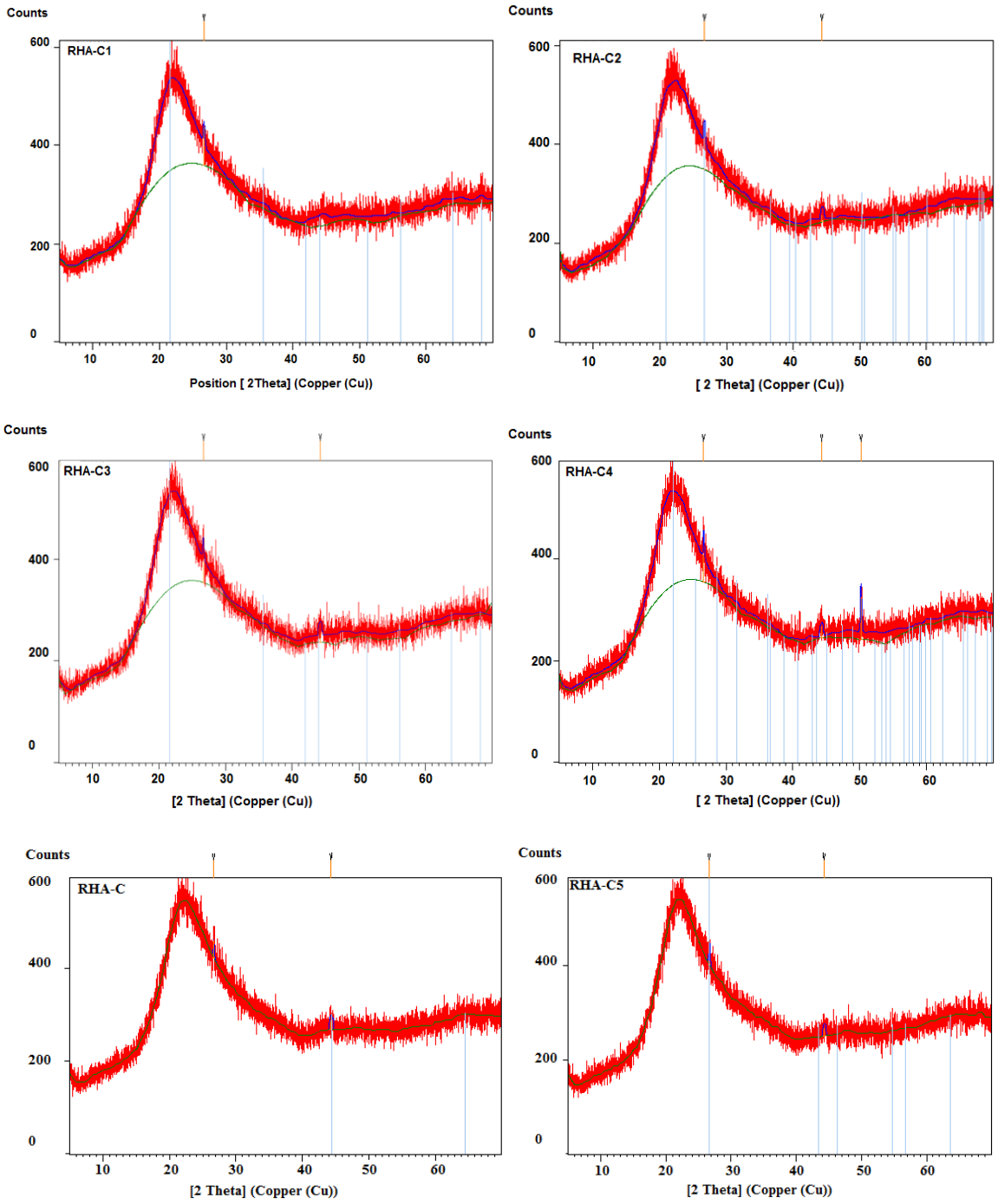

Figure 5. 18: X-ray diffractograms of re-incinerated RHA ashes.

Table 5.24: X-ray diffractogram peaks of RHA-C1, C2, C3 and C4.

RHA	Position [°2θ]	Height [Counts]	Peak assignment
RHA-C	26.6621	37.69	Quartz
RHA-C1	26.6493	28.45	Quartz
RHA-C2	26.7001	36.90	Quartz
	44.3420	15.47	Brownleeite
RHA-C3	26.6340	40.69	Quartz
	44.1745	17.95	Brownleeite
RHA-C4	26.6771	54.29	Quartz
	44.2994	23.98	Brownleeite
RHA-C5	26.6662	52.39	Quartz

5.6.2.6 Pozzolanic reactivity

The method to determine the activity of a pozzolanic material by measuring the electrical conductivity of saturated solution of calcium hydroxide is presented in section 3.3.4 (Chapter 3). The electrical conductivity curves of RHA-C, C1, C2, C3, C4 and C5 are presented in Fig.5.23. Comparison the conductivity of RHA-C to RHA-C series (C1, C2, C3, C4 and C5) it clear that with decrease amount of LOI and maintain silica in amorphous form, the reactivity of ash increased (RHA-C1 and C2) as a result of increase silica content. Even though, the LOI of RHA-C3 and C4, are decreased about 65.11% and 74.45% than RHA-C; however, increase amount of crystalline silica adversely effected on the reactivity of ash. Based on Luxán, et al., (1989) method, RHA-C1 and C2 considered a very high pozzolanic material.

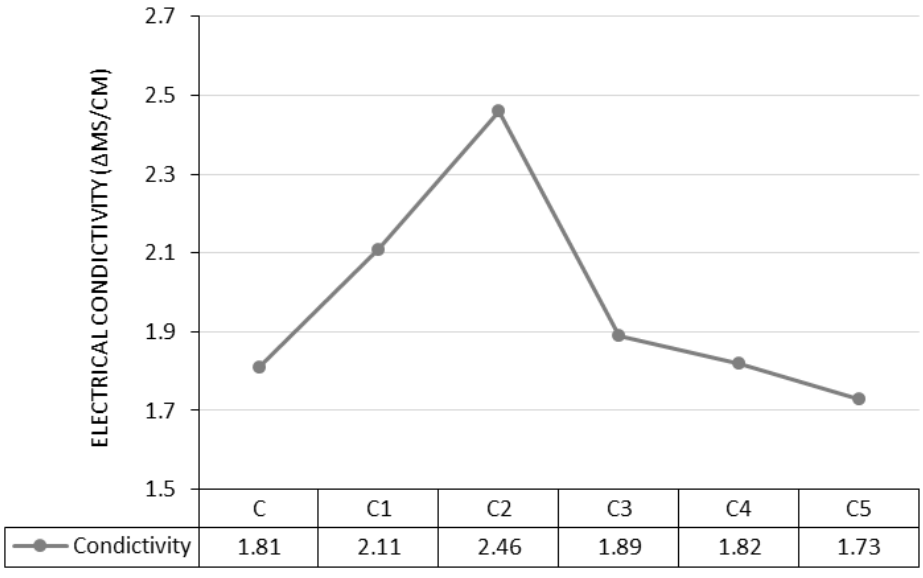

Figure 5.19: Electrical conductivity of RHA-C series at 40°C.

5.6.2.7 Microstructure of RHA samples

Fig. 5.24 shows SEM images of RHA-C to C5. Together with the increase in mean particle size (MPS), the morphology of RHA-C1 and C2, particles seem to be more uniform as seen in Fig.6.3, (a) and (b). The RHA-C1 and C2 particles are fine and uniformly sized, with some smaller particles clumped together. An observation of the microstructure of the RHA-C2 indicates significant degradation of the RHA-C structure from the re-burning process. However, RHA-C3 and C4 particles are irregular, with variation in particle size. The pore size distribution of RHA particles at different combustion times shown that RHA is a porous material including mostly mesoporous (2-50 nm).

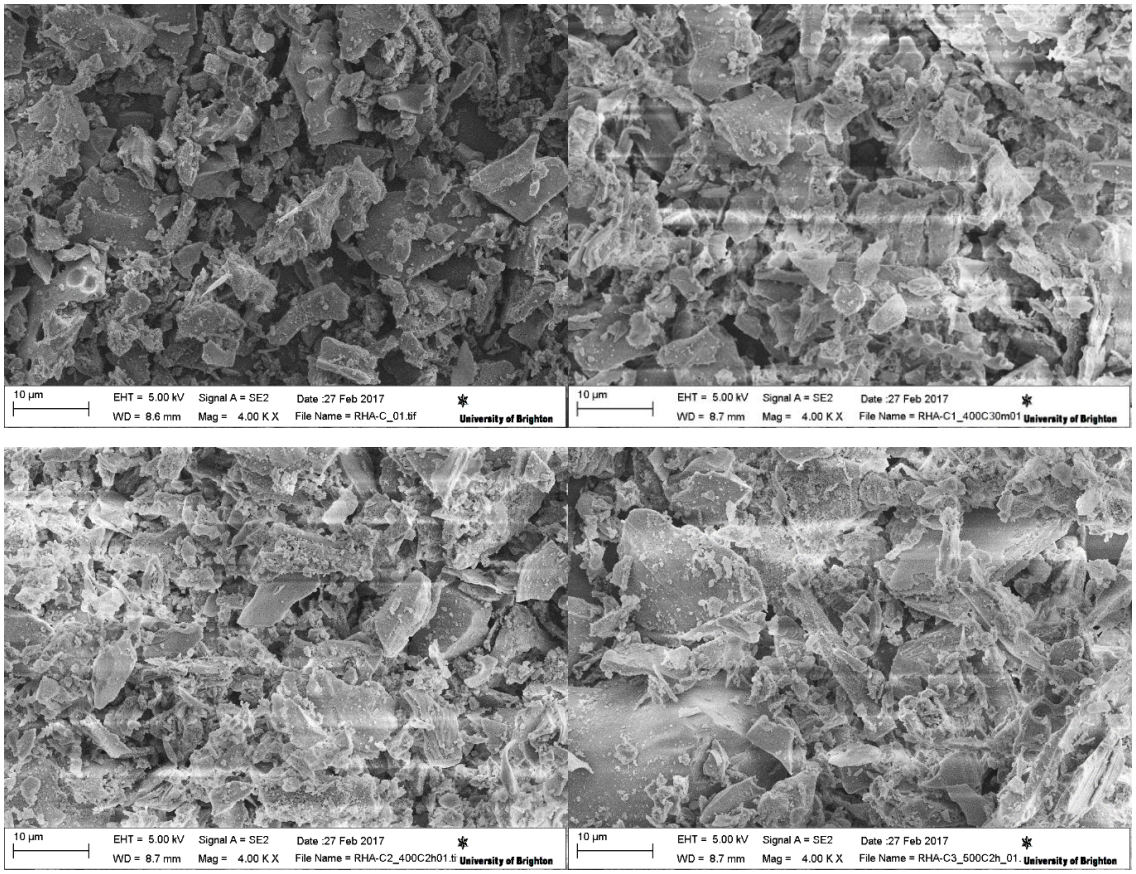

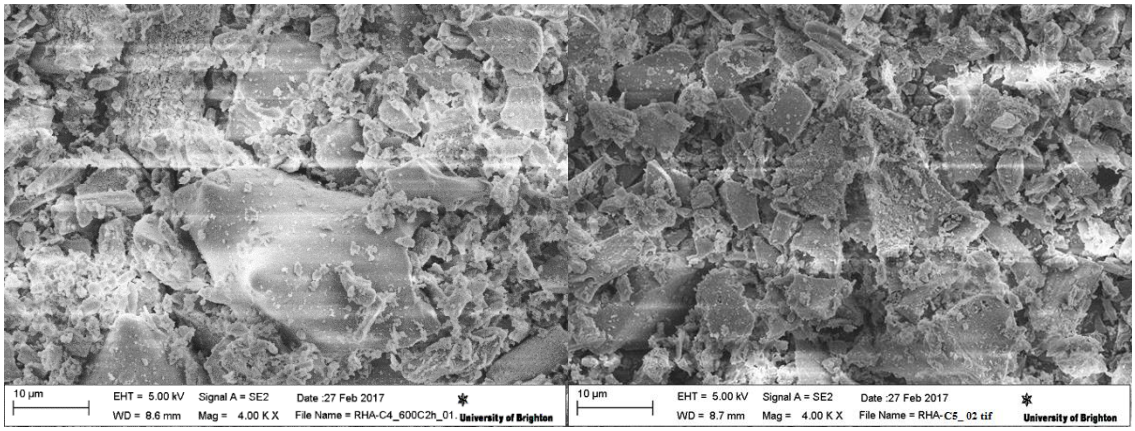

Figure 5. 20: Particle size distribution of RHA at different burning periods by SEM imaging.

5.6.3 Designation for control and RHA mortar

Mortar was mixed in, cast and cured in the same way as described in Chapter 3, section 3.10.1. The investigation was divided into two sections: the first section used one replacement ratio (5% wt. of cement) and four different RHA types (C1, C2, C3 and C4). Generally, the reason of use 5% replacement ratio for RHA-C1, C3 and C4, was due to the limitation of quantity were produced. Section two includes 8 replacement ratios (5% to 60%) and three types of RHA (C, C2 and C5). Water to binder ration and superplasticizer contents were the same as in the previous chapters.

5.6.4 Experimental results

5.6.4.1 Workability of RHA mortar

The flowability of RHA-C series mortars with 5% replacement were first determined to find out the flow characteristics of the mortars. Fig.5.25 (a), shows the influence of the different RHA types on the flowability of RHA mortar mixtures. The flow curve expressed good correlation between flowability of mixtures and specific surface area, and inverse relationship between losses on ignition to flowability. The result shows that the use of RHA with coarser average particle size (RHA-C3, C4, and C5) increases the water demand. RHA-C1 and C2, presented slightly increased in flowability about 0.42% and 1.24%, compare to RHA-C. The mechanism behind this water demand reduction is attributed to a part of water fill in the void, and the rest part of water forms a lubricating membrane which wraps around the particles and increases flowability (Givi et al., 2010). Test results of flowability of RHA-C, C2 and C5 are presented in Table 5.25, and 5.26, and illustrated in Fig. 5.25, (b).

It shows the Influence of RHA residual carbon content and particle fineness on the flowability of mixtures at constant water to binder ratio of 0.50. The results show that the incorporation of RHA-C2 lead to a slightly higher flowability compared to RHA-C. According to the Van Tuan et al. (2011), an increase in specific surface are of RHA lead to the collapse of the porous structure of RHA particles, and as a result reduce the absorbed water content in RHA during mixing. Same conclusion was reported by each of Maurice et al. (2012), Givi, et al. (2010) and Abu Bakar et al., (2011). On the other hand, despite of high specific surface area and fineness of particles, RHA-C5 exhibited lower flowability in comparison to RHA-C2. The only explanation for that is due to the amount of LOI and crystalline silica content. This is justified by the reason higher water absorbing demand and larger surface area. This property promotes faster reaction to occur.

Table 5. 25: Flowability of the RHA mixtures at 5% replacement ratio.

RHA %	Flow table (mm)						
	C	C1	C2	C3	C4	C5	SP*
5%	239	240	242	233	228	231	0.25
MPS (μm)	15.8	15.85	15.93	17.08	17.51	12.6	
SSA (m^2/g)	0.691	0.695	0.741	0.663	0.639	0.808	

SP*: Superplasticizer

Table 5.26: Comparison of RHA-C2 to RHA-C and C5 flowability.

RHA replacement (%)	Flow table (mm)			
	RHA-C	RHA-C2	RHA-C5	SP* (%)
5%	239	242	231	0.25
10%	214	219	205	0.25
15%	196	201	186	0.25
20%	179	185	174	0.25
30%	168	175	165	0.50
40%	157	164	153	1.00
50%	153	159	150	2.00
60%	147	153	144	4.00
OPC	255			0.25

SP*: Superplasticizer

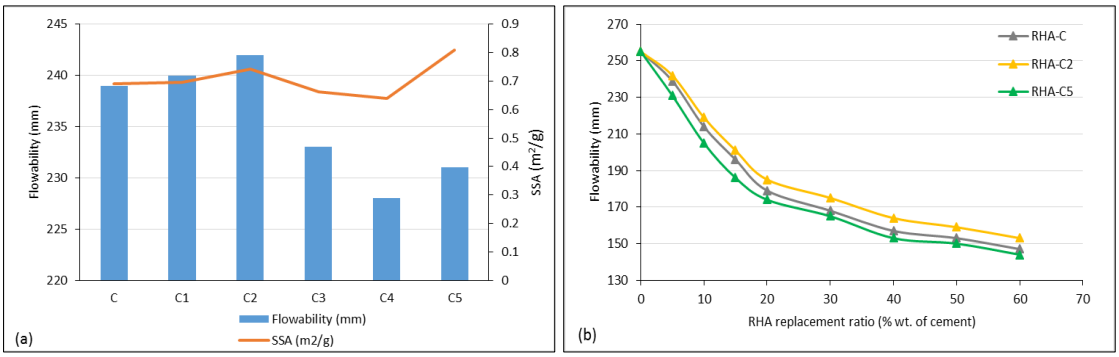

Figure 5. 21: Flowability of RHAs mortar mixture; a) 5% RHA C to C5; b) RHA-C2 to C and C5 up to 60% replacement ratio.

5.6.4.2 Compressive strength

a. Compressive strength of 5%RHA (C, C1, C2, C3 and C4) mortars.

The contribution of the loss on ignition (LOI) of RHA on the compressive strength of mortar are presented in Table 5.27, and plotted in Fig.5.26. The experimental results however, indicated that, with reducing of LOI amount and maintaining the silica structure in amorphous form, RHA showing a dominating role on the compressive strength development. As shown in Fig.7.6 and Table 7.6, the compressive strength of RHA-C1 and C2, increased about 1.00%, and 2.72% at 7 days compared to RHA-C. After 28 days, the strength increased up to 6.15%, 7.51%, 7.16% and 9.08% after 91 days compared to RHA-C. The positive effect of RHA-C1 and C2 on compressive strength is most likely to the high pozzolanity of RHA resulting from increased amount of amorphous silica content as a result of reduction in LOI.

According to Bie et al. (2015), the effect of the increased strength is due to the amorphous silica content and high specific surface area of the RHA. It is obvious that the exciting of residual carbon reduce overall quality of ash (Yamamoto and Lakho, 1982). RHA reacts intensively with the water and the calcium hydroxide generated from the hydration of cement to produce additional C–S–H (Bui 2001; Van Tuan et al. 2011; Safiuddin et al. 2011). RHA-C3 and C4 showed lower compressive strength. This is due to the crystalline silica present in the RHA and lower specific surface area compared to the RHA RHA-C1 and C2. Crystalline silica refers to the amorphous silica of RHA converted to non-reactive silica. The pozzolan reactivity of the crystalline silica is reduce due to it is structure and reduced surface area (Hwang, Bui & Chen, 2011).

Table 5. 27: Compressive strength of re-burned RHA-C series mortars at different ages.

Age of test	Compressive strength (MPa)				
	C	C1	C2	C3	C4
7days	37.97	38.34	39.03	36.60	36.24
28days	48.53	51.71	52.47	48.04	47.47
91days	55.65	59.94	61.21	53.19	51.48

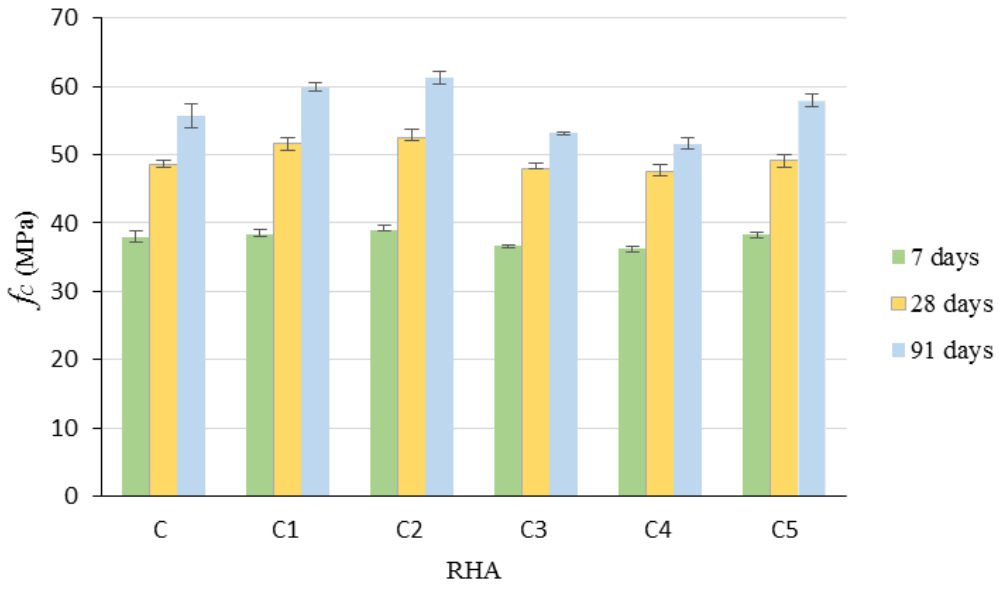

Figure 5. 22: Compressive strength of RHA at different ages.

b. Compressive strength of RHA-C2 to RHA-C and C5 mortar up to 60% replacement ratio. The results are shown in Table 5.28, and illustrated in Fig. 5.27. Unlike RHA-C and C5, the mortar incorporated with RHA-C2 shows excellent strength development at early age up to 30% replacement ratio. Generally, the reduction of early strength gained as compared to normal concrete is due to the slow pozzolanic reaction of the silica and the CH in the concrete (Shatat, 2013). However, RHA with fine grains acting as a micro-filler, promoting the cement paste pore structure, resulting in more mortar denser structure (Hamid and Ibrahim, 2015). With progression in curing time, RHA-C2 essential properties effected directly on the strength of mortars. The 28 days results shown significant improvement in strength of RHA-C2, even at 60% replacement ratio the compressive strength was increased about 6.11%, 4.67% and 14.08% compared to RHA-C, C5 and OPC control.

Table 5. 28: Compressive strength of RHA-C2 mortars compare to RHA-C at different ages.

RHA%	Compressive strength (MPa)								
	7days			28days			91days		
	C	C2	C5	C	C2	C5	C	C2	C5
5%	37.97	39.02	38.32	49.53	52.47	49.17	55.65	61.21	57.91
10%	36.13	38.86	37.4	50.24	53.62	50.56	56.15	62.68	59.41
15%	34.94	38.04	35.07	49.91	55.5	53.95	56.47	63.48	61.79
20%	32.97	37.67	33.67	47.10	57.41	56.43	60.21	66.29	63.01
30%	30.55	35.81	30.47	45.79	56.98	55.94	57.79	64.91	64.25
40%	27.24	33.70	28.64	42.43	54.84	48.96	55.71	61.26	59.24
50%	20.82	30.58	27.81	39.72	52.84	42.55	54.44	59.95	55.97
60%	16.34	25.27	23.02	32.82	49.17	39.59	53.34	56.81	54.16
OPC	35.4			45.5			48.81		

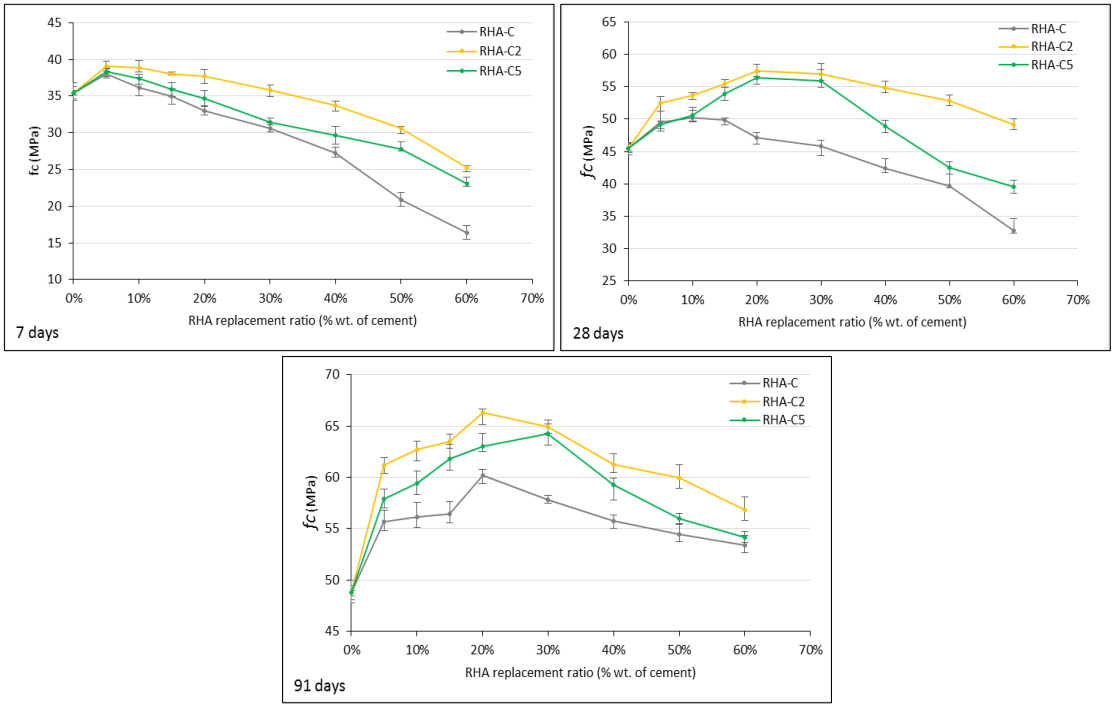

Figure 5. 23: Compressive strength of RHA-C2 compare to C and C5 mortars at different ages.

5.6.4.3 Tensile strength

i. Tensile strength of 5% RHA (C, C1, C2, C3, C4 and C5) mortar.

The tensile strength of mortars with 5% replacement of RHA-C to C5 is shown in Fig. 5.28. The results of tensile strength confirmed the compressive strength performance. The strength increased with RHA-C1 and reached optimum value with RHA-C2, then gradually decreases with increasing re-heating temperature. The significant enhancement of RHA-C2 tensile strength can be attributed mainly to the decrease in the existence of carbon. Since, carbon content exceeding 10% of RHA volume reduces the overall activity of ash (Ismail, 1979 cited in Yamamoto and Lakho. 1982). Furthermore, increase in the amount of silica content, which is entirely amorphous form. On the other hand, increase the degree of combustion temperature, led to affecting negatively on the strength performance (RHA-C4). Even though, the amount of existence carbon reduced.

However, RHA-C5 exhibited noticeable improvement, of compressive strength. The higher compressive strength of the RHA-C5 sample compared to that of other samples (RHA-C, C1, C3 and C4) is possibly due to the better filler effect (Nguyen, 2011). Moreover, strength development of mortar containing RHA depends not only on pozzolanic reactivity but also on particle size of RHA (Van, 2013). From the preceding discussion, it can be concluded that the RHA performance can be improved by removing the existence carbon. However, this improvement depends mainly on the relation between the incineration temperatures to a time.

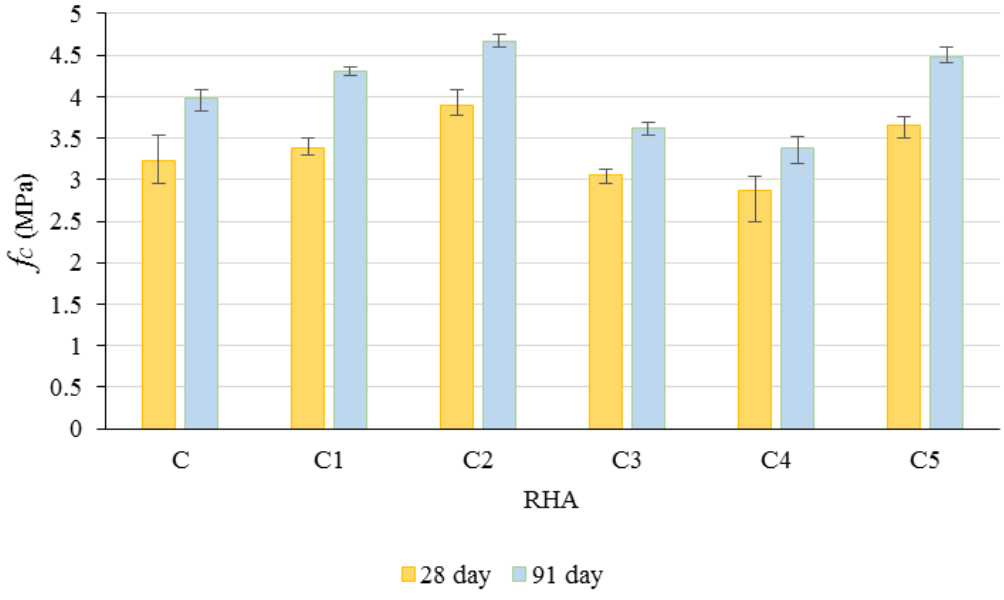

Figure 5. 24: Tensile strength performance of RHAs at age of 28 and 91-days.

ii. Tensile strength of RHA-C2 to RHA-C mortar up to 60% replacement ratio.

RHA-C2 results were comparable to RHA-C to determine the effect of re-burned RHA on tensile strength performance at different replacement ratios. Despite, the increase in tensile strength with increasing replacement ratio for both RHA ashes is identical regarding increase strength up to 20% replacement ratio then decreased. However, the results show that RHA-C2 possesses a higher compressive strength than RHA-C significantly. The rate of enhancement with application RHA-C2 is remarkable compared to RHA-C as shown in Table 5.29 and illustrated in Fig 5.29. With progressed time (91days), RHA-C2 improves the tensile strength of the mortar. Comparing to the strength of RHA-C to RHA-C2, there is a major advantage of the re-burned ash for strength.

Table 5. 29: Tensile strength of RHA-C2 mortars compare to RHA-C at different ages.

RHA%			Tensile strength (MPa)			
	RHA-C	RHA-C2	RHA-C5	RHA-C	RHA-C2	RHA-C5
		28days		91days		
5%	3.23	3.89	3.66	3.98	4.6	4.48
10%	3.61	4.02	3.82	4.19	4.81	4.58
15%	3.7	4.18	3.97	4.47	5.08	4.82
20%	3.79	4.57	4.18	4.86	5.36	5.14
30%	3.67	4.26	4.08	4.56	5.03	4.81
40%	3.55	4.03	3.78	4.22	4.8	4.32
50%	3.39	3.78	3.61	3.97	4.53	4.13
60%	3.04	3.41	3.32	3.84	4.27	4.06
OPC		28 days		91days		
		2.68		3.01		

ROI* (%): Rate of improvement (%).

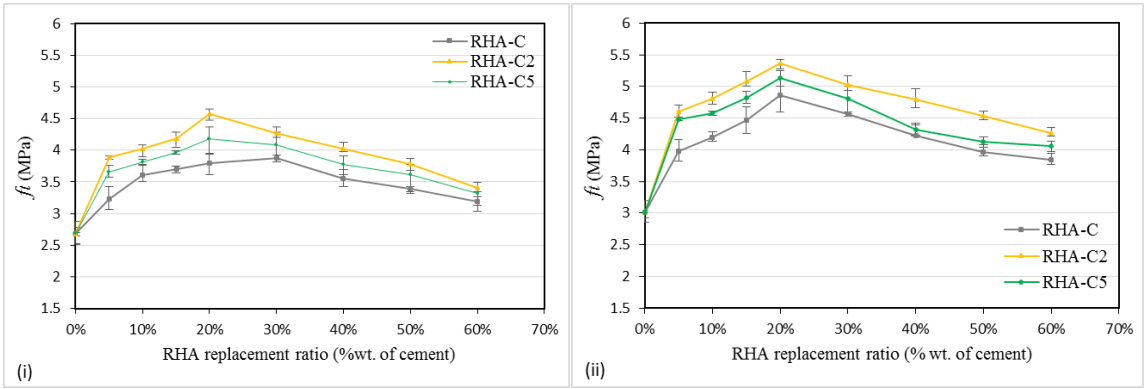

Figure 5. 25: Tensile strength performance of RHA-C and C2 mortars at age of; (i) 28-day, (ii) 91-days.

5.6.5 Discussion

The activity of RHA considered to be influenced by many factors, however burning temperature to time would be most important as far as reactivity and residual carbon content of ash are considered. Therefore, the effect of these parameters was studied step by step by examining the degree of contribution of each parameter in raising the strength of RHA mortar. Four different types of RHAs (C1, C2, C3 and C4) were produced by re-burned RHA-C at different temperatures to time. For this purpose, mortar specimens of various Portland cement –RHA mortar ratios (5% RHA-C1, C3 and C4, and 5% to 60% RHA-C2) were prepared and their compressive and tensile strength were test at 7, 28 and 91 days. For evaluating the activity of ash, the relative strength of each type of RHA with strength respective of RHA-C and C5 were compared. It can be found based on the strength results that the ash prepared in this research (RHA-C2) is highly active, where significant results observed in Table 5.28, is that even at 60% replacement ratio, mortar made with RHA-C2 exhibited 6.11% (RHA-C), 4.67% (RHA-C5), and 14.08% of OPC control. Based on that it can be say that, there is an optimum temperature to time, around 400°C for 2hrs (RHA-C2) where beyond that does not necessarily produce quality ash. Another noteworthy observation is that decrease of residual carbon content not necessarily improves the ash quality (RHA-C4). Where burning temperature above the optimum (400°C/2hrs) adversely effect on ash quality (Yamamoto and Lakho, 1982).

5.7 Effect of increase RHA fineness on flowability and strength of mortar

5.7.1 General

The effect of grinding time on the particle size distribution, specific surface area and pozzolanic activity of RHA was investigated. Different samples of RHA obtained from ultrafine grinding were characterized with respect to particle size, specific surface area and pore volume distribution using a laser diffraction particle size analyser (Malvern Mastersizer 2000). Pozzolanic activity was determined using electrical conductivity of a saturated solution of calcium hydroxide method. The evaluation was based on the change of the amount of flowability, compressive strength and tensile strength containing RHA at different grinding time compared to as received RHA.

5.7.2 Research significance

The effect of decreasing grain size of RHA on the mortar strength is useful to understand the fineness of RHA performance. Moreover, to eliminate the discrepancy of the literature on the optimum limitation of fineness of the RHA particles without inversely effecting pozzolanic reactivity, and the resulting strength of the RHA-blended mortar.

5.7.3 Method

A planetary ball mill (Planetary Mono Mill Pulverisette 6, see Fig.5.30) manufactured by FRIT ISCH (Canada) was used to mill small samples reducing the size of the particles to submicron and nanoscale. This mill works through friction and impacts caused by high-energy up to 650 rpm impacts from grinding balls and friction between balls and the grinding bowl wall. The mill shell, the grinding speed and the solid particles influence directly the outcome of size reduction. In each batch, the 225 ml mill internal volume was partially filled with 150g ±2 of the as-received RHA by weight at each time. Four different grinding time were selected (10, 20, 30, and 60 min). Particle size distributions and specific surface area was determined (see 3.3.2, Chapter 3).

Figure 5.26: The P6 Planetary Ball Mill is a bench-top grinding mill designed for powder XRF sample preparation.

5.7.4 RHA Characteristics

Fig. 5.31 shows the cumulative size distributions of ground RHAs in comparison to the RHA as received. Each curve of ground RHA corresponds to the individual adopted grinding times (varying from 10min to 60min). The ground RHA curves show very similar shapes, indicating that particles of all sizes were broken down as a result of the grinding action. As expected, the results indicate significant reductions in particle size with the increase in grinding time and the ground RHAs present values of D50 between 3.72μm and 6.91μm. The pore size distribution is the key physical property of RHA influencing pore volume, specific surface area, the water demand and the pozzolanic activity of RHA (Habeeb and Fayyadh, 2009). Theoretically, the specific surface area (SSA) of RHA derives from the internal surface area in pores and the external surface area on the surface of particles (Nguyen, 2011). During grinding, most macro-pores collapse and hence the internal specific surface area (SSA) of RHA decreases, whereas the external SSA of RHA increases (Lee, 2015).

Increasing grinding time decreases the mean particle size (MPS) of RHA, pore volume in RHA particles, and increases the SSA of RHA (Nguyen, 2011). The effect of the grinding time on mean particle size distribution, specific surface area and pozzolanic activity is summarized in Table 5.30. The ground RHA curves (Fig. 5.32, i and ii) show very similar shapes, indicating that particles of all sizes were broken down as a result of the grinding action. As expected, the results indicate significant reductions in particle size with the increase in grinding time and the ground RHAs present values of mean particle size ranged in between 3.72μm and 23.39μm. Previous investigations also had shown an increase in the SSA of RHA sample with increasing grinding time [Sugita et al., (1992); Bui, (2001); and Nguyen, (2011)].

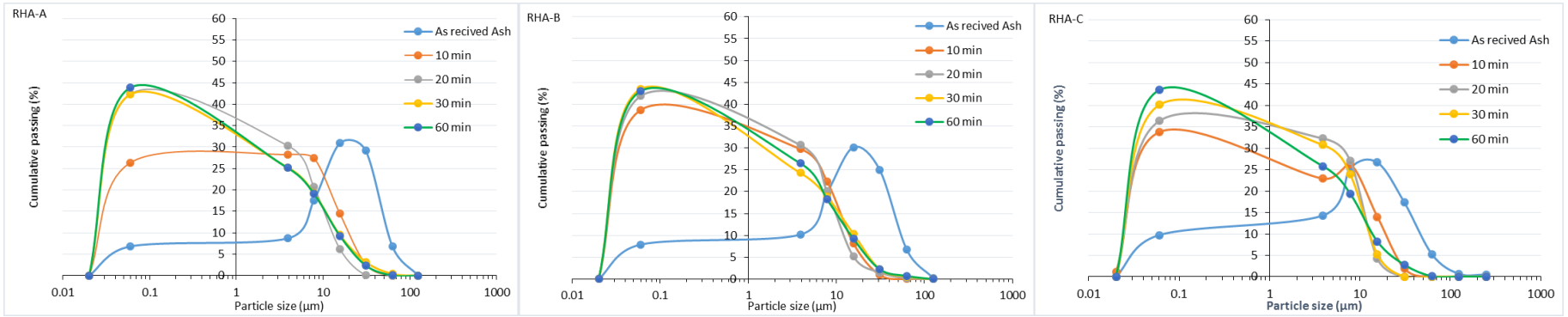

Figure 5. 27: Particle size distribution of the RHA and ground RHAs after different times of grinding (in minutes).

Table 5. 30: Variation of physical properties of RHA with grinding time.

Physical properties	RHA "as received"			Grinding time (minute)											
				10min			20min			30min			60min		
	A	B	C	A	B	C	A	B	C	A	B	C	A	B	C
MPSD* (µm)	23.39	20.94	15.80	6.91	5.07	4.33	5.62	4.67	4.12	4.78	4.35	3.91	4.07	3.91	3.72
SSA** (m^2/g)	0.53	0.58	0.69	1.26	1.31	1.43	1.71	1.77	1.86	1.85	1.92	2.09	1.88	2.13	2.38
PAEC***(mS/cm)	0.9	1.07	1.73	0.98	1.19	1.83	1.13	1.28	1.91	1.25	1.37	2.02	1.22	1.35	2.11

MPSD*: Mean particle size distribution
SSA**: Specific surface area
PAEC***: Pozzolanic activity based on the electrical conductivity test results (Luxán, et al., 1989)

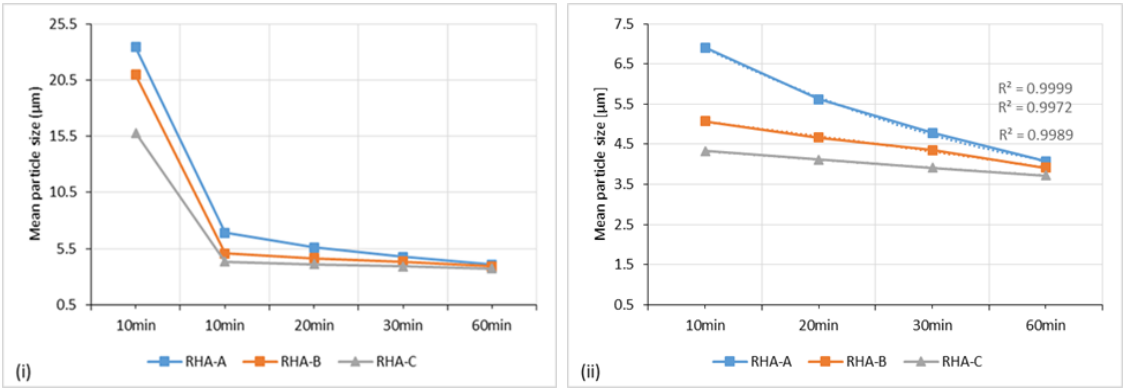

Figure 5.28: Variation of the mean particle size and grinding time, (ii) Correlation between grinding time and mean particle size.

5.7.5 Effect of reduced grain size on the pozzolanic activity of RHA

The correlation between the pozzolanic reactivity index and fineness was determined using electrical conductivity of a saturated solution of calcium hydroxide. Any change in structure of particles is expected to have an effect of the pozzolanic activity (Cordeiro et al., 2011). It can be seen from Table 5.30 that the pozzolanic reactivity of RHA increases with reducing RHA grain size. Mehta (1973) argued that, since RHA derives it is pozzolanicity from it is internal surface area, grinding of RHA to a high degree of fineness should be avoided. Bui et al., (2005) also stated that at a certain stage of grinding the RHA, the porous structure of particles would collapse, resulting in reduced surface area.

5.7.5.1 Correlation between grinding time and mean particle size

Fig. 5.33, shows the mean particles distributions of ground RHAs in comparison to the grinding time. As expected, the results indicate significant reductions in particle size with the increase in grinding time. A comparison between the grinding time and mean particles size values it is quite interesting that the conductivity after 10 minutes grinding is very similar to the conductivity of the as received RHA. The only explanation for this behaviour is that the RHA grains are clumped together, which gives some internal porosity. The short grinding time breaks these clumps apart but does not creates new surfaces. Grinding longer creates new surfaces and therefore increases the reactivity. However, with increase grinding time, pozzolanic activity increased remarkability, which is confirmed the results obtained each of Cordeiro et al. (2011), Habeeb and Mahmud (2010) and Al-Khalaf and Yousif (1984).

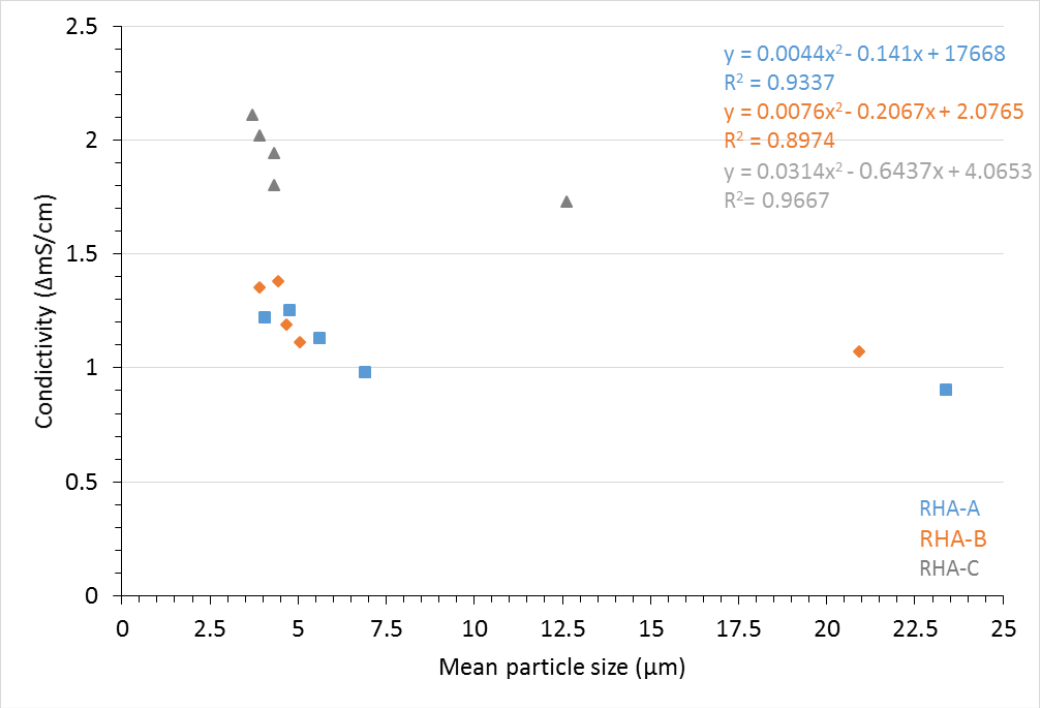

Figure 5. 29: Relationship between pozzolanic activity and mean particles size of RHA.

5.7.6 Results and Discussion

5.7.6.1 Flowability of RHA mixtures

Mini-slump cone tests were performed to evaluate the flowability of fresh RHA mortar according to BS EN 1015-03:2004. The measured slump was then plotted against RHA grain size as shown in Fig.5.34 and Table 5.31. The results show a general trend that, the slump increase with reducing grain size regardless of the type of RHA. Reducing the grain size of RHA by mechanical grinding was found to improve the flowability of RHA blended cement mortar. These surprising results may be explained that the finer particles will fill the pores of the cement paste and release the water in these pores. In this way, the flowability will be improved as part of the trapped water is transferred to free water (Luo et al., 2013). This confirms the point view of Van Tuan et al. (2011) who stated that an increase in specific surface area of RHA leads to the collapse of the porous structure of RHA particles, and as a result reduce the absorbed water content in RHA during mixing. The same conclusion was reported by Maurice et al. (2012), Givi, et al. (2010) and Abu Bakar et al., (2011). Paya et al. (1993) named this phenomenon lubricant effect, where increasing RHA fineness, reduces the internal friction in fresh mortar.

Table 5. 31: Flowability of RHA mixtures in related to fineness degree.

RHA	Mean particle size (µm)	Flowabiliy (mm)
RHA-A	23.39	200
	6.91	204
	5.62	213
	4.78	218
	4.07	224
RHA-B	20.94	205
	5.07	209
	4.67	216
	4.35	221
	3.91	227
RHA-C	15.8	239
	4.33	241
	4.12	245
	3.91	247
	3.72	251

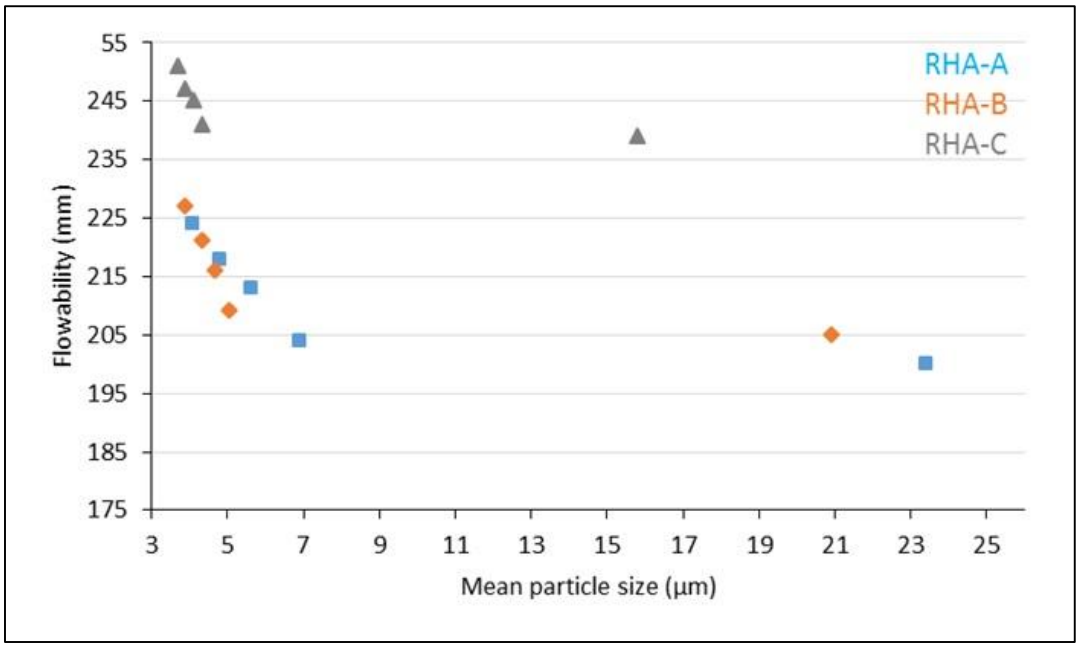

Figure 5. 30: The flowability of RHA mixtures to mean particles size.

5.7.6.2 Effect of RHA grain size on the compressive strength of RHA mortar

The compressive strength testing results of mortar with incorporation of 5% cement replaced by RHA is shown in Fig.5.35 and Table 5.32. The reactivity of rice husk ash cement extremely depends upon the specific surface area and/or particle size. The hydration starts at the surface of cement particle, the rate of hydration depends on the grain size of cement and for rapid strength development fineness is important factor (Neville, 1996). Similarly, small grain size of RHA is a beneficial for strength development of blended mortar and

concrete (Karim et al., 2012). Therefore, it can be seen that, all RHA mortar achieved an increase in strength. The increased gain in strength at early ages of mortar incorporating finer RHA, especially RHA-C may suggest an early start of the pozzolanic reaction (Aimin et al., 1994). The data in Table 5.32, show that the compressive strength generally increased with decreasing grain size to 4.78µm (RHA-A), 4.35µm (RHA-B) and 3.91 µm (RHA-C), producing high compressive strength in the range of 58.59 (RHA-B) to 75.31MPa (RHA-C) at the age of 91 days.

These positive results of ultra-fine RHA-blended mortar obtained due to the rapid consumption of $Ca(OH)_2$ produced during hydration of Portland cement at early ages are associated to the high pozzolanic reactivity of ultra-fine RHA. As a result, the hydration of cement is accelerated and larger volumes of reaction products are produced (Karim et al., 2012). The data also show that with reducing grain size of RHA particles to 4.07, 3.91 and 3.72µm, inversely affected on the strength of the RHA mortars. From previous discussion it can be conclude that the strength of mortar incorporating RHA is increased with increase in RHA grinding duration of 10–30min. However, when the RHA grinded for above of 30 min, the corresponding strength of mortar is gradually reduced. This indicates that long grinding time does not always lead to high pozzolanic activity, due to the particle aggregation by excessive grinding (Xu et al., 2015). The 30min grinding of RHA shows the best pozzolanic activity among all the ground ash samples.

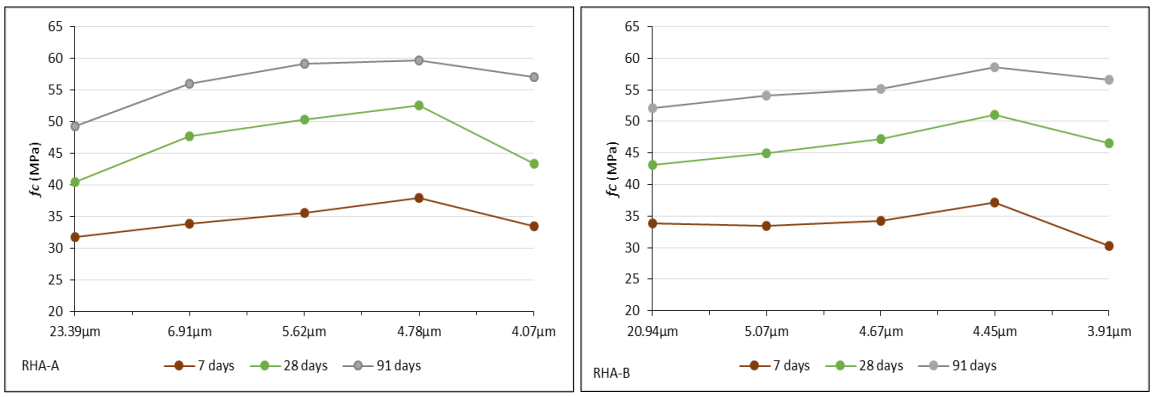

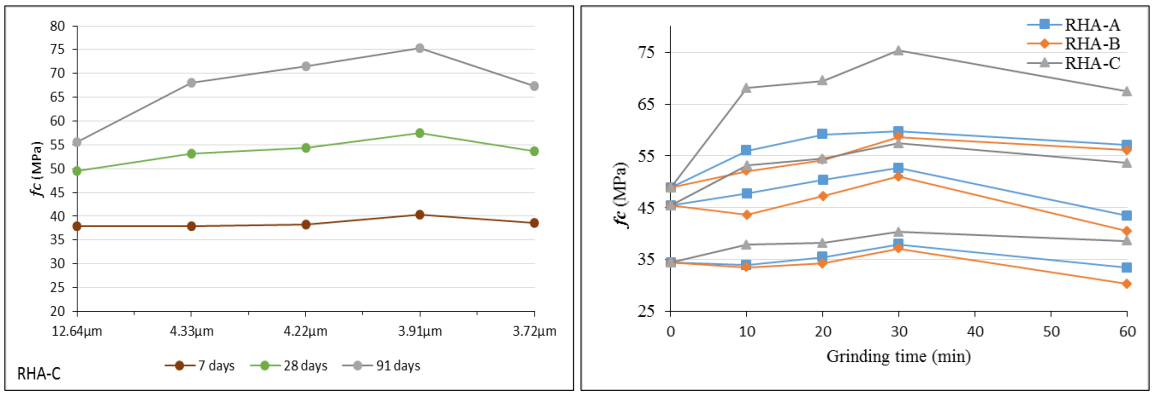

Figure 5. 31: Effect of RHA fineness on the compressive strength of RHA-A, B and C mortars; at different ages (7, 28, and 91 days).

Table 5. 32: Effect of RHA particle size on the compressive strength of mortar.

RHA	Mean grain size (µm)	Compressive strength (MPa)		
		7 days	28days	91days
RHA-A	23.39	31.75	40.42	49.25
	6.91	33.86	47.67	56.01
	5.62	35.54	50.37	59.13
	4.78	37.9	52.6	59.71
	4.07	33.41	43.35	57.07
RHA-B	20.94	33.87	43.07	52.10
	5.07	33.91	44.98	54.04
	4.67	34.77	47.23	55.18
	4.35	37.13	51.06	58.59
	3.91	33.32	46.52	56.59
RHA-C	15.8	37.97	49.53	55.65
	4.33	38.83	53.2	68.1
	4.12	39.2	54.42	71.48
	3.91	40.3	57.5	75.31
	3.72	38.59	53.6	67.4

5.7.6.3 Correlation between pozzolanic activity and compressive strength of RHA mortar

In order to understand the influence of the pozzolanic activity (the conductivity) of RHA change on the strength development of RHA mortar, a correlation between compressive strength to conductivity and mean particle size distribution were plotted in to Fig. 5.36. The results shown that, samples became more strength with increase conductivity up to 1.25 (RHA-A), 1.37 (RHA-B), and 2.02 ΔmS/cm (RHA-C), respectively. However, samples subjected to longer grinding times (60 min) the strength decreased with increasing grinding time, even with slightly increased conductivity of RHA-C. These results of compressive

strength to conductivity of RHA suggest that a certain independence relationship are exists for each type of RHA between compressive strength and conductivity for the RHA. A good logarithmic relationship (R^2>0.9) was identified between pozzolanic activity values and compressive strength. Also, clearly demonstrates that the same behavior can be observed in the relationship between D50 and the compressive strength where the correlation can be represented by a liner law with significant correlation ($R^2 \geq 0.97.5$).

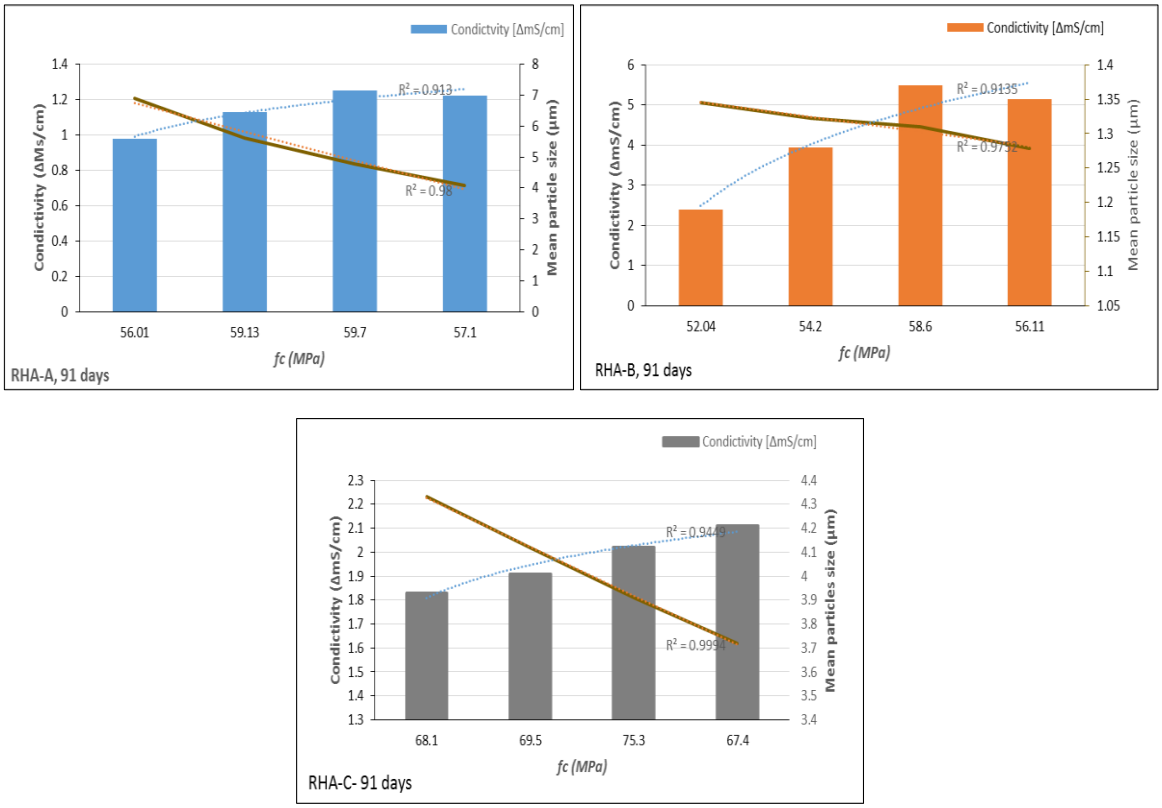

Figure 5.32: Correlation between pozzolanic reactivity to compressive strength with mean particle size of RHA mortar.

5.7.6.3 Tensile strength of RHA mortar

The tensile strength is presented in Tables 5.33 and illustrated in Fig.5.37. The results show that the development of tensile strength occurs in a similar way to that of the compressive strength. The results indicate that the increase in RHA fineness have beneficial effects on the tensile strength development. The significant improvement in the tensile strength can be attributed to the filler effect of the smaller particles in the mixture (De Sensale, 2006). According to Saravanana and Kumar (2013), the observed improvement in tensile strength of the composite is attributed to the fineness of RHA particles. However, the coarser RHA particle mixtures show smaller increments in tensile strength as reported by Habeeb and

Fayyadh (2009). Tensile strength reached the optimum values with RHA fineness ranged in between 3.91 and 4.78µm. with increase fineness of RHA particle to 4.07µm (RHA-A), 3.91µm (RHA-B), and 3.72µm (RHA-C) tensile strength decreased. A comparison of the as-received RHA-A, B and C mortar strength to the samples with RHA grinded to 30min, the strength improved by 22.62%, 20.35%, and 29.43%, respectively. This increase is attributed to the pozzolanic reaction between the $Ca(OH)_2$ in the paste and the amorphous silica in the RHA as a result of increase RHA surface area (Zhang et al., 1996).

Table 5. 33: Effect of increase RHA fineness particles on the tensile strength of mortar.

RHA	Mean grain size (µm)	Compressive strength (MPa)	
		28days	91days
RHA-A	23.39	3.19	3.25
	6.91	3.34	3.61
	5.62	3.47	3.90
	4.78	3.52	4.20
	4.07	3.26	3.90
RHA-B	20.94	3.05	3.21
	5.07	3.27	3.68
	4.67	3.35	3.89
	4.35	3.44	4.03
	3.91	3.19	3.50
RHA-C	12.64	3.23	3.98
	4.33	3.51	4.59
	4.12	3.65	5.26
	3.91	3.93	5.64
	3.72	3.77	5.04

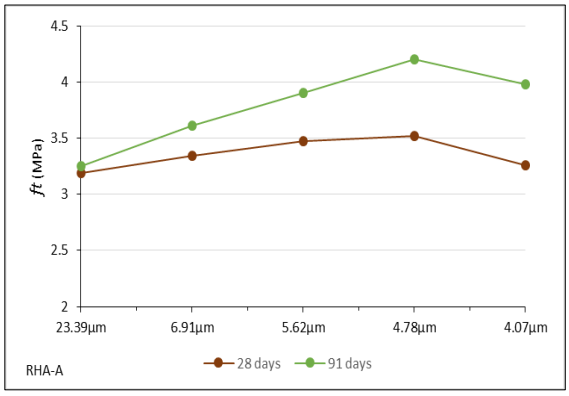

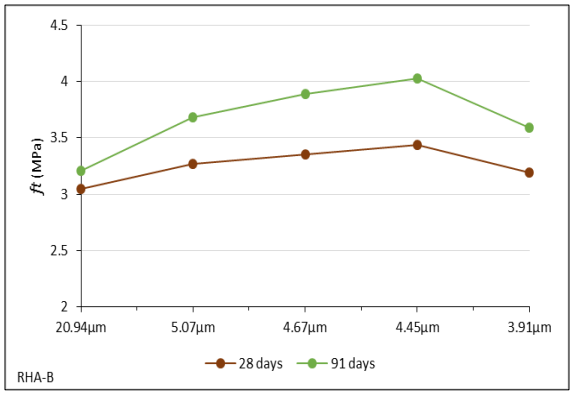

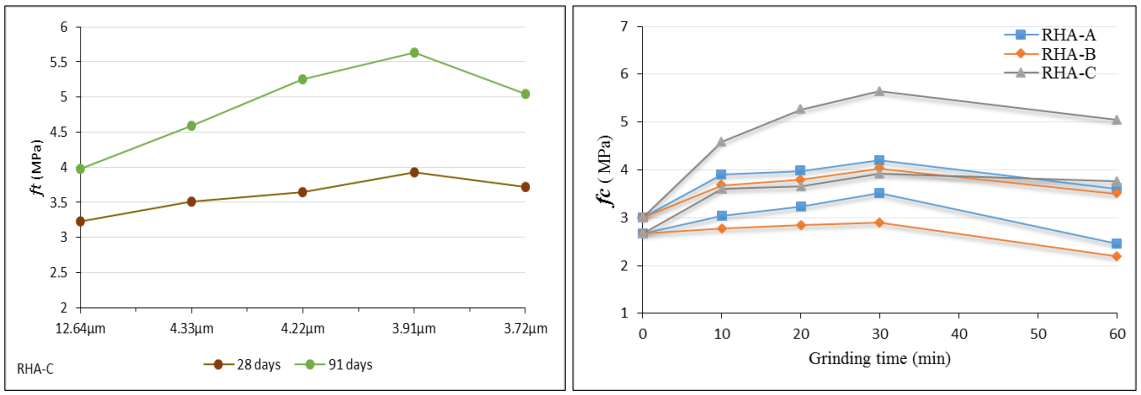

Figure 5.33: Effect of RHA grain size on the tensile strength of RHA mortars at ages of 28, and 91 days.

5.7.7 Result discussion

Regarding to the strength of the RHA re-grinded samples, the experimental results (Fig.5.35 and 37) show the positive effect of increasing fineness of RHA on the strength of mortar. Because of increases the fineness and specific surface area of RHA particles, the degree of hydration of mixture at later ages (28 and 90days) was increased, it may be attributed to the porous structure of RHA particles as discussed earlier. According to each of Khan et al. (2014); Shukla et al. (2011); Raman et al. (201); El-Dakroury and Gasser, (2008), that the hardening of mortar or concrete linked to higher fineness of RHA when applied in cementations system because of filling or densification of microstructure. Comparing the results of RHA mixtures before and after re-grinding, it is evident that increase of particles has a significant effect on the pozzolanic reactivity (conductivity) and strength development of mortars. However, this effect on increase of strength it depends on the degree of particles size and silica structure of each of RHA samples, where over this degree of fineness the strength declined.

This conclusion was supported by each of Karim et al. (2102) and Khan et al. (2015). However, Gosalvitr et al. (2015) stated that strength of RHA mixtures improved remarkably at 90min grinding time compare to conventional mortar. Van et al. (2013) stated that there is an optimum grinding time/fineness of RHA to produce the maximum compressive strength. Where, during grinding, the mean particle size of RHA decreases involving the collapse of the porous structure of RHA particles. In addition to that, Xu et al. (2015) reported that grinding for above 30 min does not always lead to high fineness due to the particle aggregation. Therefore, excessively long grinding duration should be avoided.

5.8 Conclusion

This chapter has examined the effect of RHA properties and replacement ratio on the flowability, compressive strength, tensile strength and drying shrinkage of mortar with different dosage of superplasticizer. The following conclusions are based on the results and analyses presented in this chapter.

i. The incorporation of RHA decreases the flowability, this effect is much stronger when the coarser RHA types (A and B) and high contents of RHA are used. This phenomenon can be attributed to the porosity of the RHA particles.

ii. The development of strength of RHA mortar mixtures depends mainly on the amount of reactive (amorphous) silica; however, fineness of the RHA particles is another factor that significantly improves the mortar strength.

iii. This study determines the chemical contribution of RHA on the basis of replacement percentage of RHA. This contribution will vary with the change of RHA composition or type of cement used. The theoretical results based on the hydration reactions are compared to the compressive strength result and X-Ray diffraction of RHA mortar.

iv. The compressive and tensile strength of RHA mortar were improved at high replacement ratio (40% and over) due to the micro filling effect and pozzolanic effects of RHA.

v. The strength properties of the RHA were progressively improved with the increase in RHA content up to 20% RHA-A and B, 30% RHA- C5 and RHA-C when cured for an extended period.

vi. A comparison of the RHA-C and C5 mortar results in 7days to 28 days indicated a remarkable increase in compressive strength for RHA-C5.

vii. Good correlations were observed among the compressive and tensile strength of RHA mortars.

viii. The ratio of the tensile strength to compressive strength (*ft/fc*) is influenced by the level of concrete strength. At low compressive strengths, the tensile strengths are as high as 10.7% of the compressive strength but at extremely higher compressive strengths, the ratio reduces to approximately 7% (Table 5.11).

ix. The commonly accepted 0.5 power relationship between the splitting tensile strength and compressive strength was determined to be realistic; the equations 5.1 to 5.6 are close to thus the ACI model for high-strength concrete.

x. Re-burning RHA-C at 550°C for 6hrs, created ash (RHA-C5) with best quality of ash compare to RHA-A, B and C. The amount of silica content increased from 84.30% to 93.49% also the mean particle decreased size from 15.8μm to 12.64μm.

xi. High residual carbon content (loss on ignition) does not prevent a high performance of blended cement mortar when the silica in the RHA is entirely amorphous as it is observed with RHA-C.

xii. Due to the high-water demand of RHA, it is inevitable that systems which include RHA require chemical admixtures to improve their workability. SP dosage had to be increased gradually for high RHA replacement ratios.

xiii. Typically, the results show that RHA blended cement offer higher performance at a later age (28, 91 days); mixtures with 0.50% SP also demonstrate the highest performance at a later age.

xiv. The drying shrinkage was significantly affected by RHA fineness of particles. RHA-C5 recorded the highest shrinkage value, while RHA-A exhibited the lowest values than the control, this is due to the effect of the micro-fine particles.

xv. The use of the RHA for application in mortar showed excellent performance in drying shrinkage at 60%RHA-A and B compare to control mortar.

xvi. Strains due to drying shrinkage of RHA are ranged from 1016 (RHA-A) to 1391(RHA-C5) $*10^{-4}$ (mm/mm) compare to 1143 $* 10^{-4}$ of OPC mortar at 180 days.

xvii. The effective mean particle size of RHA on mitigating drying shrinkage of RHA mixtures was suggested to be over 20.0μm. Where with coarser particles size less dry shrinkage reported.

xviii. Shrinkage strain rate linearly increases with increase fineness of RHA particles.

xix. The use of a 60 percent volume replacement of Portland cement by RHA-C5 generally leads to increased drying shrinkage, contrary to RHA-A and B, where lead to decrease drying shrinkage.

xx. Drying shrinkage strain rate factors demonstrate good correlation with compressive strength of RHA-C and C5, and less with RHA consist of coarse particles.

xxi. The behavior of RHA drying shrinkage strain is linear with RHA particles. Where, with increase in coarse particles size, lower dry shrinkage was obtained.

xxii. As the proportion of replacement ratio increases the dry shrinkage of the mortar decreased up to 15% RHA-A, and 20% RHA-B, C and C5, beyond that were increased.

xxiii. The drying shrinkage of mortar containing RHA-C5 was approximately 17.8% higher than OPC mortar at 60% replacement ratio at age of 180days. Part of the high increase in drying shrinkage of RHA-C5 is due to the very fine particles.

xxiv. According to the literature, there is some debate among researchers, for the advantageous use of RHA in mortar and concrete in respect of drying shrinkage. However, this study proves the point view of the majority of the researchers about the positive impact of RHA on the decrease of drying shrinkage as an extended period.

xxv. The use of superplasticizers in RHA mortar appears to increase drying shrinkage to a degree. The results, however, do not present a clear picture of the effect of superplasticizer dosage on shrinkage.

xxvi. The studies conducted for the material characterization of re-burned RHA on the properties yielded the following findings:

xxvii. The XRD patterns of RHA-C3, C4 and C5 showing some weak diffraction peaks of crystalline silica at 26.60°.

xxviii. The results clearly indicate that decreasing of RHA residual carbon content was found to improve the flowability of blended cement mortar as long as silica structure of ash remained in amorphous form.

xxix. The rate of strength gain of mortar was improved significantly with the decreasing of RHA-residual carbon content. The compressive strength of the RHA-C2 of 5% replacement ratio had the highest compressive strength.

xxx. The fineness of RHA is increased with increase in grinding duration from 10 to 30 min, which is attributed to the grinding effect on reduction of particle size (or incensement of surface area). Grinding for above 30 min does not always lead to high fineness due to the particle aggregation. Therefore, excessively long grinding duration should be avoided.

xxxi. RHA exhibited excellent correlation between pozzolanic activity and fineness of RHA particles.

xxxii. The flowability of mixtures was improved with increasing fineness of RHA particles. This may be due to the collapse of the porous structure of RHA particles at a high degree of grinding and reduces the resulting absorbed water content in RHA during mixing.

xxxiii. Among the four different grinding times, at 30 minutes of grinding the highest values of the compression and tensile strengths of the RHA mortars are obtained when mean particle size ranged in between 4.78μm (RHA-A) and 3.91μm (RHA-C), beyond this limitation, the strength has been decreased.

CHAPTER 6: EFFECT OF RHA ON FRESH AND HARDENED OF CONCRETES

6.1 Introduction

Strength is one of the most important characteristics of concrete, and design calculations of structural concrete members are dependent on the strength parameters of the concrete mix. The strength parameters will determine the ability of the concrete member to support the apply loads without failure. The concrete strength starts to develop after the concrete has hardened, and most of the strength is attained at 28 to 90 days. Also, strength can be attained at an early age when special types of cements are used in the concrete mix. For our investigation in this chapter, the results of the effect of RHA properties on the engineering properties of concrete such as compressive and splitting tensile strength are reported at various ages (7, 28 and 91 days). The effect of RHA on workability is also presented and discussed. A series of concrete mixtures involving three different RHA types (RHA-A, B and C) with variable replacement ratio (5% to 60%RHA-A and B, and to 80%RHA-C), were used. To neutralize the effect of w/c ratio on the fresh and hardening properties of RHA concrete, all the RHA concrete mixes were made with a water / binder ratio of 0.5. As a high demand of water, different superplasticizer dosage had to be use to maintain the workability of fresh RHA concrete mixtures in acceptable limitation. The dosages of SP were varied for different concrete mixtures to achieve acceptable a slump flow. The SP dosages were mainly dependent on the RHA content used. The compressive strength tests were carried out for all concrete mixtures at 7, 28, and 91 days, splitting tensile strength at 28 and 91days of moist curing. The minimum 28 days compressive strength of 50±3 MPa were considered for RHA concrete mixtures

6.2 Materials

6.2.1 Cement

The cement used was high strength cement type CEM I 52.5N confirming to the BS EN 197-1: 1996. The chemical composition and physical properties are presented in Table 3.1 (see Chapter 3).

6.2.2 Rice husk ash

Three different RHA types used as a supplementary cementing material (SCM). RHA was tested for specific surface area, particle size distribution, chemical composition and pozzolanic activity are presented in Tables 4.3, 4.5 and 4.7 (see Chapter 4).

6.2.3 Superplasticizers

The specification of superplasticizers was used as a water reducing admixtures for concrete was presented in section Table 3.5 (see Chapter, section 3.5).

6.2.4 Aggregate

6.2.4.1 Fine aggregate

Fine aggregate confirming to BS EN 12620:2013 was used, the sieve analysis are presented in Table 3.3 (see Chapter 3).

6.2.4.2 Coarse aggregate

The coarse aggregates included local natural un-crushed gravel with graded size 4 to 9 mm and specific density of 2678 kg/m^3 were used.

6.3 Mixture proportions

The control OPC concrete was designed to achieve Grade 50 N/mm^2 using the DOE method (DOE, 1988). Based on this, the cement content of 460kg/m^3, was adopted. The water to binder ratio (w/b) was 0.50. One binder mixture was prepared involve a control mix with 100% Portland cement and without any additive, and the others with RHA in concentrations of 0, 5, 10, 20,30, 40, 50, 60, 70 and 80% by weight of cement. The substitution concentrations chosen for tests evaluated on 9 cube specimens of dimensions 100mm ×100mm× 100mm. Tests involved determine the compressive strength at the hardened. The results are all based on average quantity obtained from the mixtures with different proportions. In addition to above mentioned, for each mix, three cylinders specimens of 100mm (diameter) × 200mm (high) prepared to evaluate tensile strength at 28 and 91 day as shown in Fig 6.1.

Increased in the amount of RHA content resulted in dry mix concrete (Kartini et al., 2004), therefore superplasticizer (SP) was used to enhance the fluidity of the mixes. The dosages of superplasticizer which is in liquid form were selected according to the guideline of the manufacturer (Fosroc International Ltd.). The total amount of superplasticizer used for each

replacement ratio was calculated as a percentage from total binder ratio and subtract from total quantity of used water. Table 6.1, summarizes the mix proportions for control OPC and various RHA concrete mixes

Table 6. 1: Details of the RHA concrete mixture proportions

RHA%	Cement (Kg/m^3)	RHA% (Kg/m^3)	Aggregate (Kg/m^3)		Water (Kg/m^3)	SP (% wt. of binder)	SP (Kg/m^3)
			fine	Coarse			
0%	460	0	785	800	228.85	0.25	1.15
5%	437	23	785	800	228.85	0.25	1.15
10%	414	46	785	800	228.85	0.25	1.15
15%	391	69	785	800	228.85	0.25	1.15
20%	368	92	785	800	228.85	0.25	1.15
30%	322	138	785	800	227.7	0.50	2.30
40%	276	184	785	800	225.4	1.00	4.60
50%	230	230	785	800	220.8	2.00	9.20
60%	184	276	785	800	211.6	4.00	18.40
70%	138	322	785	800	202.4	6.00	27.6
80%	92	368	785	800	202.4	6.00	27.6

Figure 6.1: Casting of cubes and cylinders for compressive and splitting tensile strength of concrete

6.4 Preparation of Fresh Concretes

The fresh RHA mixtures were prepared using a revolving pan type mixer conforming to BS 1881-125:2013, is shown in Figure 6.2. The nominal capacity of the pan was 50 litters. The details of preparation of OPC and RHA concrete mixtures are presented in Chapter 3, section 3.10.2.

Figure 6.2: Pan Mixer used for preparing OPC and RHA concretes mixtures.

6.5 Testing

The slump test according to BS EN 12350-2 (2009), was performed to measure the workability of concrete. The concrete was filled in three layers; each layer was roughly one third the height of the slump cone and each layer was stroked 25 times with the rounded end of the rod. After the cone was filled with concrete, the cone was lifted vertically in 3 seconds and slump value of the concrete was determined of each batch as shown in Fig 6.3. The compressive strength was computed using the formula given by BS EN 12390-3:2009 and tested on 100 mm cubes (Fig 6.4) at ages of 7, 28, and 91days, after curing in water. In determining the splitting tensile strength, BS EN 12390-6:2009 was used, and tested on cylinders 100mm in diameter and 200mm in height (Fig 6.5) at ages of 28, and 91 days, after curing in water.

Figure 6.3: Determine workability of concrete mixture according to BS EN 12350-2 (2009).

Figure 6.4: Compressive strength test on cubes size 100mm × 100mm × 100mm, according to BS EN 12390-3:2009.

Figure 6.5: Splitting tensile strength test on cylinder size 100mm (diameter) × 200mm (high), according to BS EN 12390-3:2009.

6.6 Results and Discussion of

6.6.1 Workability

Workability for the concrete is measured according to BS EN 12350-2:2009. The properties results are presented in Table 6.2, and illustrated in Fig. 6.6.

Table 6.2: Workability (slump) of OPC and RHA concrete conducted based on BS EN 12350-2 (2009).

Mixtures	Workability (mm)									
	5%	10%	15%	20%	30%	40%	50%	60%	70%	80%
RHA-A	141	110	94	68	59	48	27	13	-	-
RHA-B	176	131	98	73	64	53	35	21	-	-
RHA-C	181	143	109	81	70	61	51	44	27	11
OPC						208				

The results show that the workability of concrete decreased in the presence of RHA particles regardless of it is particle size. Generally, the use of RHA with fine average particle size (RHA-C) reduces the water demand in compare to the average of coarse particles (RHA-A and B). The mechanism behind this water demand reduction is attributed to the absorption of RHA particles by the oppositely charged surfaces of cement particles which lead to avoidance them from flocculation (Tiago, 2011). Moreover, the finer particles of RHA-C will fill the pores of the cement paste and release the water in these pores. Another reason

of high performance of RHA-C is the amount of ultra-fine particles (9.750% of total volume). According to Cordeiro et al. (2008), high ultra-fine particles (0.060µm), which tends to reduce the particle interlocking and internal friction and in results reduces the plastic viscosity of the mix. In this way, the flowability will be improved as part of the trapped water is transferred to free water (Luo et al., 2013). In addition to that, the porous structure of very finely ground RHA collapses. Therefore, the coarser RHA-A and B types have a higher water demand as less water is trapped inside the pores of the RHA particles (Bui et al., 2005).

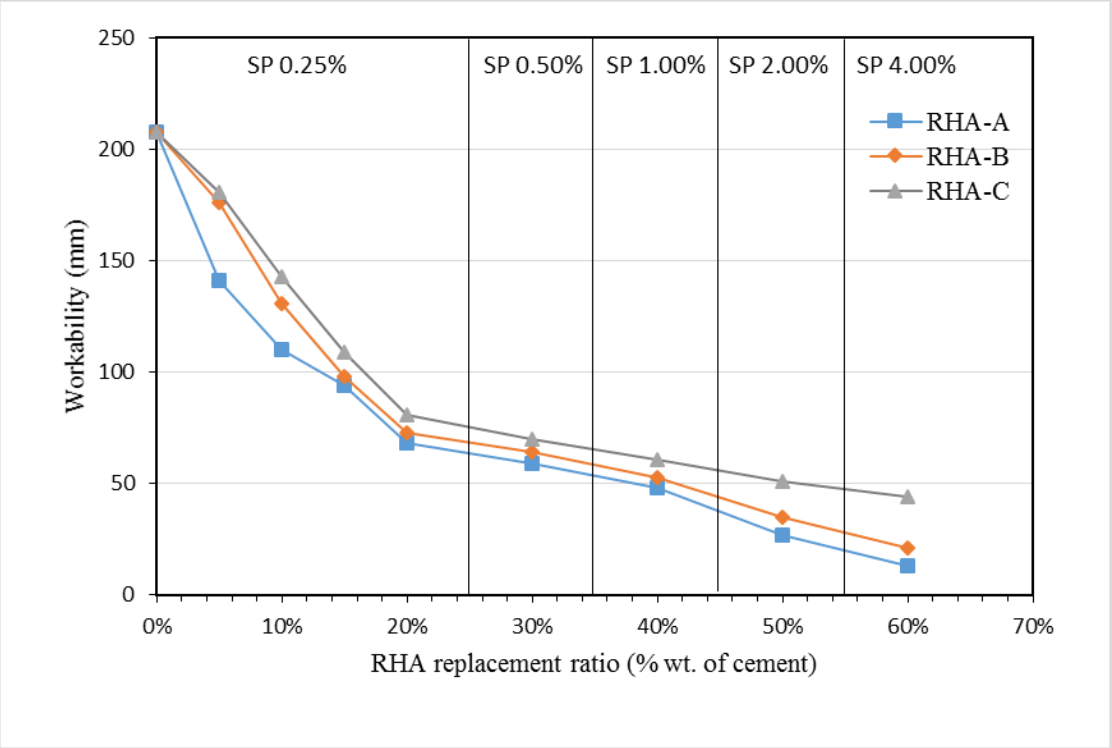

Figure 6. 6: Workability of fresh RHA mixtures at different replacement ratio.

6.6.1.1 Influence of RHA content on the workability

Generally, the total surface area of the binder strongly depends on the RHA content. For example, when 5% cement is replaced by RHA-A, the total surface area of 1g of this blend is 4.164 m^2/g comparing to the same replacement ratio of RHA-B and C, are 0.4272 m^2/g and 0.4289 m^2/g respectively. This value increased by about 28.6% (0.5812m^2/g) with 60% RHA-C. Therefore, this effect increases with increasing replacement ratio of RHA. In addition to that, the irregular shape of particles and the porous structure of RHA. Those factors reduce the workability of mixtures at a higher RHA content when the total amount of mixing water is kept constant for each replacement ratio. The similar conclusion was

reported by Krishna et al. (2016). In general, the RHA-C has better workability than RHA-A and B at all replacement ratio. Even though, RHA-C consists of high surface area, more fineness particles and abnormal amount of carbon content (LOI).

6.6.2 Compressive strength

The calculations and testing of the specimens were carried out as per BS 1881-125:2013, where $f_c = \frac{F}{Ac}$ (equation 3.3). The average compressive strength of three (3) test specimens for each of the nine (9) mixes for RHA-A and B, and eleven (11) mixes for RHA-C were obtained. The rate of all RHA concrete strength development as a percentage of 7, 28 and 91day strength development compared to OPC concretes is presented in Table 6.3, and illustrated in Fig 6.7. While the rate of development is presented in Table 6.4. The average compressive strength of the test specimens ranged from 46.32MPa (80%RHA-C) to 73.11MPa (15%RHA-C). The early age (7 days) of compressive strength results shown improvement in compressive strength of RHA concrete up to 15% replacement ratio. Further increase in the RHA content retards the strength development largely due to the higher water demand for these mixes (Anwar et al., 2014). The 28days compressive strength varied from 39.49 to 63.10 MPa while the 91days compressive strength differed from 45.46 MPa to 73.11 MPa for different concretes.

The highest level of later age compressive strength was achieved for, which contained 15%RHA-C. Conversely, the lowest level of compressive strength was at 60%RHA-B. Generally, the compressive strength of RHA concrete tends to be highest with the finer particles (RHA-C) regardless of ages. This increase in the rate of strength development of the RHA concretes over that of OPC concretes was about 24.13% (20%RHA-A), 19.22% (15%RHA-B), and 28.69% (15%RHA-C), of the average values on compressive strength. The incorporation of the porous RHA increases the degree of cement hydration at 91 days, possibly due to the internal water curing effect. Furthermore, the pozzolanic reaction of RHA indicated by the CH consumption (Table 5.13, Chapter 5) occurs to the great extent at this age inducing a significant pore refinement.

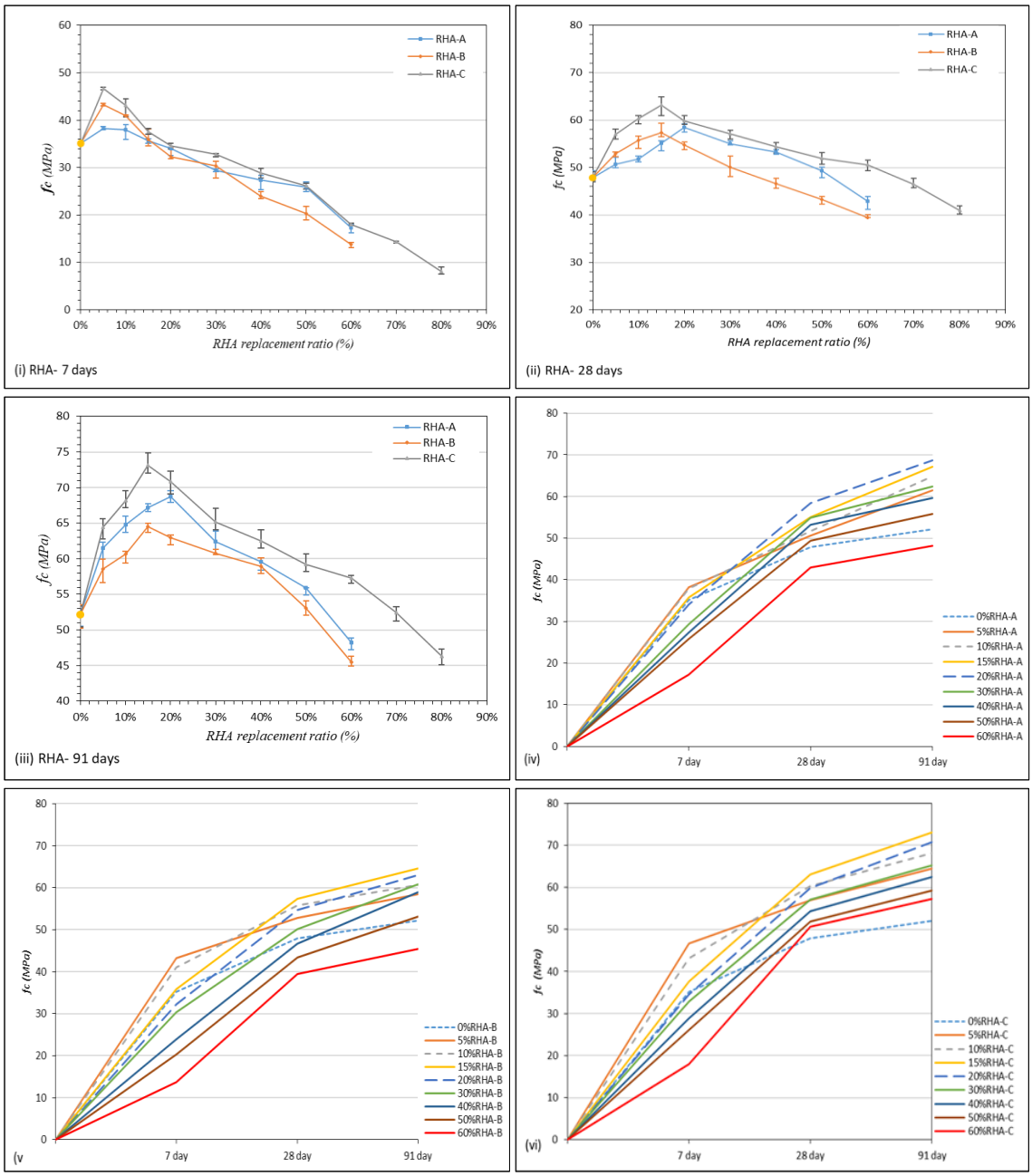

Figure 6. 7: (i, ii, and iii) Compressive strength results of RHA concrete compare to OPC concrete at different ages (7, 28 and 91-days), (iv, v and vi) progression of compressive strength development of RHA concrete separately versus time at three different ages (7, 28 and 91- days).

Table 6. 3: Compressive strength results of OPC and RHA concrete at different curing age.

RHA (%)	Compressive strength (MPa)								
	7-day			28-day			91-day		
	A	B	C	A	B	C	A	B	C
5%	38.22	43.23	46.64	50.68	52.87	56.97	61.53	58.53	64.43
10%	37.90	40.95	43.11	51.77	55.73	60.27	64.83	60.63	68.17
15%	35.70	35.91	37.59	55.14	57.32	63.10	67.20	64.53	73.11
20%	34.08	32.27	34.57	58.47	54.73	59.84	68.73	62.96	70.83
30%	29.37	30.41	32.86	54.95	50.10	57.11	62.37	60.77	65.20
40%	27.33	23.93	28.82	53.27	46.63	54.34	59.60	58.93	62.50
50%	25.88	20.33	26.09	49.36	43.31	51.90	55.87	53.07	59.23
60%	17.28	13.78	18.01	42.96	39.49	50.62	48.21	45.46	57.29
70%	-	-	14.25	-	-	46.55	-	-	52.41
80%	-	-	8.07	-	-	40.95	-	-	46.32
OPC		35.16			47.88			52.1	

Table 6. 4: The rate of RHA concrete compressive strength enhancement compare to OPC.

RHA%	rate of improvement compares to OPC control (%)								
	RHA-A			RHA-B			RHA-C		
	7day	28day	91day	7day	28day	91day	7day	28day	91day
5%	8.030	5.520	15.28	18.67	9.440	10.03	24.61	15.96	19.09
10%	7.230	7.510	19.60	14.14	14.09	14.02	18.44	20.56	23.53
15%	1.510	13.17	22.43	2.090	16.47	19.22	6.490	24.12	28.69
20%	-3.070	18.11	24.15	-8.220	12.52	16.77	-1.680	19.99	26.40
30%	-16.47	12.87	16.42	-13.51	4.420	14.22	-6.540	16.16	20.05
40%	-22.30	10.12	12.53	-31.94	-2.610	11.54	-18.03	11.89	16.59
50%	-26.39	3.000	6.690	-42.18	-9.540	1.770	-25.80	7.740	11.99
60%	-50.85	-10.28	-7.520	-60.81	-17.52	-12.79	-48.78	5.410	9.010
70%	-	-	-	-	-	-	-59.47	-2.78	0.590
80%	-	-	-	-	-	-	-77.05	-14.47	-11.0

6.6.2.1 Effect of RHA particles fineness

Fineness of RHA particles dramatically influences it is specific surface area (SSA), hence the pozzolanic reaction and the cement hydration process in the blended cement paste. Thus, results in a difference in the development of the compressive strength of concrete. The hydrated products, i.e. C-S-H phases, generated from the pozzolanic reaction of RHA, lead to refine the pore structure of the cement matrix surrounding RHA particles. Therefore, the finer particles of RHA speed up the reactions and form smaller CH crystals (Mehta, 1987). Higher fineness of RHA allowed increasing the reaction of $Ca(OH)_2$ to produce more calcium silicate hydrate (C-S-H) gel resulting in higher compressive strength (Habeeb and Bin Mahmud, 2010; Bakar et al., 2011). Moreover, fine RHA particles

contribute to strength development by acting as a micro-filler and promote the cement paste pore structure (Ismail and Walliuddin (1996).

6.6.2.2 Effect RHA content on compressive strength

The effect of RHA content on compressive strength of concrete is shown in Fig.6.7. It is obvious that at early ages, (7days), the higher the RHA content the lower the compressive strength. Generally, with replacement of cement by RHA, the pozzolanic reaction will only start when CH is released and pozzolan/CH interaction exist (Givi et al., 2010). The pozzolan reaction additionally binds Si of RHA with CH of cement hydration to form a C-S-H gel after 40 hours of cast mixture (Hwang et al., 2011). The behaviour of the delay in pozzolanic reaction will result in more permeable concrete at early ages and gradually becomes denser than plain concrete with time. This behaviour is due to two reasons: First, pozzolan particles become the precipitation sites for the early hydration C-S-H and CH that hinders pozzolanic reaction. Second, the strong dependency of the breaking down of glass phase on the alkalinity of the pore water which could only attain the high pH after some days of hydration (Givi et al., 2010).

However, RHA concrete exhibited significant performance up to 15% replacement at early age. The only explanation on the very satisfactory early age performance of RHA can be ascribed to the filler effect (Antiohos et al., 2013). Since previous studies have indicated that reactive silica cannot provide a strength contribution unless hydration at a progressed state (Feng et al., 2004; Zhang et al., 2000). De Sensale et al. (2004) attributed that to the reduction in porosity. With the progression of the hydration process, the effect of silica content begins to emerge as it is presented at age 28-days, where the performance of RHA mixtures significantly changed. The strength reached higher values than the OPC concrete even with 60%RHA-C, 50%RHA-A and 30%RHA-B. It is obvious that RHA-C with 60% replacement ratio has 9.01% enhancement in strength compare to reference concrete. Which is given an ability to increase the replacement ratio 70% without adversely effect on strength development.

6.6.2.3 Effect of impurities and crystalline phase of RHA

Generally, each of RHA-A and B, content amount of non-reactive crystalline silica (see Table 4.1, Chapter 4). With increase replacement ratio the amount of crystalline silica content of the mixture increased, for example, RHA-A consist of 23.4% crystalline silica, when replaced by 5%, the amount of crystalline silica content will be 5.38kg of totally 23kg

of RHA. However, this amount of non-reactive crystalline silica will be increased to 63.18kg at 60% replacement ratio. As referred before in Table 5.13, Chapter 5, section 5.3.4 and 5.3.5, respectively.

6.6.3 Splitting tensile strength

The testing of the specimens and the calculations were carried out as per BS EN12390-6:2009, with $f_{spt} = \frac{2 \times F}{\pi \times L \times d}$ (Equation 3.5). The average splitting tensile strength of three (3) test specimens for each of the nine (9) mixes of RHA-A and B, and eleven (11) mixes for RHA-C was obtained. The splitting tensile strength results of concrete blended RHA does not differ from the compressive strength results. The results of splitting tensile strength are plotted in Fig. 6.8 (28 and 91-days) and presented in Table 6.5. While, the splitting tensile strength development versus in time shown in Figure 6.8 (iii, iv and v). Moreover, the rate of strength development presented in Table 6.6. The splitting tensile strength of the test specimens ranged from 3.22MPa (80%RHA-C) to 5.17MPa (15%RHA-C). It can be clearly seen that the splitting tensile strength value at age of 28 days increases with RHA content up to 15% RHA-B and C, and 20%RHA-A and then decreased with increase replacement ratio. However, still higher than OPC concrete up to 50%RHA-A, 30% RHA-B and 60% RHA-C. A comparison of the 28-day results concrete containing RHA-C even with 60% replacement ratio shown higher splitting tensile strength than control concrete. This significant development in splitting tensile strength of RHA-C can be attributed to the highly reactive silica and fineness of particles. Where, the amorphous silica progressively consumption of $Ca(OH)_2$ which formed during hydration of Portland cement by RHA silica. As a consequence, larger volumes of reaction products are created. Also, SiO_2 nanoparticles of RHAs (see Table 4.4, Chapter 4) recover the particle packing density of the blended cement, directing to a reduced volume of larger pores in the cement paste.

Even though, RHA-A and B consist of crystalline silica with coarse particles; however, exhibited improvement in splitting tensile strength up to 50%RHA-A and 40%RHA-B at age of 28 days. In long term strength gain (at 91 days), the increased in splitting tensile strength become significant. For example, compare to OPC concrete RHA-C at replacement ratio of 40%, 50%, 60% and 70%, exhibited 18.07%, 15.15%, 7.73% and 1.19% improvement, respectively. This is due to the fact that the fine RHA-C particles contributed to the strength development by acting as a micro-filler and enhancing the cement paste pore structure (Habeeb and Mahmud, 2010). On the other hand, splitting tensile strength result shown less improvement by incorporation of RHA-A and B; however, exhibited

improvement about 7.49% at 50%RHA-A and 3.24% at 40% RHA-B. Furthermore, the splitting tensile strength equivalent or decreased to a value of control concrete at 60% RHA-A, 60% RHA-B and 80% RHA-C. The decrease in the strength by increasing the RHA replacement level is due to the reduction in the cement amount and as a result of that, the released amount of CH due to the hydration process is not sufficient to react with all the available silica from the addition of RHA and thus, the silica will act as inert material and will not contribute to the strength development.

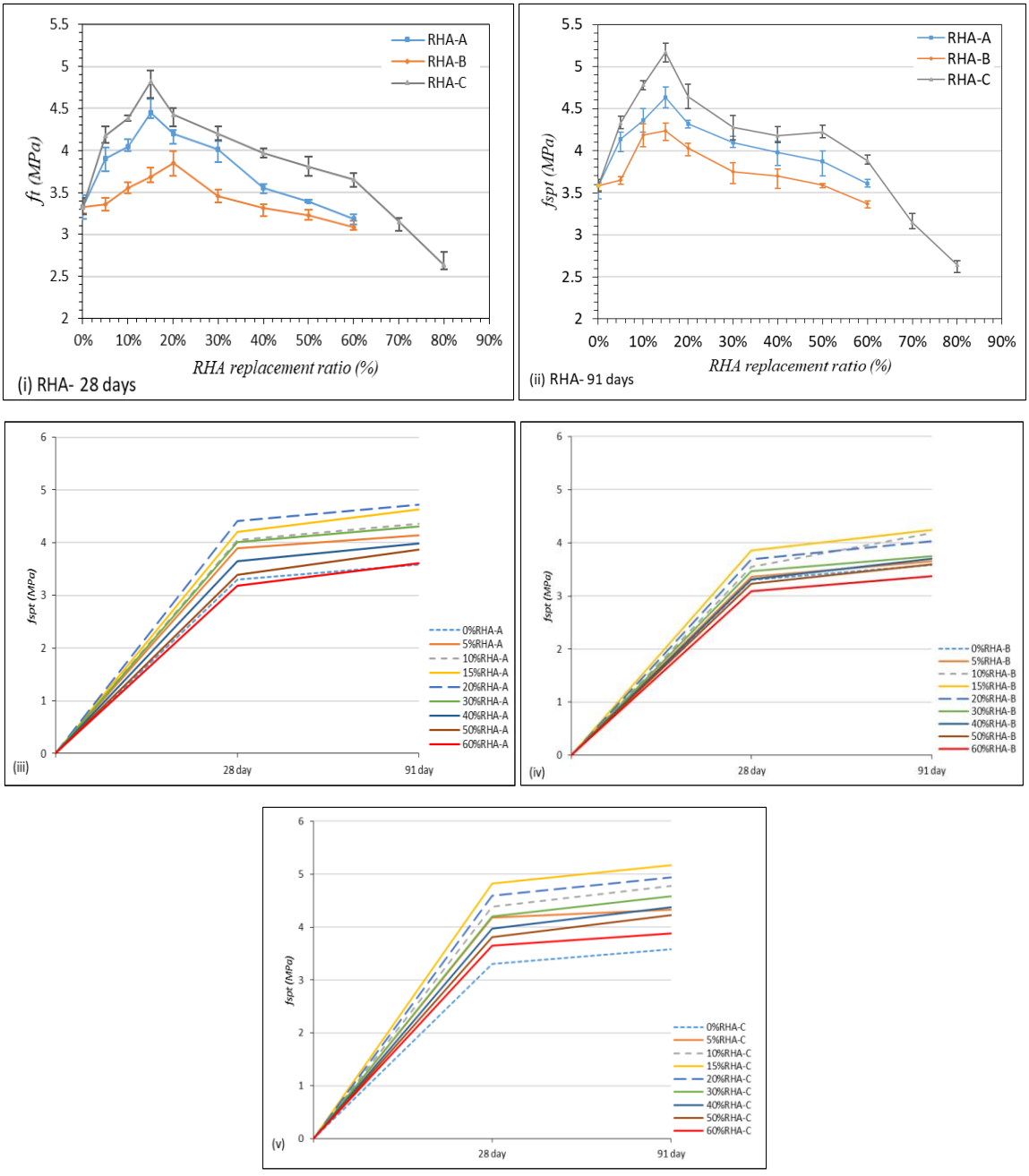

Figure 6.8: Rate RHA concrete splitting tensile strength development at the age of; (a) 28 days, (b) 91days, (iii, iv and v) rate of spitting tensile strength development of RHA- A, B and C separately versus to time (28 and 91-days).

Table 6.5: Splitting tensile strength of OPC and RHA concretes at 28 and 91 days.

RHA%	Splitting tensile strength (*fspt*, Map)					
	28-days			91-days		
	A	B	C	A	B	C
5%	3.90	3.36	4.18	4.14	3.65	4.33
10%	4.05	3.55	4.39	4.36	4.19	4.78
15%	4.20	3.85	4.82	4.63	4.24	5.17
20%	4.41	3.69	4.59	4.72	4.03	4.94
30%	4.01	3.46	4.20	4.31	3.75	4.58
40%	3.65	3.31	3.97	3.98	3.70	4.37
50%	3.39	3.23	3.81	3.87	3.59	4.22
60%	3.18	3.09	3.65	3.61	3.37	3.88
70%	-	-	3.15	-	-	3.74
80%	-	-	2.64	-	-	3.22
OPC		3.33			3.58	

Table 6.6: The rate of splitting tensile strength development of RHA concrete.

RHA%	rate of improvement compares to OPC control (%)					
	28-days			91-days		
	A	B	C	A	B	C
5%	14.42	0.890	20.33	13.53	1.920	17.32
10%	17.78	6.200	24.15	17.89	14.56	15.10
15%	20.71	13.51	30.91	22.68	15.67	30.75
20%	24.49	9.760	20.71	24.15	11.17	27.53
30%	16.96	3.760	16.12	16.93	4.530	21.83
40%	8.767	-0.600	12.60	10.05	3.240	18.07
50%	1.770	-3.001	12.60	7.490	0.280	15.15
60%	-4.800	-7.210	8.770	0.830	-5.870	7.730
70%			-5.400			1.190
80%			-20.72			-10.06

6.6.3.1 Effect of RHA percentage on splitting tensile strength of concrete

The hardened properties of the concretes were improved gradually with the increased RHA replacement ratio. The strength increased with RHA for up to 15% RHA-B and C, and 20%RHA-A which resulted in achieving the maximum value. For example, 15%RHA-C mixture resulted in 30.91% increment compared to the OPC control mix tested at 28 days age. The strength values when RHA was replaced by 40%RHA-B and C, 30%RHA-A were found to be similar to 5% replacement, in this case, the amount of silica available in the hydrated blended cement matrix is probably too high and the amount of the produced CH is most likely insufficient to react with all the available silica and as a result of that, some amount of silica was left without any chemical reaction. At 60%RHA-A and B, and

70%RHA-C, splitting tensile strength of RHA concrete exhibited equivalent or slightly less than OPC concrete. These results are agreeing with Isaia et al. (2003), results, where concrete incorporated 50% RHA showed higher strength at 91days than OPC control. However, Chindaprasirt et al. (2008) reported that strength up to 40% RHA mixed concrete is greater than control mortar after 90 days of curing. However, each of Saraswathy and Song (2007); Givi et al. (2010); Gastaldini et al. (2010); Karim et al. (2012) and Khan et al. (2015), concluded that strength of RHA associated concrete increases up to 30% replacement of cement. While, Khan et al. (2012) and Abalaka and Okoli (2013) founds that up to 25% RHA replacement ratio concrete could be attained strength without reduction compared to OPC control. Moreover, Each of Habeeb and Mahmud (2010); Hwang and et al. (2011) and Madandoust et al. (2011) considers that 20% as a suitable replacement ratio where there is no adverse in strength compared to OPC control concrete. In contrast to the previous results, Patil and Patil (2015) reported that splitting tensile strength of concrete blended RHA decreased remarkably with 8%, 12%, 16% and 20% replacement ratio compare to OPC control.

6.7 Correlation between splitting tensile strength to compressive strength

In The experimental results of splitting tensile strength (*fspt)* and compressive strength (f_c') were plotted against the calculation results by means of the existing equations shown in Figs. 6.9, and 6.10, respectively. Based on the results, the empirical relation suggested by ACI Building Code (Neville, 1995) where used.

$$fspt = 0.56\ (f_c)^{0.5} \tag{6.1}$$

According to the results, at 28-day age of RHA concretes, regression analysis defining the relationship between the two strength properties gave as follows; RHA-A results are exactly matching the equation ACI Building Code.

$$f_{sp} = 0.56\ f_c^{0.5} \tag{6.2}$$

On the other hand, RHA-B results are close to 0.47 power *fc*.

$$f_{sp} = 0.56\ f_c^{0.47} \tag{6.3}$$

While 0.485 power of *fc'* seems to be close more with the test results of RHA-C.

$$f_{spt} = 0.56\, f_c^{0.485} \quad (6.4)$$

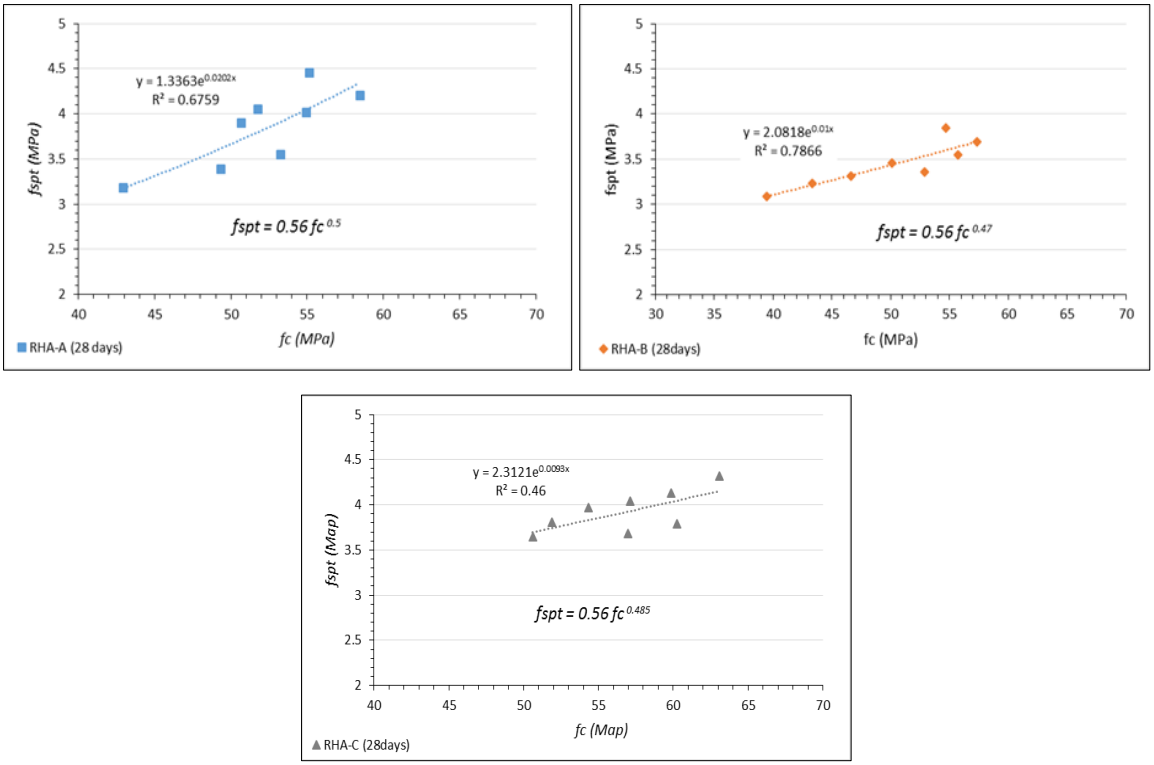

Figure 6.9: Relationship between splitting tensile strength and compressive strength of RHA concrete at 28-days.

The regression analysis trends regarding RHA concrete were slightly decreased with prolonged curing time to 91-days as follows:

For RHA-A concrete $f_{spt} = 0.56\, f_c^{0.49}$ (6.5)

For RHA-B concrete $f_{spt} = 0.56\, f_c^{0.47}$ (6.6)

For RHA-C concrete $f_{sp} = 0.56\, f_c^{0.505}$ (6.7)

These data indicate a significant correlation between splitting tensile strength and compressive strength of RHA concretes.

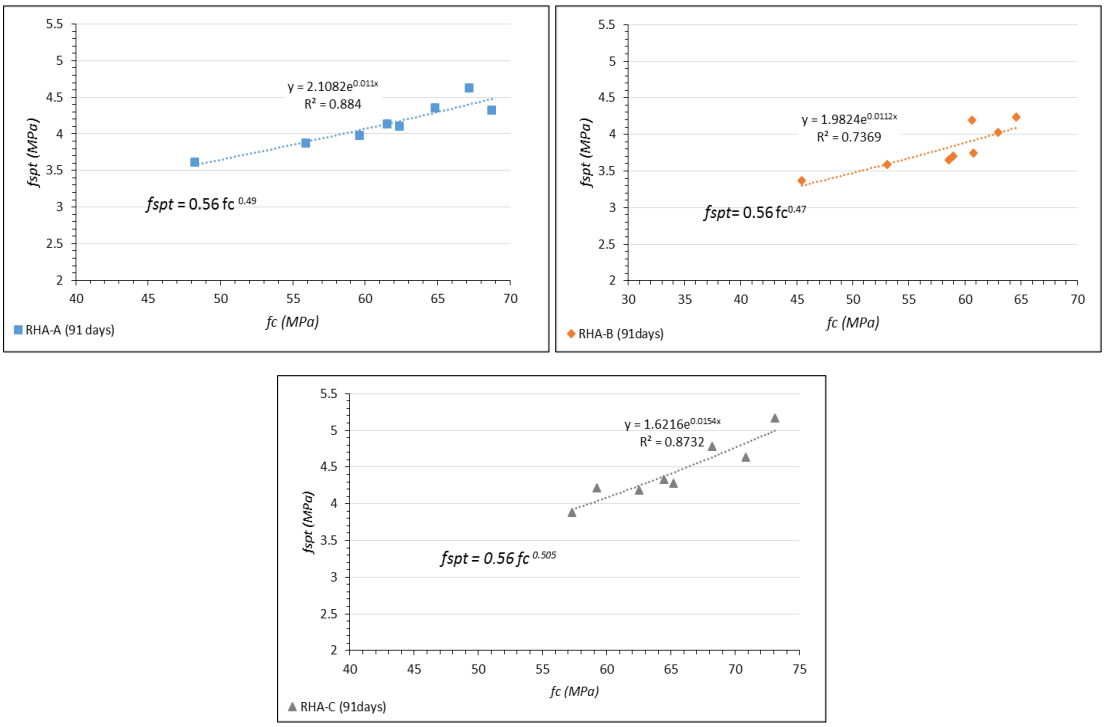

Figure 6.10: Splitting tensile-compressive strength correlation for all RHA concrete at the age of 91-days

6.8 Discussion of the results

Regarding the strength (compressive, splitting tensile) of the RHA samples, the experimental results show that RHA significantly increased the strength of concretes at the ages of 28 and 91days, as evident in Tables 6.5, 6.7, and Figures 6.4, and 6.6, respectively. The improvement of strength is mostly due to the micro filling ability and pozzolanic activity of RHA. With a smaller particle size, the RHA-C can fill the micro-voids within the cement particles. Also, the RHA readily reacts with water and calcium hydroxide, a by-product of cement hydration and produces additional calcium silicate hydrate or C-S-H (Yu et al. 1999). The additional C-S-H increases the strength of concrete since it is a major strength-contributing compound. Also, the additional C-S-H reduces the porosity of concrete by filling the capillary pores, and thus improves the microstructure of concrete in bulk paste matrix and transition zone leading to increase the strength. It should be noted that only normal curing conditions were applied in this study. The improvement of the strength of concrete by using RHA may be explained by the enhancement of the internal water curing of RHA, silica structure and the filler effect of RHA, which is primarily responsible for the strength improvement in high replacement ratio. In this respect, the substitution of cement by RHA with a smaller particle size (RHA-C) will improve the packing density of the

granular mixture and thus increase the resulting strength of concrete. Compressive strength at 7 day increases with the inclusion of all RHA concrete mixtures up to 15% replacement ratio (Figure 6.4). However, beyond that strength significantly decreased, this is ascribed to less available water in the system for the cement to hydrate because RHA absorbs a certain amount of water during mixing. This absorbed water, will promote the hydration of cement at later ages and thus increase the strength of RHA concrete.

In general, with progression of curing time (28, 91 days) the strength increases in RHA concrete, especially RHA-C, is due to combined filler and pore refinement effect. The positive effects of RHA-C can be attributed to the large number of ultra-fine particles 0.06μm (9.750% of total volume), which is possibly, caused the positive effect of RHA-C not only on the optimization of the packing density of granular mixtures, but also on the pozzolanic reaction of RHA-C. Despite of coarse particles size and crystalline silica content, RHA-A and B improved the strength of concrete up to 50% replacement ratio compare to control concrete. This large improvement of the strength of concrete blended RHA-A and B is suggested by the contribution of the amount of amorphous silica content and partially to the fine content of particles of the RHA mixture compared to that of the control mixture.

6.9 Comparison the results to the literature

To evaluate the outcome of this Chapter, the results of compression tests conducted of RHA concrete compared to the published results of similar in the literature. To neutralize the effect of water binder ratio (0.50) on strength development, the results of present study are compared to the results obtained by each of Abalaka (2013), Antiohos et al (2013), Madandoust et al. (2011), Gastaldini et al. (2007), De Sensale (2006), and Isaia et al. (2003). However, to clarify the effect of RHA properties on concrete strength, two another water binder ratio results (0.45 and 0.55) are presented. With w/b ratio 0.45, result of each of Moulick (2015), Ramezanianpour et al. (2011), and Salas et al. (2009) are included. While for w/b ratio 0.55, each of Abalaka and Okoli (2013), Ganesan et al. (2008), and Habbeb and Mahmud (2010). The comparison includes the physical properties, chemical composition of cement and RHA, fine aggregate size, coarse aggregate size and shape, and superplasticizer types and dosage. The compressive strengths at different ages, physical properties and chemical composition for cement and RHA as obtained from different literatures, are illustrated in Fig.6.11, and presented in Table 6.7, and 6.8.

The compressive strengths at age of 28 day. While, materials used in the preparation of the concrete specimens are presented in Table 6.9. To reach the purposes of this research, and

before compare the strength result of the literature to this study results, it is very important to present the process of RHA produce by each researcher and the mixing process for concrete. Therefore, the mixes proportion for the researchers is presentenced in Table 6.10. Finally, it is important to understand the methods were used by each researcher to determine the pozzolanic activity, particle size distribution, specific surface area and chemical composition. This point will help to determine the discrepancy in results.

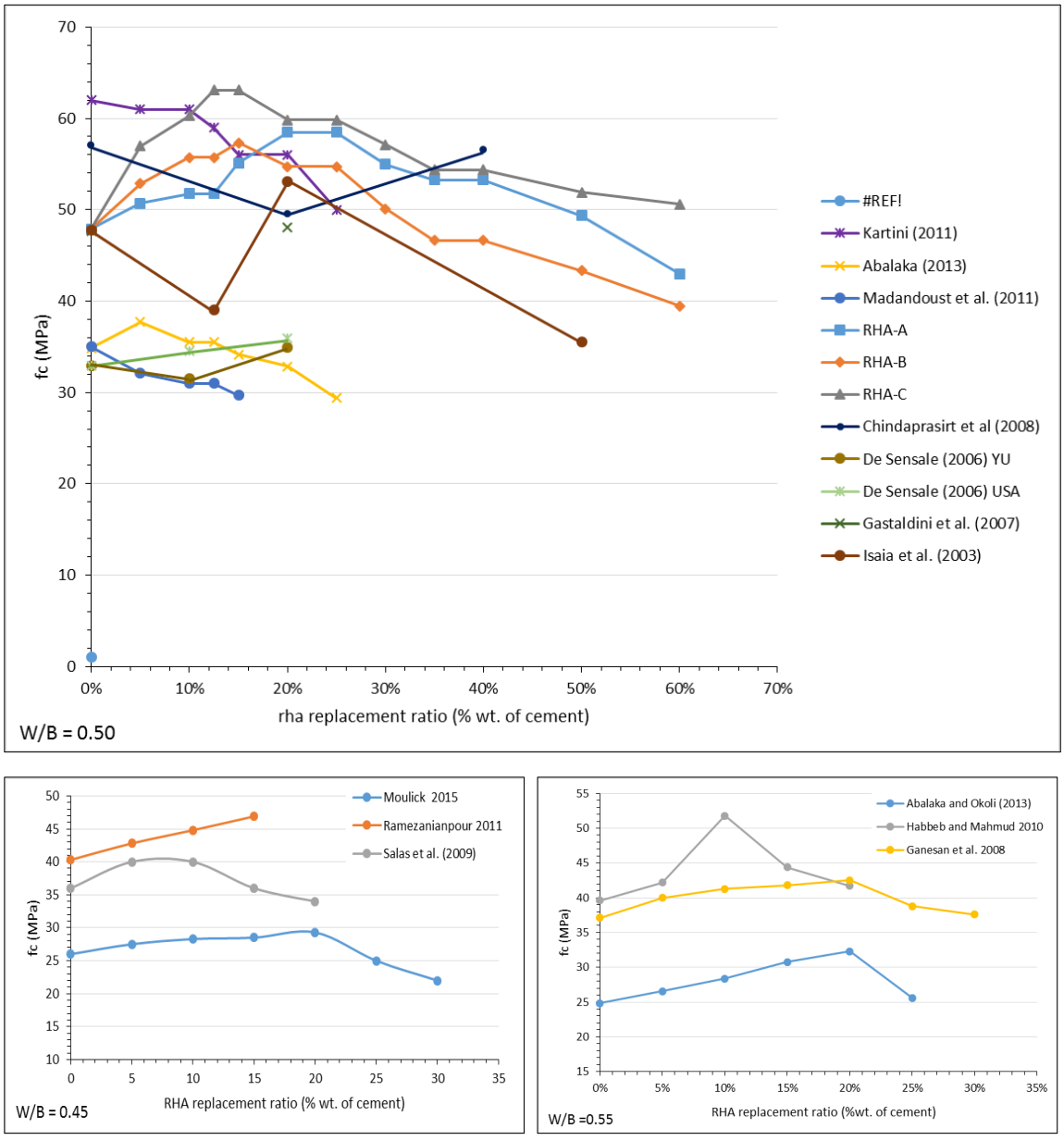

Figure 6.11: Comparison of RHA concrete compressive strength from various studies to the data of experimental results at age of 28 days.

6.9.1 Oxide composition

The oxides composition of RHA as obtained by various researchers are shown in Tables 6.7 and 6.8, shown that the RHA used by the previous researchers are consist of a very high silica content above 86%, with variation in reactivity of the ash ranged in between 81.25% to 92.93%. The residual carbon content ranged in between 0.77 to 9.10% of total ash weight, which is within the limitation of ASTM C 618-89 (≤12%). However, this significant variation in residual carbon content considers being affect directly on the mechanical properties of concrete. The other oxide elements percentage are mainly less than1%, except alkalinity (K_2O+Na_2O) are ranged in between 1.17% to 4.72%, which is consider to be enough to effect on the RHA concrete performance.

6.9.2 Fineness determination method

Based on the literature, two different methods were used to determine the fineness of cement and RHA (BET, Blaine). Each method has a different principle to present the result. The Brunauer-Emmett-Teller method (BET) is the most direct and finest length-scale measurement of specific surface area as it makes no assumption about the shape of the particles (Ferraris, 2012). While Blaine measurement as described in ASTM C204 is that the permeability of a bed of fine particles is proportional to the fineness of the particles. Generally, this method is not standardized; however, widely used in the cement industry assuming that the particles are spherical. According to Ferraris (2012), with comparison between BET and Blaine's methods, the range of surface area measured with BET is the widest of 686m^2/kg to 2000 m^2/kg, compare to the narrowest distribution is provided by the results of the Blaine method 349m^2/kg to 545 m^2/kg. This difference in measurement methods is another factor influencing the accuracy of determination of exact fineness of particles, and subsequently affected on the results.

6.9.3 Pozzolanic properties

When assessing the pozzolanic activity of RHA, it is important to take into account the method used. To determine the reactivity of RHA, two different methods were adopted according to the literature. While, each of Abalaka and Okoli (2013), Madandoust et al. (2011), Kartini (2011), Habeeb and Mahmud (2010), Salas et al. (2009) and Ganesan et al. (2008) used X-ray diffraction (XRD) method to determine the reactivity of ash (see Chapter 3, section 3.3.3). However, De Sensale (2006) used rapid analytical method to evaluate amorphous silica. The principles of the method according to the author is based on bringing

RHA into solution as glycerosilicate by treating the test material with glycerol and titrating the glycerol solution obtained with an aqueous glycerol solution of barium hydroxide, using phenolphthalein or alizarin yellow as the indicator. On the other hand, each of Moulick (2015), Ramezaianpour et al. (2011), Gastaldini et al. (2007), and Isaia et al. (2003) did not present the degree of RHA reactivity.

Table 6.7: Compressive of RHA concrete compressive strength from various studies with w/b ratio 0.50 to the data of current study.

RHA%		*fc* (MPa)		Chemical composition (%)								Physical properties		Reference
		28day	*91day*	SiO_2		Al_2O_3	Fe_2O_3	CaO	MgO	K_2O+Na_2O	LOI	Amorphous Silica (%)	SSA*(m^2/kg)	MPS**(µm)	
0%		35.4	-	RHA	90.9	0.83	0.60	0.8	0.56	1.55	4.76	81.25	377 (Blain)	-	Madandoust et al. (2011)
5%		33.6	-												
10%		32.4	-												
15%		32.1	-												
20%		30.8	-	Cement	20.0	6.0	4.2	64.5	1.2	0.8	-	-	336.5 (Blain)	-	
25%		29.7	-												
30%		26.6	-												
0%		62	65	RHA	92.05	0.96	0.05	0.49	0.19	1.17	4.81	-	10857 to 17463	5.83	Kartini (2011)
5%		61	62												
10%		59	61.5												
15%		56	61												
25%		56	59	Cement	15.05	2.56	4.00	72.17	1.27	0.49	1.33	-	-	-	
30%		50	56												
0%		47.7	53.5	RHA	96.26	0.44	0.22	0.76	0.50	1.43	4.49	-	40000 (BET)	-	Gastaldini et al. (2007)
20%		48.1	53.9	Cement	19.59	4.79	3.07	64.35	1.69	1.05	2.09	-	1480 (BET)		
YU	0%	32.9	35.9												
	10%	31.5	35.5	RHA	87.2	0.15	-	0.55	0.35	4.72	6.55	92.93	28800 (BET)	8.0	
	20%	34.9	37.9	Cement	21.98	4.65	2.27	61.55	4.27	1.15	2.30	-	309 (Blaine)	-	De Sensale (2006)
YSA	10%	34.5	44.4												
	20%	35.9	52.9	RHA	88.0	0.16	0.10	0.80	0.20	2.9	8.1	92.4	24400 (BET)	8.0	
0%		47.8	52.2	RHA	86.5	0.30	0.10	0.53	0.30	1.7	9.1	-	40100 (BET)	11.0	Isaia et al. (2003)
12.5%		39.0	49.3												
25%		53.1	61.1	Cement	19.6	4.8	3.1	64.4	1.7	1.1	2.1	-	1800 (BET)	8.0	

SSA: Specific surface area (m2/kg),* *MPS**: Mean Particle Size (µm)*

Table 6.8: Compressive of RHA concrete compressive strength from various studies with w/b ratio 0.45 and 0.55 to the data of current study.

RHA%	***fc* (MPa)**		**Chemical composition (%)**								**Physical properties**		**Reference**
	28day	***91day***	**SiO_2**		**Al_2O_3**	**Fe_2O_3**	**CaO**	**MgO**	**K_2O+Na_2O**	**LOI**	**PAI (%)**	**SSA (m^2/kg)**	**MPS (µm)**	
0%	26	-	RHA	90	0.39	0.37	0.46	0.88	3.17	3.09	-	225		Moulick (2015)
5%	27.5	-												
10%	28.3	-	Cement	17-25	4-8	0.5-0.6	61-63	0.1-4.0	0.4-1.3	-	-	-	-	
15%	28.5	-												
20%	29.3													
25%	25	-												
30%	22	-												
0%	≈36	≈44	RHA	90	0.68	0.42	1.23	0.35	3.l1	3.0	89.5	24,000 (BET)	19	Salas et al. (2009)
5%	≈40	≈45												
10%	≈40	≈47.5												
15%	≈36	≈42.5	Cement	21.27	4.63	3.96	63.05	1.56	0.34	-	-	377 (Blaine)		
20%	≈34	≈41.5												
0%	37.1	38.3	RHA	87.32	0.22	0.28	0.48	0.28	4.16	2.10	87.0	36470 (BET)	3.8	Ganesan et al. (2008)
5%	40.0	43.3												
10%	41.3	44.8												
15%	41.8	45.7												
20%	42.5	46.0	Cement	20.25	5.04	3.16	63.61	4.56	0.59	3.12	-	326 (Blain)	22.5	
25%	38.8	43.0												
30%	37.6	38.7												
35%	35.1	37.2												
0%	40.3	-	RHA	89.61	0.04	0.22	0.91	0.42	1.65	5.91	-	-	-	Ramezanianpour et al. (2011)
5%	42.8	-												
10%	44.8	-	Cement	21.5	3.68	2.76	61.5	4.8	1.07	1.35	-	-	-	
15%	46.9	-												
0%	24.83	28.84	RHA	95.41	-	0.82	-	1.24	1.87	0.77	90	235	46.45	Abalaka and Okoli (2013)
5%	26.56	30.75												
10%	28.36	32.28												
15%	30.77	34.43	Cement	24.79	6.35	0.92	58.5	2.87	1.45	-	-	-	-	
20%	32.28	37.20												
25%	25.61	30.19												
0%	39.6	-	RHA	88.32	0.46	0.67	0.67	0.44	3.03	5.81	-	30400 (BET)	11.5	Habbeb and Mahmud (2010).
5%	42.2	-												
10%	51.8	-												
15%	44.4	-	Cement	20.99	6.19	3.86	65.96	0.22	0.77	1.73	-	351 (Blaine)	22.1	
20%	41.7	-												

Table 6.9: Materials used according to the literature

Reference	**w/b**	**Materials used in the experiment**			
		Cement	**Fine aggregate**	**Coarse aggregate**	**Superplasticizer type**
Isaia et al. (2003)	0.50	High early strength Portland cement	Dmax = ¼ 4.8 mm	Diabasic coarse aggregate Dmax = ¼19 mm.	Naphthalene based superplasticizer
De Sensale (2006)		Portland cement type I (normal Portland cement)	Local natural sand Dmax = 4.75 mm	Crushed granite Dmax = of 12.5 mm	Sulfonated naphthalene formaldehyde condensate
Gastaldini et al. (2007)		High initial strength Portland cement (CP V – ARI, Brazilian standard NBR 5733)	Natural quartz sand Dmax =1.20 mm	Crushed diabasic rock Dmax = 19.00 mm	Poly-carboxylic ether
Kartini (2011)		Ordinary Portland cement	Sand (fine aggregate) Dmax = 5 mm	Granite coarse aggregate Dmax = 20 mm	Sulphonated naphthalene formaldehyde
Madandoust et al. (2011)		Ordinary Portland Cement	Natural sand	Crushed limestone Dmax =16 mm	Polyethylene sulphonate
Present study		High early strength CEM I 52.5N cement	Graded river Dmax = 4mm	Un-crushed gravel Dmax = 9mm	Poly-carboxylic polymer
Moulick (2015)	0.45	Portland Cement (OPC) grade 43	River sand Dmax = 4.75mm	Coarse Aggregate: Dmax = 20mm	Poly-carboxylic
Ramezanianpour et al. (2011)		Portland cement type I	natural sand	Crushed calcareous stone Dmax = 19 mm	-
Salas et al. (2009)		Type V Portland cement (High sulfate resistance)	River siliceous sand D max = 2.38mm D max =9.51 mm,	Crushed basalt, Dmax = 19 mm	Naphthalene formaldehyde-based
Abalaka and Okoli (2013)	0.55	Ordinary Portland cement	Natural river bed quartzite sand D max = 5mm	Crushed granite Dmax = 20mm	-
Ganesan et al. (2008)		Ordinary Portland cement (OPC) conforming to Indian standard code IS 8112-1995	Graded river sand D max = 1.18 mm	Crushed granite aggregate Dmax = 12.5 mm	-
Habbeb and Mahmud (2010)		Ordinary Portland cement type I	Dmax = 4.75 mm	Crushed granite Dmax = 19mm	Sulphonated naphthalene formaldehyde

Table 6.10: Mix proportion and superplasticizer dosage used by various researchers

Reference		RHA%	Cement (kg/m^3)	RHA (kg/m^3)	Water (kg/m^3)	Superplasticizer		Fine aggregate (kg/m^3)	Coarse aggregate (kg/m^3)
						%	(kg/m^3)		
Isaia et al. (2003)		0	359	0	178	1%	1.8	-	-
		12.5	314	45	176	2%	3.6		
		25	270	90	169	6%	10.8		
		50	180	180	160	11%	19.8		
De Sensale (2006)	UY	0	408	0	204	-	-	758	983
		10	367	40.8	204	-	-		
		20	327	81	204	-	-		
	USA	10	367	40.8	202.78	0.30	1.22		
		20	327	81	202.37	0.40	1.63		
Gastaldini et al. (2007)		0	346	0	173	-	-	757	1082
		20	277	69	171		2.07	733	1058
Kartini (2011)		0	375	-	190	1.0	3.75	580	1235
		10	338	37	190	1.0	3.75		
		15	319	56	190	1.0	3.75		
		20	300	75	190	1.0	3.75		
		25	281	94	190	1.0	3.75		
		30	262	113	190	1.0	3.75		
Madandoust et al. (2011)		0	396	0	210	1.0	-	844	951
		5	376	20	210	0.95	3.76		
		10	356	40	210	0.98	3.90		
		15	337	60	210	1.03	4.10		
		20	317	79	210	1.07	4.23		
		25	297	99	210	1.11	4.40		
		30	277	119	210	1.15	4.56		

Reference	RHA%	Cement (kg/m^3)	RHA (kg/m^3)	Water (kg/m^3)	Superplasticizer		Fine aggregate (kg/m^3)	Coarse aggregate (kg/m^3)
					%	(kg/m^3)		
Moulick (2015)	0%	360	-		2.88		652	1333
	5%	342	18		2.88			
	10%	324	36		2.88			
	15%	306	54		2.88			
	20%	288	72		2.88			
	25%	270	90		2.88			
	30%	252	108		2.88			
Ramezanianpour et al. (2011)	0%	420	-	210			929	760
	5%	390.6	29.4	210				
	10%	378	42	210				
	15%	357	63	210				
Salas et al. (2009)	0%	440	0	198	0.4	-	1123	660
	5%	418	22	198	0.8	-	1115	655
	10%	396	44	198	1.7	-	1108	651
	15%	374	66	198	1.9	-	1099	646
	20%	352	88	207	4.3	-	1098	645
Abalaka and Okoli (2013)	0%	267	-	133.5	-		486	1,537
	5%	254	13	133.5	-	-		
	10%	240	27	133.5	-	-		
	15%	227	40	133.5	-	-		
	20%	214	53	133.5	-	-		
	25%	200	67	133.5	-	-		
Ganesan et al. (2008)	0%	383	0	2.03	-	-	575	1150
	5%	364	19	2.03	-	-		
	10%	345	38	2.03	-	-		
	15%	326	57	2.03	-	-		
	20%	306	77	2.03	-	-		
	25%	287	96	2.03	-	-		
	30%	268	115	2.03	-	-		
	35	249	134	2.03	-	-		
Habbeb and Mahmud (2010)	0%	391	-	207	-	-	750	994
	5%	371	20	207	-	-		
	10%	352	39	207	-	-		
	15%	332	59	207	-	-		
	20%	313	78	207	-	-		

6.9.4 Superplasticizer

According to the literature, different type of superplasticisers was used as water reducer (Naphthalene based superplasticizer, Sulfonated naphthalene formaldehyde condensate, modified carboxylic ether, Polyethylene sulphonate complying, and Poly carboxylic). Each type of superplasticizer has properties defer to others. Each of Salas et al. (2009) and Isaia et al. (2003) used Naphthalene based superplasticizer (SNF), which is produced from naphthalene by oleum or sulphur trioxide sulfonation of β sulfonate. According to Leta (2014), using Naphthalene based superplasticizer, the compressive strength of C25/30 grade concrete recorded at 1.5% SP dosage a corresponding compressive strength gain of 27%. De Sensale (2006), Habbeb and Mahmud (2010) and Kartini (2011), they used naphthalene sulfonated formaldehyde condensate superplasticizer. Which is a highly effective dual action powder superplasticizer, production of free-flowing concrete or as a substantial water-reducing agent for promoting high early and ultimate strengths (Marco and Loren's, 2007). Ganesan et al. (2008) used modified carboxylic ether (MCE) superplasticizer, which is the latest generations, poly carboxylate ether-based superplasticizers "PCEs".

Despite the superior dispersing ability of MCE superplasticizer (Akhlaghi et al., 2017); however, does not induce any substantial modifications in paste strength values, inversely reduce the strength (Puertas et al., 2005). Madandoust et al. (2011) used polyethylene sulphonate superplasticizer (PES), which is synthesized by free radical induced polymerization of sodium ethylene sulfonate (sodium vinyl sulfonate). While each of Moulick (2015), and Gastaldini et al. (2007), they used Poly-carboxylic, which is defining as high early strength, and significant increase of strength at 28day, with high water reduction more than 40% (Nematollahi and Sanjayan, 2014).

The effect of superplasticizers (SPs) on the workability and strength of concrete has been widely evaluated by several authors' such as Hanehara and Yamada (2000), Brooks's et al. (2001), Puertas and Vazquez (2003). Recently, study has been conducted on the effect of different types of superplasticisers (Modified Polycarboxyel ether, Melamine formaldehyde, and Sulphated Naphthalene), on the workability and strength of concrerte by Zghair and Rasheed (2016). The author used five different dosage of superplasticizer ranged in between 0.5% to 2.5% of binder ratio. The results shown that the type and dosage of superplasticizer has a direct effect on the workability, compressive and splitting tensile strength of concrete as it is shown in Table 6.11. Therefore, it can be saying that one of these parameters affected on the strength presented by the literature was type and SP dosage.

Table 6.11: The effect of type and composition of chemical admixture on properties of produced concrete

Concrete mix	**SP (%)**	**Modified Polycarboxyel ether**			**Melamine Formaldehyde**			**Sulphonated Naphthalene**		
		Slump (mm)	*fc* (MPa)/28 day	*fspt* (MPa)/28 day	Slump (mm)	*fc* (MPa)/28 day	*fspt* (MPa)/28 day	Slump (mm)	*fc* (MPa)/28 day	*fspt* (MPa)/28 day
M1	0.5	60	31.5	4.2	35	29.3	2.9	27	28.6	2.3
M2	1.0	135	32.4	5.3	70	28.3	3.4	65	28.9	2.5
M3	1.5	240	39.6	6.5	110	31.4	4.1	98	32.6	3.9
M4	2.0	collapse	38.1	6.8	160	32.4	3.8	145	30.6	3.4
M5	2.5	collapse	30.3	3.6	collapse	25.6	3.1	collapse	27.3	2

6.10 Factors affecting the compressive strength variation

Results of the 28day compressive strength test on concrete according on the literature are illustrated in Fig 6.11, and presented in Table 6.7. With reference to the Tables 6.7, 6.8, 6.9 and 6.10, respectively. There are several factors affected on the compressive strength of concrete blended RHA. Some of these factors are related to the RHA physical properties and chemical composition, while more other factors related to the cement type, fine and coarse aggregate size and shape, and type of superplasticizers. Linking all these factors, to determine one's relationship is difficult; therefore, each factor will be studied separately and then the effect of all these factors will eventually be linked to the strength of RHA concrete to explain the contradiction.

6.10.1 Effect of physical properties of RHA

The physical characteristics of RHA like fineness, particle shape and size are mainly depending on the combustion temperature and time of the rice husk. The physical properties of RHA have a greater influence on the performance of fresh concrete such as workability. Moreover, fineness of the RHA have a direct influence on the pozzolanic activity of ash, and hence the strength of concrete.

6.10.1.1 Particle size distribution and Specific Surface Area (SSA)

The particle size distribution of the RHA has been identified as influencing the compressive strength, where with an increase of finesses leading to an increase compressive strength [Khan et al., (2014); Shukla et al. (2011) and El-Dakroury and Gasser, (2008)]. Fineness is generally defined as the percentage of particles passing at a specified sieve size (Gunasekara, 2016). The specific surface area and mean particle size distribution according

to the literature are presented in Tables 6.7, and 6.8, respectively. To evaluate the effect of RHA particles size distribution on the strength development of concrete, a comparison in between four different researches [Ganesan et al. (2008), Abalaka and Okoli (2013), Habeeb and Mahmud (2010) and Salas et al. (2009)] are presented in Fig.6.12. It was observed that, the best correlation is achieved between the mean particles size distribution to the compressive strength of RHA. This result is aligned with the results of present study and confirm that, fineness of RHA particles effects on the compressive strength characteristics of the mixture through the physical micro-filler action (Jaya 2011). Which is giving a logical explanation for further improvement in strength of RHA concrete.

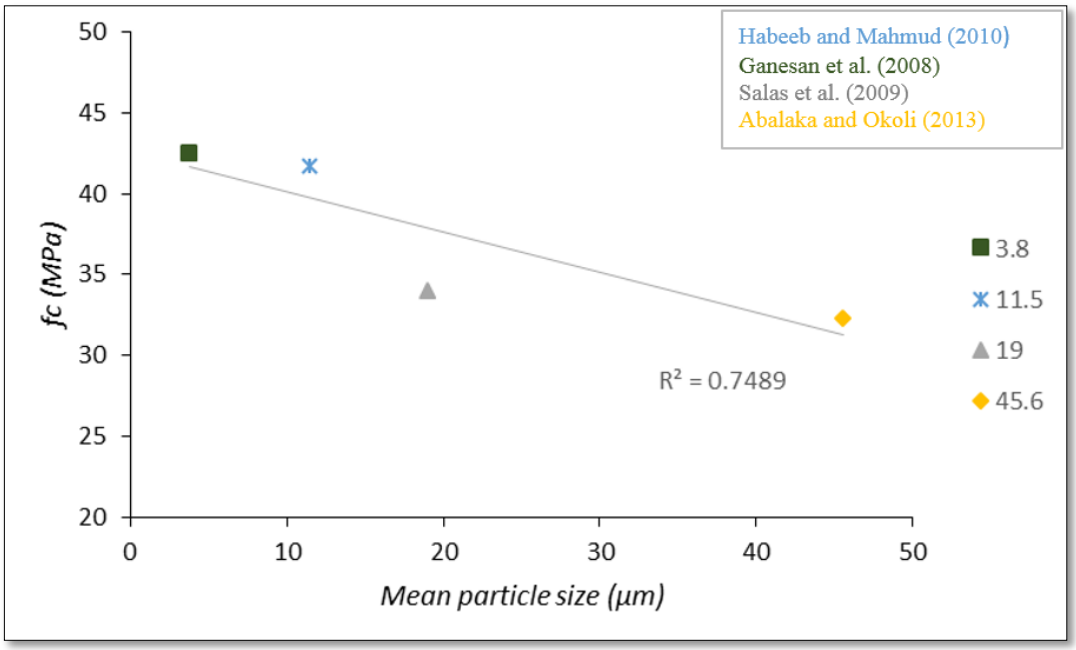

Figure 6.12: Compressive strength vs. mean particle size distribution.

6.10.2 Effect of chemical composition of RHA

6.12.2.1 Effect of SiO_2 to the reactivity of the ash

RHA is a fine particulate material with the main chemical constituent of SiO_2. This oxide element is responsible for it is pozzolanic activity. The reactive silica content has been reported as an important factor affecting final compressive strength in RHA concrete. The optimum 28day compressive strength vs. SiO_2 content and reactivity percentage are presented in Tables 6.7, and 6.8, respectively. While, the exact reactive silica of RHA based on the literature are presented in Table 6.12. An extensive research on the RHA in concrete showed that the reactivity of ash significantly affected on the compressive strength. Abalaka

and Okoli (2013) have highest SiO_2 content with highest amount of reactive silica; however, achieved the third highest strength. Salas et al. (2009) RHA has second highest SiO_2 with significantly high reactive silica; however, achieved the second highest compressive strength. While Ganesan et al. (2008); has a third highest reactive silica (SiO_2); however, achieved the best compressive strength out of the four RHA concretes. Which is can be attributed to the very high specific surface area (36470 m^2/kg) and very fine particles (3.8μm). On the other hand, less reactive of silica even with high amount of silica content, explains the decrease in the compressive strength as evidence in result of Madandoust et al. (2011). Overall, these results indicated that while the SiO_2 content and reactivity has a significant impact on the strength development of concrete.

Table 6.12: The exact reactive silica for 1kg/m^3 of RHA according to the literature.

Reference	SiO_2	Reactivity (%)	SiO_2 reactive for each 1kg/m^3 of RHA
Abalaka and Okoli (2013)	95.41	90.00	858.69 g/m^2
Salas et al. (2009)	90.00	89.50	805.50 g/m^2
Ganesan et al. (2008)	87.32	87.00	759.68 g/m^2
Madandoust et al. (2011)	90.90	81.25	738.56 g/m^2

6.10.3 Effect of cement type

Cement defined as the key ingredient of concrete, which mainly consists of calcium, aluminum, iron and small amounts of other materials. It is obvious that the type and fineness of cement effect directly on the strength of concrete; therefore, the variation in strength result partially can be attributed to the cement type. The chemical composition, fineness and mean particle size of cement used by the literature are presented in Tables 6.7, and 6.8, respectively. Strength properties are known to much depend on the tricalcium silicate (C_3S) content, which is means that the higher the CaO content in the clinker, the better the hardening conditions (Talaber, 1982). In addition to the CaO, each of SiO_2 and Fe_2O_3 also provides strength to cement. Therefore, concrete strength can be deduced from the total amount of $CaO+SiO_2+Fe_2O_3$ in cement.

A comparison in between the amount of $CaO+SiO_2+Fe_2O_3$ and the results of 28-day compressive strength of concrete are present in Table 6.13. In general, the type of cement used are divided to different groups, each of De Sensale (2006), Kartini (2011), Abalaka and Okoli (2013), and Ganesan et al. (2008) are used Ordinary Portland cement. The correlation between assume of $CaO+SiO_2+Fe_2O_3$ to the compressive strength are shown in Fig.6.13. While, the second group consist of different types of cement, and the correlation

between assume of $CaO+SiO_2+Fe_2O_3$ to the compressive strength are shown in Fig.6.14. Therefore, it can be concluded in addition to the RHA properties, type of cement was another main reason to the contradiction in the strength variation results of literature.

Table 6.13: Total amount of $CaO+SiO_2+Fe_2O_3$, vs compressive strength of RHA concrete.

Reference		CaO	SiO_2	Fe_2O_3	$CaO+SiO_2+Fe_2O_3$	W/B	*fc (MPa)*			
							OPC	5%	10%	15%
Kartini (2011)		72.17	15.05	4.00	91.22	0.50	62.0	61.0	59.0	56.0
Madandoust et al. (2011)		64.50	20.00	4.20	88.70	0.53	35.4	33.6	32.4	32.1
Ramezanianpour et al. (2011)		61.50	21.50	2.76	85.76	0.45	40.3	42.8	44.8	46.9
Salas et al. (2009)		63.05	21.27	3.96	88.28	0.45	36.0	40.0	40.0	36.0
Abalaka and Okoli (2013)		58.50	24.79	0.92	84.21	0.45-0.55	24.8	26.5	28.3	30.7
Ganesan et al. (2008)		63.61	20.25	3.16	87.02	0.53	37.1	40.0	41.3	41.8
Habbeb and Mahmud (2010)		65.96	20.99	3.86	90.81	0.53	39.6	42.2	51.8	44.4
Present Study	RHA-A	63.9	19.7	3.10	86.7	0.50	47.8	50.6	51.7	55.1
	RHA-B					0.50		52.8	55.7	57.3
	RHA-C					0.50		56.9	60.2	63.1

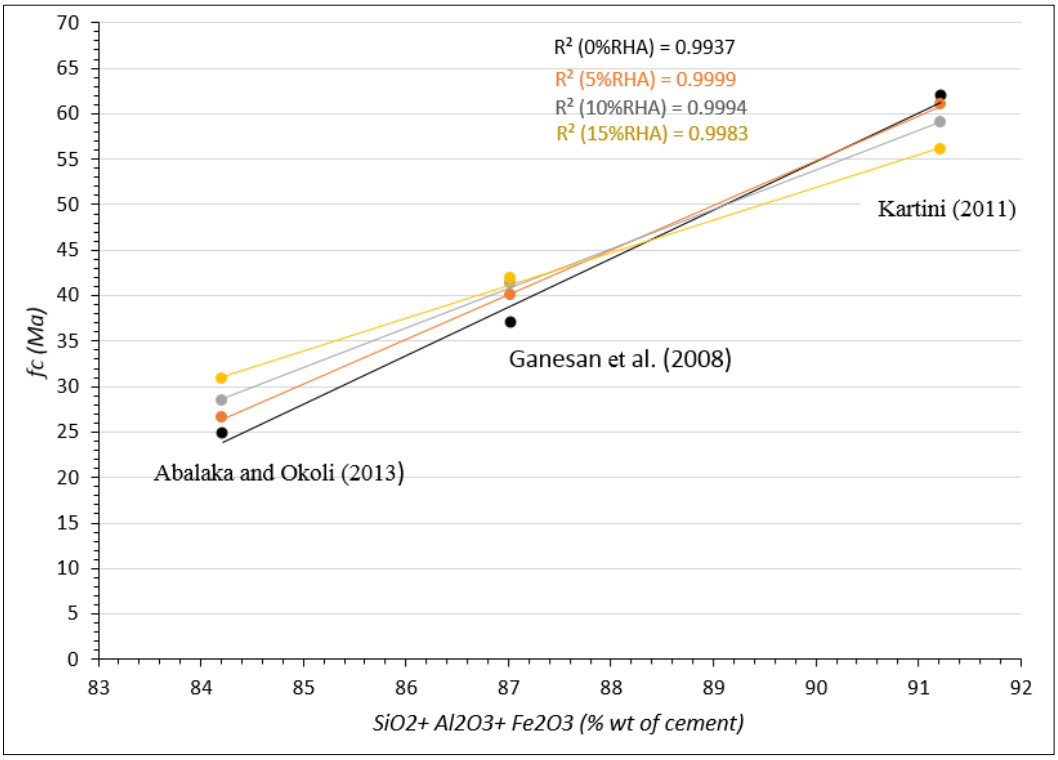

Figure 6.13: Total amount of $CaO+SiO_2+Fe_2O_3$, vs compressive strength of first group.

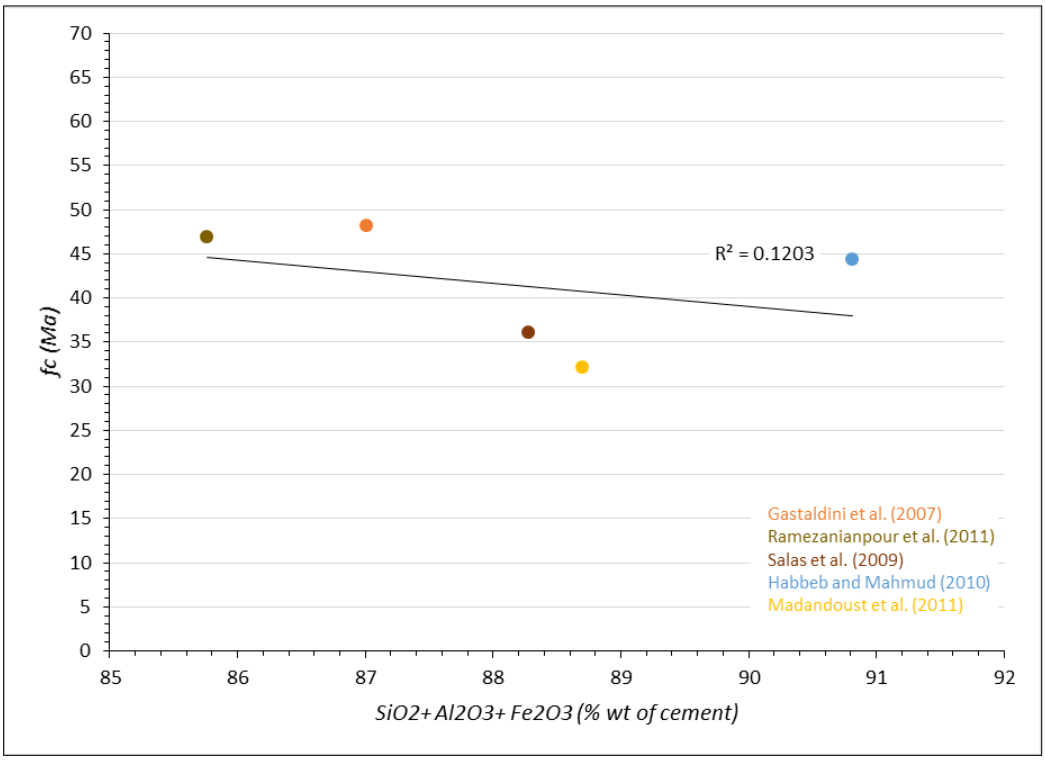

Figure 6.14: Total amount of $CaO+SiO_2+Fe_2O_3$, vs compressive strength of second group.

6.10.4 Effect of coarse aggregate

6.10.4.1 Size and type

It is well recognized that coarse aggregate plays an important role in concrete. Coarse aggregate typically occupies over one-third of the volume of concrete, and research indicates that changes in coarse aggregate can change the strength and fracture properties of concrete. To predict the behavior of concrete under general loading requires an understanding of the effects of aggregate type, aggregate size, and aggregate content. Generally, the factors influencing the strength of concrete in addition to the amount and type of cement and w/c ratio, it is the aggregate type and grading (Kılıc et al., 2008). All type and size of coarse aggregate used by the previous researcher are present in Table 6.9, shown four different types with variable in size were used. There is strong evidence that aggregate type is a factor in the strength of concrete. Bentz et al., (1963) compared concretes with elven types of crushed aggregate (diabase, dolomite, dolomitic limestone, high absorption limestone, quartzite and sandstone, micritic limestone, granite, granitic gneiss, siliceous gravel, marble, and meta-basalt) for the same mix proportions containing. The obtained results presented that the compressive strength with Micritic limestone, Dolomite limestone,

Diabase, Granite, and high absorption limestone at 91days were 51.8, 51.1, 50.7, 48.7, and 41.3MPa, respectively.

Another research has compared the effects of limestone and basalt on the compressive strength of high-strength concrete (Giaccio et al., 1992). In concretes containing basalt, load induced cracks developed primarily at the matrix-aggregate interface, while in concretes containing limestone; nearly all of the coarse aggregate particles were fractured. Which is confirming the compressive strength result presented by Madandoust et al. (2011). Size aggregate is another factor effect on the strength of concrete. The test results of each of Gastaldini et al. (2007) and Ganesan et al. (2008) containing the smaller maximum aggregate size (12.5mm) yield higher compressive strength than the concretes containing the larger aggregate (20mm). These results are aligned with the result of present study, where the maximum size of coarse aggregate used was 9.5mm. Thus, the considerable difference in maximum aggregate size may contribute to the contradictory results of previous study.

6.11 Conclusion

In this chapter, the effect of RHA on the workability, the compressive strength, and splitting tensile strength of concrete mixtures was studied. Based on the experimental results and discussion, the following conclusions can be drawn:

i. Partial replacement of the Portland cement with up to 15% RHA by mass increased the early-age compressive strength values. However, the amount of increase in compressive strength it depends on the RHA reactivity.
ii. As high as 70% by weight of OPC can be replaced with RHA-C without any adverse effect on the strength of concrete. This would reduce the amount of Portland cement use and the greenhouse gas.
iii. The addition of RHA increases the compressive strength of RHA compared to that of the control sample. In particular, the compressive strength of the RHA-C mixtures is greater than control concrete mixture even at 60% replacement ratio.
iv. Strength decreased with incorporation of RHA-A and B, compare to RHA-C this reduction in strength could be due to the coarse particles size, and also associated to the crystalline silica content.

v. Although the early compressive strength of concrete produced with RHA-A and B were found to be low. However, at ages of 28 and 91 days showed a continued rate of development of hydration, superior to that of the normal concrete.

vi. Maximum compressive strength associated with an increase in content of RHA up to 15% RHA-B, C, and 20% RHA-A. The strength enhancement achieved about 132%, 124% and 140%, compared to the control concrete at 91 days. The same trend was observed for the splitting tensile strength.

vii. A simple power function is proposed to evaluate the ratio of the splitting tensile to the compressive strength (*fspt/fc*) as a function of the cylinder compressive strength (Table 6.4, Eq. 1, 2 and 3). Based on that the correlation are close to ACI Building Code (*fspt*= 0.56 ($f_c^{0.5}$).

viii. The strength of RHA concrete development relay on the fineness of RHA particles more than the silica content, as is seen in the results of the comparison literature.

ix. Type of superplasticizer play great role on the strength development of RHA concrete, proven that was in comparison of the literature results.

x. The characteristics of the constituent materials of the concrete (cement, RHA aggregates, and admixtures) considerably effected on the strength development of RHA concrete and require greater attention when RHA used as a supplementary cementitious material.

CHAPTER 7: CHLORIDE PENETRATION RESISTANCE

7.1 General

Besides the strength requirements of concrete relevant to structural and fire resistance, it is also essential to consider the durability, which has received more attention over the last twenty years. In fact, it is necessary to take into account the final location of the structure, as this can lead to various impact conditions. Generally, the integrity of concrete can be altered due to absorbed chloride, sulphates and CO_2. Under normal circumstances chloride levels in raw materials (i.e. cement, aggregates and mixing water) are negligible. However, chloride-induced corrosion is a consequence of the diffusion of chloride ions from the environment through the porous structure of the concrete cover. Therefore, improve the durability of concrete is essential to increase resistance to corrosion. It is a known fact that RHA is suitable for partial replacement because of it is very high silica content (Bui et al., 2005; Mehta, 1977).

The reactivity of RHA is attributed to it is high content of amorphous silica, and to it is very large surface area governed by the porous structure of the particles (James & Rao, 1986; Mehta, 1994). It is generally accepted that incorporation of a pozzolan improves the resistance to chloride penetration and reduces chloride- induced corrosion initiation period of steel reinforcement. The improvement is mainly caused by the reduction of permeability/diffusivity, particularly to chloride ion transportation of the blended cement concrete (Stanish et al., 1997). In addition to that, RHA properties are different (i.e. particle size, silica content, silica form) and these differences in properties influence the ingress of chloride ion (Rasoul et al., 2017). Therefore, durability is an important parameter, hence is being measured for developed RHA based concrete and compared against normal concrete. Despite of several papers have been published on the effect of RHA properties on the strength performance of RHA blended concrete; however, only limited information is available on the chloride diffusion resistance. Therefore, the aim of this Chapter to determine the influence of RHA properties and replacement ratio on the chloride diffusion resistance, and compare that to the literature. To evaluate that diffusion coefficient is the

parameter which characterizes a concrete in order to predict it is long term performance that it is resistance to the penetration of ions. In the chloride diffusion test, the concrete being completely water saturated, the chloride penetrated by pure diffusion mechanism, being the difference in concentration, the driving force. The calculation of diffusion coefficient (D) from electrical measurement is based on non-steady-state migration (*Dnssm*) method. The results of the tests within the period of 28 and 91 days are presented.

7.2 Chloride ions

chloride ions can be divided in two categories: internal chlorides (when the chloride solution is intermixed with the cement powder [Hussain et al., (1994), Buenfeld et al., (1990)], or external chlorides (when chloride ions intrude in already hardened cement paste or concrete (Tang and Nilsson,1993).

7.2.1 Chloride binding

The numerous reviews on chloride binding over the years show just how important the understanding of this phenomenon is, especially in terms of obtaining a fundamental diffusion value that is useful in-service life modelling of concrete structures in chloride environment (Yuan et al., 2009). Some of the chloride ions that make their way into concrete are captured by a physical and chemical process called chloride binding. In general binding occurs as part of the diffusing chloride reacts chemically with the hydrating cement matrix forming Friedel's salt - $3CaO{\cdot}Al_2O_3{\cdot}CaC_{l2}{\cdot}10H_2O$, or physically with the adsorption of chloride ion to the C–S–H phase of the concrete. Friedel's salt is a complex calcium chloroaluminate hydrate compound that forms as C_3A or C_4AF combines with chlorides that diffuses through the concrete or chlorides added in the mix (Mehta, 1991).

7.2.1.1 Effect of Pozzolanic materials

It is known that fly ash, GGBS and metakaolin have a naturally high C_3A content and it has been shown that concrete with these constituents have low diffusion coefficient as a result of their binding capacity (Glass and Buenfeld, 2000). It has been reported that optimum replacement level for fly ash is 30%, with reduced binding capacity at 50% replacement (Dhir et al., 1997). With GGBS, replacement levels of up to 70% results in better chloride binding (Mohammed et al., 2002). Earlier, Dhir et al., (1996) has shown the effect of GGBS on the intrinsic permeability and chloride binding capacity on chloride

diffusion coefficient at several replacement levels up to 70%. Silica fume concrete, although having a low binding capacity (Justnes, 1998), blocks the ingress of chlorides with a much-improved particle packing. At a similar strength level, fly ash, GGBS and metakaolin concretes are better at resisting chloride ingress. Blending Portland cement (PC) with either fly ash, GGBS or metakaolin cements increases the ratio of monosulphate to formation of ettringite (AFt), as monosulphate is the important precursor phase thereby increasing the potential binding sites (Jones et al., 2003). Geiker et al., (2007) in their investigation found that the content of alkali metal ions (K_2O and Na_2O) has an important role to play in the distribution of chlorides between the pore solution, formation of ettringite (Aft), and C-S-H.

7.2.2 External Chloride transport

The transportation of chloride ions into concrete is a complicated process which involves diffusion, capillary suction, permeation and convective flow through the pore system and microcracking network, accompanied by physical adsorption and chemical binding (Kropp, 1995). With such a complex transportation process, it is necessary to understand individual transport mechanisms and the predominant transport process in order to pinpoint the appropriate method for quantifying the chloride resistance of concrete.

7.2.2.1 Diffusion

Diffusion is a transfer of mass of free molecules or ions in the pore solution resulting in a net flow from regions of higher concentration to regions of lower concentration of the diffusing substance. This mode of transport operates in fully saturated media such as fully submerged concrete structures. For porous material like concrete, the diffusion coefficient, D, is the material characteristic property describing the transfer of a given substance driven by concentration gradient.

7.3 Effect of RHA on the chloride diffusion resistance

The incorporation of RHA improves the resistance to chloride penetration of concrete as confirmed by many researches [Chindaprasirt et al., 2007; Gastaldini et al., 2007)]. This is due to the reduction in the average of pore size of paste and the improvement at the interfacial zone (Chindaprasirt et al., 2007). Saraswathy and Song (2007) reported that

chloride-induced corrosion resistance of concrete is significantly improved with the use of 30%RHA compare to OPC concrete. Ganesan et al. (2008) stated that chloride diffusion coefficient decreased with increasing of RHA replacement ratio up to 20- 25%. Beyond that, any increase in replacement ratio will increase the chloride diffusion coefficient. While Zahedi et al. (2015) reveal that RHA concrete reached the maximum enhancement of chloride resistivity at 20% replacement ratio. Moreover, Kannan and Ganesan (2014) reported that even with mean particle size of 6.27µm and 87.89% silica content, RHA reduces the total charge passed up to 15% replacement ratio, however beyond that increased. Chindaprasirt et al. (2008) compared the performance of RHA at two different replacement ratios (20 and 40%). RHA reduced the charge passed to 750 and 200 coulombs at 20% and 40% replacement levels. According to the author, with incorporation of RHA, significantly improve the resistance to chloride penetration of mortar by increasing nucleation sites for precipitation of hydration products, reducing $Ca(OH)_2$ and improving the permeability of mortar. Anwar et al. (2001) concluded that, chloride diffusion coefficient is correlated with the RHA replacement ratio. Where, the chloride diffusion coefficient values of concrete blended RHA decreased with increasing the RHA content from 10% to 20% and reached maximum at 40% replacement ratio.

According to the author, with partially replacement of cement by RHA in concrete results in changing the pore structure. Where, formation of fine and discontinuous pores and the pores are blocked by the effect of RHA and hydration products which improves the durability of concrete. Based on the previous researches the improvement of concrete resistance to chloride diffusion coefficient companied with discrepancy in optimum replacement levels of RHA. Moreover, there is no study is conducted to determine the effect of RHA properties on the durability of concrete with high replacement ratio (>40%).

7.4 Chloride diffusion techniques: review

In general, the tests for diffusion of chloride into concrete can be divided into two types: steady and non-steady state tests. Steady-state means that the chloride diffusion the concrete at a constant rate of flux causing the concentration to increase at a constant rate. While with none-steady state conditions the rate of chloride ion concentration will change continuously with the time at any position. The variation into the type of chloride penetration is presented in Figure 7.1.

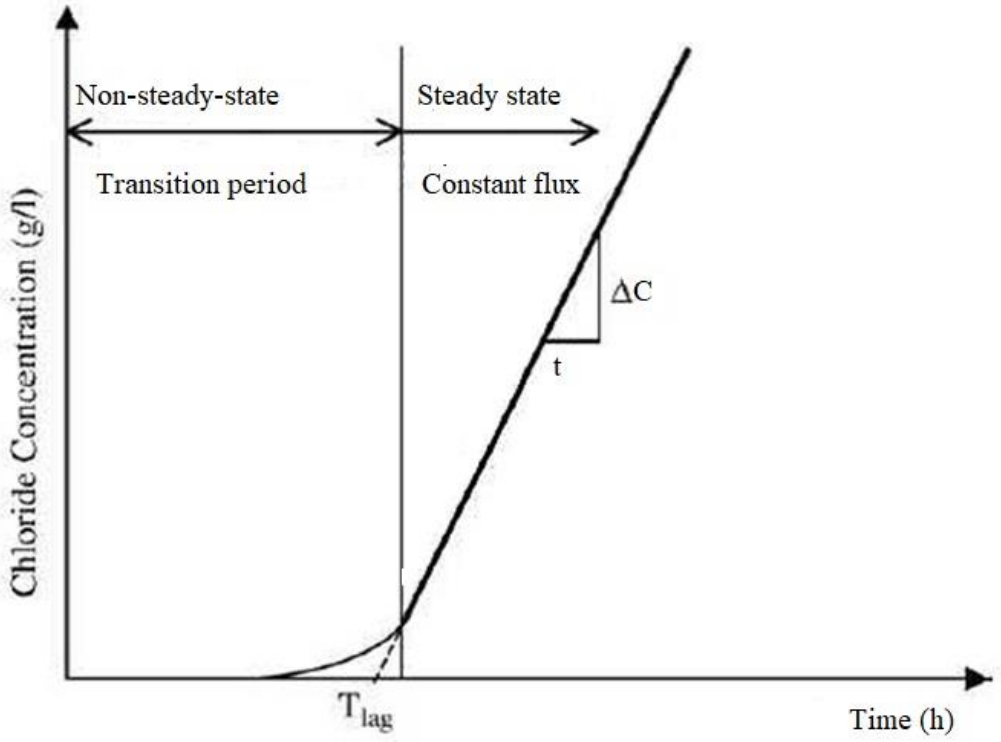

Figure 7. 1: The non-steady- state condition of chloride ingress schematic.

The none-steady state diffusion process which is mainly controlled by Fick's second law (Eq. 7.1), which is developed by Adolf Fick in the 19th century: The molar flux due to diffusion is proportional to the concentration gradient. The rate of change of concentration at a point in space is proportional to the second derivative of concentration with space is typically used for high-performance concrete (Stanish et al., 1997). For the above reason, only non-steady state conditions were adopted to calculate the chloride diffusion/migration coefficients in the present study.

$$\frac{\partial c}{\partial t} = D\frac{\partial^2 c}{\partial x^2}. \qquad (7.1)$$

Where
D: is the diffusion coefficient, (cm^2/sec)
c: constant
t: is the time of first exposure
x: is the distance from the exposed surface

7.5 Tests and analysis method

7.5.1 Chloride diffusion method NT Build 492

In the 1990s, a practical accelerated test method for chloride penetration was developed in Scandinavia, NT Build 492 or Rapid Chloride Migration test, RCM [NT Build 492 1999, Tang & Nilsson 1992, Tang 1996, Tang & Sørensen 2001]. This method was adopted as an important element of service life evaluation and a method for quality control based on resistivity was proposed. This enables the calculation of the apparent chloride diffusion coefficient (D*ns*) from an accelerated test (Nordtest method: BUILD-492, 1999). Among the different proposed laboratory accelerated chloride tests such as ASTM C1202 (steady state), NT Build 355 (steady state), NT Build 443(non-steady state), NT Build 492 (non-steady state- Electrical migration) is considered as the most similar test method to the real condition for the submerged concrete structure where the apparent non-steady state chloride diffusion (D*nss*) could be obtained (Kim et al., 2009).

Chloride diffusion coefficients was assessed by means of the non-steady state rapid chloride migration test (RCMT) specified in NTDbuild492 (1999). An external electrical potential was applied, and the chlorides ions were forced to migrate into the specimen. The testing time which is variable (6, 24, 48, and 96 h) and depends on the applied voltage. The non-steady-state chloride migration coefficient of diffusion (D_{nssm}) was calculated from Eq. (2).

$$Dnssm = \frac{0.0239\,(273+T)L}{(U-2)t}\left[Xd - 0.0238\sqrt{\frac{(273+T)L\,Xd}{U-2}}\right] \qquad (7.2)$$

Where:

D_{nssm}: non-steady-state migration coefficient, $\times 10^{-12}$ m^2/s;

U: absolute value of the applied voltage, V;

T: average value of the initial and final temperatures in the anolyte solution, °C;

L: thickness of the specimen, mm;

x_d: average value of the penetration depths, mm;

t: test duration, hour.

The test uses the principle of electro transfer to drive chloride ions through a 50mm thick concrete disc and 100mm in diameter (see Chapter 3.11.2). Samples are first cut using a water-cooled saw to the required thickness as shown in Fig.10.2. After preparation of the samples, they were placed in the vacuum desiccator for one hour under evacuation pressure. The specimens were then saturated with calcium hydroxide [$Ca(OH)_2$] solutions for 3hours

under vacuum. Saturated $Ca(OH)_2$ solutions were prepared by dissolving 1.6 grams of $Ca(OH)_2$ per liter of water (NT BUILD-492, 1999). Samples were left in a saturated solution for 18 ± 2 hours before the test. The test involves mounting the specimens in a rubber sleeve and then clamping them to ensure there is not any leakage.

Besides, the circumference of the rubber sleeve is covered with a thin layer of silicone grease to provide water resistance. This allows samples to be kept wet during the entire preparation period prior to the start of the NT building test. 10% NaCl solution is used as an anolyte and 0.3M sodium hydroxide (NaOH) is used as the catholyte solution. The test runs between 24 and 96 hours, depending on the initial current observed at 30V, and then adapting to the proposed initial current and voltage specified in the standard. At the end of the test, the temperature of the analyte solution and the final current was recorded before the samples were removed from the rubber sleeve and splatted to two halves. The 0.1M $AgNO_3$ solution is then sprayed onto the split surface to induce a chemical reaction between the chloride in the sample and silver in a solution to precipitate silver chloride. The process of preparation, set, measurement and determination of chloride diffusion coefficient are presented in Figure 7.2.

.

Figure 7.2: Preparation, set up test and determine the chloride diffusion coefficient of OPC and RHA concrete mixtures; (i)sample cut, (ii)samples after cut,(iii)vacuum of samples for 3h, (iv) vacuum of samples with $Ca(OH)_2$ solution for 1h,(v) set up of samplewith $Ca(OH)_2$ solution for 1h,(v) set up of sample used NT BUILD 492 method, (vi) press sample to two halves, (vii)samples after pressed to two halves, (viii) samples after spread by $AgNO_3$, (xi) samples width determination, (x) depth of chloride diffusion determination.

7.6 Materials and mixture proportioning

The materials used to cast the concrete specimens are presented in detail in Chapter 6 (see section 6.2.1, 6.2.2, 6.2.3, and 6.2.4). The mix design of the mixtures was obtained based on the British (DOE) method (see Chapter 6, section 3) is presented in Table 7.1. Nine binder mixtures were investigated. The first with 100% Portland cement, and the others with rice husk ash in concentrations of 5%, 10%, 15%, 20%, 30%, 40%, 50% and 60%, by weight of cement in dry condition.

Table 7.1: Mix proportion of concrete blended RHA.

RHA (% wt. of cement)	Batch quantities (kg/m^3)						SP (%)
	Cement	RHA	Aggregate		Water	SP% wt.	
			Fine	Coarse			
OPC	1592	-	2720	2770	792.02	3.98	0.25%
5%	1512	80	2720	2770	792.02	3.98	0.25%
10%	1433	159	2720	2770	792.02	3.98	0.25%
15%	1353	239	2720	2770	792.02	3.98	0.25%
20%	1274	318	2720	2770	792.02	3.98	0.25%
30%	1114	478	2720	2770	788.04	7.96	0.50%
40%	955	637	2720	2770	780.08	15.92	1.00%
50%	796	796	2720	2770	764.16	32.84	2.00%
60%	637	955	2720	2770	732.32	63.68	4.00%

SP*; Superplasticizer (%wt. of binder)

7.7 Results and discussion

The application of the electrical field was variable between 24 to 96hrs in all the experiments. After testing each series of three concrete samples using the RCM test set-up, three samples were split and sprayed with $AgNO_3$, a colorimetric indicator for chlorides. AgCl, being the product of the reaction of $AgNO_3$ with chlorides, has a white colour, while AgOH (which is later transformed to Ag_2O), formed in the chloride-free regions of sample, is brownish. Therefore, the boundary between the regions with and without chlorides becomes clearly visible and the chloride penetration depth can be measured as shown in Fig. 7.3.

Figure 7. 3: RHA concrete sample after spraying with $AgNO_3$.

As expected, in all the investigated samples the chloride penetration fronts were not straight and distorted because of the aggregates were present in the concrete. As explained earlier (see Section 1 and Fig. 1), the voltage and the duration of the RCM test are adjusted based on the initial value of the current at the voltage of 30 V. the initial currents measured at 30V on concrete samples were in the target range of 25–60mA as shown in Table 7.2. Generally, the depth of chloride penetration it depends on RHA replacement ratio. Hence, the applied voltage (U) was increased with increase replacement ratio (see Table, 7.2).

7.7.1 Apparent diffusion coefficient at 28-days

Apparent values of non-steady-state migration coefficient (D_{nssm}) for all concrete at age of 28-days was reported in Table 7.2, and presented in Fig.7.4. Data presented are the average values from 2 test cylinders. From this, six measurements as a minimum of average chloride depths were taken and the diffusion coefficient is calculated. Outliers are determined visually by observation of the overall data especially regression trends and the expected behavior. These outliers were excluded from the calculation of the average value presentation. The chloride diffusion coefficient of concrete without RHA was $11.55 \times 10^{-12} m^2/s$. As seen in Table7.2, inclusion of RHA greatly reduced the chloride diffusion coefficient which indicates better resistance to chloride ion penetration. The results of RHA-C, at 28-day cured concrete showed the least chloride diffusion coefficient (D_{nssm}) values. For example, with 30%RHA-C concrete, the D_{nssm} values are found to be $2.44 \times 10^{-12} m^2/s$, respectively. The considerably lower D_{nssm} values for RHA-C blended cements were attributed to their un-permeability nature that is due to the refinement of their pore structure. Due to the completely amorphous silica, and fineness of particles, the higher reactivity of SiO_2 with $Ca(OH)_2$ leads to the formation of C-S-H gel which reduced the micro and macro-pores present in the concrete (Saraswathy et al., 2017). For this reason, the chloride diffusion coefficient reduced considerably in RHA-C concrete when compared to RHA-A, and B concrete. The refinement of the pore structure occurring in blended cements considerably reduced the permeation of aggressive chloride ions. The same trend was observed by Saraswathy and Song (2007) by replacing 15 and 30% RHA. In addition to that, D_{nssm} of RHA-C is improved with increasing replacement ratio continually but modestly to reach $0.76 \times 10^{-12} m^2/s$ at 50%, in comparison, the chloride diffusion coefficient of RHA-A and B were $1.77 \times 10^{-12} m^2/s$, and $2.09 \times 10^{-12} m^2/s$, respectively. Migration coefficient of RHA mixtures continuously decreases with increase replacement ratio up to 60% RHA-A, and 50% RHA-B and C, as the applied voltage (U) increased to reach 60V at 40% RHA-A,

50%RHA-B and 20%RHA-C. This increase in applied voltage of RHA-C concrete is mainly due to the improvement of degeneration of the pore structure of concrete (Zahedi et al., 2015).

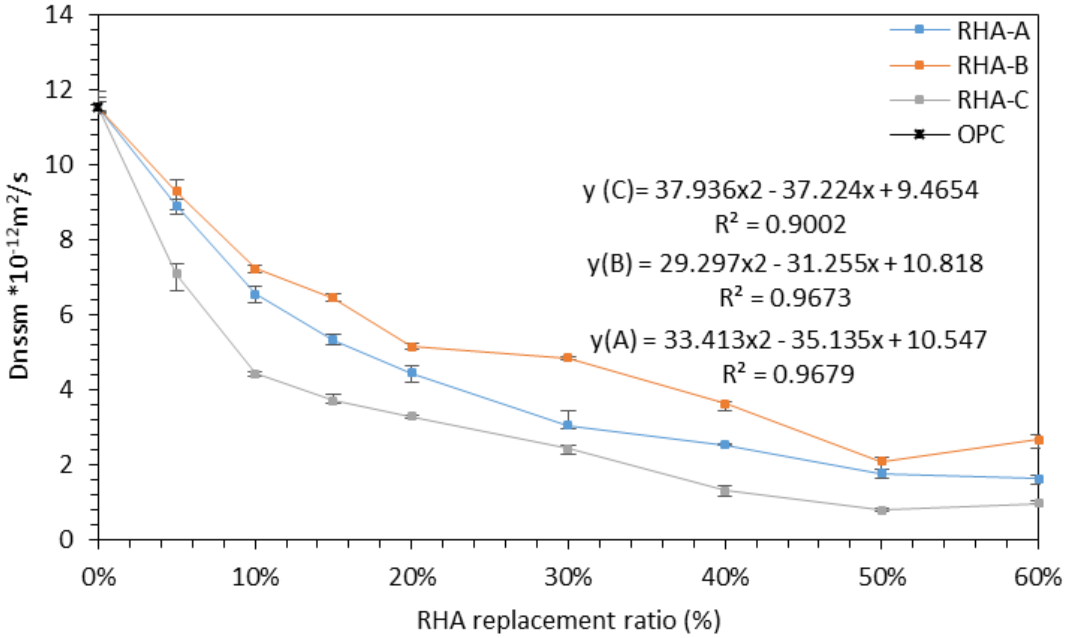

Figure 7.4: Diffusion coefficient values of OPC and RHA concretes at the age of 28-days.

Table 7.2: Correlation of RHA replacement ratio to chloride diffusion coefficient at age of 28-days.

%RHA	Applied voltage (U)			initial current (mA)			Test duration (t, hour)			Depth of Cl^- (mm)			*Dnssm* $\times 10^{-12}$ m^2/s		
	A	B	C	A	B	C	A	B	C	A	B	C	A	B	C
5%	25	25	30	50.7	58.7	56.3	24	24	24	16.14	16.39	15.71	8.91	9.30	8.50
10%	35	30	35	42.0	48.4	37.7	24	24	24	16.86	15.69	11.65	6.55	7.23	4.44
15%	40	35	40	38.6	42.3	32.4	24	24	24	15.71	16.41	11.27	5.33	6.45	3.73
20%	40	35	60	26.5	37.6	26.6	24	24	48	13.06	13.14	14.50	4.45	5.15	3.29
30%	50	40	60	26.8	38.7	14.6	24	24	48	11.31	14.17	21.14	3.07	4.85	2.44
40%	60	50	60	24.7	31.5	18.9	24	24	48	11.34	13.31	11.53	2.55	3.63	1.32
50%	60	60	60	15.7	16.2	9.5	48	48	96	15.17	17.70	13.81	1.77	2.09	0.79
60%	60	60	60	10.8	21.3	6.6	48	24	96	14.53	11.65	16.76	1.64	2.67	0.97
OPC		25			59.0			24			20.38			11.55	

7.7.2 Apparent diffusion coefficient at 91-days

The chloride migration diffusion coefficients of RHA blended mix concrete specimens at age of 91days are presented in Table 7.3, and plotted in Figure 7.5. While the improvement rate of chloride diffusion resistance is presented in Table 7.4. It is observed that, longer curing times improved the diffusion coefficient resistance of RHA concrete specimens. From the results, it can be seen that extending the wet curing period to 91days has reduced the diffusion coefficient in comparison with 28 days specimens. As an example, the D_{nssm} of 30%RHA-C mixture was $2.44\times10^{-12}m^2/s$ when cured for 28days, and became $1.26\times10^{-12}m^2/s$ as curing extended to 91days. That indicated long-term curing results in higher resistance to chloride permeability. It is reasonable to assume that this decrease was achieved by a continuation of RHA silica reacting with CH of cement hydration. Where RHA with fine particles causes segmentation of large pores and increases nucleation sites for precipitation of hydration products in cement paste (Mehta et al 1983). This increases the hydration and refines the pore structure of paste, leads to a reduction of calcium hydroxide in paste, for RHA concrete (Chindaprasirt et al 2007).

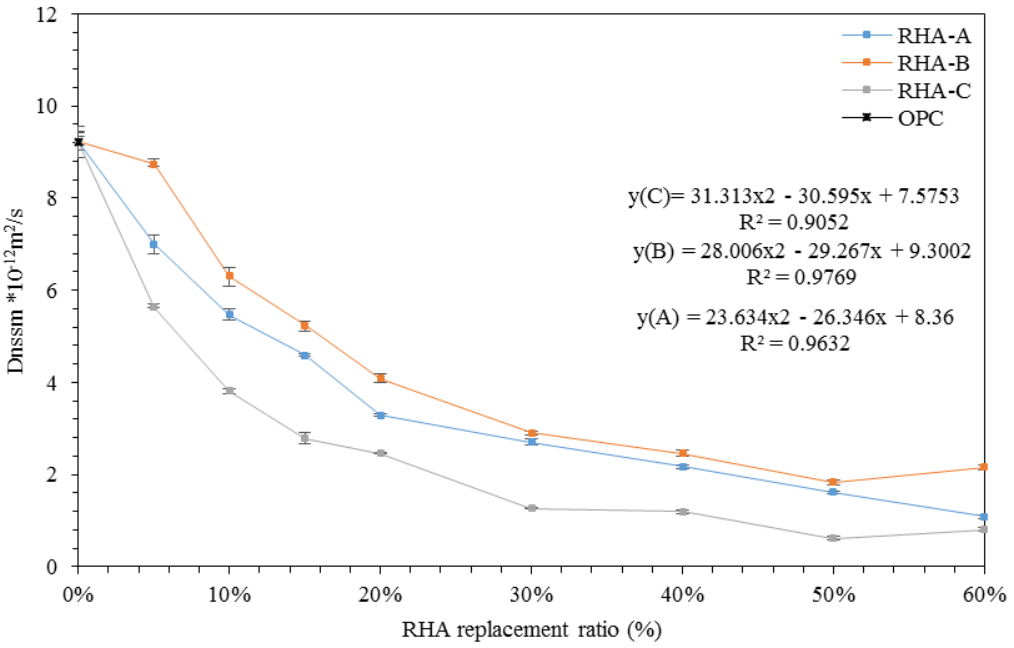

Figure 7.5: Chloride diffusion of RHA blended concrete at the age of 91-days.

Table 7. 3: Correlation between RHA replacement ratios to depth of chloride diffusion at age of 91-days.

RHA (%)	Applied voltage (U)			initial current (mA)			Test duration (t, hour)			Depth of Cl^- (mm)			*Dnssm* $\times 10^{-12}$ $m^{2/}s$		
	A	B	C	A	B	C	A	B	C	A	B	C	A	B	C
5%	30	30	35	49.3	50.6	42.8	24	24	24	15.52	18.89	14.55	7.00	8.74	5.63
10%	35	30	40	42.7	43.2	35.4	24	24	24	14.11	13.96	1145	5.47	6.31	3.81
15%	40	35	50	31.7	37.8	33.9	24	24	24	13.53	13.55	10.46	4.59	5.24	2.78
20%	50	40	60	29.3	32.6	25.1	24	24	48	12.14	12.01	11.89	3.29	4.08	2.46
30%	50	50	60	26.9	29.3	14.7	24	24	48	10.01	10.82	11.20	2.70	2.91	1.26
40%	60	50	60	23.3	26.9	18.4	24	24	48	9.610	9.190	10.63	2.17	2.46	1.20
50%	60	60	60	13.1	17.1	4.3	48	48	96	14.19	15.72	11.05	1.62	1.83	0.61
60%	60	60	60	11.4	23.1	4.9	96	48	96	18.76	9.820	14.06	1.09	2.16	0.81
OPC	30			49.07			30			20.00			9.22		

Table 7. 4: Improvement rate in chloride diffusion resistance of RHA mixtures compare to OPC concrete at ages of 28 and 91-days.

RHA [%]	Rate of improvement (%)					
	28-days			91-days		
	A	B	C	A	B	C
5%	22.81	19.44	38.57	24.29	16.24	39.12
10%	43.26	37.37	61.50	40.77	31.68	58.77
15%	53.82	44.10	67.70	50.29	43.34	69.93
20%	60.68	55.35	71.46	64.33	55.84	73.33
30%	73.34	57.99	78.82	70.74	68.44	86.28
40%	77.93	68.52	88.55	76.50	73.41	89.12
50%	84.65	81.86	93.10	80.40	80.22	93.30
60%	85.79	76.85	91.52	82.80	76.62	91.21

7.7.3 Effect of high replacement ratio on the chloride diffusion resistance

The results of chloride diffusion resistance at 28 and 91-days show the relative enhancement in resistivity of RHA concrete with increasing replacement ratio. From the coefficient of chloride diffusion values of RHA blended concrete specimens presented in Table 7.2, it can be seen from the results the higher the mix proportion became, the lower the chloride diffusion coefficient. Where latent hydraulic property and pozzolanic reaction made the concrete denser, which caused the chloride ions to be less penetrated (Chang et al., 2013). To demonstrate better the correlation between chloride diffusion resistance and replacement ratio results at 28 and 91-days, are presented graphically in Fig.7.6. The coefficient of chloride diffusion values of RHA concrete at different replacement levels were in the range of 0.79 (50%RHA-C) to 9.30 (5%RHA-B) $\times 10^{-12}$ m^2/s at 28 days of curing compare to 11.55 $\times 10^{-12}$ m^2 /s of control concrete specimens. These values became 0.61 to 8.74 $\times$ 10^{-12} m^2/s at 91 days of curing, compare to 9.22 $\times$ 10^{-12} m^2/s of control concrete specimens. Better chloride ion resistance of high volume of RHA concretes was also shown in other studies (Sivasundaram et al., 1991; Zhang et al., 1999).

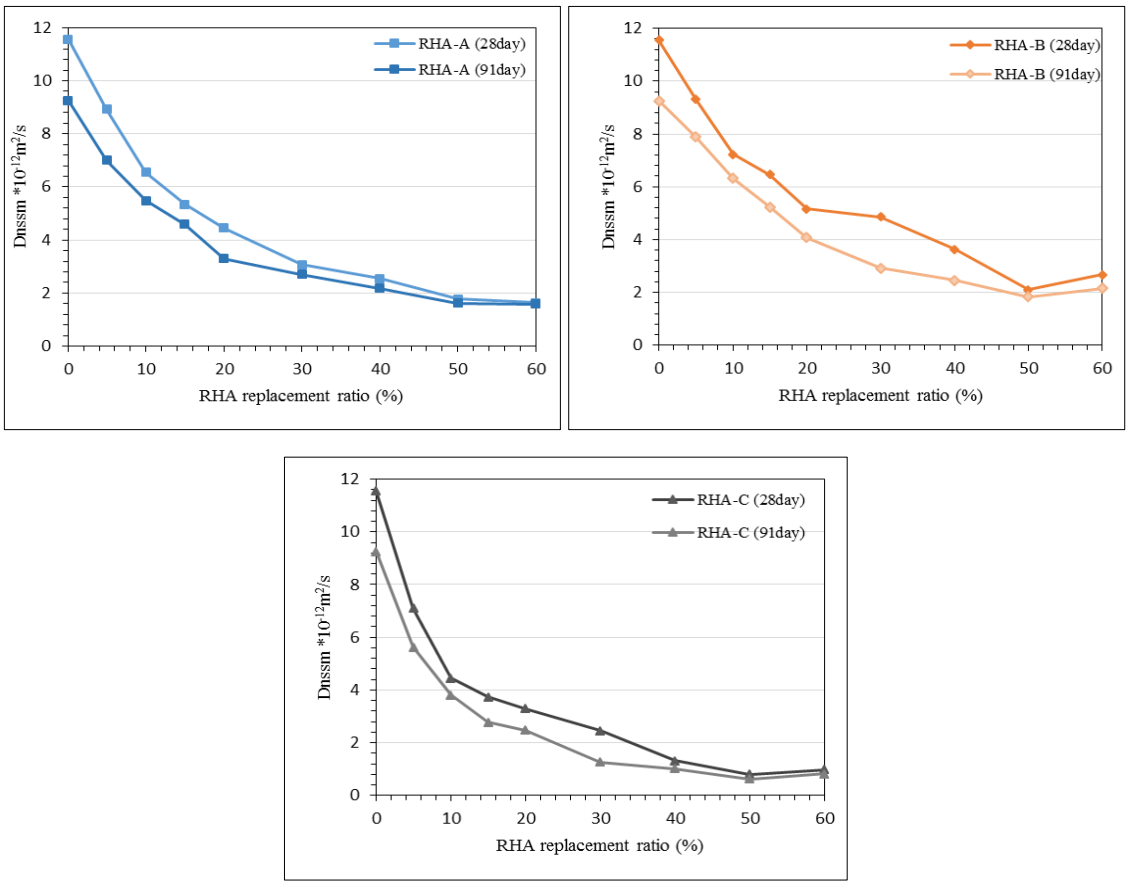

Figure 7.6: Correlate the D_{nssm} values versus to the curing time.

7.7.4 Effect of fineness of RHA

The fineness is one of the most important properties of RHA which relates to both the physical - and the chemical effects, i.e. the porous structure, the filler effect, and the pozzolanic reaction of RHA (Nguyen, 2011). It is clear that RHA particles are particularly effective in chloride migration coefficient when the mean size of RHA particles about 15.80μm. Particle size distribution of RHA samples (see Chapter 4.2.4) has shown an excellent correlation between RHA fineness and the chloride diffusion coefficient. Where the use of fine RHA (RHA-C) further reduces the diffusion coefficient. The average pore size of the cement paste is further reduced with the use of finer RHA (Chindaprasirt et al., 2007). The reduced average pore size as well as the improvement of the interfacial zone would increase the resistance to the ingress of the harmful chloride solution, and decreases the chloride ion diffusion of the RHA concrete. Therefore, it can be said that the coarser RHA has less effect on chloride diffusion resistance. This result of chloride diffusion resistance fit is well with the result of the pozzolanic reactivity of RHA analyzed previously.

7.7.5 Characterization of age factor in chloride diffusion coefficient

The age refers, according to the test specification, to the period of the sample when exposed to chlorides. Therefore, it should take into consideration the retarding effect on the diffusion process resulting from the refinement of the pore structure over time by introducing a so-called age factor. This factor characterizes the time-variant of chloride diffusion coefficient and has larger influence on the prediction of chloride penetration (Tran et al., 2016). The result shows that as the age of test increases, diffusion coefficient decreases for all replacement ratios. Where the reduction rate of chloride ion diffusion coefficient of RHA samples are significantly increased as compared to those of normal concrete.

The subsequent pozzolanic reaction provides an improvement in compressive strength, and it is high aluminate content binds the chloride ion, resulting in a reduction in the value of D with increased cure time. The decrease in diffusion coefficients (D) with age shows an exponential decay effect. Corresponding values for the apparent diffusion coefficients (D) with standard diffusion are plotted in Figure 7.7. Hydration of cement may continue up to 20-30 years, while all available water in the system does not react with un-hydrated particles. Theoretically, the effects of ageing will continue at the same time as hydration (Hassan, 2012).

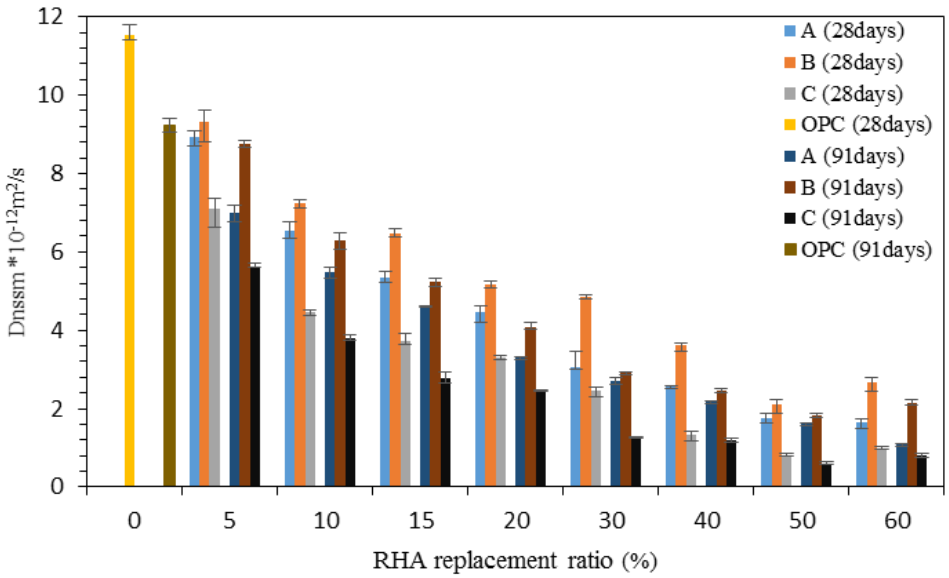

Figure 7.7: Correlation between RHA replacement ratio and D_{nssm} at age of 28, and 91 days.

7.8 Discussion

The overall results show that the diffusion resistance of concrete blended RHA specimens continuously decreases with increase in RHA content up to 50% of RHA-B and C and 60%RHA-A. At 60% RHA-B and C, there is an increase in diffusion coefficient and these values are significantly lower in compared to that of OPC control. This observation is true for both 28 and 91 days cured specimens. The range of diffusion coefficient of RHA-A concrete various from 1.64 $\times 10^{-12}$ m^2/s (60%RHA) to 8.91$\times 10^{-12}$ m^2/s (5%RHA) at 28days, and from 1.09 $\times 10^{-12}$ m^2/s (60%RHA) to 7.0 $\times 10^{-12}$ m^2/s (5%RHA) at 91-day curing. Similarly, the chloride diffusion coefficient of RHA-B concrete is various from 2.09 $\times 10^{-12}$ m^2/s (50%RHA) to 9.30$\times 10^{-12}$ m^2/s (5%RHA) at 28 days, and from 1.83$\times 10^{-12}$ m^2/s (50%RHA) to 8.74$\times 10^{-12}$ m^2/s (5%RHA) at 91 days. While the chloride diffusion coefficient of RHA-C concrete ranged in between 0.79 $\times 10^{-12}$ m^2/s (50% RHA) to 8.50$\times 10^{-12}$ m^2/s (5%RHA) at 28 days and 0.61 $\times 10^{-12}$ m^2/s (50%RHA) to 5.63$\times 10^{-12}$ m^2/s (5%RHA) at 91 days of curing, respectively. These values also indicted that reduction of diffusion coefficient value observed by 8.46 times for RHA-A concrete at 60% replacement ratio, 5.03 times for RHA-B concrete at 50% replacement ratio, and 15.11 times for RHA-C concrete at 50% replacement ratio compare to OPC concrete, respectively.

Generally, the significant performance of RHA-C in reduction of chloride diffusion coefficient can be attributed to an increase in fineness of the ashes. Where, the finer particles

of ashes develop discontinuous pore in concrete structure. Moreover, the micro and macro pores present in the concrete are completely filled up by finer particles (Ganesan et al., 2008). Unexpected results can sometimes be observed with this test. Table 7.2, shows for RHA-C mix the D_{nssm} value measured at 28 days shows a considerable jump from an average of 8.5×10^{-12} m^2/s at 5% replacement ratio to 44.4×10^{-12} m^2/s at 10%RHA. Test results and calculations have been checked but nothing could be found to suggest an error. The present work indicates that the permeability properties are considerably improved due to pore refinement by the finer particles of RHA in blended concretes.

7.9 Conclusions

From the experimental investigation the following conclusions were made: -

i. The application of RHA brings a considerable improvement of durability of concrete. This improvement is a consequence of the pozzolanic activity of the RHA, which results in the generation of additional C-S-H gel. The fine C-S-H gel is responsible for a reduced porosity and in turn also reduced permeability.

ii. According to the experimental results as much as 60% by weight of OPC can be replaced by all RHA types used in this study, improving the durability of concrete (chloride ion resistance). The best results were achieved with RHA-C about 93% reduction of chloride penetration; this can be attributed to the high reactivity of the amorphous silica and fine grain size of RHA-C. This is a much higher reduction than previously reported in the literature where only about 15% to 40% reduction could be achieved.

iii. At the curing age of 28 and 91 days, RHA shows significant resistance to chloride ion diffusion, which is in consistence with findings in the literature. However, in most literatures (Chapter 2, section 2.6.4), the RHA concrete has reached maximum chloride diffusion resistance at 30%. In this study, chloride diffusion reached maximum reduction at 50%RHA-B and C, and 60%RHA-A concrete.

iv. In general, an excellent correlation exists between the diffusion coefficient, depth of chloride ingress, time, and applied voltage.

v. The enhancement of chloride diffusion resistance of RHA concrete depends on the reaction of amorphous silica and fineness of particles size.

vi. Concerning the test method, the non-steady state tests (NT BUILD 492) have an excellent compatibility with the ageing factor.

CHAPTER 8: EFFECT OF COMBUSTION DEGREE TO TIME ON THE SILICA STRUCTURE OF RHA

8.1 Introduction

The aim of this preliminary laboratory research in this Chapter was to identify the time-temperature relationship on the onset of silica crystallization in rice husk ash. The raw rice husk sample was used on 'as received' basis without any pretreatment. The experimental methods and procedures are taken in the laboratory for the ash and analytical methods used to assess the reactivity of the ash. A set of three groups of ashes was produced by changing the incineration temperature and time of combustion. Used X-ray diffraction methods test evaluated the crystallization of the ashes.

8.2 Review of literature

Rice husk ash is generated by the incineration of rice husk under controlled condition. The standard form of RHA silica is amorphous, however crystalline also present as the other forms of RHA silica. The structure of silica produced is dependent on the conditions of incineration (temperature degree to time). Where burning rice husk under controlled conditions below 700°C yielded an amorphous ash; however, with short duration of incineration time (Mehta, 1979; Stroeven et al., 1999 and Maeda et al., 2001). In addition to that, other researchers concluded that the combustion environment affects specific surface area of RHA [Khalaf and Yousif, 1984 and James and Rao, 1986]. Therefore time, temperature, and environment must be carefully selected in the pyro processing of rice husks to ensure ash of maximum reactivity [Mehta, 1979; Yoeh et al., 1979; Ankra, 1976; Nehdi, et al., 2003]. Since then, many similar studies had been carried out, as shown in Table 8.1. Crystallization is the process of transformation amount of highly reactive amorphous silica into non-reactively crystalline silica when incineration temperature to time exceeds a specific limitation (Lun, 2015). Amorphous silica contains the molecules which are arranged in a random three-dimensional repeating pattern. The specific surface area is large, and the chaotic formation of the structure is open with holes in the network where electrical neutrality is not satisfied. While, crystalline silica structure is a repetition of a basic unit.

Therefore, the structure of crystalline silica reduces the surface area of RHA and thus decreased the reactivity of RHA (Lun, 2015).

Mehta (1979) suggested that maintaining the combustion temperature below 500°C under oxidizing conditions for prolonged periods or temperature up to 680°C with less than one minute could produce amorphous silica. According to the author, prolonged heating above this temperature may cause the material to convert, at least in part to, crystalline silica; first to cristobalite and then tridymite. Hamad and Khattab (1981) prepared an amorphous silica ash at a temperature of about 500 to 600°C. While, Nehdi et al., (2003) states that silica in RHA can remain in amorphous form at combustion temperatures of up to 900°C if the combustion time is less than one hour, whereas crystalline silica is produced at 1000°C with combustion time greater than five minutes. Same conclusion was reported by Yoeh et al., (1979). On the other hand, Bui (2001) claimed that crystalline ash could also be formed at temperatures as low as 350°C under prolonged exposure of about 15 hours. Chandrasekhar et al., (2003) observed that RHA produced at below 400°C contained un-burnt cellulose material, while sintering of RHA starts only at and above 600°C. And also, maximum reactivity was observed at 400°C with 6-12 hours and 500°C with 8- 12 hours incinerating time.

Based on the previous researches conclusions, the results of different researchers are divided into two groups. Some researcher suggested that RHA silica maintained in amorphous form under or equal to 500°C, i.e. Mehta (1979), Al- Khalaf and Yuosif (1984), and Chandrasekhar et al., (2003). While some other researchers like Yoeh et al., (1979) and Nehdi et al., (2003), they reported that RHA silica retains it is properties as amorphous form even at 900°C. Add to the above, a researcher like Habeed and Fayyadh (2009), and Abu Baker et al. (2010) produced RHA with entirely amorphous silica at 700°C. According to the previous research, there is no exact temperature to the time of transformation of silica to crystalline. Therefore, in order to identify the most suitable production condition (combustion degree to time), it is imperative to establish the amorphous silica content in RHA samples by investigated that at various temperature to time.

Table 8.1: Composition of RHA found at different temperatures.

Researcher	Incarnation temperature (°C)	
Mehta (1979)	Essentially amorphous silica can be produced by maintaining the combustion temperature below 500°C under oxidizing conditions for prolonged periods or up to 680°C with a hold time less than 1 min.	
Yeoh et al. (1979)	RHA can remain in the amorphous form at combustion temperatures of up to 900°C if the combustion time is less than 1h, while crystalline silica is produced at 1000°C with combustion time greater than 5 min.	
Hamad & Khattab (1981)	At a temperature of about 500 to 600°C consists of amorphous silica. Cristobalite was detected at 800°C and after burning at 1150°C both cristobalite and tridymite were present.	
Chopra et al. (1981)	At incineration temperatures up to 700°C the silica was predominantly in amorphous form and that the crystals present in the ashes grew with time of burning.	
Khalaf & Yousif (1984)	500°C for 2 hours High reactivity RHA is produced.	
Smith & Kamwanja (1986)	800°C for 12 hours Resulted in small proportions of crystalline silica.	
James & Rao (1986)	400°C -900°C for 1-30 hours Reactivity of ash is dependent mainly on temperature and duration has small effect. High reactivity of ash around 500°C.	
Boating and Skeet (1990)	550-700°C amorphous, while silica transformed to crystalline at 900°C.	
Isamil and Waliuddin (1996)	400-700°C for 24 hours Amorphous silica.	
Nehdi etal. (2003)	RHA-A 750°C RHA-B 830°C RHA-C 750°C+air	Less than one hour the silica in RHA can remain in amorphous form. While, Greater than five minutes converted to crystalline silica.
Benjamin and Shah (2003)	•Rice husk placed in an electric furnace at 500°C for 5hours. •The effect of time of burning was also studied on RHA by burning RHA for one hour before burning in the electric furnace for two hours at 500°C.	
Chandrasekhar et al. (2003)	400°C for 6-12 hours and 500°C for 8-12 hours reactive RHA is produced.	
Bui (2005)	350°C for 15 hours crystalline ash is formed	
Asavapisit & Ruengrit (2005)	Ash burned at 400-800°C for one hour, where 650°C as optimum temperature for producing reactive RHA based on strength activity index.	
Reddy (2006)	At burning temperatures of 550°C– 800°C, amorphous silica is formed, but at higher temperatures crystalline silica is produced.	

Researcher	Incarnation temperature (°C)
Nair et al. (2008)	500°C-700°C for 12 hours. Highest amount of amorphous silica is formed.
Habeeb and Fayyadh (2009)	Incineration temperature not acceding 700°C, resulting amorphous silica.
Madandoust et al. (2011)	Amorphous RHA was obtained by burning at relatively high temperatures in the range of 650°C.
Zain et al. (2011)	The average temperature to produce amorphous ash was 500–600°C during 2h of combustion.
Onojah et al. (2013)	Crystallization in rice husk ash begins at temperature above 500°C; below this temperature rice husk ash is purely amorphous. The phase transformation in rice husk ash is shown below. Amorphous Silica 600°C⭤ Quartz 800°C→ Tridymite→ 1470°C →Cristobalite.
Moghadam and Khoshbin (2013)	The RHA was obtained by burning at relatively high temperatures (450-550°C) which led to the crystallization of the amorphous silica. To be used as a pozzolanic material, the ash was ground by means of a laboratory 2ball mill until certain fineness.
Shatat (2013)	Amorphous RHA was prepared by burning of rice husk (RHA) for 2h at 600°C.
Kannan and Ganesan (2014)	Temperature of 650°C over a period of one hour resulted amorphous ash.
Khassaf et al. (2014)	The Rice Husks Ash (RHA) used in this investigation was obtained from Al- Abasia Farms in Kufa city. Burning of rice husks was carried out in a furnace with controlled in order to establish the optimum burning temperature and burning time. The combustion temperature was about 550°C and duration time was 2 hours produced an ash with optimum properties.

8.3 Rice husk sample

Locally rice husk from Iraq was brought for the present study. The husk particles have an average length of 6.4 - 9.1mm and width of 1.5 - 3.08mm, as shown in Fig. 8.1. The husk sample was gathered in a single lot. Rice husk samples were split into different groups based on the burning temperature to time.

Figure 8.1: Boat-like shape of the as received whole rice husk.

8.4 Combustion method

8.4.1 Furnace

Laboratory-type muffle furnace model Carbolite ELF 11/14B, which is a drop-down door laboratory furnace with a chamber capacity of 14 liter's and maximum operating temperature of 1100 º C, was used for ash production (Fig. 8.2).

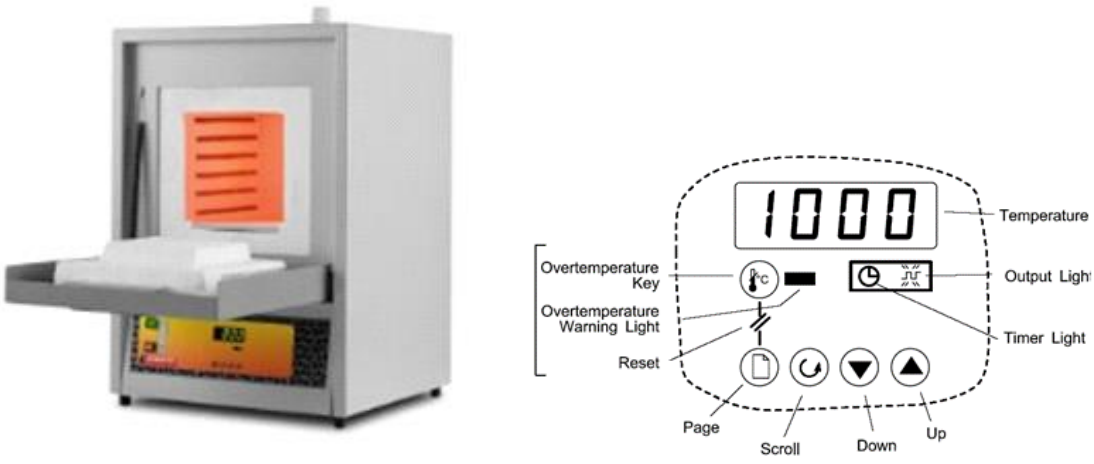

Figure 8.2: Carbolite ELF 11/6, Muffle Furnace.

The main features of the furnace consist of Controlled heat up rate eliminate thermal shock to the material. Energy efficient moldatherm insulation is suitable for high interior-exterior temperature differential. The unit is rated for a maximum operating temperature of 1100°C. The furnace consists of standard exhaust vent, vacuum formed, low thermal mass insulation, digital instrumentation for precise temperature set point and display, the microprocessor automatically optimizes control parameter during furnace operation, and hard ceramic hearth fitted as standard and ventilated via the top mounted ceramic chimney. The set temperature was maintained for the required duration. Then it was cooled down from the set temperature to the room temperature directly by bring out the sample from the chamber to avoid crystallization of silica as a result of long proses of cool down inside of the chamber. Then, the ash samples were kept in air-tight polythene bags.

8.4.2 Ash preparation

The muffle furnace used in the preparation of the ash samples has two heating rates and the cooling regime, illustrated in Fig.8.3. The heating rate was 28°C per minute up to 500°C and 20°C per minute above 500°C. while the cooling regime began at a rate of 7°C per minute from the set temperature to 500°C and 5°C per minute from 500°C to ambient temperature. Incineration of husk was carried out in the furnace when the temperature of the furnace chamber reached the set point by put of 5g ± 0.5 of the hulls for each sample. The aim of putting the samples directly to the chamber room after heating reaches the set point, was to avoid any per longed time which my effect on the silica structure.

During that time, there was a sudden increase in temperature for a short period, due to the heat energy supplied from the burning husk. This rise in temperature was neglected, as it existed for a brief period. The minimum and maximum duration of burning temperatures were selected based on that husk have to be converted into ash leaving the least permissible level of unburnt carbon and presenting the start point of converting silica into crystalline. Based on these factors, the duration of incineration was varied from five minutes to nineteen minutes. The combinations of burning degree to time were investigated based on the available literature information. Which is showing that, if the temperature is low, long duration of incineration is required and if the temperature is high, a brief period of combustion is enough.

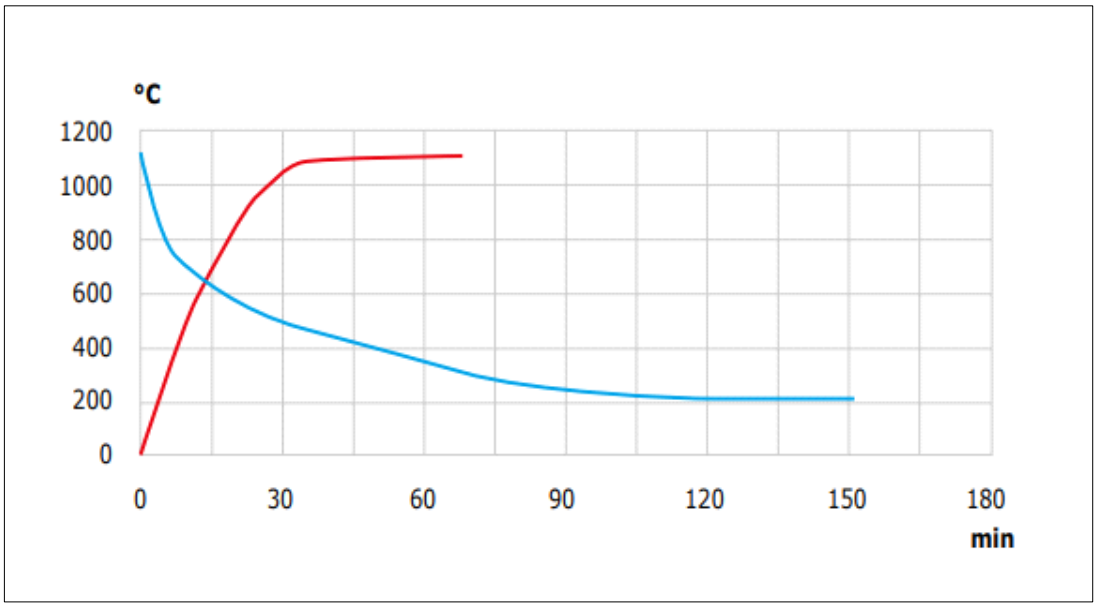

Figure 8.3: Heat –up and cool down rate for ELF11/6 Carbolite Muffle Furnace

8.4.3 Chemical composition of RHA

The Rice Husks used in this investigation was provided from Babylon Province /Iraq. The burning of rice husks was carried out in a muffle furnace at 500°C for 60 minutes. X-Ray Fluorescence (XRF) test used to identify the chemical composition of the ash. Residual carbon content (Loss on ignition) obtained according to EN 196-2:1994 (see Chapter 4, section 4.2.5). The results are shown in Table 8.2.

Table 8.2: Chemical composition of ash prepared at 500°C for 60 minutes.

SiO_2	Al_2O_3	Fe_2O_3	CaO	K_2O	P_2O_5	SO_3	MnO	TiO_2	SrO	Cl	WO_3	LOI
82.85	1.42	0.58	1.61	3.23	0.44	0.98	0.07	0.03	0.01	0.80	0.44	8.40

8.5 Determination of RHA silica structure

8.5.1 Introduction

Rice husk ash samples (obtained from combustion experiments) were subjected to X-Ray Diffraction (XRD) analysis using X-Ray Diffractometer to determine their silica structure. Before analysis, the ash samples were ground to a powder form using Planetary Mono Mill Pulverisette 6 for one minute. Cu Kα radiation analyzed the ground samples with a scanning rate of 0.05° per second (see Chapter 3, section 3.3.3). The resulting phase diagram (diffractogram) showed the different phases present in the sample via various peak positions. A background hump indicates the amorphous structure at peak position on the diffractogram. Three different categories of ash have been prepared in the present investigation from rice husk. These are labelled as D, E and F, respectively. Group A of rice husk ash samples are prepared at six different temperatures, 350, 400, 425, 450, 475 and 500 ºC, with two different of times (60 and 90 minutes). Followed by group B, were prepared at four different temperatures 525, 550, 575 and 600°C with two different time (15 and 30 minutes). While, the third group (group C) prepared at ten different temperatures, 625, 650, 675, 700, 725, 750, 775, 800, 825 and 850°C, with two different periods (5 and 10 minutes).

8.5.2 RHA group D

8.5.2.1Ash sample preparation

Generally, the ignition temperature of husk was 340°C and based on these facts, the temperature of incineration in this series was fixed at 350°C to 500°C at two different

periods of times (60 and 90 minutes). The oven was set up at the desired temperature before each test. When the rice husk sample (5.0g) was placed onto the steel plate inside the muffle furnace at 350°C, it was observed that the rice husk particles immediately flashed or devolatilized, resulting in flaming combustion (long trailing orange flame) for 5-9 seconds. The resulting char particles took another 35-50 seconds to burn out entirely into ash in the form of glowing combustion with short, slight bluish flame surrounding the char particles. In fact, the final ash product from the combustion of these raw rice husk particles were not completely burned, which is clear from the color of the ash (brown). With increasing time of combustion to 90min, the ash turned to the black color indicated to wholly burned raw materials.

Sudden exposure of raw rice husk particle, when the incineration temperature increased to 400°C, caused the alkali metal compounds of potassium and sodium oxide to melt, thus forming a surface melts mixture on the char and/or ash particles. Therefore, any unburnt carbon molecules 'trapped' in this melted mixture and were unavailable for further oxidation (Krishnarao et al., 2001). In addition, resulted ash presented a variable color indicating the variation in silica structure and residual of carbon content. Comparison the color of ash samples incinerated at 400°C for 60 min and 90 min it is clear that with increasing time the color turned to a brighter indication of low residual carbon content. This trend became more apparent with ash prepared at 425°C and 450°C and became white color at 475°C to 500°C. These results are in contrary to the conclusion reported by Bin Taib (2007). According to the author, because of the phenomenon of surface melting, it has never been possible to obtain utterly white ash from the burning of raw rice particles, irrespective of how long the particles were stored in the muffle furnace.

8.5.2.2 Silica structure

Series A of RHA samples ashes is consisted of six variables incineration temperatures (350°C, 400°C, 425°C, 450°C, 475°C and 500°C), where each sample burned at two different periods of time (60 and 90 minutes). All particle samples were analyzed for their silica structures using X-Ray Diffraction (XRD) analysis at the University of Brighton Laboratories (see Chapter 4, section 4.2.2.3). The color and representative XRD patterns of the RHA samples are shown in Tables 8.4, and 8.5, respectively. Fresh rice husk contained amorphous silica 'as received' (Fig.8-1), Incineration at 350°C for 60 min. Based on the NIOSH manual of analytical methods (NMAM, 2003) presented in Table 8. 4, the husk burned at 350°C for 60minute shown a weak peak of XRD.

Thus, barely observed peaks could be assigned to cristobalite and quartz was estimated to be negligible. Indicated that the ash remained in an amorphous form. As can be seen, with increasing time of burning to 90 min, a single diffuse band is shown at around 26.7° with slightly increase intensity from 22.03 counts (60min) to 39.71 counts. Indicated that, the silica in RHA at 350°C/90m sustains in an amorphous state. However, a comparison in between each type of rice husk ash degree, only peaks at or near of 26.66° (quartz), 21.93° (cristobalite) and 21.62° (tridymite) will be take in account as the primary 2°theta diffraction patterns to determine the crystallinity of ash silica. After 60 min of heating, the peak intensity of quartz and cristobalite (secondary) was increased at sample exposure to 400°C. These weak peaks of quartz at 26.64° are augmented with an additional weak peak at 35.55° (secondary) and 30.91° (tertiary). These weak peaks were identified as cristobalite.

Nonetheless, the ash properties remain nearly amorphous. With increasing degree of burning degree to 425°C for 60 min, the XRD patterns show a trace of tridymite at 23.40° (tertiary) show up on top of the broad amorphous background. As well as, quartz at 26.71°, calcite at 29.40° and cristobalite at 35.77° (secondary) and 31.17° (tertiary) presented. Contrary to 60 minutes of heating, XRD patterns of 90-minute show low peaks at 2θ (secondary and tertiary) of cristobalite at 36.07° and 31.23°, accompanied with a slightly sharp Calcite peak at 29.47°. Similarly, to the XRD results of previous burning degrees, there was no significant difference in XRD patterns of other combustion degrees 450°C, 475°C and 500°C /60min and 90min. Except for 2θ of 29.4° where presenting with the sharp intensity of calcite at 475°C/60min (113.18 counts). In general, based on the results burning rice husk at temperatures ranged in between 350°C to 500°C for 60 to 90minute, exhibited weak peaks of crystalline silica, indicating that ash sustained in amorphous form.

Table 8.3: Qualitative X-ray diffraction according to NIOSH Manual of Analytical Methods (NMAM).

Mineral	Peak (2-Theta Degrees)		
	Primary	Secondary	Tertiary
Quartz	26.66	20.85	50.16
Cristobalite	21.93	36.11	31.46
Tridymite	21.62	20.50	23.28

Table 8.4: Effect of temperature and residence time on the formation of the rice husk ash in the muffle furnace.

Time (min)	Temperature degree of burning rice husk (°C)					
	350°C	400°C	425°C	450°C	475°C	500°C
60						
90						

Table 8.5: X-ray diffraction of rice husk ash samples in a muffle furnace at different temperatures and residence times.

Temp. (°C)	Time (min)	Peaks		Time (min)	Peaks	
	60 (min)	Pos.[°2Th.]	Height.[cts]	90 (min)	Pos. [°2Th.]	Height.[cts]
350	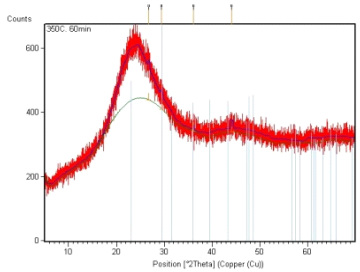	26.8083 29.4703 36.1190 44.1143	22.03 18.39 29.32 18.33	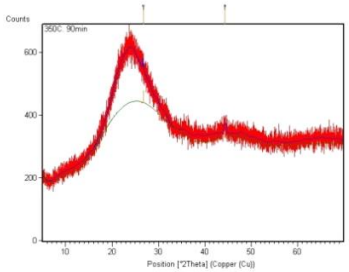	26.711 44.3590	39.71 21.38
400	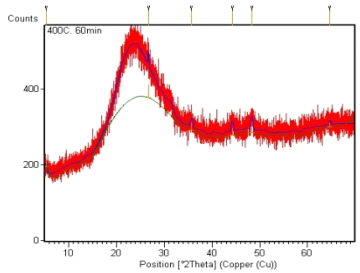	5.2734 26.6901 35.7475 44.2214 48.3308 64.6724	22.34 35.77 20.07 21.31 32.75 12.83	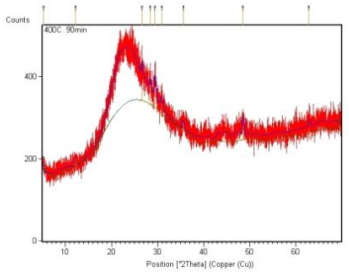	5.2261 12.1744 26.6499 28.3875 29.4774 30.9161 35.5553 48.5377 62.8626	24.65 17.21 26.30 24.67 50.93 23.19 17.22 35.48 10.58
425	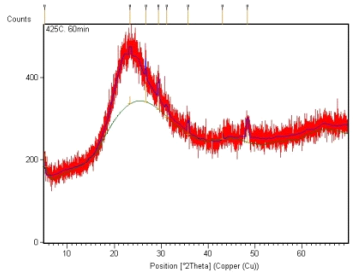	5.1311 23.4072 26.7163 29.4027 31.1781 35.7709 43.1209 48.3922	32.35 19.39 48.52 52.63 10.99 27.33 26.79 31.39	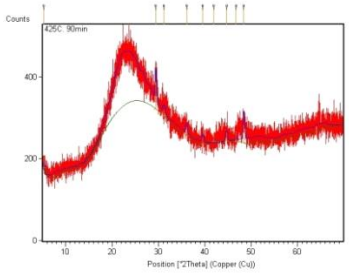	5.2471 29.4707 31.2368 36.0791 39.5425 41.9505 44.6810 46.7298 48.4322	28.26 67.60 15.89 21.32 17.13 24.54 22.41 24.63 45.23

Temp (°C)	Time (min)	Peaks		Time (min)	Peaks	
	60 (min)	Pos. [°2Th.]	Height [cts]	90 (min)	Pos. [°2Th.]	Height [cts]
450	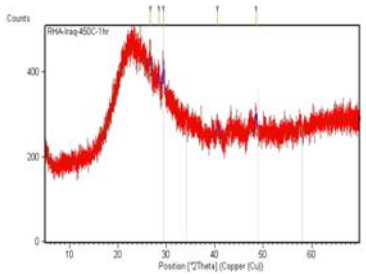	26.7179 28.4602 29.3922 40.5998 48.5416	28.13 28.68 92.34 28.83 32.17	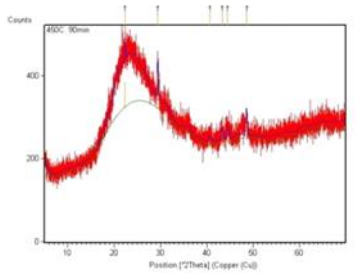	22.3454 29.4680 40.6206 43.3106 44.5223 48.5886	60.70 86.32 13.16 26.17 25.58 46.94
475	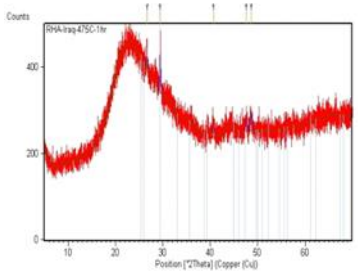	26.6578 29.4280 40.6696 47.5663 48.6096	54.78 113.18 17.55 29.57 31.81	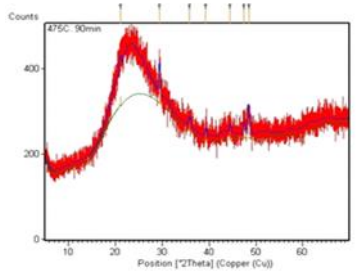	21.0764 29.4275 35.8989 39.3276 44.5062 47.4072 48.4584	22.80 75.03 18.25 17.71 18.67 26.99 46.93
500	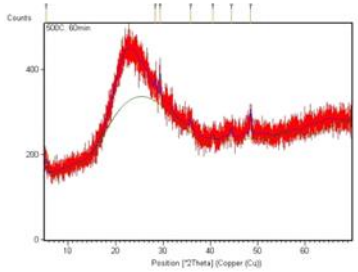	5.3634 28.4558 29.3829 35.8776 40.5042 44.4400 48.4534	26.97 20.20 58.62 19.82 9.42 17.18 39.11	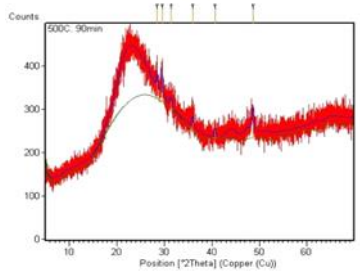	28.4524 29.5489 31.3828 35.9354 40.6241 48.5995	34.36 58.81 17.75 21.05 18.92 33.81

8.5.3 RHA group E

8.5.3.1 Sample preparation

Samples prepared at 525°C, 550°C, 575°C and 600°C for 15 and 30 minutes. The flaming time was observed ranged in between 3-5 seconds. The char burning time were 25-35 seconds. In total, combustion time for samples reached in between 28 to 40 seconds.

8.5.3.2 Silica structure of group E

The color and XRD diffractograms results are shown in Table 8.6, and 8.7, respectively. At 525°C for 15 minutes, a single diffuse of quartz peak presented at 26.75° indicated that ash sustained in amorphous form. Even with increasing burning time to 30 minutes, a weak peak of quartz was barely observed at 26.6° accompanied with cristobalite (tertiary) at 31.24°, confirming that ash remained in an amorphous state. With increasing combustion degree to 550°C for 15 minutes, a weak peak of quartz was observed at 26.7°, accompanied with calcite silica at 29.46°. While a trace of tridymite observed at 23.16° (tertiary) accompanied by the weak peak of each of quartz at 26.69°, calcite at 29.42° and cristobalite at 31.43 (tertiary) for 30 minutes to burning time. At combustion degree of 575°C for 15 and 30 minutes, some weak diffraction peaks of quartz (26.76°), cristobalite (31.62° tertiary) and calcite (29.52°) exhibited. Same determination was observed at 600°C for 15 and 30 minutes.

Table 8.6: Effect of temperature to time on the formation of black char particles of raw rice husk in the muffle furnace.

Time (min)	Temperature (°C)			
	525	550	575	600
15				
30				

Table 8.7: X-ray diffraction of rice husk ash samples in a muffle furnace at different temperatures and residence times.

Temp.(°C)	Time (min)	Peaks		Time (min)	Peaks	
	15 (min)	Position.[°2Th.]	Height.[cts]	30 (min)	Position.[°2Th.]	Height.[cts]
525	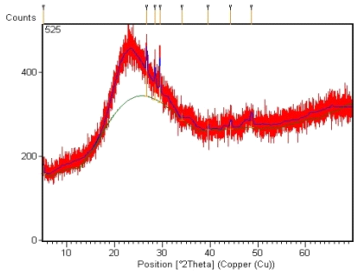	5.1463 26.7597 28.5209 29.4909 34.1358 39.5660 44.3504 48.7006	20.57 59.90 37.08 86.46 19.36 22.08 16.33 16.42	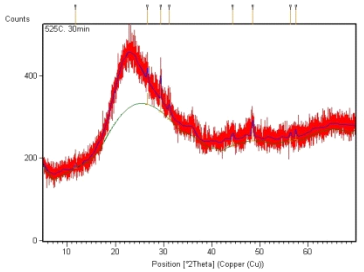	11.7376 26.6901 29.4527 31.2470 44.3743 48.4978 56.3228 57.4278	10.58 28.63 69.71 16.14 12.42 37.79 12.47 15.43
550	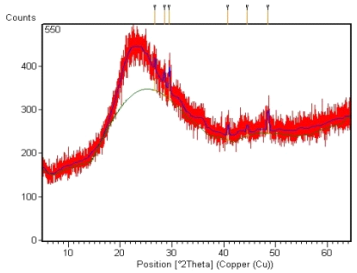	26.7033 28.5132 29.4682 40.7773 44.5403 48.5418	29.80 26.28 53.42 23.65 13.64 30.18	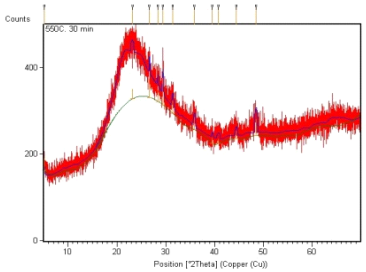	5.1229 23.1622 26.6918 28.3943 29.4252 31.4383 35.8605 39.5576 40.7945 44.4518 48.4916	28.56 23.55 43.33 26.25 63.43 29.86 29.70 13.23 10.81 18.98 39.03

Temp (°C)	Time (min)	Peaks		Time (min)	Peaks	
	15 (min)	Position [°2Th.]	Height [cts]	30 (min)	Position [°2Th.]	Height [cts]
575	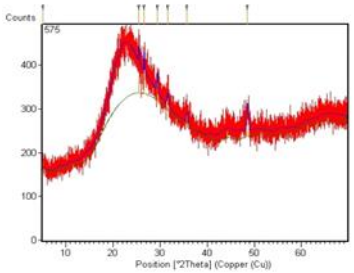	5.1192 25.5175 26.6660 29.4251 31.6240 35.7271 48.5768	23.13 35.75 46.55 41.90 25.94 21.33 40.19	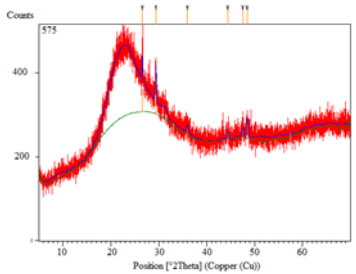	26.5832 29.3973 35.9812 44.4067 47.4841 48.4333	55.43 82.84 16.45 16.41 20.37 33.27
600	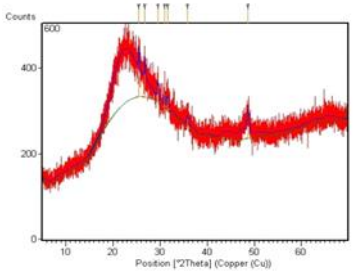	25.5595 26.7664 29.5219 30.9662 31.5942 35.8652 48.6391	46.59 55.32 40.11 31.72 25.44 20.20 31.28	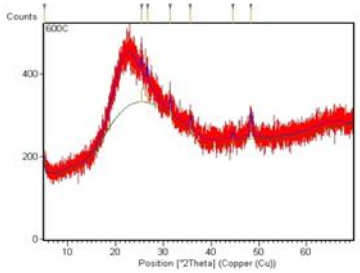	5.1806 25.4528 26.6779 31.4930 35.7254 44.5341 48.3341	33.43 29.69 35.07 30.16 28.75 13.24 40.12

8.5.4 RHA group F

8.5.4.1 Sample preparation

The color change according to temperature/time relationship during the combustion of rice husk was shown in Table 8.10. A wide range of high incineration temperature ranged in between 625°C to 850°C (whereby crystallization of the siliceous ash occurs according to the literature) was used at two different periods (5 and 10 minutes). In fact, color changes are associated with the completeness of the combustion process as well as the structural transformation of silica in the ash. In general, ash produced for 5 minutes' combustion degree is in white with the amount of black char indication of un-complete oxidation of the carbon. While, with the increase, the period to 10 minutes, intense interaction between potassium and silica ions causes the formation of potassium polysilicate combined with carbon resulting in white color ash. The husk samples immediately flashed or devolatilized, accompanied by sudden exposure of the raw rice husk resulting in flaming combustion for 2-3 seconds. The resulting char particles took another 11-16 seconds to burn out entirely into ash in the form of glowing combustion with short, slight bluish flame surrounding the char particles.

8.5.4.2 Silica structure

The XRD pattern results are shown in Table 8.11. Generally, ash samples prepared at 625-850°C retained their amorphous structure despite being exposed to high degree of temperature. This could be ascribed to the short exposure time (5 minutes), which did not allow for crystal formation (Gorthy and Pudukottah, 1999). However, XRD scan of sample burned at 650°C for 5 minutes exhibited a single peak confirming the presence of quartz at 26.68° accompanied with cristobalite at 31.47° (tertiary) and calcite at 29.46°. Moreover, at 10 minutes of combustion, the intensity of the quartz peak is slightly increased accompanied with a trace of quartz and cristobalite.

Likewise, XRD patterns representative of RHA burned at 675°C for 5 minutes, is showing the amorphous nature of silica. Where weak peaks of quartz and cristobalite were barely observed at 26.7° and 31.4° (tertiary) respectively. Meanwhile, with increasing time to 10 minutes, the crystalline quartz exhibited with sharp peaks at 26.68° indicating to improve the crystallinity of particles. The XRD patterns of ash obtained at 700°C for 5 and 10min shown a little variation of the broad peaks. As evidenced by a very low-intensity peak in the XRD pattern, where the broad peaks at a round of 26.71° (quartz), 31.51°, 35.69° (cristobalite), 44.45° (quartz) confirm of the amorphous silica of ash.

The Illustrated XRD patterns of the RHA sample incinerated at 725°C, for 5 and 10 minutes shown variable peaks with low intensity at 25.48°, 26.75°, 31.49° and 35.79°, were assigned as a trace of quartz and cristobalite. However, these phases disappeared utterly at a burned temperature at 750°C. The formation of cristobalite was detected as low-intensity signals at 31.44° and 35.67°, while no sign of quartz at both periods. Generally, this contradiction in the intensity of peaks can be attributed to the impurity of husk. As the degree of incineration was increased to 775°C, 800°C, 825°C and 850°C, almost same intensities of the diffraction peaks are exhibited.

Table 8.8: Effect of temperature to time on the formation of rice husk in the muffle furnace.

Time (min)	Temperature (°C)				
	625	650	675	700	725
5					
10					

Time (min)	Temperature (°C) 750	775	800	825	850
5					
10					

Table 8.9: X-ray diffraction of rice husk ash samples in a muffle furnace at different temperatures and residence times.

Temp. (°C)	Time (min)	Peaks		Time (min)	Peaks	
	5 (min)	Position [°2Th.]	Height [cts]	10 (min)	Position [°2Th.]	Height [cts]
625	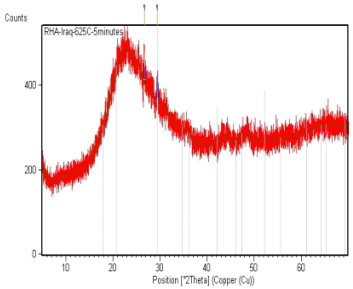	26.6755 29.4217	23.90 30.14	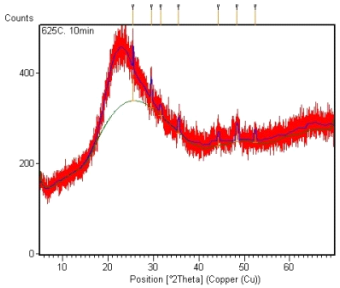	25.5606 29.5112 31.5648 35.5683 44.3123 48.4208 52.3637	58.12 52.79 18.14 29.59 19.65 35.75 18.53
650	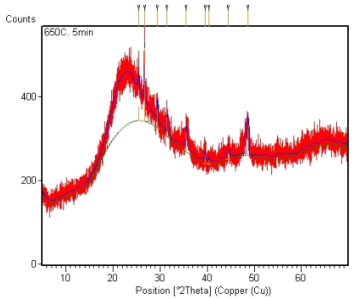	25.5108 26.6860 29.4619 31.4798 35.5938 39.5107 40.2989 44.4862 48.5924	35.72 46.14 48.26 48.31 50.26 22.86 10.90 16.67 62.29	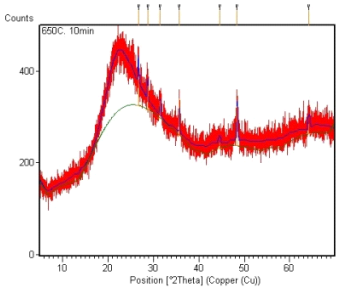	26.6959 28.7190 31.4554 35.7236 44.5158 48.3951 64.1762	58.02 51.82 38.17 81.55 13.17 87.06 21.07
675	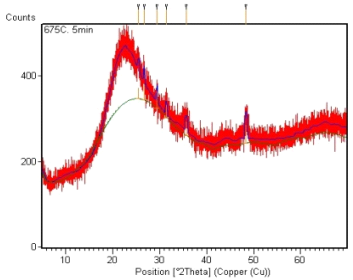	25.5177 26.7044 29.4303 31.4003 35.6593 48.3132	26.25 38.23 39.87 28.70 33.19 42.99	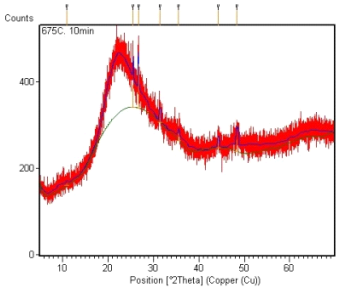	10.9982 25.5326 26.6897 31.4270 35.5870 44.2743 48.4186	4.28 51.63 102.91 30.18 16.89 25.36 28.75

Temp.(°C)	Time (min)	Peaks		Time (min)	Peaks	
	5 (min)	Position [°2Th.]	Height [cts]	10 (min)	Position [°2Th.]	Height [cts]
700	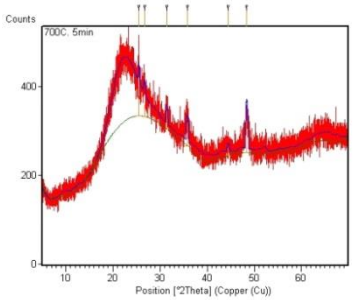	25.5113 26.6832 31.4260 35.7897 44.4637 48.3341	46.44 28.37 40.55 52.04 17.38 74.30	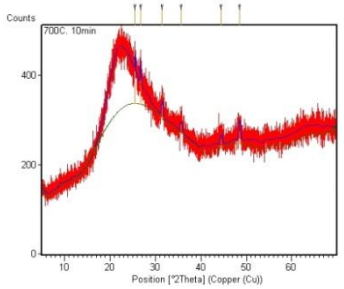	25.5312 26.7157 31.5128 35.6964 44.4597 48.5550	42.44 56.90 29.65 21.36 17.16 28.83
725	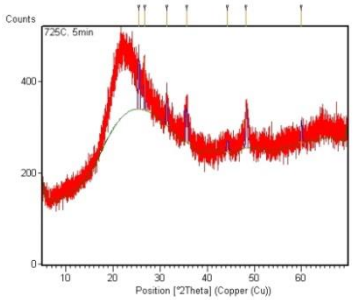	25.4758 26.7059 31.3968 35.6172 44.3176 48.2715 59.9801	31.18 66.67 40.06 56.95 11.91 80.71 27.03	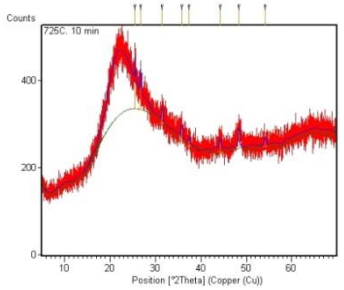	25.4874 26.7537 31.4924 35.7944 37.4305 44.2274 48.3770 54.0771	57.90 52.12 28.71 26.52 13.71 21.53 41.37 11.70
750	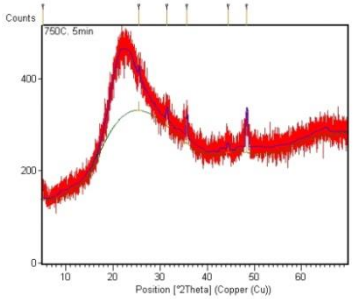	5.0950 25.5607 31.4489 35.6789 44.3853 48.3579	19.56 20.65 25.79 53.81 12.16 57.05	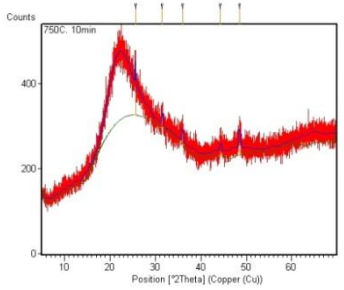	25.5826 31.5169 35.9380 44.3471 48.4510	54.24 26.21 28.43 14.10 28.95

Temp. (°C)	Time (min)	Peaks		Time (min)	Peaks	
	5 (min)	Position [°2Th.]	Height [cts]	10 (min)	Position [°2Th.]	Height [cts]
775	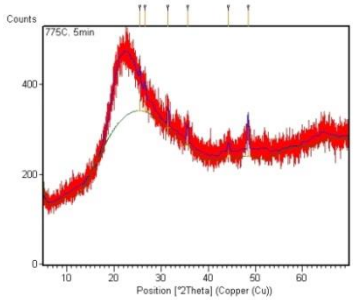	25.4849 26.6146 31.4512 35.6114 44.2813 48.4472	26.59 25.45 37.88 36.89 18.00 65.32	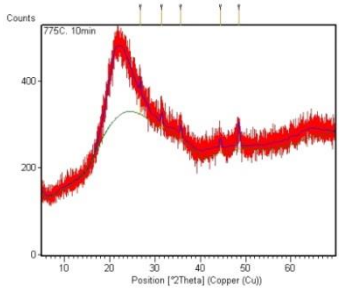	26.7447 31.5080 35.7401 44.3963 48.5219	39.02 21.47 21.25 17.73 35.96
800	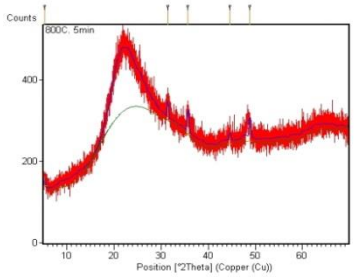	5.3271 31.3919 35.7021 44.5432 48.8057	22.86 34.95 45.39 16.15 32.49	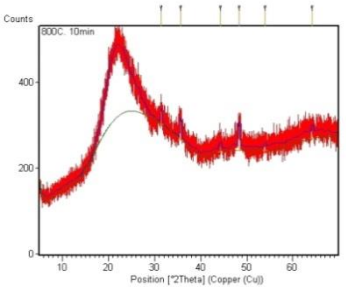	31.5142 35.7131 44.2046 48.2743 53.9314 64.1663	31.44 41.57 13.71 54.51 7.75 10.65

Temp.(°C)	Time (min)	Peaks		Time (min)	Peaks	
	5 (min)	Position [°2Th.]	Height [cts]	10 (min)	Position [°2Th.]	Height [cts]
825	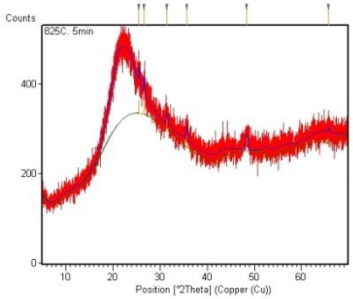	25.5595 26.6646 31.4641 35.6133 48.4253 65.7914	30.79 35.15 22.67 25.12 30.33 12.30	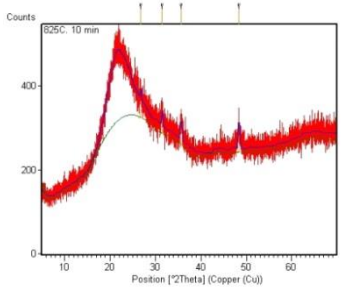	26.7677 31.4944 35.6513 48.3668	21.88 29.70 38.77 41.62
850	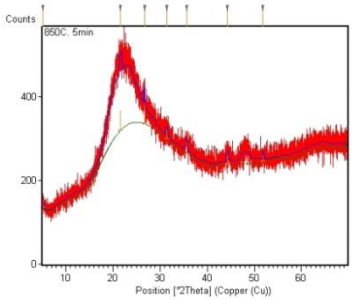	5.2194 21.6563 26.6939 31.3927 35.6310 44.3437 51.8342	16.72 47.40 46.81 22.36 26.50 23.09 15.97	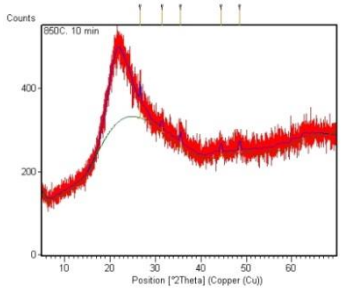	26.6600 31.4092 35.5692 44.4162 48.5506	36.37 14.75 23.16 16.61 14.23

8.6 Comparison the results to the literature

In this study, a set of 20 experimental sequences of combustion temperature, each consisting of two different times was conducted to investigate the effect of set time set to incineration degree on the silica structure of RHA. Many similar studies carried out as shown in Table 8.12. Therefore, temperature and time must be carefully selected in the pyro-processing of rice husks to ensure time-temperature relationship with the onset of silica crystallization in rice husk ash. As can be seen, all the ash samples retained their amorphous structures despite being exposed to combustion temperatures more than 350°C to 500°C for 60 and 90 minutes. However, some crystal peaks of the diffractograms at 2θ presented at 26.67°, 29.47°, 31.23°, 36.07°, 44.68° and 48.43° in the form of quartz and cristobalite due, to slight contamination of the husk sample as it was not washed or retreatment to remove the impurities. In comparing the obtained results to the literature, they are aligned with Mehta (1979), Zain et al. (2012) and Onojah et al. (2013) conclusion.

The relationship between time to burning temperature on the formation of crystallization is more explicit with samples was subjected to a temperature of 525-600°C for 15 and 30 minutes (Group B). Results from the XRD analysis showed that the residence time of up to 30 minutes was still insufficient for the crystallization of silica to take place, where all the samples yet retained their amorphous form. However, traces of quartz and cristobalite are present in some samples due to impurities of husk. These results are aligned with results obtained by Hamad and Khattab (1981), Sugita (1993), Salas et al. (2011), Ramezanianpour et al. (2009) and Bui et al. (2012). Exposure of the rice husk to the temperatures in the range of 600°C-850°C (which were the reported temperatures for crystallization of silica in rice husk ash). For a brief period (5 to 10 minutes) were found to be insufficient for the formation of high intensity of background hump at peaks position of crystalline. However, enough to present trace of quartz, cristobalite and tridymite to take place. In general, all these ash samples were still in their amorphous form, as indicated by a background hump peak.

Table 8.10: Silica structure of RHA in related to the degree and period of combustion by various researches.

Authors	Findings		Remarks
	Temperature	Duration	
Mehta (1979)	≤500°C	Per- longed period	Amorphous silica is produced.
	680°C	Less than one minute	
Yoeh et al. (1979)	900°C	60 minutes	Amorphous form of silica is produced.
	1000°C	5 minutes	Crystalline silica is formed.
Chopra et al. (1981)	Up to 700C	Not discussed	Predominantly in amorphous form and particle size is increased with increase in time of burn.
Hamad & Khattab (1981)	At 500°C & 600°C		Amorphous silica is formed.
	800°C	Not discussed	Cristobalite silica is formed.
	1150°C		Formation of cristobalite and tridymite.
Yamamoto (1982)	400°C	4 hours	Formed amorphous silica
	600°C	2-3 hours	
Khalaf & Yousif (1984)	500°C	2 hours	High reactivity RHA is produced.
Smith & Kamwanja (1986)	800°C	12 hours	Resulted in small proportions of crystalline silica.
James & Rao (1986)	400°C - 900°C	1-30 hours	Reactivity of ash is dependent mainly on temperature and duration has small effect. High reactivity of ash around 500°C.
Boating and Skeet (1990)	550-700°C	Not discussed	Amorphous, while silica transformed to crystalline at 900°C and over.
Sugita (1993)	<600°C	Not discussed	Ash with higher pozzolanic activity is achieved.
Isamil and Waliuddin (1996)	400-700°C	24 hours	Amorphous silica is formed.

Authors	Findings		Remarks
	Temperature	Duration	
Nehdi et al. (2003)	Up to 900°C	< one hour	Silica in RHA can remain in amorphous form.
	450°C	6 hours	Trace of quartz
		22 hours	Trace of quartz
	700°C		Trace of quartz plus cristobalite less than 5%
	800°C		10% Tridmite plus 53% Cristobalte
Shinohara and Kohyama (2004)	900°C		12% Tridmite plus 53% Cristobalte
	1000°C		34% Tridmite plus 38% Cristobalte
	1100°C	6 hours	58% Tridmite plus 29% Cristobalte
	1200°C		46% Tridmite plus 3% Cristobalte
	1350°C		66% Tridmite plus 16% Cristobalte
Bui (2005)	350°C	15 hours	Crystalline ash is formed.
Asavapisit & Ruengrit (2005)	400-800°C	60 minutes	650°C as optimum temperature for producing reactive RHA based on strength activity index.
Reddy (2006)	550°C– 800°C	Not discussed	Amorphous silica is formed.
Nair et al. (2008)	500°C-700°C	12 hours	Highest amount of amorphous silica is formed.
Salas et al. (2009)	600°C	3hour	RHA amorphous silica is formed.
Ramezanianpour et al. (2009)	550, 600, 650, 700 and 750°C	30 minutes 60 minutes	They suggested that RHA Produced at 650°C for 60 min can be considered to be non-crystalline RHA and also save the RHA production time.
		90 minutes	
Abu Bakar et al. (2010)	6 hours	≤700°C	Reactive RHA is produced.
Zain et al. (2011)	500°C- 700°C	2hour	The furnace is able to produce amorphous silica with the constant furnace combustion temperature at 500–700°C for 2 h.

Authors	Findings		Remarks
	Temperature	Duration	
Bui et al. (2012)	300°C,400°C,500°C,600°C and 700°C		Amorphous silica (no sharp peaks) indicating the absence of crystalline
Onojah et al. (2013)	<500	Not discussed	Below this temperature rice husk ash is purely amorphous.
	>500°C		Crystallization in rice husk ash begins at temperature above 500°C; The phase transformation in rice husk ash is shown below. Amorphous Silica 600°C→ Quartz 800°C→ Tridymite→ 1470°C →Cristobalite.
Kannan and Ganesan (2014)	650°C	60 minutes	Crystalline silica
Khassaf et al. (2014)	550°C	2 hours	RHA produced with optimum properties.
Zahedi et al. (2015)	650°C	60 minutes	Amorphous silica.
Abu Bakar et al. (2016)	500, 600, 700 and 800°C		Amorphous silica.
	900°C	2 hours	Crystallization transformation of silica starts to occur.
Zareei et al. (2017)	550-700°C	60 minutes	Amorphous silica.

8.7 Conclusions and recommendations

Incinerating temperature degree of burning rice husk essentially control the quality of ash, which may result either in entirely amorphous form or partially crystalline. Based on this relationship according to the experimental results presented in this chapter, the following concluding remarks could be drawn:

i. The reasonably good correlation between the set of time to the burning temperature and the detected reference peaks from the XRD analysis might indicate that the degree of the ash can be transformed to crystalline silica form.
ii. In general, compared to the results of the RHA ashes, an increase of burning time for each sample was not able to exhibit a noticeable increment in the intensity of the peaks of XRD. Therefore, it is believed that effect of incineration degree might be responsible for producing less crystallization silica rather than the time.
iii. The appearance of crystallization traces peaks was highly dependent on impurity content of the rice husk. In order word, the higher the impurities, the higher the intensity of peaks.
iv. Rice husk ash is produced at 350°C, for 90 minutes altogether black color, indicating of none-completion of husk combustion resulting in high amount of residual carbon content.
v. Exposure of rice husk to temperature up to 850°C for 10 minutes was insufficient to cause crystallization of silica.
vi. The results confirmed the point view of some researchers that RHA can be produced at high temperature (850°C) with entirely amorphous form.
vii. The theoretical recommended minimum required the temperature to deliver ash from an economic point of view in the way of saving energy and time, RHA produced at 625°C for 5 minutes, considers being the ideal one.
viii. In spite of low combustion degree (350°C), a trace of quartz and cristobalite can be an exhibit.
ix. The time of starting husk flaming it depends on the degree of combustion, were decreased with increased temperature.
x. As a result of relatively high amount of potassium (3.23%) consists, some char skeletons resulted in the ash samples incinerated at 625°C to 850°C. The presence of potassium (low melting degree) surface melts on these particles, which form a ‘barrier’ to prevent direct contact between the carbon molecules and oxygen.

CHAPTER 9: SUMMARY, CONTRIBUTIONS AND RECOMMENDATIONS

9.1 General

In this Chapter, the general conclusion, findings and list of the contributions from the results of the tests are presented in response to the aims and objectives set out in the first chapter of the thesis with several recommendations for future research.

9.2 Summary

Recently RHA has become one of the promising supplementary cementations materials in concrete because of availability and low cost as byproduct materials. However, regarding the material properties, the use of RHA in mortar and concrete presented a contradiction in strength, drying shrinkage, durability characteristics, and even fluidity. According to the literature, many researchers stated that use of RHA will cause some apparent disadvantages in terms of the reduction compressive and tensile strength even at very low replacement ratio (5-10%). However, some others of researchers found that RHA strongly influences the strength and durability development of mortar and concrete up to 30% replacement ratio. Most of the RHAs used by authors have a similar chemical composition where $SiO_2 \geq 85\%$ and LOI <12 (Table 2.2).

However, with variation the reactivity and fineness of ash (high specific surface and particle size, Table 2.4). This contradiction in the applications of RHA in mortar and concrete gives a motivation to investigate the reason of discrepancy on effect of RHA on the mortar and concrete performance. Therefore, the overall objective of the research, i.e. the possibility of RHA characteristics as a mineral admixture at high replacement ratio (over 30%) without effect negatively to the strength of concrete, was proposed. In addition, a review of the properties of RHA and it is effects on the hydration process and microstructure development as well as the drying shrinkage and durability were also dealt with. For this, the constituent materials, mortar and concrete were primarily investigated for fundamental properties. Later, critical fresh features and the hardened properties of the concrete were determined. The results of the research indicated that neither crystalline silica, nor a higher amount of carbon content are detrimental the pozzolanic reactivity of the ash, if the crystalline silica and carbon content both provided finely ground.

The experimental studies in Chapters 5, 6 and 7 demonstrated these differences. One of the very important results observed in Chapter 5 was that mortar blended RHA increases the degree of cement hydration at later stages. This may be attributed to the absorbed water from the porous RHA particles. These water-saturated RHA particles will act as water reservoirs distributed throughout the system. With progress of the hydration process, the water from these pores will be released and will promote the hydration of the cement.

Additionally, it was also found that the fineness of RHA strongly influences the hydration and microstructure development of cement paste. In fact, the fineness of RHA is depended on the grinding process. Intensive grinding will cause the collapse of the RHA particles and their porous structure. This collapse causes a reduction of water absorption by RHA, and thus the positive effect of RHA on both the hydration and the microstructure of cement paste are decreased. The experimental results also revealed that there is an appropriate fineness of RHA, i.e. 4μm, with regard to the grinding time and the silica structure of RHA. Where, the finer RHA particles improve the workability of mortar and concrete mixtures. This may be caused by the partial collapse of the porous structure of RHA particles at a certain degree of grinding. This leads to a reduction of the amount of absorbed water in the RHA particles. Therefore, more free water available in the system can make the mixture more workable. In addition to that, the experimental results demonstrated that the addition of RHA increases the compressive strength of mortar and concrete up to 70% replacement ratio (RHA-C), compared to that of the control sample. Besides, the compressive strength, tensile strength higher than that of the control samples, especially at later ages. This confirms that RHA can be used as a mineral admixture to produce concrete at high replacement ratio.

Incorporation of RHA in such high replacement ratio accompanied by an increase of water demand. To avoid that, superplasticizer (SP), was used to produce RHA mortars mixtures with high workability. To understand the effect of SP on the strength development, a comparative study was made between two different dosages of SP at the same replacement ratio. Where the results pronounced tendency of increase strength at same replacement ratio with increase SP dosage, as an example the compressive strength of RHA-C at 15% replacement ratio at 91 days was increased from 59.72MPa at 0.25%SP to 68.04MPa with 0.50% SP, respectively. A synergic effect between RHA and SP was also found to improve the flowability. This leads to an increase of the total cement replacement percentage, which is very important for the sustainable development of the construction industry.

Drying shrinkage is one of most disadvantages of mortar and concrete, because of self-desiccation caused by the loss of water. In the experimental studies, it was observed that the addition of RHA reduced the drying shrinkage of OPC mixtures. This positive effect is possibly attributed to the absorbed water in the porous structure of RHA, which influences the distribution of water and compensates for the drop of relative humidity in mortar during the hydration process (An Van, 2013). Data obtained show that RHA with coarse grain and partially crystalline silica content is preferable to reduce drying shrinkage of mortar. Additionally, it was also found that the silica structure and fineness of RHA strongly influences the chloride diffusion coefficient of concrete blended RHA. Where, experimental results revealed that concrete blended RHA reached the maximum resistance to chloride diffusion at 50% RHA-C (0.61×10^{-12} $m^{2/}s$ compare to 1.62 and 1.83×10^{-12} $m^{2/}s$ of RHA-A and B, respectively).

Silica in the RHA initially exists in amorphous form, however may become crystalline when rice husk burnt at high temperature (Ramezanianpour et al., 2013). Therefore, the duration and temperature of furnace are important parameters, influencing the reactivity of RHA pozzolans. By incineration rice husk under controlled process condition, ash with high amorphous silica content can be produced. The literature reveled an argument between the researchers on the exact temperature to time, where amorphous silica transformed to crystalline. According to Mehta (1978), silica remains in amorphous form under oxidizing condition with prolonged time at temperature below 500°C.

Contrary to that other researcher such as James and Rao (1986), Al Khalaf and Yuosif (1984) reveled that even at 700-800°C; silica mainly remained in amorphous form. On the other side, some other studies like Bui (2005) stated that even at low temperature (350°C) for prolonged time (15 hours) crystalline ash is formed. Most of these studies concern ashes produced by controlled burning conditions, at specified temperature, time of burning, heating rate, type of furnace, and oxidizing conditions. In such conditions, highly reactive pozzolan with non-crystalline silica, small carbon content, and high specific surface area is produced. Electrical laboratory furnace was used for such investigation with small sample (usually not more than 5g for one run). Different temperature degree to time was investigated. The XRD analysis test present very small trace of crystalline can be neglected even at high degree of temperature (850°C) for 5minutes.

9.3 Overall Conclusions

The conclusions drawn from this investigation are summarized at the end of each Chapter; however, the overall major conclusions derived from this study are given in below.

1. The rice husk ashes in this study are a macro-mesoporous amorphous siliceous material which possesses variable amorphous silica content, and porous structure with macro and mesoporous inside it is particles. The pore size distribution is the key physical property of RHA influencing specific surface area (SSA), the water demand and the pozzolanic reactivity of RHA. The SSA of RHA derives from the internal surface area in pores and the external surface area on the surface of particles. During grinding, most macro-pores collapse and hence the internal SSA of RHA decreases, whereas the external SSA of RHA increases.
2. Some researchers in the literature review with the opinion that the performance of RHA with amorphous silica structure content is the decisive factor. According to the results of the experiment of this research, it is possible to improve the performance of RHA even with high crystalline silica content (RHA-A) with increase fineness particle size.
3. The particle size distribution and specific surface area of RHA influences on the workability and strength of the mortar and concrete. In other words, increase fineness of the RHA effect on the increase of pozzolanic activity which in term effect on the strength of mortar and concrete performance positively.
4. The strength of the mortar and concrete increased by the addition of RHA compared to conventional samples up to 70% replacement percentage (RHA-C). In particular, the increment of RHAs samples strength (compressive, splitting tensile) improvement is higher at a later age than that of the conventional samples, as a result of water reservoirs act of RHA porous particles. This water promotes the mixture strength at a later age when released during the hydration progress.
5. Optimum compressive strength of RHA mortar is variable, and it depends on the RHA properties. Where at the age of 91 days, RHA-A reached maximum compressive strength at 30% (54.7MPa), RHA-B at 20% (55.00MPa), RHA-C at 20% (60.21MPa) and RHA-C5 at 30% (64.25MPa), compared to OPC mortar (48.81MPa), respectively.
6. The maximum replacement ratio of cement by RHA without decreasing the strength lowers than OPC mortar is variable. Where, it was 40% of RHA-B (51.86MPa) and

50% of RHA-A (50.38MPa); however, reached 60% of RHA-C5 (54.16 MPa) and 70% of RHA-C (51.76MPa) compare to OPC mortar (48.81MPa).

7. The incorporation of RHA increases the degree of cement hydration in mortar. RHA-C and C5 are more effective at early ages (7 days), possibly due to the better nucleation site effect, whereas RHA, particularly the coarse RHA-A, dominates at the later ages (28, 91 days) possibly due to the higher internal water curing effect.
8. The graphical plot has interpreted the synergic effects of RHA and SP dosage on flowability and strength (compressive, tensile). Where, 15%RHA-C flowability was 226 mm at 0.50% SP compare to 155mm and 196mm at 0% SP and 0.25% SP, respectively. Furthermore, compressive strength at 0.50% SP increase about 12.23% and 18.15% compare to 0.25%SP and 0%SP, while tensile strength increased about 11.82% and 22.51%, respectively.
9. The high content of residual carbon content (RHA-C, 11.35% of total weight) relatively effected on the reactivity of ash. With decreasing loss on ignition proportion gradually to 7.57% (RHA-C1) and 5.08 (RHA-C2), the compressive strength of 5%RHA-C2 mortar increased about 18.57% and 20.26% compared to RHA-C.
10. The incorporation of RHA increases the compressive strength of mortar especially at the ages of 28, 91 days. At w/b of 0.50, compressive strength of mortar reaches the highest value with 20%RHA-C2. The increase in RHA-C2 content over 20% replacement ratio companied with decreases in the compressive strength. However, the compressive strength of the sample at 60%RHA-C2 was higher than that of the OPC mortar about 6.11%.
11. With the same amorphous silica content, increase fineness of RHA-A, B and C particles (the difference in MPS of RHA) results in an increase of pozzolanic reactivity of RHA and as a result increase in strength (compressive, tensile) of RHA mortar in compression with the same samples of ashes before re-grinded.
12. The calcium hydroxide phase of cement hydration is completely consumed in RHA-A, B, C and C5 mortar at 17.1%, 15.5%, 14.66% and 13.43% replacement ratio, at age of 12 months.
13. The study shown that the drying shrinkage deformation of RHA mortar was significantly affected by RHA properties. Mortar blended with RHA consists of coarse particles (RHA-A and B) showed lower drying shrinkage than those have fine particles (RHA-C, and C5). Where, the drying shrinkage of RHA at 60%

replacement ratio are ranged from 1016 (RHA-A) to 1391(RHA-C5) $*10^{-4}$ mm/mm compare to 1143 * 10^{-4} mm/mm of OPC mortar at 180 days.

14. It has been found that, chloride diffusion resistance of RHA-C concrete is much better than other RHA (A and B) and ordinary Portland cement concrete. The rich amorphous content of silica reduces free calcium hydroxide during hydration of concrete which ultimately improves the chloride ion diffusion resistance of RHA concrete.
15. According to the chloride migration test, the coefficient of permeability of concrete incorporating high volume RHA (60%) is very low resulted in highest resistance to chloride diffusion. Concrete reached the maximum chloride diffusion resistance at 60% RHA-A (1.09×10^{-12} m^2/s), 50% RHA-B (1.83×10^{-12} m^2/s) and 50% RHA-C (0.61×10^{-12} m^2/s) compared to OPC concrete (9.22×10^{-12} m^2/s) at 91 days.
16. X-ray diffraction studies made it possible to gain a better understanding of the structural changes of RHA with combustion temperature to time, producing ash with totally amorphous form and minimum residual carbon content.
17. Trace of crystalline (quartz phase) was found to transform into upon heat treatment at 350°C for 60 minutes of incineration. While, with increasing temperature in the range of 400 to 500°C, a trace of tridymite and cristobalite observed. The crystallization temperature was variable dependent on impurity content in the order higher than the impurities and lower than the transformation temperature.

9.4 Contributions

The present study has contributed to the current state of knowledge on RHA mortar and concrete. The main contributions are:

i. The discrepancy in the literature results of RHA characteristics effect on the mechanical properties and durability of mortar and concrete, are mainly related to the inconsistency in characteristics of ash namely physical properties (specific surface area, mean particles size), chemical (mineralogical) content and reactivity of ash. However, cement type and properties, aggregate size and type, and admixture specification (superplasticizers), were other factors led to this contradiction. The strength results are clarifying these factors influence and presented clear figuration of effectiveness of RHA on development of mortar and concrete properties.

ii. In this research, it was found that the maximum cement replacement level by RHA in producing OPC was variable and depends on the properties of ash. Where,

50%RHA-A and B, considered as a maximum replacement of cement for RHA consist of crystalline silica. However, strength at 70% RHA-C and C5 mortars, considered as an acceptable value compare to control mortar.

iii. At 60% replacement ratio, RHA-C2 mortar exhibited 14.08% increase in compressive strength compared to 9.06% of RHA-C5, and 8.49% of RHA-C at the same age (91day). This is an essential contribution to sustainable development of OPC.

iv. RHA-C content high amount of residual carbon (loss on ignition) has proven successful in the overall response improvement of OPC properties.

v. The fineness of RHA grain affect positively on increasing the strength of mortar up to 4.0μm, beyond that strength (compressive, tensile) decreased.

vi. There is a considerable advantage of re-burning RHA on the strength of mortar. This indicates that with reduction of RHA residual carbon content the strength development is improved.

vii. Effect of RHA characteristics (crystalline silica, mean particle size) has a direct effect on the drying shrinkage of mortar. Where with RHA consist of relatively crystalline silica and coarse particle size, RHA mortar exhibited a significant reduction in drying shrinkage.

viii. Effect of RHA with entirely amorphous silica (RHA-C) on the durability of OPC was significantly higher than the resistance to chloride diffusion than a similar mixture of OPC. Moreover, RHA even with partially crystalline silica content (RHA-A and B) dramatically improves the durability characteristics compare to OPC concrete.

ix. The significant performance of RHA-C concrete up to 60% replacement ratio to resist chloride diffusion give an idea that the total cement replacement level can be expected to increase further by using RHA.

x. Concerning the test method, the non-steady state tests, NT Build 492 has excellent compatibility with the ageing factor.

xi. Re-burned RHA at suitable temperature leads to increasing specific surface area and reduce mean particle size, and results an increase in the reactivity of ash.

xii. Increase of fineness particles can improve the performance of RHA relatively consist of crystalline silica (RHA-A and B). Where the RHA particle size influence on the pore structure by refinement and chain the development of unfavorable crystals produced in hydration process.

xiii. Even at very low combustion temperature (350°C), a trace of crystalline silica appears. However, cannot be taken in account as it is very small and does not effect on the reactivity of ash.

xiv. There is an inverse relationship between the combustion degrees to the amorphous silica structure of ash. However, the period of incineration is balancing this relationship.

xv. Freeboard temperatures of 350 – 500°C for 60 minutes gave the lowest XRD patterns, indicating to preserve the amorphous structure of silica.

xvi. The optimum burning temperature to obtain the desired properties was set at 500°C (60 minute of burning). The comparative XRD plot of the RHA obtained by burning rice husk at various temperatures showed the difference between the amorphous and crystalline silica. However, the theoretical recommended minimum required the temperature to deliver ash from an economic point of view in the way of saving energy and time, RHA produced at 625°C for 5 minutes, considers to be the ideal one.

9.5 Further research

The findings of this thesis suggest a number of potential topics for future studies. Some open questions are pointed out as follows:

i. The effects of various curing conditions on the hardened properties of OPC mortar and concrete, including the drying shrinkage, should be examined.

ii. The impact of RHA properties on the fresh and hardened properties of OPC concrete should be investigated for different types and sizes of coarse aggregate.

iii. The effects of unburnt carbon content and the internal water curing of RHA on the hydration and microstructure development of cement paste should be evaluated.

iv. Chloride diffusion resistance of RHA concrete may be studied for a different type of cement rather than one type of cement (high strength cement).

v. The effect of RHA on the durability of OPC concrete at low water to binder ratio (w/b), should be investigated.

vi. The effect of mineral admixtures may also have a positive impact on the durability of concrete should be evaluated.

vii. Effect of combustion temperature on the time of the silica structure transformation needs more investigation to produce ash with ultimate reactivity.

REFERENCES

Abalaka, A., 2013. Strength and Some Durability Properties of Concrete Containing Rice Husk Ash Produced in a Charcoal Incinerator at Low Specific Surface. International Journal of Concrete Structures and Materials. 7(4), pp. 287-293.

Abalaka, E., 2013. Influence of water-binder ratio on normal strength concrete with rice husk ash. International Journal of Sciences 2(2), pp. 28-36.

ACI Committee 318. Building code requirements for structural concrete (ACI318-99) and commentary (318R-99). Farmington Hills, MI: American Concrete Institute; 1999.

Agrawal, Y.C., McCave, I.N. and Riley, J.B., 1991. Laser diffraction size analysis. Principles, methods, and application of particle size analysis, pp.119-128.

Ahmad, S., Nawaz, M. and Elahi, A., 2005, August. Effect of superplasticizers on workability and strength of concrete. In Proceedings of 30th Conference on our World in Concrete & Structures, Singapore (pp. 23-24).

Aitcin, P.C., Jolicoeur, C. and Mac Gregor, J.G., 1994. Superplasticizers: how they work and why they occasionally don't. Concrete International, 16(5), pp.45-52.

Akasaki, J.L., Tashima, M.M., da Silva, C.A.R., da Silva, E.J., Barbosa, M.B. and Payá, J., 2005. Comparative studies between the rice husk ash (RHA) amorphous and crystalline, [in]. In Congreso Nacional de Materiales Compuestos-2005 (p. 1).

Al-Khalaf, M.N. and Yousif, H.A., 1984. Use of rice husk ash in concrete. International Journal of Cement Composites and Lightweight Concrete, 6(4), pp.241-248.

Alsadey, S., 2012. Influence of superplasticizer on strength of concrete. International Journal of Research in Engineering and Technology, 1(3), pp.164-166.

Al-Tayeb, M.M., Hamouda, H., 2015. Effect of Superplasticizer on Workability of Concrete Containing Crumb Rubber. Civil and Environmental Research, Vol.7 (2).

Alvarez, M. and Arboleda, D., 2009. Rice Husk Ash as a Sustainable Concrete Material for the Marine Environment. Sixth LACCEI International Latin American and Caribbean Conference for Engineering and Technology (LACCEI'2008). June 4 – June 6 2008, Tegucigalpa, Honduras.

Alvarez, M., 2006. Marine durability characteristics of rice husk ash-modified reinforced concrete. Proceedings of the 4th LACCEI International Latin American and Caribbean Conference for Engineering and Technology (LACCET'06), Breaking Frontiers and Barriers in Engineering: Education, Research and Practice.

American Society for Testing and Materials C1202–12. Committee C-9 on Concrete and Concrete Aggregates, 2012. Standard test method for electrical indication of concrete's ability to resist chloride ion penetration. ASTM International.

American Society for Testing and Materials. 2000. ASTM C204: Standard Test Method for Fineness of Hydraulic Cement by Air Permeability Apparatus.

Antiohos, S.K., Papadakis, V.G. and Tsimas, S., 2014. Rice husk ash (RHA) effectiveness in cement and concrete as a function of reactive silica and fineness. Cement and Concrete Research, 61, pp.20-27.

Antiohos, S.K., Tapali, J.G., Zervaki, M., Sousa-Coutinho, J., Tsimas, S. and Papadakis, V.G., 2013. Low embodied energy cement containing untreated RHA: A strength development and durability study. Construction and Building Materials, 49, pp.455-463.

Anwar, M., Miyagawa, T. and Gaweesh, M., 2000. Using rice husk ash as a cement replacement material in concrete. In Waste management series (Vol. 1, pp. 671-684). Elsevier.

Aprianti, E., Shafigh, P., Bahri, S. and Farahani, J.N., 2015. Supplementary cementitious materials origin from agricultural wastes–A review. Construction and Building Materials, 74, pp.176-187.

ASTM, C., 1984. Standard Test Method for Sieve Analysis of Fine and Coarse Aggregates.

Atiş, C.D., 2005. Strength properties of high-volume fly ash roller compacted and workable concrete, and influence of curing condition. Cement and Concrete Research, 35(6), pp.1112-1121.

Bamforth, P.B., Price, W.F. and Emerson, M., 1997. An international review of chloride ingress into structural concrete (Vol. 359). Thomas Telford.

Bapat, J.D., 2012. Mineral admixtures in cement and concrete. CRC Press.

Begum, R., Habib, A. and Mostafa, S., 2014. Effects of Rice Husk Ash on the Non-Autoclaved Aerated Concrete. IJEIR, 3(1), pp.116-121.

Bensted, J., 1983. Hydration of Portland cement. In Advances in cement technology (pp. 307-347).

Bhanumathidas, N. and Mehta, P.K., 2001. Concrete mixtures made with ternary blended cements containing fly ash and rice-husk ash. Special Publication, 199, pp.379-392.

Björnström, J. and Chandra, S., 2003. Effect of superplasticizers on the rheological properties of cements. Materials and Structures, 36(10), pp.685-692.

Boateng, A. and Skeete, D., 1990. Incineration of rice hull for use as a cementitious material: the Guyana experience. Cement and Concrete Research 20(5): 795-802.

Bouzoubaâ, N. and Fournier, B., 2003. Current situation of SCMs in Canada. Materials Technology Laboratory Report MTL, 4.

British Standards Institution, BS 1881-102: 1983. Testing concrete. Method for determination of slump.

British Standards Institution, BS EN 12390-1:2012. Testing hardened concrete. Shape, dimensions and other, requirements for specimens and molds.

British Standards Institution, BS EN 12390-2:2009. Testing hardened concrete. Making and curing specimens for strength tests.

British Standards Institution, BS EN 197-1:2000. Cement. Composition, specifications and conformity criteria for common cements.

Bui, D. D., 2001. Rice husk ash a mineral admixture for high performance concrete, TU Delft, Delft University of Technology.

Bui, D.D., Hu, J. and Stroeven, P., 2005. Particle size effect on the strength of rice husk ash blended gap-graded Portland cement concrete. Cement and concrete composites, 27(3), pp.357-366.

Burhan, S., 2011. Development of strength and Durability of Concrete incorporation Local Metakaolin, University of Engineering & Technology, Lahore.

Byfors, K., 1986. “Chloride Binding in Cement Paste”, Nordic Concrete Research, Vol. 5, pp. 27-38.

Calica Jr, M.G., 2008. Influence of rice husk ash as supplementary material in cement paste and concrete. Nat. Aero. Lab. J., 2, pp.81-92.

Cao, Y. and R. J. Detwiler., 1995. Backscattered electron imaging of cement pastes cured at elevated temperatures. Cement and Concrete Research 25(3): 627-638.

Celik, K., Jackson, M.D., Mancio, M., Meral, C., Emwas, A.H., Mehta, P.K. and Monteiro, P.J.M., 2014. High-volume natural volcanic pozzolan and limestone powder as partial replacements for Portland cement in self-compacting and sustainable concrete. Cement and concrete composites, 45, pp.136-147.

Chakraverty, A., Mishra, P. and Banerjee, H.D., 1988. Investigation of combustion of raw and acid-leached rice husk for production of pure amorphous white silica. Journal of Materials Science, 23(1), pp.21-24.

Chang, P.K, and Peng Y.N., 2001. Influence of mixing techniques on properties of high-performance concrete. Cement and Concrete Research 31(1): 87-95.

Chao-Lung, H., Le Anh-Tuan, B. and Chun-Tsun, C., 2011. Effect of rice husk ash on the strength and durability characteristics of concrete. Construction and building materials, 25(9), pp.3768-3772.

Chindaprasirt, P., Chotithanorm, C., Cao, H.T. and Sirivivatnanon, V., 2007. Influence of fly ash fineness on the chloride penetration of concrete. Construction and Building Materials, 21(2), pp.356-361.

Chindaprasirt, P., Rukzon, S. and Sirivivatnanon, V., 2008. Resistance to chloride penetration of blended Portland cement mortar containing palm oil fuel ash, rice husk ash and fly ash. Construction and Building Materials, 22(5), pp.932-938.

Chungsangunsit, T., Gheewala, S.H. and Patumsawad, S., 2009. Emission assessment of rice husk combustion for power production. World Academy of science, engineering and technology, 53, pp.1070-1075.

Cizer, Ö., Van Balen, K., Van Gemert, D. and Elsen, J., 2007, January. Carbonation and hydration of mortars with calcium hydroxide and calcium silicate binders. In Proc. International Conference on Sustainable Construction Materials and Technologies (pp. 611-621). Taylor&Francis Group.

Cook, D.J., 1984. Development of microstructure and other properties in rice husk ash-OPC systems. In Australasian Conference on the Mechanics of Structures and Materials, 9th, 1984, Sydney, Australia.

Cook, D.J., 1986. Cement replacement material-Rice husk ash. Concrete technology and design, 3, pp.171-195.

Cook, D.J., Pama, R.P. and Paul, B.K., 1977. Rice husk ash-lime-cement mixes for use in masonry units. Building and Environment, 12(4), pp.281-288.

Cook, J.D. and Swamy, R.N., 1986. Concrete technology and design: Cement replacement material, 3. Concrete technology and design: Cement replacement material, 3.

Cordeiro, G.C., Toledo Filho, R.D. and Fairbairn, E.D.M.R., 2009. Use of ultrafine rice husk ash with high-carbon content as pozzolan in high performance concrete. Materials and Structures, 42(7), pp.983-992.

Cordeiro, G.C., Toledo Filho, R.D., Tavares, L.M., Fairbairn, E.D.M.R. and Hempel, S., 2011. Influence of particle size and specific surface area on the pozzolanic activity of residual rice husk ash. Cement and Concrete Composites, 33(5), pp.529-534.

Cordeiro, G.C., Toledo Filho, R.D. and Fairbairn, E.D.M.R., 2009. Use of ultrafine rice husk ash with high-carbon content as pozzolan in high performance concrete. Materials and Structures, 42(7), pp.983-992.

Coutinho, J.S., 2003. The combined benefit is of CPF and RHA in improving the durability of concrete structures. Cement and Concrete Composites, 25(1), pp.51-59.

Dabai, M.U., Muhammad, C., Bagudo, B.U. and Musa, A., 2009. Studies on the effect of rice husk ash as cement admixture. Nigerian Journal of Basic and Applied Sciences, 17(2), pp.252-256.

Damodhara, B. R, Jyothy, S. A, Reddy, I. V. R., 2013. Effect of rice husk ash on the properties of ordinary Portland cement and Portland slag cement with and without superplasticizers. International Journal of Civil, Structural, Environmental and Infrastructure Engineering Research and Development (IJCSEIERD) Vol. 3, Issue 2.

Darweesh, H., 2013. Hydration, Strength Development and Sulphate Attack of Some Cement Composites. World Applied Sciences Journal 23(2): 137-144.

Da Silva, F.G., Liborio, J. and Helene, P., 2011. Improvement of physical and chemical properties of concrete with Brazilian silica rice husk (SRH). Revista Ingeniería de Construcción, 23(1), pp.18-25.

De Sensale, G. R., 2006. Strength development of concrete with rice-husk ash. Cement and Concrete Composites 28(2): 158-160.

De Sensale.G.R., 2010. Effect of rice-husk ash on durability of cementitious materials. Cement & Concrete Composites, 32, pp 718 – 725.

De Souza Rodrigues, C., Ghavami, K. and Stroeven, P., 2010. Rice husk ash as a supplementary raw material for the production of cellulose–cement composites with improved performance. Waste and Biomass Valorization, 1(2), pp.241-249.

Debasish, S. and Bandyopadhyay, A., 2010. Adsorptive mass transport of dye on rice husk ash. Journal of Water Resource and Protection, 2(05), p.424.

Della, V.P., Kühn, I. and Hotza, D., 2002. Rice husk ash as an alternate source for active silica production. Materials Letters, 57(4), pp.818-821.

Deshpande, S., Darwin, D. and Browning, J., 2007. Evaluating free shrinkage of concrete for control of cracking in bridge decks. University of Kansas Centre for Research, Inc.

Deshpande, V.S., Mrksich, M., McMeeking, R.M. and Evans, A.G., 2008. A bio-mechanical model for coupling cell contractility with focal adhesion formation. Journal of the Mechanics and Physics of Solids, 56(4), pp.1484-1510.

Detwiler, R.J., Kjellsen, K.O. and Gjorv, O.E., 1991. Resistance to chloride intrusion of concrete cured at different temperatures. Materials Journal, 88(1), pp.19-24.

Devi, R.B., Chanu, Y.J. and Singh, K.M., 2016. A Survey on Different Background Subtraction Method for Moving Object Detection. International Journal for Research in Emerging Science and Technology, 3(10).

Dhir, R.K., El-Mohr, M.A.K. and Dyer, T.D., 1996. Chloride binding in GGBS concrete. Cement and Concrete Research, 26(12), pp.1767-1773.

Dhir, R.K., El-Mohr, M.A.K. and Dyer, T.D., 1997. Developing chloride resisting concrete using PFA. Cement and Concrete Research, 27(11), pp.1633-1639.

Efficiency, E., 2007. Tracking Industrial Energy Efficiency and CO2 Emissions. International Energy Agency 34(2): 1-12.

El-Dakroury, A. and M. Gasser., 2008. Rice husk ash (RHA) as cement admixture for immobilization of liquid radioactive waste at different temperatures. Journal of Nuclear Materials 381(3): 271-277.

El-Gamal, S.M., Al-Nowaiser, F.M. and Al-Baity, A.O., 2012. Effect of superplasticizers on the hydration kinetic and mechanical properties of Portland cement pastes. Journal of Advanced Research, 3(2), pp.119-124.

Englehardt, J. D. and C. Peng., 1995. Pozzolanic filtration/solidification of radionuclides in nuclear reactor cooling water. Waste Management 15(8): 585-592.

Ettu, L.O., Ajoku, C.A., Nwachukwu, K.C., Awodiji, C.T.G. and Eziefula, U.G., 2013. Strength variation of OPC-rice husk ash composites with percentage rice husk ash. Int J Appl Sci Eng Res, 2(3), pp.420-4.

Fairbairn, E.M., Americano, B.B., Cordeiro, G.C., Paula, T.P., Toledo Filho, R.D. and Silvoso, M.M., 2010. Cement replacement by sugar cane bagasse ash: CO2 emissions reduction and potential for carbon credits. Journal of environmental management, 91(9), pp.1864-1871.

Farny, J.A. and Kosmatka, S.H., 1997. Diagnosis and control of alkali-aggregate reactions in concrete. Portland cement Association.

Farooque, K.N., Zaman, M., Halim, E., Islam, S., Hossain, M., Mollah, Y.A. and Mahmood, A.J., 2009. Characterization and utilization of rice husk ash (RHA) from rice mill of Bangladesh. Bangladesh Journal of Scientific and Industrial Research, 44(2), pp.157-162.

Feng, Q., Yamamichi, H., Shoya, M. and Sugita, S., 2004. Study on the pozzolanic properties of rice husk ash by hydrochloric acid pretreatment. Cement and concrete research, 34(3), pp.521-526.

Feng, Q., Lin, Q., Gong, F., Sugita, S. and Shoya, M., 2004. Adsorption of lead and mercury by rice husk ash. Journal of Colloid and Interface Science, 278(1), pp.1-8.

Ferraris, C. and Garboczi, E., 2013. Identifying improved standardized tests for measuring cement particle size and surface area. Transportation Research Record: Journal of the Transportation Research Board, (2342), pp.10-16.

Food and Agriculture Organization of the United Nations (FAO)., 2013. Rice market monitor journal, 16 (1).

Gajendran, K.A., Anuradha, R., Venkatasubramani, G.S., 2015. Studies on relationship between compressive and splitting tensile strength of high-performance concrete. QJournal of Engineering and Applied Science, 10 (14), pp: 6151–6156

Gambhir, M.L., 2006. Fundamentals of reinforced concrete design. PHI Learning Pvt. Ltd.

Ganesan, K., et al., 2007. Chloride resisting concrete containing rice husk ash and bagasse ash. Indian journal of engineering & materials sciences 14: 257-265.

Ganesan, K., Rajagopal, K. and Thangavel, K., 2008. Rice husk ash blended cement: assessment of optimal level of replacement for strength and permeability properties of concrete. Construction and building materials, 22(8), pp.1675-1683.

Gastaldini, A.L.G., Da Silva, M.P., Zamberlan, F.B. and Neto, C.M., 2014. Total shrinkage, chloride penetration, and compressive strength of concretes that contain clear-colored rice husk ash. Construction and Building Materials, 54, pp.369-377.

Gastaldini, A.L.G., Isaia, G.C., Gomes, N.S. and Sperb, J.E.K., 2007. Chloride penetration and carbonation in concrete with rice husk ash and chemical activators. Cement and concrete composites, 29(3), pp.176-180.

Gastaldini, A.L.G., Isaia, G.C., Saciloto, A.P., Missau, F. and Hoppe, T.F., 2010. Influence of curing time on the chloride penetration resistance of concrete containing rice husk ash: A technical and economic feasibility study. Cement and Concrete Composites, 32(10), pp.783-793.

Gaynor, R., 1987. Understanding Chloride Percentages. Steel Corrosion in Concrete: Causes and Restraints, ACI, SP-102, pp. 161-165, 1987.

Geiker, M.R., Ekstrand, J.P. and Hansen, R., 2007. Effect of mixing on properties of SCC. In 5th International Symposium on Self-Compacting Concrete (pp. 231-238). RILEM Publishing SARL.

Gelb, L.D. and Gubbins, K.E., 1998. Characterization of porous glasses: Simulation models, adsorption isotherms, and the Brunauer− Emmett− Teller analysis method. Langmuir, 14(8), pp.2097-2111.

Giaccio, G., de Sensale, G.R. and Zerbino, R., 2007. Failure mechanism of normal and high-strength concrete with rice-husk ash. Cement and concrete composites, 29(7), pp.566-574.

Givi, A.N., Rashid, S.A., Aziz, F.N.A. and Salleh, M.A.M., 2010. Assessment of the effects of rice husk ash particle size on strength, water permeability and workability of binary blended concrete. Construction and Building Materials, 24(11), pp.2145-2150.

Givi, A.N., Rashid, S.A., Aziz, F.N.A. and Salleh, M.A.M., 2010. Contribution of rice husk ash to the properties of mortar and concrete: a review. Journal of American science, 6(3), pp.157-165.

Glass, G.K. and Buenfeld, N.R., 2000. The influence of chloride binding on the chloride induced corrosion risk in reinforced concrete. Corrosion Science, 42(2), pp.329-344.

Govindarao, V., 1980. Utilization of rice husk-a preliminary-analysis. Journal of Scientific & Industrial Research (JSIR) 39(9): 495-515.

Grist, E., Paine, K. and Heath, A., 2016. Hydraulic lime – pozzolan concretes: Properties, uses and research needs. University of Bath.

Gunasekara, C., 2016. Influence of properties of fly ash from different sources on the mix design and performance of geopolymer concrete.

Gupta, M.A. and Wayal, A.S., 2015. Use of Rice Husk Ash in Concrete: A Review. IOSR Journal of Mechanical and Civil Engineering (IOSR-JMCE), 12(4), pp 29-31.

Habeeb, G. and M. Fayyadh., 2009. Rice husk ash concrete: the effect of RHA average particle size on mechanical properties and drying shrinkage. Australian Journal of Basic and Applied Sciences 3(3): 1616-1622.

Habeeb, G.A. and Mahmud, H.B., 2010. Study on properties of rice husk ash and it is use as cement replacement material. Materials Research, 13(2), pp.185-190.

Hamada, D., Sato, T., Yamato, F. and Mizunuma, T., 2000. Development of new superplasticizer and it is application to self-compacting concrete. Special Publication, 195, pp.291-304.

Hanle, L.J., Jayaraman, K.R. and Smith, J.S., 2004. CO2 emissions profile of the US cement industry. Washington DC: Environmental Protection Agency.

Hansen, W., 1987. Drying shrinkage mechanisms in Portland cement paste. Journal of the American Ceramic society, 70(5), pp.323-328.

Harish, K. V. and R. R. Prasada., 2013. Material characterization studies on low-and high-carbon rice husk ash and their performance in Portland cement mixtures. Advances in Civil Engineering Materials 2(1): 266-287.

Hasparyk, N.P, Farias. L.A, Moacir A. S. A, and Bittencourt. R.M., 2004. Study of the influence of amorphous rice husk-ash on concrete properties. In PRO 40: International RILEM Conference on the Use of Recycled Materials in Buildings and Structures (Volume 2) (Vol. 2, p. 751). RILEM Publications.

He, F., Shi, C., Yuan, Q., Chen, C. and Zheng, K., 2012. AgNO3-based colorimetric methods for measurement of chloride penetration in concrete. Construction and Building Materials, 26(1), pp.1-8.

Hearn, N., Hooton, R.D. and Nokken, M.R., 2006. Pore structure, permeability, and penetration resistance characteristics of concrete. Significance of Tests and Properties of Concrete and Concrete-Making Materials. ASTM International.

Heath, A. and Paine, K., 2014. Reducing CO2: Optimum blend of binders in the UK. 34th Cement and Concrete Science Conference. University of Sheffield, 14-17 September 2014.

Hewlett, P., 2003. Lea's chemistry of cement and concrete, Butterworth-Heinemann.

Hewlett, P.C. Leas, 1998. Chemistry of Cement and Concrete, 4th edition. John Wiley & Sons Inc, New York, NY.

Hooton, R.D., Thomas, M.D.A. and Stanish, K., 2001. Prediction of chloride penetration in concrete (No. FHWA-RD-00-142,).

Hossain, M.M., Karim, M.R., Hasan, M., Hossain, M.K. and Zain, M.F.M., 2016. Durability of mortar and concrete made up of pozzolans as a partial replacement of cement: A review. Construction and Building Materials, 116, pp.128-140.

Houston, D. F., 1972. Rice bran and polish. Rice chemistry and technology. American Association of Cereal Chemists, Inc. pp. 12–15.

Hsu, S.L., 2010. Life cycle assessment of materials and construction in commercial structures: variability and limitations (Doctoral dissertation, Massachusetts Institute of Technology).

Hung, H.H., 1997. Properties of high-volume fly ash concrete (Doctoral dissertation, University of Sheffield).

Hussain, S.E. and Al-Gahtani, A.S., 1994. Influence of sulfates on chloride binding in cements. *Cement and Concrete Research*, *24*(1), pp.8-24.

Hwang, C.L., and Wu. D.S., 1989. Properties of cement paste containing rice husk ash. Special Publication 114: 733-762.

Ibrahim, D.M., El-Hemally, S.A., Abo-El-Enein, S.A., Hanafi, S. and Helmy, M., 1980. Thermal treatment of rice-husk ash: Effect of time of firing on pore structure and crystallite size. Thermochimica Acta, 37(3), pp.347-351.

Ikpong, A. and Okpala. D., 1992. Strength characteristics of medium workability ordinary Portland cement-rice husk ash concrete. Building and Environment 27(1): 105-111.

Imbabi, M.S., Carrigan, C. and McKenna, S., 2012. Trends and developments in green cement and concrete technology. International Journal of Sustainable Built Environment, 1(2), pp.194-216.

Isaia, G.C., Gastaldini, A.L.G. and Moraes, R., 2003. Physical and pozzolanic action of mineral additions on the mechanical strength of high-performance concrete. Cement and concrete composites, 25(1), pp.69-76.

Ismail, M. S. and A. Waliuddin., 1996. Effect of rice husk ash on high strength concrete. Construction and building materials 10(7): 521-526.

Jamil, M., Khan, M.N.N., Karim, M.R., Kaish, A.B.M.A. and Zain, M.F.M., 2016. Physical and chemical contributions of Rice Husk Ash on the properties of mortar. Construction and Building Materials, 128, pp.185-198.

Janković, K., Nikolić, D., Bojović, D., Lončar, L. and Romakov, Z., 2011. The estimation of compressive strength of normal and recycled aggregate concrete. Facta universities-series: Architecture and Civil Engineering, 9(3), pp.419-431.

Jensen, O.M. and Hansen, P.F., 2001. Water-entrained cement-based materials: I. Principles and theoretical background. Cement and concrete research, 31(4), pp.647-654.

Jones, A.E.K., Marsh, B., Clark, L., Seymour, D., Basheer, P. and Long, A., 1997. Development of a holistic approach to ensure the durability of new concrete construction. Camberley, UK: British Cement Association.

Jones, M.R., Macphee, D.E., Chudek, J.A., Hunter, G., Lannegrand, R., Talero, R. and Scrimgeour, S.N., 2003. Studies using 27Al MAS NMR of AFm and AFt phases and the formation of Friedel's salt. Cement and Concrete Research, 33(2), pp.177-182.

Justnes, H., 1998. A review of chloride binding in cementitious systems. NORDIC CONCRETE RESEARCH-PUBLICATIONS-, 21, pp.48-63.

Kachwala, A., Pamnani, A. and Raval, A., 2015. Effect of Rice Husk Ash as a Partial Replacement of Ordinary Portland cement in Concrete. Int. Res. J. Eng. Technol., 2(5), pp.175-177.

Kapur, P.C., Singh, R. and Srinivasan, J., 1984. Tube-in-Basket burner for rice husk. I: Properties of husk as a fuel and basic design considerations. Sadhana, 7(4), pp.291-300.

Karim, M.R., Zain, M.F.M., Jamil, M., Lai, F.C. and Islam, M.N., 2012. Strength of mortar and concrete as influenced by rice husk ash: a review. World Applied Sciences Journal, 19(10), pp.1501-1513.

Kartini, K., Mahmud, B.H. and Hamidah, M.S., 2008. Improvement on mechanical properties of rice husk ash concrete with super plasticizer. The International Conference of Construction and Building Material (Vol. 20, pp. 221-230).

Khan, M.N.N., Jamil, M., Karim, M.R., Zain, M.F.M. and Kaish, A.A., 2015. Utilization of rice husk ash for sustainable construction: a review. Research Journal of Applied Sciences, Engineering and Technology, 9(12), pp.1119-1127.

Khan, R., Jabbar, A., Ahmad, I., Khan, W., Khan, A.N. and Mirza, J., 2012. Reduction in environmental problems using rice-husk ash in concrete. Construction and Building Materials, 30, pp.360-365.

Khana, M., Jamil, M., Karimc, M. and Zaind, M., 2014. Strength and durability of mortar and concrete containing rice husk ash: a review. World Applied Sciences Journal32 (5), pp.752-765.

Khatri, D.S., 2014. Impact of admixture and rice husk ash in concrete mix design. IOSR Journal of Mechanical and Civil Engineering E-ISSN, pp.2278-1684.

Kılıç, A., Atiş, C.D., Teymen, A., Karahan, O., Özcan, F., Bilim, C. and Özdemir, M., 2008. The influence of aggregate type on the strength and abrasion resistance of high strength concrete. Cement and Concrete Composites, 30(4), pp.290-296.

Kosmatka, S.H. and Panarese, W.C., 2002. Design and control of concrete mixtures (Vol. 5420). Skokie, IL: Portland cement Association.

Kraiwood K, Chai J, Smith S, Seksun C, 2001. A study of ground coarse fly ashes with different fineness's from various sources as pozzolanic materials. Cement Concrete Comp; Volume 23, pp:335–43

Krishna, R., 2008. Rice husk ash an ideal admixture for concrete in aggressive environment. Recycling construction Waste for sustainable development. Organized by CREAM, UiTM, ACCI and CSM, Kuala Lumpur.

Krishnarao, R.V., Subrahmanyam, J. and Kumar, T.J., 2001. Studies on the formation of black particles in rice husk silica ash. Journal of the European Ceramic Society, 21(1), pp.99-104.

Kropp, J., 1995. Chlorides in concrete. Performance criteria for concrete durability, pp.139-164.

Kugler, V.M., Söderlind, F., Music, D., Helmersson, U., Andreasson, J. and Lindbäck, T., 2003. Low temperature growth and characterization of (Na, K) NbOx thin films. Journal of crystal growth, 254(3-4), pp.400-404.

Kumar, S., Sangwan, P., Dhankhar, R.M.V. and Bidra, S., 2013. Utilization of rice husk and their ash: A review. Res. J. Chem. Env. Sci, 1(5), pp.126-129.

Kunchariyakun, K., Asavapisit, S. and Sombatsompop, K., 2015. Properties of autoclaved aerated concrete incorporating rice husk ash as partial replacement for fine aggregate. Cement and Concrete Composites, 55, pp.11-16.

Lafarge. 2014. The annual report. http://www.lafarge.com/sites/customers_activities-cement_market.

Laskar, A.I. and Talukdar, S., 2008. Rheological behavior of high-performance concrete with mineral admixtures and their blending. Construction and Building materials, 22(12), pp.2345-2354.

Le, H.T., Nguyen, S.T. and Ludwig, H.M., 2014. A study on high performance fine-grained concrete containing rice husk ash. International Journal of Concrete Structures and Materials, 8(4), pp.301-307.

Leta, H., 2014. The effects of mega flow SP1 super plasticizing admixture on the properties of concrete. Msc. Addis Ababa University.

Locher, F.W. and Richartz, W., 1976. Setting of cement: I, Reaction and development of structure. Zem.-Kalk-Gips, 29(10), pp.435-42.

Loupilov, A., Sokolov, A. and Gostilo, V., 2001. X-ray Peltier cooled detectors for X-ray fluorescence analysis. Radiation Physics and Chemistry, 61(3-6), pp.463-464.

Luping, T. and Nilsson, L.O., 1993. Chloride binding capacity and binding isotherms of OPC pastes and mortars. Cement and concrete research, 23(2), pp.247-253.

Ma, B.G., Wang, X.G., Liang, W.Q., Li, X.G. and He, Z., 2007. Study on early-age cracking of cement-based materials with superplasticizers. Construction and Building Materials, 21(11), pp.2017-2022.

Madandoust, R., Ranjbar, M.M., Moghadam, H.A. and Mousavi, S.Y., 2011. Mechanical properties and durability assessment of rice husk ash concrete. Biosystems engineering, 110(2), pp.144-152.

Mahmud, H., 2010. Absorption and permeability performance of Selangor rice husk ash blended grade 30 concrete. Journal of engineering science and technology 5(1): 1-16.

Mahmud, H.B., Malik, M.F.A., Kahar, R.A., Zain, M.F.M. and Raman, S.N., 2009. Mechanical properties and durability of normal and water reduced high strength grade 60 concrete containing rice husk ash. Journal of advanced concrete technology, 7(1), pp.21-30.

Malathy, R. and Subramanian, K., 2007. Drying shrinkage of cementitious composites with mineral admixtures. Indian journal engineering material science, 14, pp. 146-150.

Malhotra, V.M. and Mehta, P.K., 2014. Pozzolanic and cementitious materials. CRC Press.

Malhotra, V.M., 2006. Reducing CO2 emissions. Concrete international, 28(09), pp.42-45.

Marco, P. and Llorens, J., 2007. Understanding of naphthalene sulfonate formaldehyde condensates as a dispersing agent to stabilize raw porcelain gres suspensions: surface adsorption and rheological behavior. Colloids and Surfaces A: Physicochemical and Engineering Aspects, 299(1-3), pp.180-185.

Marthong, C., 2012. Effect of rice husk ash (RHA) as partial replacement of cement on concrete properties. International Journal of Engineering Research and Technology, ESRSA Publications1 (6).

McGrath, P.F., 1997. Development of test methods for predicting chloride penetration into high performance concrete. National Library of Canada= Bibliothèque nationale du Canada.

Mehta, P.K. and Monteiro, P.J., 2017. Concrete Microstructure, Properties and Materials.

Mehta, P.K. and Monteiro, P.J.M., 1986. Concrete: structure, properties, and materials, ‖ Prentice Hall. Inc. Englewood Cliffs, New Jersey.

Mehta, P.K. and Pirtz, D., 1978. Use of rice hull ash to reduce temperature in high-strength mass concrete. In ACI Journal Proceedings (Vol. 75, No. 2, pp. 60-63).

Mehta, P.K. and Pitt, N., 1976. Energy and industrial materials from crop residues. Resource Recovery and Conservation, 2(1), pp.23-38.

Mehta, P.K., 1973. Mechanism of expansion associated with ettringite formation. Cement and Concrete Research, 3(1), pp.1-6.

Mehta, P.K., 1977. Properties of blended cements made from rice husk ash. In Journal Proceedings (Vol. 74, No. 9, pp. 440-442).

Mehta, P.K., 1989, June. Rice husk ash as a mineral admixture in concrete. In Proceedings of the 2nd international seminar on durability of concrete: aspects of admixtures and industrial by-products, Gothenburg, Sweden (pp. 131-6).

Mehta, P.K., 1991. "Concrete in marine environment". Elsevier applied science. London and New York

Mehta, P.K., 1992. Rice Hush Ash-A unique supplementary cementing material. Advances in concrete technology.

Mehta, P.K., 2006. Monteiro. PJM Concrete–Microstructure, Properties, and Materials, United States: McGraw-Hill, pp.85-86.

Mehta, P.K., the Regents of the University of California., 1978. Siliceous ashes and hydraulic cements prepared therefrom. U.S. Patent 4,105,459.

Mehtra, P.K. and Folliard, K.J., 1995. Rice Husk Ash--a Unique Supplementary Cementing Material: Durability Aspects. Special Publication, 154, pp.531-542.

Moghadam, H.A. and Khoshbin, O.A., 2012. Effect of Water-Cement Ratio (w/c) on Mechanical Properties of Self-Compacting Concrete (Case Study). World Academy of Science, Engineering and Technology, International Journal of Civil, Environmental, Structural, Construction and Architectural Engineering, 6(5), pp.317-320.

Moghadam, H.M., Khoshbin. O.A., 2013. Mechanical properties and shrinkage and expansion assessment of rice husk ash concrete and it's comparison with the control concrete. Recent Researches in Urban Sustainability, Architecture and Structures. Baltimore, MD, USA September 17-19.

Monitor, R.M., 2010. Trade and Markets Division, Food and Agriculture Organization of the United Nations. Vol. XIII. Issue, (1).

Muthadhi, A. and S. Kothandaraman., 2010. Optimum production conditions for reactive rice husk ash. Materials and structures 43(9): 1303-1315.

Nagataki, S., 1994. Mineral admixtures in concrete: state of the art and trends. Special Publication 144: 447-482.

Naik, T.R., 2008. Sustainability of concrete construction. Practice Periodical on Structural Design and Construction, 13(2), pp.98-103.

Nair, D.G., Fraaij, A., Klaassen, A.A. and Kentgens, A.P., 2008. A structural investigation relating to the pozzolanic activity of rice husk ashes. Cement and Concrete Research, 38(6), pp.861-869.

Nazari, A., Riahi, S., Riahi, S., Shamekhi, S.F. and Khademno, A., 2010. Mechanical properties of cement mortar with Al2O3 nanoparticles. Journal of American Science, 6(4), pp.94-97.

Nehdi, M., 2001. Ternary and quaternary cements for sustainable development. Concrete international 23(04): 36-44.

Nehdi, M., Duquette, J. and El Damatty, A., 2003. Performance of rice husk ash produced using a new technology as a mineral admixture in concrete. Cement and concrete research, 33(8), pp.1203-1210.

Nematollahi, B. and Sanjayan, J., 2014. Effect of different superplasticizers and activator combinations on workability and strength of fly ash based geopolymer. Materials & Design, 57, pp.667-672.

Neville, A.M. and Brooks, J.J., 1987. Concrete Technology. 2010. Essex, England: Pearson Education Limited.

Ngun, B.K., Mohamad, H., Sakai, E. and Ahmad, Z.A., 2010. Effect of rice husk ash and silica fume in ternary system on the properties of blended cement paste and concrete. Journal of Ceramic Processing Research, 11(3), pp.311-315.

Nguyen, V.T., 2011. Rice husk ash as a mineral admixture for ultra-high-performance concrete.

Nikam, V.S. and Tambvekar, V.Y., 2003. Effect of different supplementary cementitious material on the microstructure and it is resistance against chloride penetration of concrete.

Okamura, H. and Ozawa, K., 1995. Mix design for self-compacting concrete. Concrete library of JSCE, 25(6), pp.107-120.

Okpalla, D.C., 1987. Rice Husk Ash as a Partial Replacement for Cement in Concrete, Proceedings of the Annual Conference of the Nigerian Society of Engineers, Port Harcourt, Nigeria, pp. 1-12

Olawale, O. and F. A. Oyawale., 2012. Characterization of rice husk via atomic absorption spectrophotometer for optimal silica production. International Journal of Science and Technology 2(4): 210-213.

Omatola, K. and A. Onojah., 2009. Elemental analysis of rice husk ash using X-ray fluorescence technique. International journal of physical sciences 4(4): 189-193.

Onojah, A.D., Agbendeh, N.A. and Mbakaan, C., 2013. Rice Husk Ash Refractory: The Temperature Dependent Crystalline Phase Aspects. International Journal of research and reviews in applied sciences (IJRRAS). pp, 247.

Osuji, S.O. and Ikogho, D., 2018. Current Effects of Naphthalene Based Superplasticizer's Addition Process on Water Reduction and Grade C20/25 Concrete's Compressive Strength. Journal of Civil Engineering Research, 8(1), pp.9-14.

Oyejobi, D.O., Abdulkadir, T.S. and Ajibola, V.M., 2014. Investigation of rice husk ash cementitious constituent in concrete. International Journal of Agricultural Technology, 10(3), pp.533-542.

Papatzani, S., Paine, K. and Calabria-Holley, J., 2014. Strength and microstructure of colloidal nanosilica enhanced cement pastes. Cement Application, 4, pp.80-85.

Patel, M., Karera, A. and Prasanna, P., 1987. Effect of thermal and chemical treatments on carbon and silica contents in rice husk. Journal of Materials Science, 22(7), pp.2457-2464.

Patil, B.P., 2015. Evaluation of Mechanical Properties of Rice Husk Ash Concrete for M25 Grade.

Patil, R., Dongre, R. and Meshram, J., 2014. Preparation of silica powder from rice husk. Journal of Applied Chemistry, 27, pp.26-29.

Payá, J., Monzó, J., Borrachero, M.V., Mellado, A. and Ordoñez, L.M., 2001. Determination of amorphous silica in rice husk ash by a rapid analytical method. Cement and Concrete Research, 31(2), pp.227-231.

Plank, J. and Winter, C., 2008. Competitive adsorption between superplasticizer and retarder molecules on mineral binder surface. Cement and Concrete Research. Vol. 38, Issue 5. – P. 599–605.

Puertas, F., Santos, H., Palacios, M. and Martínez-Ramírez, S., 2005. Polycarboxylate superplasticizer admixtures: effect on hydration, microstructure and rheological behavior in cement pastes. Advances in Cement Research, 17(2), pp.77-89.

Putra, J. R, B.H. Abu Bakar, Che Wan and Dewi, S. J., 2014. Chloride resistance of concrete containing rice husk ash by rapid migration test. Australian Journal of Basic and Applied Sciences, 8 (19). pp. 218-222.

Raheem, A.A., Soyingbe, A.A. and Emenike, A.J., 2013. Effect of curing methods on density and compressive strength of concrete. International Journal of Applied Science and Technology, 3(4).

Ramakrishnan, S., Velrajkumar, G. and Ranjith, S., 2014. Behaviour of cement-rice husk ash concrete for pavement. Int. J. Emerg. Tren. Eng. Dev., 11(4), pp.31-41.

Raman, S.N., Ngo, T., Mendis, P. and Mahmud, H.B., 2011. High-strength rice husk ash concrete incorporating quarry dust as a partial substitute for sand. Construction and Building Materials, 25(7), pp.3123-3130.

Ramasamy, V., 2012. Compressive strength and durability properties of rice husk ash concrete. KSCE Journal of Civil Engineering, 16(1), pp.93-102.

Ramezanianpour, A. A., 2014. Cement Replacement Materials. Page 257-290.

Ramezanianpour, A.A., Mahdikhani, M. and Ahmadibeni, G., 2009. The effect of rice husk ash on mechanical properties and durability of sustainable concretes.

Rasoul, B.I., Gunzel, F.K. and Rafiq, M.I., 2017. The effect of rice husk ash properties on the strength and durability of concrete at high replacement ratio. In 3rd International conference on Structural, Civil, and Architectural Engineering (ICSCAE), Montreal, Canada, 5-6 June 2017.

Rasoul, B.I., Günzel, F.K. and Rafiq, M.I., 2018. Effect of rice husk ash properties on the early age and long-term strength of mortar. High Tech Concrete: Where Technology and Engineering Meet (pp. 207-214). Springer, Cham.

Reddy, D.V., Alvarez, M. and Arboleda, D., 2008, June. Sustainable Concrete Materials for the Marine Environment. In Sixth LACCEI International Latin American and Caribbean Conference for Engineering and Technology (LACCEI'2008).

Rizwan, S.A. and Bier, T.A., 2005, April. Inclusion of Mineral Admixtures in Cement Pastes for High Performance Concrete. In 2nd International Conference on" Concrete and Development", CD7-004 (pp. 1-12).

Rößler, C., Bui, D.D. and Ludwig, H.M., 2013. Mesoporous structure and pozzolanic reactivity of rice husk ash in cementitious system. Construction and Building Materials, 43, pp.208-216.

Rukzon, S., Chindaprasirt, P. and Mahachai, R., 2009. Effect of grinding on chemical and physical properties of rice husk ash. International Journal of Minerals, Metallurgy and Materials, 16(2), pp.242-247.

Safiuddin, M., West, J.S. and Soudki, K.A., 2011. Flowing ability of the mortars formulated from self-compacting concretes incorporating rice husk ash. Construction and Building Materials, 25(2), pp.973-978.

Salas, A., Delvasto, S., De Gutierrez, R.M. and Lange, D., 2009. Comparison of two processes for treating rice husk ash for use in high performance concrete. Cement and concrete research, 39(9), pp.773-778.

Sandberg, P. and Larsson, J., 1993. Chloride binding in cement pastes in equilibrium with synthetic pore solutions. Chloride Penetration into Concrete Structures, Nordic Miniseminar, pp.98-107.

Saraswathy, V., Karthick, S. and Kwon, S.J., 2014. Improved durability performances in cement mortar with rice husk ash. Journal of the Korean Recycled Construction Resources Institute, 2(1), pp.66-73.

Saraswathy.V and Song. H.W., 2007. Corrosion performance of rice husk ash blended concrete. Construction and Building Materials, 21(8), pp. 1779-1784.

Setina, J., Gabrene, A. and Juhnevica, I., 2013. Effect of pozzolanic additives on structure and chemical durability of concrete. Procedia Engineering, 57, pp.1005-1012.

Shah, R.A., Khan, A.H., Chaudhry, M.A., and Quaiser, M.A., 1979. Utilization of rice husk ash for the production of cement like materials in rural areas. UNIDO/ESCAP/RCTT/ workshop on rice husk ash cement, Peshawar, Pakistan, January, Regional Centre for Technology Transfer, Bangalore, India, pp.57-60.

Shahroodi, A., 2010. Development of Test Methods for Assessment of Concrete Durability for Use in Performance-Based Specifications (Doctoral dissertation, University of Toronto).

Shannon, J., Howard, I.L., Cost, V.T. and Wilson, W.M., 2015. Benefit is of Portland-limestone cement for concrete with rounded gravel aggregates and higher fly ash replacement rates. In Proc., Transportation Research Board 94th Annual Meeting, Washington, DC.

Shetty, M.S. 2005. Concrete technology. New Delhi: S. Chand and Company.

Shinohara, Y. and Kohyama, N., 2004. Quantitative analysis of tridymite and cristobalite crystallized in rice husk ash by heating. Industrial Health, 42(2), pp.277-285.

Shukla, A., Singh, C.K. and Sharma, A.K., 2011. Study of the properties of concrete by partial replacement of ordinary Portland cement by rice husk ash. International Journal of Earth Sciences and Engineering, 4(6), pp.965-968.

Siddique, R. and Khan, M.I., 2011. Supplementary cementing materials. Springer Science & Business Media.

Siddique, R. and Klaus, J., 2009. Influence of Metakaolin on the properties of mortar and concrete: A review. Applied Clay Science, 43(3), pp.392-400.

Singh, D., Kumar, R., Kumar, A. and Rai, K.N., 2008. Synthesis and characterization of rice husk silica, silica-carbon composite and H3PO4 activated silica. Cerâmica, 54(330), pp.203-212.

Sivakumar, G. and Ravibaskar, R., 2009. Investigation on the hydration properties of the rice husk ash cement using FTIR and SEM. Applied Physics Research, 1(2), p.71.

Sousa-Coutinho, J. and Papadakis, V.G., 2011, April. Rice husk ash: importance of fineness for it is use as a pozzolanic and chloride-resistant material. In Proceedings of the 12th International Conference on Durability of Building Materials and Components, Porto, Portugal.

Spiesz, P. and Brouwers, H.J.H., 2009, September. Evaluation of the rapid chloride migration (rcm) test. In Proceedings of the 17th Ibausil, International Conference on Building Materials (nternational Baustofftagung), Weimar, edited by HB Fischer and KA Bode, FA Finger-Institut für Baustoffkunde, Weimar, Germany.

Srinivasreddy, A.B., McCarthy, T.J. and Lume, E., 2013. Effect of rice husk ash on workability and strength of concrete.

Stanish, K.D., Hooton, R.D. and Thomas, M.D.A., 1997. Testing the chloride penetration resistance of concrete: a literature review. FHWA contract DTFH61, pp.19-22.

Struble, L. and Godfrey, J., 2004. How sustainable is concrete. In International workshop on sustainable development and concrete technology (pp. 201-211).

Sugita, S., Shoya, M. and Tokuda, H., 1992. Evaluation of pozzolanic activity of rice husk ash. In Proceedings of the 4th CANMET/ACI International Conference on Fly Ash, Silica Fume, Slag and Natural Pozzolans in Concrete, Istanbul, Am. Concr. Inst., Detroit, USA (Vol. 1, pp. 495-512).

Suhendro, B., 2014. Toward green concrete for better sustainable environment. Procedia Engineering 95: 305-320.

Sumadi, S. & Lee, Y.L., 2008. Development of Blended Cements for Water Proofing Application. Jabatan Struktur dan Bahan Fakulti Kejuruteraan Awam Universiti Teknologi Malaysia.

Sutter, L.L., Hooton, R.D. and Schlorholtz, S., 2013. Methods for evaluating fly ash for use in highway concrete (Vol. 749). Transportation Research Board.

Swaminathen, A.N. and Ravi, S.R., 2016. Use of Rice Husk Ash and Metakaolin as Pozzolonas for Concrete: A Review. International Journal of Applied Engineering Research, 11(1), pp.656-664.

Taib, M.R.B., 2007. Production of amorphous silica from rice husk in fluidized bed system, PhD thesis.

Talaber, J., 1982. Factors influencing the quality of cement. Periodica Polytechnica Civil Engineering, 26(1-2), pp.27-39.

Tang, L. and Nilsson, L.O., 1992. Chloride diffusivity in high strength concrete at different ages. Nordic Concrete Research. Publication no 11.

Tang, L. and Nilsson, L.O., 1992. Rapid determination of the chloride diffusivity in concrete by applying an electrical field. ACI materials journal, 89(1), pp.49-53.

Tang, L. and Sørensen, H.E., 2001. Precision of the Nordic test methods for measuring the chloride diffusion/migration coefficients of concrete. Materials and Structures, 34(8), p.479.

Tang, L., 1996. Chloride transport in concrete-measurement and prediction. PhD Thesis, Chalmers University of Technology, Gotenburg, Sweden.

Tang, L., Nilsson, L. O. and Basheer, P. A. M., 2012. Resistance of Concrete to Chloride Ingress: Testing and modelling. Spon Press.

Taylor, H.F.W., 1997. Cement Chemistry. Second Edition, Thomas Telford Services Ltd.

Tazawa, E.I., Miyazawa, S. and Kasai, T., 1995. Chemical shrinkage and autogenous shrinkage of hydrating cement paste. Cement and concrete research, 25(2), pp.288-292.

Thomas, M., 1996. Chloride thresholds in marine concrete. Cement and concrete Research, 26(4), pp.513-519.

Thomas, M.D.A., Pantazopoulou, S.J. and Martin-Perez, B., 1995. Service Life Modelling of Reinforced Concrete Structures Exposed to Chlorides-A Literature Review. Prepared for the Ministry of Transportation, Ontario, at the University of Toronto.

Thuadaij, N. and Nuntiya, A., 2008. Preparation of nanosilica powder from rice husk ash by precipitation method. Chiang Mai Journal of Science, 35(1), pp.206-211.

Triantafyllou, D., Ahmed, A. and Kamau, J., 2017. Performance of Recycled Aggregate Concrete after Washing Treatment of Aggregates. European Journal of Engineering Research and Science, 2(9), pp.49-53.

Tushir, M and G. Kumar, G., 2016. Effect of Rice Husk Ash on Split Tensile Strength of Concrete. International Journal on Emerging Technologies 7(1): pp. 78-82, 2016.

Van, V.T.A., 2013. Characteristics of rice husk ash and application in Ultra-High-Performance Concrete. Bauhaus University Weimar, the Netherlands. PhD thesis.

Van Tuan, N., Ye, G. and van Breugel, K., 2010, August. Effect of rice husk ash on autogenous shrinkage of ultra-high-performance concrete. In *Proceedings of International RILEM Conference on Advances in Construction Materials Through Science and Engineering, Hong-Kong*.

Van Tuan, N., Ye, G., Van Breugel, K. and Copuroglu, O., 2011. Hydration and microstructure of ultra-high-performance concrete incorporating rice husk ash. *Cement and Concrete Research*, *41*(11), pp.1104-1111.

Vayghan, A.G., Khaloo, A.R. and Rajabipour, F., 2013. The effects of a hydrochloric acid pre-treatment on the physicochemical properties and pozzolanic performance of rice husk ash. *Cement and Concrete Composites*, *39*, pp.131-140.

Venkatanarayan, A., Raulji, P., Norton, W., Chakravarti, D., Coarfa, C., Su, X., Sandur, S.K., Ramirez, M.S., Lee, J., Kingsley, C.V. and Sananikone, E.F., 2015. IAPP-driven metabolic reprogramming induces regression of p53-deficient tumours in vivo. Nature, 517(7536), p.626.

Venkatanarayanan, H.K. and Rangaraju, P.R., 2013. Decoupling the effects of chemical composition and fineness of fly ash in mitigating alkali-silica reaction. Cement and Concrete Composites, 43, pp.54-68.

Wansom, S., Janjaturaphan, S. and Sinthupinyo, S., 2010. Characterizing pozzolanic activity of rice husk ash by impedance spectroscopy. Cement and concrete research, 40(12), pp.1714-1722.

Wasserbau, B.B., 2004. Merkblatt Chlorideindringwiderstand von Beton. Bundesanstalt für Wasserbau.

Wen-ping, L., Jian, W., Zhen, Z., Li-jiang, G. and Li, H., 2009. Practical integrated design of a condenser-objective lens for transmission electron microscope. In Journal of Physics: Conference Series (Vol. 188, No. 1, p. 012045). IOP Publishing.

Wolford, I.M., 2016. Quantifying Amorphous Content of Commercially Available Silicon Carbide Fibres.

Wongkeo, W., Thongsanitgarn, P. and Chaipanich, A., 2012. Compressive strength and drying shrinkage of fly ash-bottom ash-silica fume multi-blended cement mortars. Materials & Design (1980-2015), 36, pp.655-662.

Wu, D.S. and Peng, Y.N., 2003. The macro-and micro properties of cement pastes with silica-rich materials cured by wet-mixed steaming injection. Cement and Concrete Research, 33(9), pp.1331-1345.

Xu, W., Lo, T.Y. and Memon, S.A., 2012. Microstructure and reactivity of rich husk ash. Construction and Building Materials, 29, pp.541-547.

Yalcin, N. and V. Sevinc., 2001. Studies on silica obtained from rice husk. Ceramics international 27(2): 219-224.

Yamada, K., Takahashi, T., Hanehara, S. and Matsuhisa, M., 2000. Effects of the chemical structure on the properties of polycarboxylate-type superplasticizer. Cement and concrete research, 30(2), pp.197-207.

Yamamoto, Y. and Lakho, S.M., 1982. Production and utilization of active rice husk ash as a substitute for cement. In Proceedings of JSCE (No. 322, pp. 157-166).

Yang, J., Wang, Q. and Zhou, Y., 2017. Influence of curing time on the drying shrinkage of concretes with different binders and water-to-binder ratios. Advances in Materials Science and Engineering, 2017.

Yap, S.P., Foong, K.Y., Alengaram, U.J. and Zumaat, M.Z., 2013. Waste Materials in Malaysia for Development of Sustainable Concrete: A Review. Electronic Journal of Structural Engineering, 13, p.1.

Yeoh, A.K., Bidin, R., Chong, C.N. and Tay, C.Y., 1979. The relationship between temperature and duration of burning of rice-husk in the development of amorphous rice-husk ash silica. In Proceedings of UNIDO/ESCAP/RCTT, Follow-up Meeting on Rice-Husk Ash Cement, Alor Setar, Malaysia.

Yuan, Q., Shi, C., De Schutter, G., Audenaert, K. and Deng, D., 2009. Chloride binding of cement-based materials subjected to external chloride environment–a review. Construction and Building Materials, 23(1), pp.1-13.

Yuan, Y., S. P. Shah, S.P., and H. L. Lu, H.L., 2003. Advance in concrete and structures. Proceeding of the international conference ICACS 2, pp. 786-791.

Zain, M.F.M., Islam, M.N., Mahmud, F. and Jamil, M., 2011. Production of rice husk ash for use in concrete as a supplementary cementitious material. Construction and building materials, 25(2), pp.798-805.

Zhang, M.H. and Malhotra, V., 1996. High-performance concrete incorporating rice husk ash as a supplementary cementing material. ACI Materials Journal, 93(6), pp.629-636.

Zhang, M.H., Lastra, R. and Malhotra, V.M., 1996. Rice-husk ash paste and concrete: some aspects of hydration and the microstructure of the interfacial zone between the aggregate and paste. Cement and Concrete Research, 26(6), pp.963-977.

Zulu, S.N., 2017. Optimizing the usage of fly ash in concrete mixes (Doctoral dissertation).

Zych, T., 2015. Test methods of concrete resistance to chloride ingress. Czasopismo Techniczne.

PUBLICATION

Rasoul, B.I., Günzel, F.K. and Rafiq, M.I., 2018. Effect of rice husk ash properties on the early age and long-term strength of mortar. In *High Tech Concrete: Where Technology and Engineering Meet* (pp. 207-214). Springer, Cham.

Rasoul, Binyamien I; Gunzel, Friederike K; Rafiq, Imran M., 2017. The effect of rice husk ash on the strength and durability of concrete at high replacement ratio. *Mechanics, Materials Science & Engineering, 12* (1), 2017, ISSN: 2412-5954.

Rasoul, B., 2018. Influence of rice husk ash (RHA) on the on the drying shrinking of mortar. *European Chemical Bulletin, 7*(3), pp.115-119.

APPENDIX A

Table1. Chemical composition of RHA according to literature, where strength of concrete and mortar are increased.

Author		SiO_2	Al_2O_3	Fe_2O_3	CaO	MgO	Na_2O	K_2O	P_2O_5	TiO_3	MnO	SO_3	Cl^-	C	LOI
	RHA	86.5	0.3	0.1	0.5	0.3	0.1	1.6	-	-	-	0.1	-	-	9.10
Isaia et al. (2001)	Cement	19.6	4.8	3.1	64.4	1.7	0.1	1.0	-	-	-	2.8	-	-	2.10
De Sensale (2006)	RHA- Uruguay	87.2	0.15	0.16	0.55	0.35	1.12	3.60	-	-	-	0.32	-	-	6.55
	RHA-USA	88	-	0.1	0.8	0.2	0.7	2.2	-	-	0.2	-	-	-	8.10
	Cement type I	21.98	4.65	2.27	61.55	4.27	0.11	1.04	-	-	-	2.19	-	-	2.30
Saraswathy and Song (2006)	RHA	92.95	0.31	0.26	0.53	0.55	0.08	2.06	-	-	-	-	-	-	1.97
	OPC Cement	22.00	5.60	4.00	63.90	1.70	-	-	-	-	-	2.30	-	-	1.10
Gastaldini et al. (2007)	RHA	96.26	0.41	0.22	0.76	0.50	0.03	1.44	-	-	-	0.04	-	-	4.49
	OPC Cement	19.59	4.79	3.07	64.35	1.69	0.07	0.98	-	-	-	2.75	-	-	2.09
Ganesan et al. (2008)	RHA	87.32	0.22	0.28	0.48	0.28	1.02	3.14	-	-	-	-	-	-	2.10
	OPC Cement	20.25	5.04	3.16	63.61	4.56	0.08	0.51	-	-	-	-	-	-	3.12
Da Silva et al. (2008)	RHA	97.53	-	0.21	0.22	-	0.01	0.04	-	-	-	-	-	-	1.72
	OPC Cement	31.16	4.71	1.89	68.08	0.48	0.29	0.48	0.28	-	-	-	-	-	0.81
Chindaprasirt et al. (2008)	RHA	93.2	0.4	0.1	1.1	0.1	0.1	1.3	-	-	-	0.9	-	-	3.7
	Cement type I	20.9	4.8	3.4	65.4	1.3	0.2	0.4	-	-	-	2.7	-	-	0.9
Ramezanianpour et al. (2009)	RHA	89.61	0.04	0.22	0.91	0.42	0.07	1.58	-	-	-	-	-	-	5.91
	Cement type I	21.50	3.68	2.76	61.50	4.80	0.12	0.95	-	-	-	-	-	-	1.35
Habeeb and Fayyadh (2009)	RHA	88.32	0.46	0.67	0.67	0.44	0.12	2.91	-	-	-	-	-	-	5.81
	OPC Cement	20.99	6.19	3.86	65.96	0.22	0.17	0.6	-	-	-	-	-	-	1.73
Givi et al. (2010)	RHA	87.86	0.68	0.93	1.30	0.35	0.12	2.37	-	-	-	-	-	-	-
	OPC Cement	21.89	5.3	3.34	53.27	6.45	0.18	0.98	-	-	-	3.67	-	-	3,21
Gastaldini et al. (2010)	RHA	90	0.28	0.14	0.45	0.28	0.08	1.55	-	-	-	0.02	-	-	5.0
	High early strength Cement	19.59	4.79	3.07	64.35	1.69	0.07	0.98	-	-	-	2.75	-	-	2.09
Zerbino et al. (2011)	RHA-natural	95.04	0.30	0.44	1.25	0.45	0.09	1.40	-	-	-	0.01	-	-	0.51
	RHA- Grinded	94.84	0.39	0.54	1.32	0.40	0.11	1.45	-	-	-	0.01	-	-	0.25
	OPC Cement	21.8	3.7	4.0	64.8	0.7	0.1	1.1	-	-	-	2.5	-	-	1.3
Madandoust et al. (2011)	RHA	90.9	0.83	0.6	0.8	0.56	1.55		-	-	-	-	-	-	-
	Cement type I	20.0	6.0	4.20	64.5	1.2	0.8		-	-	-	-	-	-	-
Chao-Lung et al. (2011)	RHA	91	0.35	0.41		0.81	0.08	3.21	0.98	-	-	1.21	-	-	8.5
	Cement type I	22.01	5.51	3.44		2.59	0.40	0.70	0.05	-	-	2.03	-	-	0.51
Xu et al. (2012)	RHA	91.71	0.36	0.9	0.86	0.31	0.12	1.67	-	-	-	-	-	-	3.13
	Cement OPC	-	-	-	-	-	-	-	-	-	-	-	-	-	-
De Souza et al. (2014)	RHA	93.25	0.1	0.02	0.57	0.19	-	2.18	0.51	0.01`	0.25	-	-	-	3.20
Shatat (2014)	RHA	86.0	1.16	1.85	0.64	0.77	1.14	2.54	0.06	-	-	0.32	-	-	4.77
	OPC cement	20.48	4.76	4.69	62.15	1.47	0.46	0.27	0.15	0.58	-	-2.63	-	-	1.85

Table 2: Physical Properties of RHA according to literature, where strength of concrete and mortar are increased.

Author		Specific gravity (g/cm^3)	Blaine specific surface area (cm^2/g)	Average particle size (µm)	Specific surface area BET (m^2/kg)
Isaia et al. (2001)	RHA	2.02		11	40100
	Cement	3.12		8	1800
De Sensale (2006)	RHA- Uruguay	2.06	-		28800
	RHA-USA	2.16	-		24300
	Cement	3.14	309		
Gastaldini et al. (2007)	RHA	2.11			40000
	Cement	3.14			14800
Ganesan et al. (2008)	RHA	2.06	-	3.80	36470
	Cement OPC	3.1	326	22.50	-
Da Silva et al. (2008)	RHA	2.2			9360
	Cement OPC	3.10			440
Chindaprasirt et al. (2008)	RHA	2.23	11200	10	
	Cement OPC	3.14	3600	15	
Ramezanianpour et al. (2009)	RHA	2.15	3600		
	OPC cement type I	3.21	3200		
Habeeb and Fayyadh (2009)	RHA	2.11		11.5	30400
	Cement OPC type I	2.94	351.4	22.1	-
Givi et al. (2010)	RHA average particle size 95 microns	-	-		24000
	Ultra-fine RHA	-	-		36470
	Cement OPC	1.7	314		-
Gastaldini et al. (2010)	RHA	2.17			40000
	High early strength Cement	3.11			14800
Zerbino et al. (2011)	RHA-Natural	1.45-1.60			
	RHA- Grinded	2-2.1			
	OPC Cement	3.13			
Madandoust et al. (2011)	RHA	-	376.8		
	Cement type I OPC		336.5		
W. Xu et al. (2012)	RHA			150 nm	77420
	Cement OPC	3.14			39500

Table 3: Chemical composition of RHA according to literature, where strength of concrete and mortar are decreased.

Author		**Chemical composition**													
		SiO_2	**Al_2O_3**	**Fe_2O_3**	**CaO**	**MgO**	**Na_2O**	**K_2O**	**P_2O_5**	**TiO_3**	**MnO**	**SO_3**	**Cl^-**	**C**	**LOI**
Ikpong and Okpala (1992)	RHA	82.13	4.27	0.38	0.16	1.65	0.14	1.23	1.44	-	-	-	-	-	8.60
	Cement	-	-	-		--		-	-	-	-	-	-	-	-
Ismail and Waliuddin (1996)	RHA	80.0	3.93	0.41	3.82	0.25	0.67	1.45	-	-		0.78	-	-	8.56
	Cement	22	4.9	4.4	62.0	2.25	-	-	-	-	-	1.4	-	-	2.2
Marshal and Galica (2008)		85.77	0.24	0.32	0.67	0.17	0.09	0.81	-	-		-	-	-	-
	RHA0	92.00	0.29	0.1	1.28	0.37	0.05	2.19	0.94	-	-	-	-	-	3.43
Rukzon et al. (2008)	RHA1	92.50	0.28	0.1	1.40	0.20	0.06	2.35	0.93	-	-	-	-	-	3.65
	RHA2	90.10	0.25	0.1	1.45	0.01	0.08	2.42	0.92	-	-	-	-	-	3.56
	RHA3	93.24	0.44	0.1	1.10	0.01	0.03	1.27	0.96	-	-	-	-	-	3.72
	OPC Cement	20.90	4.76	3.41	65.41	1.25	0.24	0.35	-	-	-	2.71	--	-	0.96
Dabai et al. (2009)	RHA	68.12	1.06	0.78	1.01	1.31	-	21.23	-	-	-	0.137	-	-	18.25
	Cement	23.43	4.48	4.08	64.40	1.34	-	0.29	-	-	-	2.79	-	-	5.68
Kartini et al. (2010)	RHA	96.70	1.01	0.05	0.49	0.19	0.26	0.91	0.01	0.16	-	-	-	-	4.4
	Cement II	21.38	5.60	3.36	64.64	2.06	0.05	-	-	-	-	2.14	-	-	0.64
Rodrigues et al. (2010)	RHA-I	73.60	0.075	0.26	0.76	0.27	0.09	1.17	-	-	-	-	-	-	22.90
	RHA-II	94.60	0.09	0.15	0.93	0.28	0.06	1.12	-	-	-	-	-	-	1.40
	Cement type I	17.90	4.85	2.70	64.45	2.15	0.30	-	-	-		2.40	-	-	1.60
Abalaka and Babalaga (2011)	RHA	95.41	-	0.82	-	1.24	0.22	1.65	3.97	0.03	0.19	0.03	-	-	3.88

Author	**SiO_2**	**Al_2O_3**	**Fe_2O_3**	**CaO**	**MgO**	**Na_2O**	**K_2O**	**P_2O_5**	**TiO_3**	**MnO**	**SO_3**	**Cl^-**	**C**	**LOI**	**SiO_2**
Abu Baker et al. (2014)	RHA0	93.00	0.20	0.13	0.49	0.73	0.02	1.30	-	-	-	0.15	-	-	3.98
	RHA1	90.00	0.39	0.37	0.46	0.88	0.02	3.10	-	-	-	0.15	-	-	4.63
	RHA2	91.00	0.10	0.10	0.40	0.90	0.15	3.30	-	-	-	0.50	-	-	3.55
	RHA3	90.99	0.23	0.26	0.41	0.73	0.02	2.19	-	-	-	0.08	-	-	5.09
	RHA4	90.87	0.14	0.95	0.49	0.65	0.25	2.16	-	-	-	0.09	-	-	4.40
	RHA5	90.70	0.40	0.40	0.40	0.50	0.10	2.20	-	-	-	0.10	-	-	5.20
	RHA6	93.70	0.30	0.20	0.60	0.40	0.20	1.40	-	-	-	0.10	-	-	3.10
	RHA7	92.90	0.18	0.43	0.41	0.35	0.02	0.72	-	-	-	0.10	-	-	4.89
	OPC cement	17.00	3.90	3.20	70.00	1.50	0.02	0.53	-	-	-	3.60	-	-	0.25
Chatveera and Lertwattanaruk (2011)	RHA	78.12	0.31	0.23	0.03	0.34	0.17	0.82	-	-	-	0.09	-	-	8.31
Khan et al. (2012)	Rapid cooled RHA	84.00	1.39	2.01	0.60	0.85	-	-	-	-	-	-	-	-	5.85
	Slow cooled RHA	89.50	0.40	2.86	0.30	0.25	-	-	-	-	-	-	-	-	4.0
	Cement OPC	19.80	6.9	3.85	62.45	2.35	-	-	-	-	-	2.95	-	-	-
Antiohos et al. (2013)	RHA.A	89.05	0.25	0.41	0.85	0.17	1.32	-	-	0.13	0.13	0.01	0.09	-	6.34
	RHA-Ʊ	86.50	0.92	0.56	1.12	0.43	1.58	-	-	0.12	0.12	0.05	0.09	-	6.30
	Cement	20.41	4.74	3.08	62.28	1.90	0.19	0.59	-	-	0.02	2.82	0.01	-	2.85
Abakaka (2013)	RHA	95.41	-	0.82	-	1.24	0.22	1.65	3.97	-	0.19	0.07	-	-	0.77
	OPC Cement	24.79	6.35	0.92	58.50	2.87	0.65	0.80	0.15	0.06	-	4.91	-	-	-

Table 4: Physical Properties of RHA according to literature, where strength of concrete and mortar are increased.

Author		Specific gravity (g/cm^3)	Blaine surface area (cm^2/g)	Average particle size (μm)	Specific surface area BET (m^2/kg)	Fineness passing (45μm) _
Ismail and Waliuddin (1996)	RHA	2.11				
	Cement		3315			
	RHA0	1.98		42		
Rukzon et al. (2008)	RHA1	2.15	3200 cm^2/g	28		
	RHA2	2.21	7800 cm^2/g	17		
	RHA3	2.23	12500 cm^2/g	10		
	OPC cement	3.14		15		
Kartini et al. (2010)	RHA		20500 cm^2/g	25.83		78.13
	Cement		17570 cm^2/g	21.20		93.88
Rodrigues etal.(2010)	RHA-I			1.8	119	
	RHA-II			4.0	15	
	Cement type I			10	$1.89 m^2/g$	
Shukla,Singh and Sharma(2011)	RHA	2.06				Fineness passing 45-micron sieve 96%
	Cement	3.15				Fineness passing 90-micron sieve 95%
Abu Baker et al. (2014)	RHA0			17.96		
	RHA1			10.93		
	RHA2			9.74		
	RHA3			9.52		
	RHA4			9.34		
	RHA5			8.70		
	RHA6			6.85		
	RHA7			6.65		

Chatveera and Lertwattanaruk (2011)	OPC cement RHA Cement type I	 2.02 3.11	 6200 3248		 110 -	

APPENDIX B

Table 5: Chloride diffusion resistance of RHA concrete at ages of 28 day.

Replacement ratio (%)	Chloride diffusion coefficient of RHA concrete at 28 day		
	A	B	C
5%	8.778	9.468	8.665
	9.034	8.898	8.503
	8.946	9.557	8.341
10%	6.396	7.736	4.175
	6.761	7.059	4.909
	6.511	6.913	4.261
15%	5.555	6.562	3.665
	5.100	6.445	3.811
	5.354	6.369	3.720
20%	4.561	5.233	3.126
	4.509	5.213	3.375
	4.290	5.030	3.395
30%	2.893	4.896	2.504
	3.003	4.750	2.399
	3.315	4.917	2.439
40%	2.957	3.585	1.226
	2.056	3.698	1.469
	2.638	3.627	1.274
50%	1.803	1.971	0.774
	1.750	2.140	0.680
	1.765	2.178	0.937
60%	1.609	2.547	1.034
	1.786	2.581	0.900
	1.530	2.893	0.997
70%	-	-	1.367
	-	-	1.351
	-	-	1.394
80%	-	-	5.418
	-	-	5.427
	-	-	5.553
OPC	11.679		
	11.300		
	11.683		

Table 6: Chloride diffusion resistance of RHA concrete at ages of 91-days.

Replacement ratio (%)	Chloride diffusion coefficient of RHA concrete at 28 day		
	A	B	C
5%	7.352	7.727	5.278
	6.669	8.072	5.789
	6.983	7.870	5.824
10%	5.276	6.380	4.175
	5.458	6.213	4.909
	5.701	6.360	4.261
15%	4.726	5.465	2.718
	4.606	5.067	2.852
	4.460	5.180	2.772
20%	3.283	4.051	2.332
	3.298	4.215	2.578
	3.316	3.985	2.488
30%	2.708	2.962	1.284
	2.671	2.808	1.253
	2.739	2.985	1.269
40%	2.244	2.440	1.189
	2.094	2.438	1.209
	2.181	2.498	1.221
50%	1.617	1.893	0.581
	1.590	1.822	0.670
	1.676	1.772	0.608
60%	1.059	2.166	0.768
	1.079	2.105	0.852
	1.136	2.216	0.819
70%	-	-	1.179
	-	-	1.177
	-	-	1.223
80%	-	-	4.480
	-	-	4.711
	-	-	4.877
OPC	9.0331		
	9.3958		
	9.3154		